NASA CONTRACTOR REPORT

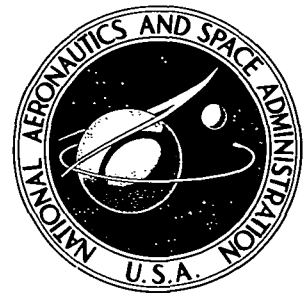

NASA CR-2208

NASA CR-2208

A DESIGN STUDY FOR A SIMPLE-TO-FLY, CONSTANT ATTITUDE LIGHT AIRCRAFT

by Frederick O. Smetana, Douglas E. Humphreys, Rafael J. Montoya, William W. Rickard, and Ivan E. Wilkinson

Prepared by
NORTH CAROLINA STATE UNIVERSITY
Raleigh, N.C. 27607
for Langley Research Center

NATIONAL AERONAUTICS AND SPACE ADMINISTRATION • WASHINGTON, D. C. • MARCH 1973

1. Report No.	2. Government Accession No.	3. Recipient's Catalog No.
NASA CR-2208		

4. Title and Subtitle	5. Report Date
A DESIGN STUDY FOR A SIMPLE-TO-FLY, CONSTANT ATTITUDE LIGHT AIRCRAFT	March 1973
	6. Performing Organization Code

7. Author(s)	8. Performing Organization Report No.
Frederick O. Smetana, Douglas E. Humphreys, Rafael J. Montoya William W. Rickard, and Ivan E. Wilkinson	

9. Performing Organization Name and Address	10. Work Unit No.
North Carolina State University Raleigh, N.C. 27607	760-71-03-01
	11. Contract or Grant No. 34-002-086

12. Sponsoring Agency Name and Address	13. Type of Report and Period Covered
National Aeronautics and Space Administration Washington, D.C. 20546	Contractor Report
	14. Sponsoring Agency Code

15. Supplementary Notes

16. Abstract

The activities during a four-year study by doctoral students to evolve in detail a design for a simple-to-fly, constant attitude light airplane are described. The study indicated that such aircraft could materially reduce the hazards to light airplane occupants which arise from the high pilot work load and poor visibility that occur during landing. Preliminary cost studies indicate that in volume production this system would increase the cost of the aircraft in roughly the same fashion that automatic transmission, power steering, power brakes, and cruise control increase the cost of a compact car.

17. Key Words (Suggested by Author(s))	18. Distribution Statement
Design Light aircraft Automatic control system Constant pitch attitude	

19. Security Classif. (of this report)	20. Security Classif. (of this page)	21. No. of Pages	22. Price*
Unclassified	Unclassified	322	$6.00

*For sale by the National Technical Information Service, Springfield, Virginia 22151

TABLE OF CONTENTS

LIST OF FIGURES

LIST OF TABLES

GENERAL INTRODUCTION

PROJECT BACKGROUND

The task of designing a simple-to-fly, constant attitude light aircraft developed in a rather unusual fashion. NASA had long been concerned about the high percentage of light aircraft accidents which occur during landing and takeoff ($\sim$ 75% of all accidents). There was a feeling among senior NASA engineers that a major contributor to this statistic was the greatly increased pilot workload required on these occasions. Some also felt that the loss of visual reference which often occurs when the nose is pulled up just prior to touchdown can be very disconcerting to the novice pilot and therefore can be a cause of accidents. There was also some concern among senior NASA engineers over two aspects of the training of future aerospace engineers: (1) Relatively few students were being exposed to the design problems of light aircraft; as a consequence few well-trained engineers, those able to apply modern analysis and technology to improve the safety and performance of light aircraft, would ever seek employment with this industry. (2) Engineers tend to concentrate during their education almost exclusively on the narrow high-level technical aspects of their speciality; they acquire little appreciation for the personnel and fiscal management of major projects or even for the technical contributions from other fields which are needed to insure project success.

North Carolina State University had heard this last concern voiced by several other groups over a period of some years and had determined to respond to this need by introducing a graduate program in Major Systems Design. Thus, when the University suggested that an interdisciplinary group of faculty members and doctoral students undertake the design of a simple-to-fly, constant-attitude light airplane, this activity was recognized as having the potential for contributing to the solution of a number of problems. This report is a record both of the technical accomplishments of the program and of its educational activity. The reader may therefore judge for himself whether this type of educational activity is capable of providing both a sound technical accomplishment and training in the conduct of realistic, advanced technology detail design and development tasks.

The faculty group consisted of three members of the Department of Mechanical and Aerospace Engineering, two with backgrounds largely in aerodynamics and the other with a background largely in stress analysis; a member of the Department of Electrical Engineering with an interest in control system design; and a member of the Department of Industrial Engineering faculty with an interest in manufacturing processes. Other members of the Industrial Engineering faculty with specializations in human factors and operations research also worked closely with the project. Except for the Principal Investigator, the role of the other faculty members was

largely advisory. They responded to specific questions, offered special courses - some on an individual reading basis, and criticized the interim reports and briefings. They also served as dissertation supervisors for two of the students.

Five students performed the majority of the work. Two had undergraduate training in Aerospace Engineering, one in Mechanical Engineering, and one in Electrical Engineering. A fifth student with an undergraduate major in Mechanical Engineering became disenchanted with the program and dropped out after receiving a Master's degree. He was replaced by an M.S. student with an undergraduate major in Aerospace Engineering.

The original concept was to assign one student to study the aerodynamic requirements of the constant attitude airplane including its static stability and propulsion. A second student was to develop the stability derivatives for use in the control system design. A third student was responsible for the design of the control systems. A fourth student, for the structural design. The fifth student was to study the means by which the simple-to-fly concept could be implemented and to investigate construction aspects which would lead to the lowest cost aircraft with the requisite performance.

The students were housed together in a series of contiguous offices, one of which was that of the principal investigator. In this way there was frequent communication between all concerned and the principal investigator could closely supervise all the activity. All concerned felt this was an essential ingredient to technical progress. The students devoted 20 hours per week to the task during the academic year and 30 hours per week during the summer. The principal investigator also devoted approximately 20 hours per week to the project.

One aspect of project activity which had a particularly stimulating effect on technical progress was the presentation, at 6-9 month intervals, of oral briefings at the Langley Research Center. These briefings were well rehearsed and well supplied with visual aids. The stimulus of wishing to report competent, coherent, and continuing technical effort served on several occasions to speed the solution of technical difficulties and to force decisions on the technical approach to be followed. The briefings were also very valuable in that the students had the opportunity to have their approaches criticized by knowledgeable professionals and to obtain information relative to the problems they were then wrestling with.

The Langley Research Center also supplied a series of five lecturers - one in each of the major task areas - at the onset of the activity to help orient all those on the project to the state of the art in that area.

It was originally planned to include a large number of undergraduates in the activity as the project developed. During the second of the four years of effort which this report covers, half the senior class (some 26 students) in Flight Vehicle Design was assigned to assist in the project. The seniors were divided into 5 groups of about equal size, each headed by a graduate student. They were asked to assist in various detailed analyses. While they accepted their assignments with enthusiasm and were very complimentary on the way the course was run, feeling they had for the first time during their educations come to grips with a real problem, the graduate students spent so much time bringing them (the seniors) up to date, as it were, that the semester went by with no real progress being made on the project. As a result, the experiment was not repeated.

Several changes also had to be made in personnel assignments as the work progressed. The aerodynamic analysis turned out to be relatively simple and was completed in about 18 months. The development of suitable control system concepts and details, on the other hand, proved to be relatively difficult. None of the faculty group had had experience with multi-input, multi-output control systems, the type which would be required in this vehicle. Nor was there much experience with non-linear control systems. As a result, the decision was made to attempt to obtain the desired result from linear systems. The control system design task was then divided as follows: the aerodynamicist undertook the design of the lateral control system (turn coordinator). The controls analyst restricted his efforts to the development of the longitudinal control subsystems. The human factors - manufacturing technology analyst undertook the analysis of control system reliability and the design of a suitable backup system. The principal investigator and the M.S. student undertook the development of an electrical means to obtain the desired flap responsiveness and an analysis of the response of an aircraft with this type of control system to gusts. The latter three aspects were chosen for very detailed analysis because questions about them were asked repeatedly during the briefing sessions. The fifth student continued to work on the structural design details.

As a result of these changes in emphasis, progress on the total design task was not uniform. Some areas were given as complete an analysis as is warranted by the present state of knowledge. Only actual construction and test can provide a more accurate picture of the validity of these design analyses. In other areas, the work has progressed only to the point of some preliminary estimates. It is of course difficult to forecast accurately at the beginning of such a project just what problems are likely to be encountered and how long it will take to solve them. Because the problems to which the major emphasis was devoted during the last two years seemed to be the ones upon which acceptance of the simple-to-fly, constant attitude concept hinged, it was felt that these questions should be resolved, insofar as possible, even at the expense of little progress on the more routine aspects of the detail design.

The reader will note that the report reflects the state of completion of each phase of the work. The structural and material analysis given here, for example, was initially prepared prior to the beginning of detail design activity. Although detail design of the new wing carry through structure was later completed as were a stress analysis of the fuselage extension structure and the new horizontal stabilator, these tasks were not regarded as presenting a sufficiently comprehensive view of the structural design to warrant their inclusion in this report. Despite some editorial attention this section may therefore contain references to other aspects of the work which were later altered. The aerodynamics work, on the other hand, is essentially complete as presented here, although the lateral control studies were utilized in a slightly different way in the latest concept (spoilers became part of the manual back-up system rather than the primary control system).

The fact that the discussion on system dynamic considerations seems to repeat some of the earlier treatment of air frame dynamics reflects to an unavoidable degree the increasing emphasis which had to be devoted to the control system design. Originally, all of the airframe dynamic analysis was intended to be included in this section. As the complexity of the control system design task became evident, however, and additional staff were assigned to the task, each of them undertook individual dynamic analysis which are integral parts of their respective discussions.

Unfortunately, there are several other instances in the report where the editorial task of updating material prepared earlier and molding it with later analyses was simply too great to obtain a completely self-consistent narrative although an effort was made to remove the more glaring inconsistencies. For these remaining faults, the reader's forebearance is earnestly solicited.

It should be mentioned also that two areas of the report - control subsystem I and effective, low-cost means of improving overall control system reliability - are continuing to receive study as part of as yet incomplete doctoral dissertations.

Educationally at least, the activity can already be called a success. Two students have completed the requirements for the Ph.D.; one used his work on the project as the basis for his dissertation; the other did not. Another student is presently writing his dissertation. A fourth, has had his dissertation outline accepted. The M.S. student is also writing his thesis. Employers generally have viewed the project activity enthusiastically. The two students who have completed their work both accepted responsible design positions, one with industry and the other with the government. Both have already been promoted to supervisory positions.

One other evidence of success in the submission of five disclosures of invention for evaluation by the Research Corporation. On two of these, students were the senior inventor. Although four of these will not be prosecuted because of the current economic climate and the fact that with "paper" inventions development costs cannot be estimated, sales price determined, and the possible market estimated, the

An analysis of accident statistics, illustrated by Table 2, indicates that though a majority of accidents are avoidable by proper piloting, there is still much the designer can do to prevent accidents. Stall can be prevented by limiting control deflection, or use of a stick-shaker. Prevention of the stall prevents the spin. Spiral divergence can be prevented by use of a wings leveler.

TABLE 2. AIRCRAFT ACCIDENTS BY CAUSE

(Source: Ref. 1)

Engine failure	17.8%
Groundloop, waterloop, swerve	13.7%
Wheels up landing	6.5%
Gear collapsed	3.8%
Gear retracted	3.5%
Hard landing	8.5%
Nose over/down	5.0%
Airframe failure: in flight	0.6%
Airframe failure: on ground	0.08%
Engine tearaway	0.06%
Stall, spin, spiral, mush	8.5%
All other	32%

Lest the data be misleading, it should be pointed out that the actual cause of an accident is often human error though the immediate cause is an aircraft failure. For example, most engine failures are due to faulty maintenance, faulty operation technique, fuel mismanagement, fuel exhaustion, et cetera. In a like manner, most airframe failures are due to pilot loss of control associated with pilot disorientation in weather.

Table 3 illustrates the fact that fully two-thirds of all aircraft accidents occur in the landing phase of flight, making it the most dangerous phase. Only 16% of the accidents occur during takeoff, though it is second most dangerous. Only 8% of the accidents occur during cruise, though a majority of all flight hours are

accumulated in this phase. One can only conclude that to improve safety through design, he should examine the landing phase most carefully.

TABLE 3. AIRCRAFT ACCIDENTS BY PHASE OF OPERATION

(Source: Ref. 1)

Taxi	7%
Takeoff	16%
Cruise	8%
Landing	67%
Static	2%
	100%

Landing is a very difficult tracking task, requiring precise control of a six degree of freedom system having three oscillatory modes, two of which are only lightly damped, and several first order modes. Though one of the first order modes (the roll root) is very fast, there is another which can be slow or even unstable (the spiral root). The presence of disturbance inputs (gusts) is quite likely during the landing phase. Added to the tracking task workload are the problems of navigation within a controlled system, communication with air traffic control, approach control, tower control, or other traffic, and other problems of which a pilot must be aware. This can obviously be a very heavy workload, especially when considerations of mortality are superimposed. The difficulty of the tracking task and the excessive workload appear to be the causes of the high accident rate for the landing phase. Thus, reduction of the difficulty of the tracking task and of the workload is the logical approach to the prevention of accidents. Table 4 lists the relative frequency of occurence of several types of pilot errors which can cause accidents, according to two Air Force studies (Ref. 6).

Most of the errors appear to be mistakes that no competent pilot would ever make, yet they were made by professional pilots. For example, when a pilot observes a situation and undertakes a response which is the opposite of the correct response, worsening the situation, he has committed a reversal error. The designer should keep these errors in mind when designing an aircraft control system.

It is also helpful for the designer to reflect on the typical private pilot and the type of flying he does. The average utilization

TABLE 4. PILOT ERRORS

Errors in interpreting multi-revolution instruments	18%
Reversal errors	17%
Signal interpretation errors	14%
Legibility errors	14%
Substitution errors	13%
Using an inoperative instrument	9%
Scale interpretation errors	6%
Errors due to illusions	5%
Forgetting errors	4%
	100%

of personal owner aircraft in the United States is about 80 hours per year, or 1 1/2 hours per week (Ref. 1). Since many of these planes have multiple owners, the average private pilot could be expected to get little more than 1 hour flying time per week. Such a pilot cannot be expected to maintain a reasonable level of proficiency, especially in aspects such as slow flight, stalls, and engine out or other emergency procedures. This pilot is reasonably safe under normal conditions, but should the weather turn bad, an instrument fail, or the traffic get heavy, he may become overloaded, confused, and lose control of the situation.

It is obvious that major gains in safety can be realized by application of the factors discussed to aircraft design. One could reduce the pilot's workload; simplify pilot tasks; reduce the required precision of tracking, the effect of disturbances, and the number of tracked variables; reduce the amount of signal interpretation required; and make the control inputs compatible with resulting aircraft responses and instrument displays. Since the typical private pilot flies much less than he drives, one could take advantage of the set of reflex reactions he has developed driving by modeling the aircraft control system after that of the car.

The control simplifications which one would choose for a safe, simple-to-fly light aircraft would, in general, remove tasks from the pilot's schedule of duties and assign them to machines. One of the major pilot tasks throughout the flight profile is the

maintainence of trim, both longitudinal and lateral, in the presence of speed and altitude changes and disturbance inputs. In the simple-to-fly concept, control is accomplished by a pitch angle control system, a bank angle or turn rate command system, and an airspeed and rate of climb command system. The pilot flies the plane by commanding airspeed (from 1.1 V_{STALL} to V_{MAX}) with a foot throttle, rate of climb (from RS_{MAX} through zero to RC_{MAX}) with fore and aft motion of the yoke, and turn rate (from 0° to $\pm 45^{\circ}$ bank angle) by turning the wheel. The pitch angle control system maintains the fuselage inertial pitch angle at 0°, without pilot intervention. The command systems allow the pilot to control the variables he really wants to control, rather than deflecting the control surfaces required to obtain the desired results. He need only command the desired values for each of the variables, and feedback controllers deflect the control surfaces as required to attain and maintain these values. Pitch angle stabilization has the effect of neutralizing the short period and phugoid oscillations and vertical gust disturbances. It also makes the aircraft stall-proof and thus spin-proof. The bank angle command system controls rudder and ailerons to produce co-ordinated turns by driving the side-slip angle to 0° as the aircraft banks. This neutralizes the dutch roll oscillations, and prevents spiral divergence.

The aircraft will require the following sensors: a vertical gyro (for pitch angle and roll angle), differential pressure transducer (for airspeed, which is proportional to the difference between total pressure and static pressure), two wind angle vanes (one for angle of attack, one for sideslip angle). There are several rates which may be generated as derivatives, or measured using rate gyros and accelerometers. There must also be servos to drive each control surface or powerplant control: left flap, right flap, elevator, rudder, manifold pressure, and propeller speed. Use of full span flaps requires that aileron deflection be simulated by differential flap deflection.

These control systems entirely replace the conventional aircraft control system. There is no direct mechanical connection between the pilot and any control surface. The pilot simply commands the desired values of the flight path variables, and the control systems obey. Servos, sensors, and circuitry have been designed to meet these requirements. The details of their analysis and design are treated in subsequent sections. Such a control system would seem to accomplish the objective of making the aircraft very simple to fly, and thus very safe to fly. However, because of the complexity of the system, extreme measures must be taken to avoid exchanging one source of accidents (pilot error) for another (control system failure). Design for reliability was therefore included as an integral part of this study.

The techniques of reliability engineering can be used to calculate the probability that the system will perform without failure over a period of time. Conversely, one can require that the system be designed such that it have a specified reliability, or probability of failure free operation over a period of time. The cost of the system will increase as the reliability requirement is increased, so the requirement should be made as low as is practical. The system will be useless if it fails too often, or if it costs to much to build, so a trade-off must be made. It would appear reasonable to design the system so that it requires repair or overhaul at about the same interval as other aircraft systems, such as the airframe or powerplant. Light aircraft powerplants generally require complete major overhauls every 1200 to 2000 hours operating time, depending on the engine. The interval for airframe and control system inspection is 100 hours or 1 year, whichever comes first. A 1000 hour life of failure-free operation amounts to about 12.5 years in the life of a typical privately owned aircraft, or 2 2/3 years for a typical instructional aircraft. Thus it would seem that a reasonable design goal for the control system would be that it have a very good chance of lasting 1000 hours under normal conditions of use. Appendix F discusses the analysis and design of additions to the control system to insure this level of reliability.

CONTROL SYSTEM SIMPLIFICATION

INTRODUCTION

The primary purpose of designing a constant attitude, simple-to-fly light aircraft was to minimize flight accidents due to pilot error. Simplification of pilot duties is especially important for the non-professional pilot who, according to Pazmaney (Ref. 1), flies only 80 hours per year, which is little more than 1 1/2 hours per week. Accident statistics show that 87% of all aircraft accidents involve general-aviation aircraft, making these vehicles in the hands of novice pilots a hazard to jet transports carrying from 100 to 400 passengers at a time.

An obvious solution to this problem is to design flight controls that are as familiar to the pilot as those in his accustomed vehicle, the car. This approach, of course must take into account the specialized aircraft functions that are much more complex than those of an automobile.

The design of any vehicle should properly include careful attention to design of controls, considering size, shape, and location; minimum activation force; maximum force; and overall system dynamic response. It should be a "perfect fit" for the pilot: The seat should be the right size and properly located in relation to controls and displays; the yoke should have the right size, shape, and distance from the operator; the knobs and switches should be located conveniently and be the right size; and all controls should require sufficient but not excessive force for activation.

The minimum and maximum allowable forces for the various control types and their motions have been examined. Setting the proper minimum force reduces the likelihood of accidental activation of a control, especially those controls on which the pilot must continuously keep his hands or feet. Upper constraints are needed to insure that the control forces required do not go beyond the capabilities of the pilot. Coupling desirable control size and travel with pilot strength determines the forces and moments available to manipulate the control surfaces.

The force capability which 95%, or the fifth percentile, of a population can be expected to exert is considered the standard. Human strength has been measured and recorded for various populations, especially servicemen and college students. Such compilations give the mean and sometimes the 95th percentile and fifth percentile.

The standard for leg extension and ankle flexion, according to Damon (Ref. 2), is 192 lbs. Woodson and Conover (Ref. 3) give the strength limit of the average man, within an envelope of pedal

position, as 10" maximum pedal travel. Dreyfuss (Ref. 4) limits travel to 4" maximum travel as the comfort limit. Damon shows the standard for pedal pressure to be 50 lbs. for eye level, 41" above heel and pedal angle, with vertical of 50°. This angle increases slightly with added seat height. The arm forces for which standards are set are push, pull, up, down, and rotation, all for the standard left hand, since it is usually weaker than the right. McCormick (Ref. 5) gives the standards for forearm level and upper arm at 30° to vertical as push, 26 lbs.; pull, 34 lbs.; up, 17 lbs.; and down, 21 lbs. These need not be the limits on wheel forces if a worst case analysis shows them to be impractical; the pilot can use both hands if necessary. Use of two hands on the wheel should be avoided on landing, from pattern altitude down, as the pilot may need his right hand to do other tasks. Damon gives left rotation as 25 lbs. and right rotation as 30 lbs. It is not considered necessary to set standards for switches and dials, as they will most likely not require limit forces. No trouble is anticipated if their forces are kept below 4 oz., except that knobs over 1" in diameter can sustain higher loads.

The design of any airplane control system should take into account these human limitations as well as performing its major function of directing the airframe motions within the limitations of its aerodynamic characteristics and structural strength. Figure 1 illustrates, in general, the airplane control problem.

Conventionally, an airplane is controlled through the elevator (equilibrium angle of attack), the rudder (angle of sideslip), the ailerons (angle of bank), and the throttle (output of the power plant). Since the modifications resulting from this design effort will lead to an airplane substantially different from those of conventional configurations, it is reasonable to expect that the control system of this airplane would also be somewhat different.

A simplified control system capable of controlling the airplane through specialized control functions in order to meet the requirements of constant attitude flying is desired. These specialized functions are listed in Table 5.

The design of a safe, simple-to-fly aircraft control system, first of all, must attempt to reduce the most common sources of pilot errors. Fitts (Ref. 6) undertook several surveys to determine the major sources of pilot errors. Although he is most concerned with instrument reading errors, his conclusions carry over into the realm of controls, since they are used in the same environment as the instruments. Fitts showed that pilot errors increase greatly with the number and complexity of tasks. He found that most errors could be prevented by changing the design and implementation of the system. A common error, he found, is that of reversal. The pilot observes a situation and makes a control input that is exactly opposite from what it should be.

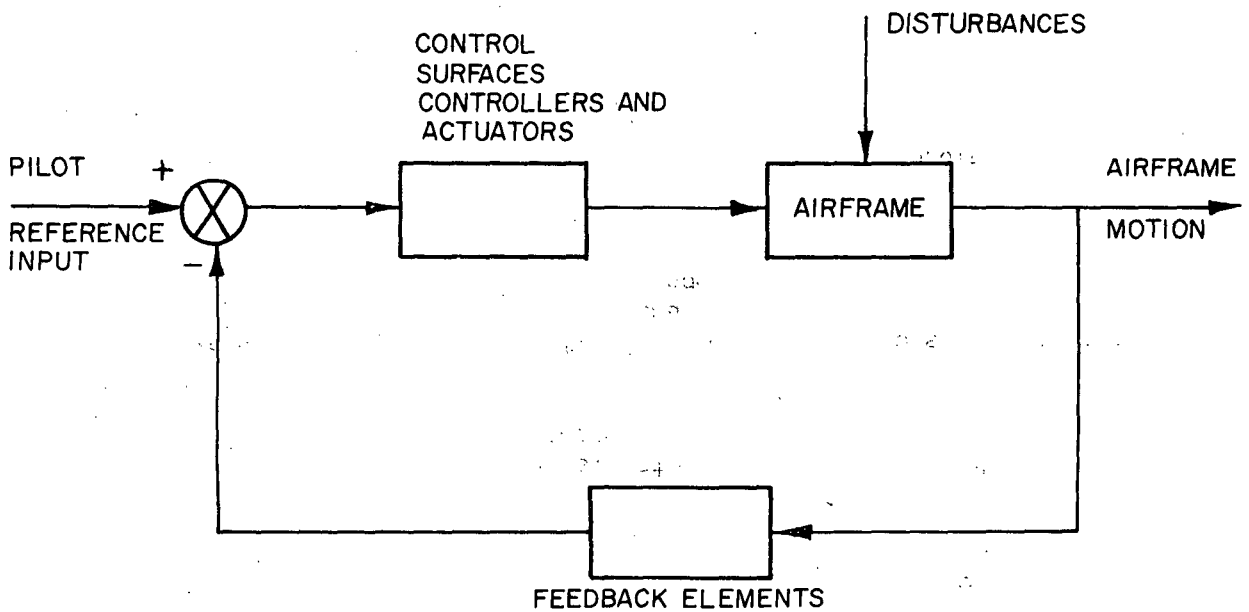

Figure 1. Generalized airplane control problem.

TABLE 5. SPECIALIZED CONTROL FUNCTIONS FOR A SIMPLE-TO-FLY, CONSTANT ATTITUDE AIRPLANE

Control Surface	Controlled By	Control Function
Flaps Throttle	Yoke Push-Pull	Rate of climb or descent
Flaps Throttle	Accelerator Press-Depress	Forward speed
Elevator	Attitude gyro-servomechanism arrangement	Constant attitude
Ailerons Rudder	Yoke Twisting	Coordinated turns

Since the study was based on experienced military pilots, the conclusion is that control motions and resultant aircraft motions must be strictly analogous to each other. This is known as S-R (signal-to-response) compatibility in human factors engineering, where it has been proven that reaction time and errors increase with decreasing S-R compatibility.

Gagne (Ref. 7) emphasized what he called "job aids," which can, by their nature, reduce the amount of training and experience needed to perform successfully certain tasks. By definition, a job aid is an item that assists an operator in the performance of his task. Proper attention to design allows the inclusion of job aids into a system, reducing its operating complexity. He also emphasized that the system should be analyzed and that assignment of tasks to man and machine should insure that capabilities match requirements.

Morgan (Ref. 8) and Woodson have published extensive handbooks on the concepts and physical characteristics involved in good design from a human factors standpoint. Woodson's manual is a commercial version of the report of the joint Army-Navy-Air Force committee on human factors in design, a substantial portion of which is devoted to aircraft. This book covers the details, such a control shape, color, size, motion, throw, activation force, and location, related to both use and user.

From these sources, the philosophy of control design for a new aircraft evolved. The control system must be simple, with as few variables as possible requiring the pilot's attention. Those functions which require constant attention should be linked to as few controls as possible or shifted to automatic controllers which will maintain a condition the pilot desires to be held constant, such as airspeed or altitude. It must have a high S-R compatibility so that the pilot need not think out his response but merely react. High S-R compatibility implies that the correct response must be the pilot's natural reaction. It should employ job aids which make the system require fewer inputs to accomplish an objective. It should assign to man that portion of the system tasks which he is better qualified to handle, and to machine those tasks which require the constant maintenance of a variable, as airspeed, while the man should make the decision of when and what to do.

Four control systems were conceived to satisfy these requirements, with the basic philosophy of simplification through integration of several control functions. These integrations are based on observations of the interplay of the different control surfaces of an airplane to obtain a desired control over its motions, e.g., elevator deflection and throttle setting to obtain a change in rate of climb in the conventional case or flaps and throttle settings to obtain the same objective in the

specialized simple-to-fly aircraft. All the simplified control systems employ three automatic devices not controlled by the pilot: wing leveler, turn coordinator, and fuselage leveler.

For the purpose of identification, the control systems were labeled Control Systems I-IV. These systems can be divided broadly into two categories: Control Systems I-III, in which the systems are manually operated by the pilot; and Control System IV, in which an attempt is made to control the airplane automatically, with minimal manual control.

The feasibility of the control systems were established on the basis of whether or not they can be implemented, e.g., weight, cost reliability, market appeal, and regulatory agency requirements.

Control System I

This system is the simplest to design and build but reduces pilot workload only slightly, requiring the pilot to track with the yoke and a foot throttle. The yoke controls vertical and turning flight; rate of climb is proportional to fore or aft yoke deflection and turning rate proportional to angular deflection of the wheel. The foot throttle controls only forward velocity, which is proportional to foot pedal depression. Fore or aft deflection of the foot throttle and yoke combine to control flap setting and engine throttle position. Thus, holding the foot throttle steady while the yoke is pulled or twisted keeps the forward airspeed constant during climbs and turns. Holding the yoke steady while depressing the foot pedal causes acceleration, with rate-of-climb unchanged.

A speed monitor relieves the pilot of keeping his foot on the foot throttle for extended periods of time. The pilot can set the speed monitor to hold any given airspeed within the capabilities of the aircraft, in which case the foot throttle is used only to override the speed monitor.

Control System II

This system reduces the pilot's workload more than the first but is more complicated to design and build. With the absence of the foot throttle, the yoke takes on the additional function of regulating speed. Fore and aft travel of the yoke determine not only the rate of climb, but also an airspeed corresponding to that rate of climb, e.g., best airspeed for a desired rate of climb or airspeed inversely proportional to rate of sink. Once an airspeed and rate of climb for each yoke position have been chosen, the throttle setting and flap deflection required to attain them are determined.

It appears likely that there is no single, continuous relationship between yoke position, throttle setting, and flap deflection, so a mode selector is provided. This allows one set of control ratios for cruise, one for climb, and another for descent. The speed monitor, as before, serves to keep the aircraft flying at a constant speed automatically, at the discretion of the pilot.

Control System III

In this system, the yoke has the same form and function as in Control System II, controlling airspeed, rate of climb, and turns. The speed monitor has the same function as before.

A throttle lock is added as a fail-safe device on the power plant controls for take-off and landing, allowing the pilot to lock the power full on for takeoff and climb or full off for landing. This protects the aircraft against the possibility that a control system or component failure could cause a loss of power on take-off or an addition of power on touch-down.

Control System IV

In the fourth system, man serves as a monitor, and the system does the tracking. The pilot can, of course, override any control at any time. The pilot sets in his instructions and sits back to see that the desired flight path results. This system is the most complicated to design and build but the simplest to fly.

The system has six modes--taxi, takeoff, climb, cruise, descent, and landing; and four input parameters--velocity, rate of climb, altitude, and heading. The modes may be necessary to allow for changes in the relations between control ratios in the various flight phases, or to remind the pilot of what he has commanded the airplane to do and to remind him to change commands between flight phases.

The taxi phase returns all control to the pilot. This is necessary to allow taxiing of the airplane and also permits it to be flown as a standard airplane. In this phase, the pilot must taxi to the end of the runway and prepare for the takeoff. He sets the velocity for his desired climb velocity, rate of climb for the desired rate of climb, altitude for the altitude at which he wishes to discontinue climbing, and heading is not necessarily set at all. The pilot must steer the airplane out of the terminal in the normal manner or set the heading to steer him properly, according to procedures observed at the particular terminal, as 90° left at 800 feet above the runway and 45° right at 1200 feet above the runway. Having prepared for take-off, the pilot switches

the mode to "take-off," and releases the brakes when power comes up. The system immediately applies full power and proceeds to fly the plane off the ground. The pilot must keep the plane straight on the runway, while the system drops flaps, inducing lift-off and climb, at some preselected velocity, as $1.2V_{stall}$. The pilot then switches to "climb," and the plane will climb at the speed and rate of climb he has chosen until it reaches the prescribed altitude.

The aircraft then levels off and flies at the pre-set altitude and velocity until the pilot changes to "cruise" and modifies the velocity. In this setting, the system will maintain speed, altitude, and heading, with rate of climb set at zero. If he wishes to change airspeed, altitude, or heading, the pilot merely dials them into the system, and the changes are made gradually, in comparison to climbing maneuvers.

When he is ready to descend, the pilot merely shifts to "descend" and dials in the necessary information, as rate of descent, velocity of descent, altitude at which to end descent, and heading or omni station to hold while descending. The descent ends at the altitude which the pilot has chosen to allow him to set up in the pattern and begin landing procedures.

Although the landing mode may not be possible to achieve, it is considered desirable. The pilot dials in the velocity, altitude, and rate of sink he wishes at touchdown. It will be necessary for him to steer the plane or re-set the heading desired at each turn in the landing pattern. If this procedure proves unfeasible on landing, it may be necessary to return all control except velocity to the pilot and make provision for him to cut power on touchdown.

This system incorporates the autopilot into the simplified control system, with provisions for both inertial and radio control of heading. It constitutes a radical departure from conventional general aviation control systems in that it would control the airplane automatically, reducing the pilot tasks to those of dialing reference values of the airplane outputs and monitoring the system. Its implementation would require the construction of what may be called a "flight computer." This would be responsible for the generation and channeling of error signals to activate the actuators of the various control surfaces. The mode selector would provide for the airplane to be flown entirely manually.

There are indications that a considerable amount of automation will be found in general aviation airplanes in the near future. It should be recognized, however, that the incorporation of Control System IV in today's airplanes probably represents an

over-optimistic outlook, since a very sophisticated, hence expensive, control system would be required.

Choice of Control System

To assist in choosing a power source and the actuator types and sizes and to generate some preliminary cost information, limited investigations were made on all four control systems to determine

1. The response rates required of the different control surfaces based on the dynamic behavior of the airplane and the desired flight profiles

2. Methods for exciting the control actuators

3. Design criteria to insure that all systems were fail-safe.

Control System I was chosen as the basis of the modification kit to be incorporated into the PA-28 235C. The decision was based on four considerations.

1. Detailed design of this system is basic to the optional implementation of the other three systems.

2. Several subsystems of this system are common to all other systems, for example, the automatic constant attitude controller and the wings leveler.

3. On the basis of mechanical failures being the least likely to occur, this system is the safest since it is the least automated of all the systems proposed.

4. Preliminary estimate of the weight of major components indicated that this parameter is not critical.

It may be recalled that the aim of this control approach is to simplify the pilot's control task by integrating several control functions into a few controls. For example, the deflection of the control surfaces necessary to obtain coordinated turns are achieved by one pilot command, twisting the yoke. Further, the system is intended to produce a close correlation between automobile driving and aircraft piloting so as to reduce the familiarization period needed when moving from one vehicle to the other.

The implementation of this control concept in flight hardware was viewed initially in terms of three essentially independent subsystems: a forward speed, rate-of-climb controller; a fuselage

leveler; and a turn coordinator. The discussion below indicates the manner in which these subsystems evolved and integrated as the analysis developed and additional influences were considered.

SUBSYSTEM I.

This subsystem obtains rate-of-climb (+ or -) from aft and fore motion of the yoke, respectively, and changes in forward airspeed by "accelerator" depression (throttle movement). Since both flap and throttle motions are required to change either airspeed or rate of climb, the system must actuate the same two outputs with either of two inputs, but in an entirely different manner. The analysis of such multi-input, multi-output control systems had not, at the time the project began, appeared in accessible literature and the prospect of developing these techniques in a rigorous fashion and yet meet a design timetable was not very appealing. Thus an effort was made to find a simpler means of providing the necessary control actuations.

It became obvious at this point that, to control the aircraft in the manner envisioned, a "fly-by-wire" system would have to be employed. Thus it did not matter whether the control linkages were fully mechanical, power-boosted mechanical, all hydraulic, or all electric. In examining the aerodynamic requirements (flap setting and power setting as functions of speed, rate of climb, altitude, and weight) of constant attitude flight, it was found that if δ_F were plotted against the ratio of dynamic pressure to weight with rate of climb and percent power as parameters, the curves were essentially independent of altitude for the operating range of the aircraft. The fact that these curves were universal suggested that they might be used as the contours of three-dimensional cams which could be used to actuate the flaps and the throttle.

Accordingly, such a system was devised. One cam follower controls the flap position (probably by exciting an electric or hydraulic servo, although direct mechanical action is possible, at least in theory), the other, the engine throttle position. The yoke position determines the angular position of the flap cam; an electric or hydraulic actuator positions the flap cam axially according to a measurement of the ratio of dynamic pressure to aircraft weight. The cam follower is a ball. It is held by an arm which can move about a fixed axis. The rotation of the follower arm is thus controlled both by yoke position and by Q/W or either separately.

The foot throttle position controls the axial position of the power cam. Its angular position is determined by the yoke position. It is seen, therefore, that the follower position (which operates the engine throttle) is determined by either a command to change speed or a command to change rate of climb, or both. Reasonably accurate models of the two cams along with actuators and followers were built to investigate the operation of the system. The cams had a maximum diameter of 4" and a length of about 6". Studies

with the model indicated that the required flap and engine operation could be achieved in this fashion. The flight profile of these two three-dimensional cams is shown in Figure 2.

It should be noted that a cam-type control system provides only a continuous variation of equilibrium flap and power settings. It does not provide inherent control over airframe dynamics or attenuation of gust responses. It is therefore essential that the airframe dynamics with the control system in the loop be investigated. Since a suitable characterization of the cam-type control system dynamics would have to be developed, since the desirability of the resulting airframe dynamics was not known beforehand, and since various interested parties had repeatedly expressed concern over the safety of light aircraft operation in turbulent air, the cam-type system was abandoned in favor of a full feedback control system.

To simplify the analysis of such a system, it was assumed that a fuselage leveler of such effectiveness could be built that θ would always be zero (or some other command value). For purposes of the forward-speed, rate-of-climb control system design, then, the aircraft was treated as a two-degree-of-freedom system (u,α). This design is discussed in detail below. Some effects of coupling with the pitching mode were later investigated as part of a detailed study (Ref. 9) of the response of aircraft of this type to atmospheric turbulence. For the present discussion it is sufficient to mention that management of the coupling requires no change in the type of compensation employed in the control system but does entail a small change in the time constants. Satisfactory operation in gusty as well as in still air also means that the rate-of-climb sensor must be of the inertial type (integrating accelerometer) rather than of the simpler aerodynamic type (vane).

The forward speed-rate of climb control subsystem for this aircraft is a fly-by-wire subsystem designed for the automatic control of the forward airspeed (u) and the rate of climb (w). The requirement of constant attitude flying constrains the manner in which these variables can be controlled. This is done by the lift and drag modulation resulting from deflections of the full span, Fowler flaps and by the adjustment of engine horsepower resulting from rpm changes at constant manifold pressure. The goals of minimization of piloting tasks and introduction of automobile type controls dictated that u be controlled by fore and aft motions of the foot throttle and that w be controlled by fore and aft motions of the yoke.

The aircraft as a dynamic plant outputs a u which is the resultant of the combined effect of flap deflection (δ_F), elevator deflection (δ_E), changes in engine rpm (δ_{RPM}), and changes in engine manifold

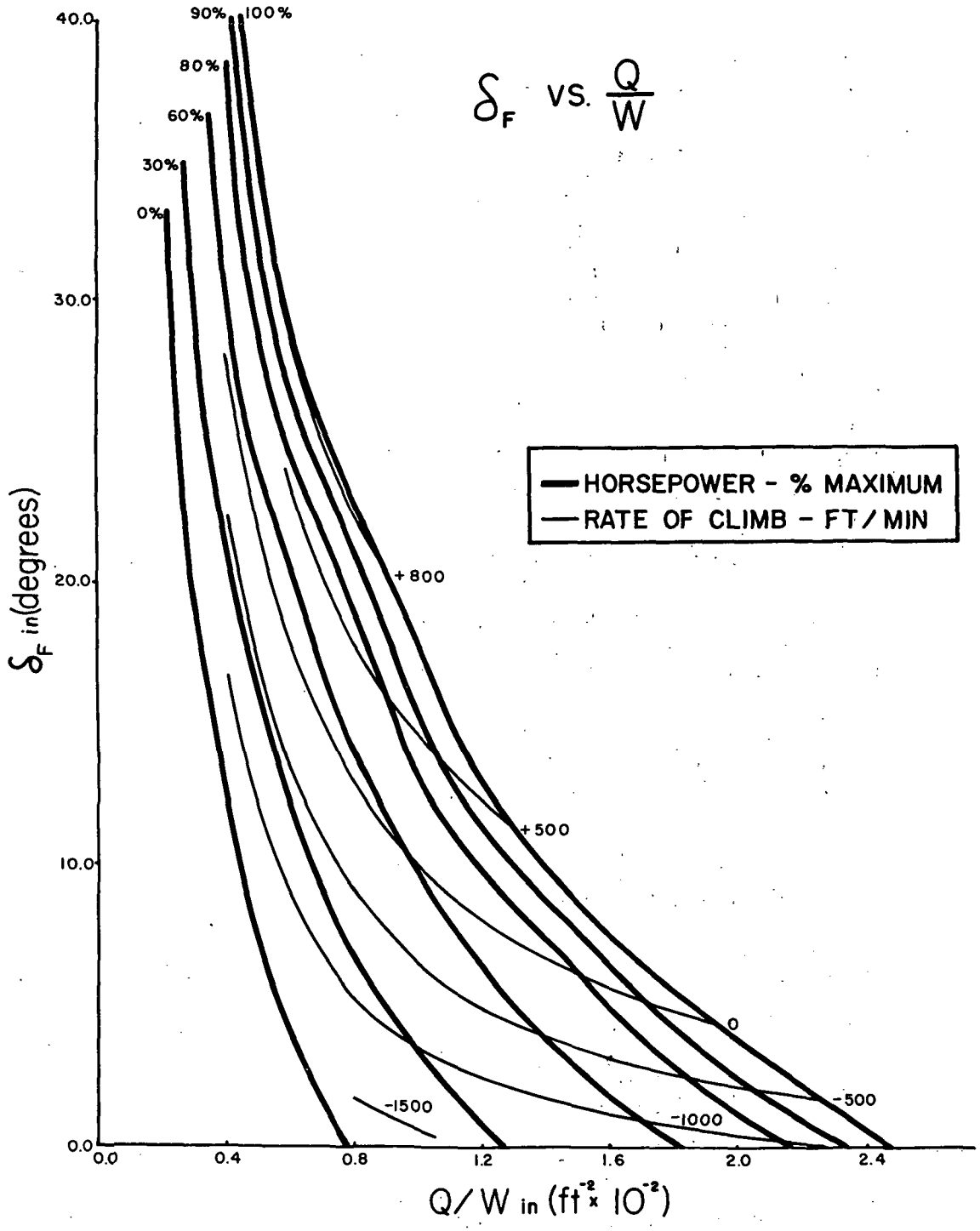

Figure 2. Flight profile of the three dimensional cams used in early mechanization of forward speed-rate of climb control.

pressure (δ_{MAP}). These deflections of the control surfaces* also affect w in a similar fashion. Hence, it is necessary that both control inputs to the subsystem (u_c and w_c) command all these manipulated variables (δ_F, δ_E, δ_{RPM}, and δ_{MAP}) to achieve control over both output variables (u and w). This dynamic model can be simplified by the use of an engine control strategy that keeps manifold pressure constant and by considering that the elevator deflections produce internal disturbances in u and w the effect of which will be rejected by the feedback control subsystem. The proposed subsystem is shown conceptually in Figure 3. The operation is as follows: a foot throttle depression is transduced into a u_c voltage which is added algebraically to a voltage proportional to the airspeed of the aircraft as sensed and transduced by the u sensor. This addition is performed by the airspeed error generator the output of which, (ε_u), actuates the flap and engine servos to produce a δ_F and a δ_{RPM} respectively. These changes in the manipulated variables produce, through the aircraft dynamics, a change in u that tends to drive the error to zero. Similarly, a yoke deflection is transduced into a w_c voltage which is added algebraically to a voltage proportional to the rate of climb of the aircraft as sensed and transduced by the w sensor. This addition is performed by the rate of climb error generator the output of which, (ε_w), actuates the flap and engine servos to produce a δ_F and a δ_{RPM} respectively. These deflections produce a change in w that tends to drive the error to zero. The purpose of the compensator matrix will become clear when the requirement of noninteraction of the control channels is discussed below.

Longitudinal Open Loop Behavior of the Aircraft

In order to set dynamic specifications for the subsystem described conceptually above, it is necessary to examine the open loop behavior of the aircraft. The equations describing this behavior are found elsewhere in this report.

The transfer functions of interest are those relating u and w to the control surface deflections δ_F and δ_{RPM}. These transfer functions are ratios of polynomials in the Laplace variable s with a common fourth order denominator and second or third order numerators. The coefficients of the polynomials making up these transfer functions are dependent on geometric parameters, airspeed, and non-dimensional

---

*The term control surface deflection as used in this text applies also to changes in engine rpm and manifold pressure.

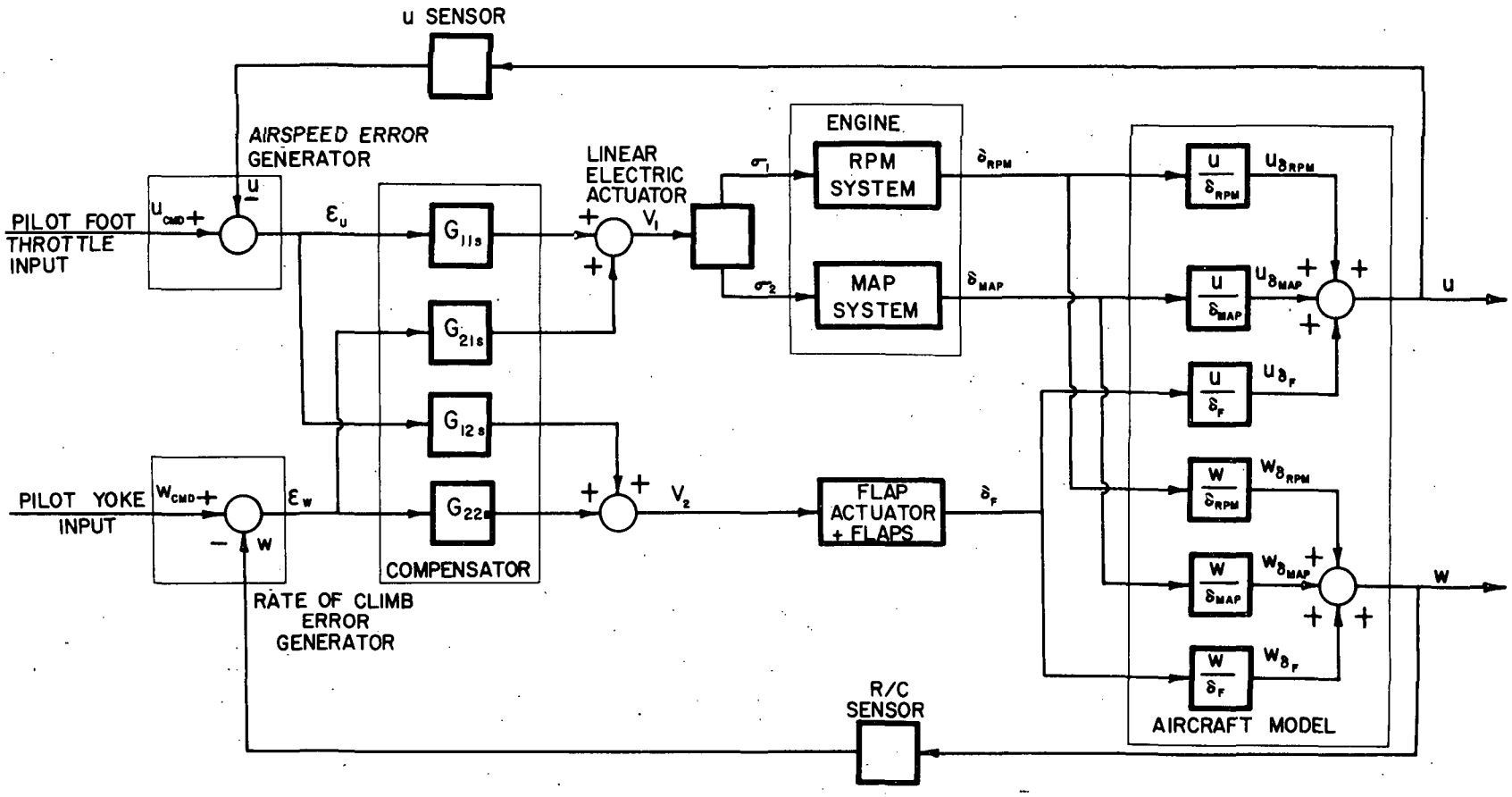

Figure 3. Forward speed-rate of climb controller.

stability derivatives. These coefficients were evaluated for representative conditions in the flight profile of the aircraft. These conditions are: light-weight cruise, climb, and land; and heavy-weight cruise, climb, and land. Appendices D and E list the required information to compute these coefficients as well as their values for the unmodified and modified aircraft respectively.

The flight condition chosen as the basis for design was the heavy-weight cruise (FC #4). A step response test was performed on the individual transfer functions resulting from the substitution of the coefficients for this flight condition from the appendices. This test shows the dynamic behavior of the aircraft in u and w due to flap deflections and changes in engine rpm. These transient responses were evaluated by a computer program which is based on the method of residues. Figure 4a shows the u and w responses of the unmodified aircraft and modified aircraft to a one degree step in flap deflection; similarly Figure 4b shows the u and w responses of the two aircraft to a 50 rpm step change of the engine. Examination of these figures shows that the geometric modifications have improved the dynamics of the short period mode while virtually unchanging the dynamics of the phugoid mode. It is also seen that the flap and rpm power have increased due to the geometric modifications. The long settling time (due to the phugoid mode dynamics) shows that any attempt at controlling these variables accurately in an automatic fashion requires a quickening of this settling time.

Closed Loop Performance Specifications

The operational description of the subsystem given above and the open loop dynamic behavior of the aircraft as shown in Figures 4a and 4b dictated that the following specifications be set:

i) noninteraction between the u and w control channels; i.e., a command in u should not affect the present value of w and a command in w should not affect the present value of u;

ii) position to rate controls; this means that a u corresponds to a foot throttle position (δ_{FT}) and a w corresponds to a yoke position (δ_{Y});

iii) the dynamic responses of w and u should be changed from the typical second order behavior with long settling time depicted in Figures 4a and 4b to that of a typical first order system with time constant of the order of 2-3 seconds, i.e., a system with settling time of the order of 6-10 seconds;

iv) zero compliance of the control channels, i.e., perfect rejection of internal and external disturbances by both u and w channels;

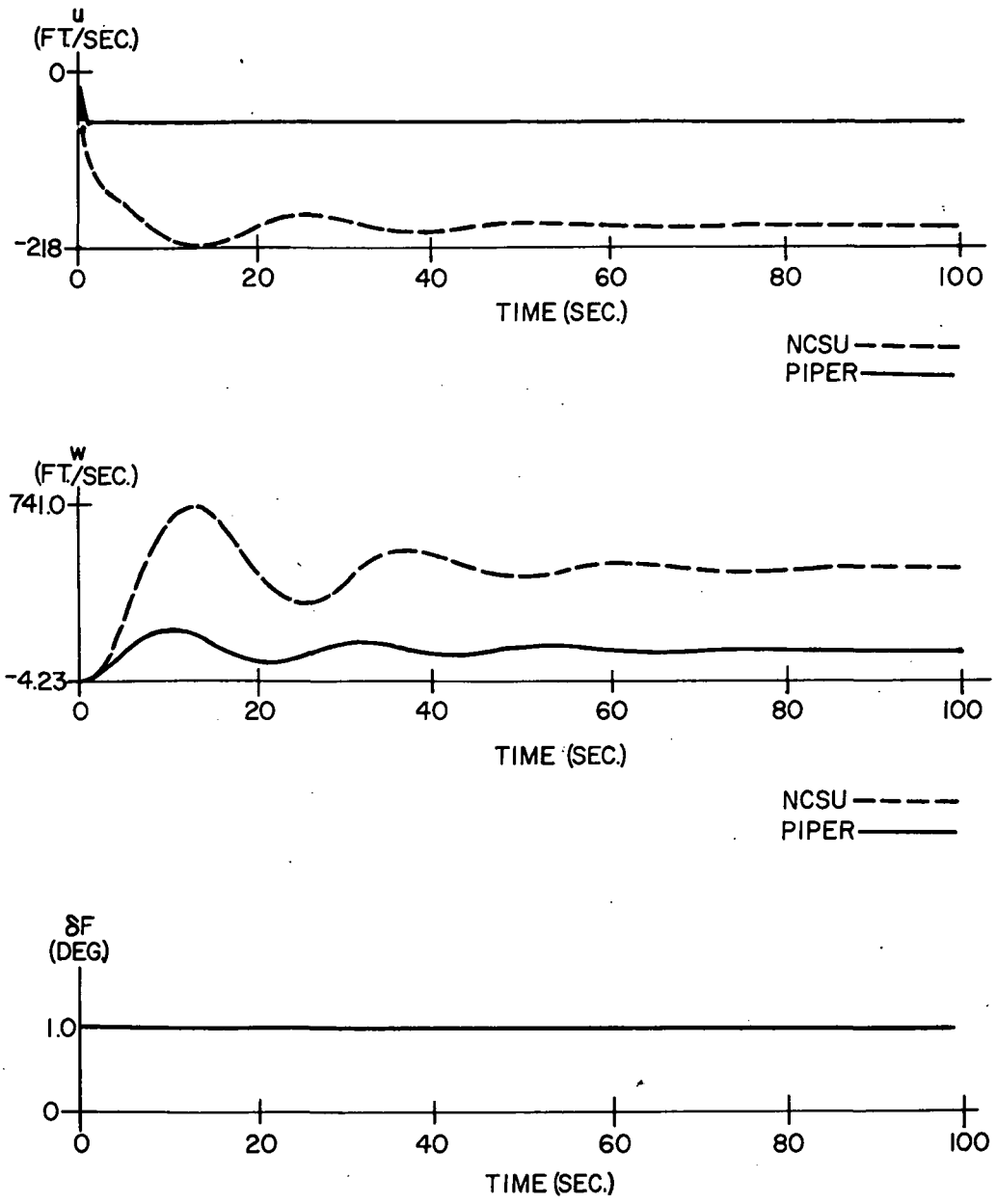

Figure 4a. Aircraft response to a one degree step in flap deflection.

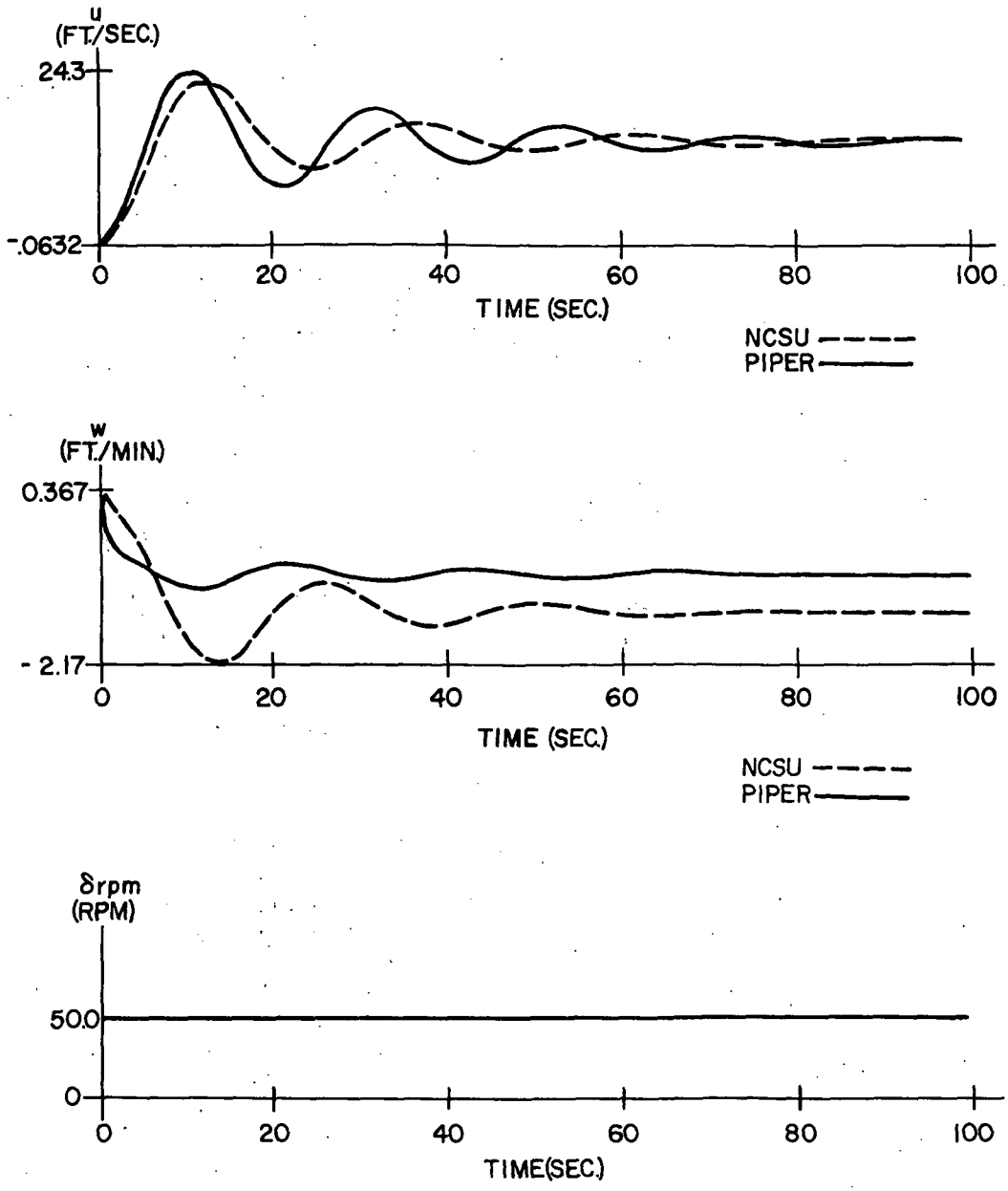

Figure 4b. Aircraft response to a 50 rpm step in engine speed.

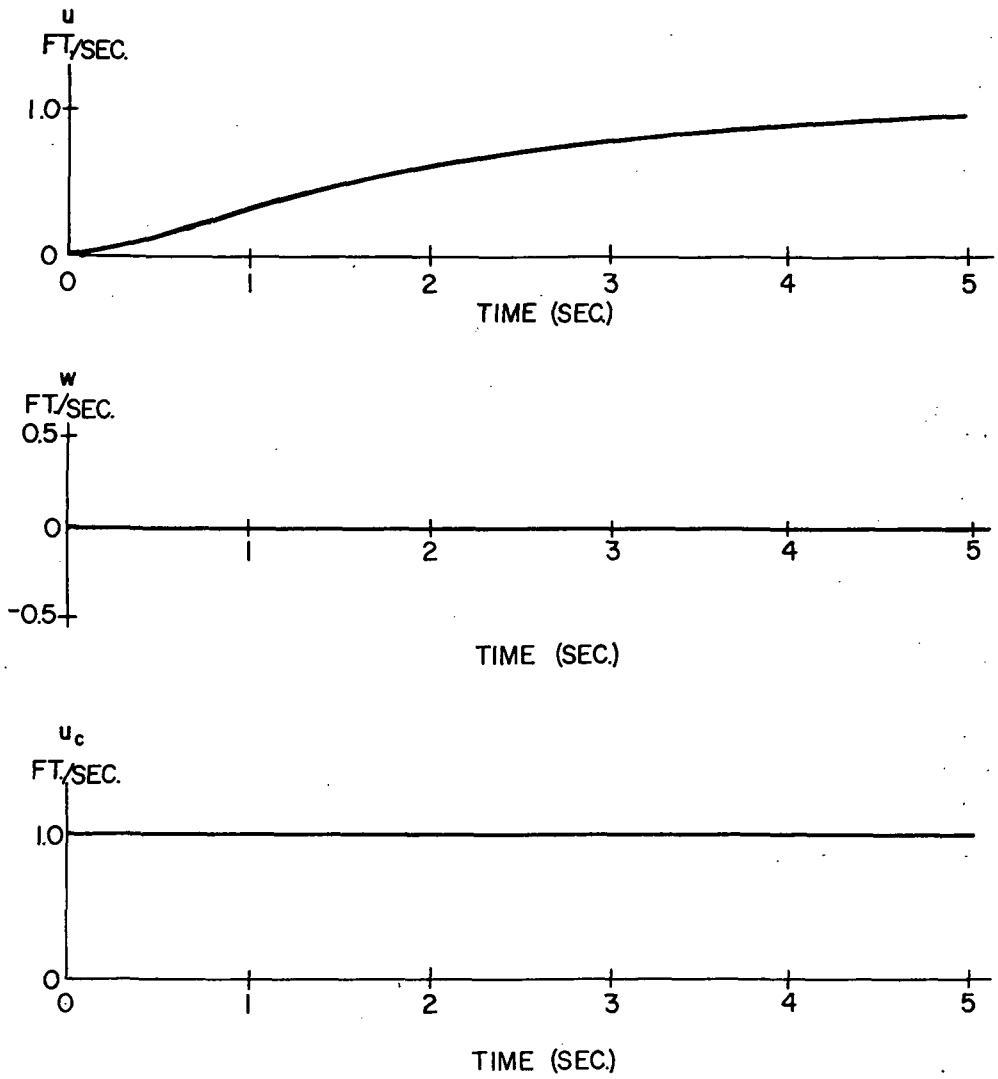

Figure 4c. Closed loop responses of the forward airspeed-rate of climb control subsystem to a step command in u_c.

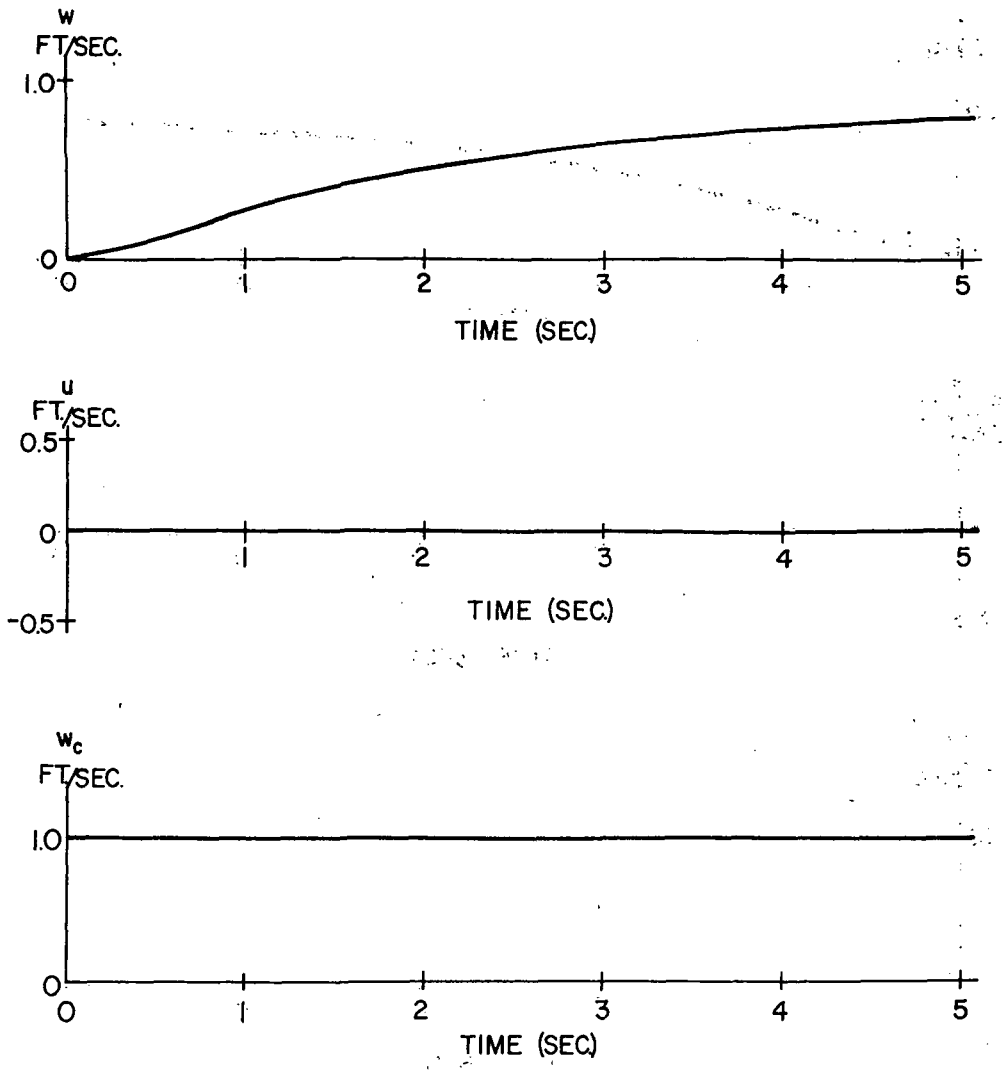

Figure 4d. Closed loop responses of the forward airspeed-rate of climb control subsystem to a step command in w_c.

v) the flap actuating system must be at least ten times faster than the rpm actuating system to account for the inherent lag between lift build up and engine horsepower build up; and

vi) the maximum allowable static error should be 2.6 fps in u and 20 fpm in w.

The first four specifications will serve as a guide for the synthesis of the subsystem whereas the last two will set a bound on the characteristics of the fixed elements of the subsystem. These characteristics are developed in Appendix G.

Synthesis of the Forward Airspeed, Rate of Climb Automatic Control Subsystem

The model of the control subsystem proposed as shown in Figure 3 and its operational description and specifications indicate that the subsystem is of the multiple input-multiple output (MIMO) type. The two input-two output case for this type of systems has been formulated in a number of ways in the literature. See for example Stevens, et al., Ref. (41) and Takahashi, et al., Ref. (42). The procedure followed in this design is presented in Appendix H and was chosen for its simplicity and clarity. The steps required by this method can be summarized as follows:

i) determination of the plant transfer functions $\frac{u}{\delta_{RPM}}$, $\frac{u}{\delta_F}$, $\frac{w}{\delta_{RPM}}$, and $\frac{w}{\delta_F}$ under the assumption of zero pitch angle;

ii) determination of the closed loop transfer functions relating u to u_c and w_c relating w to u_c and w_c;

iii) determination of the relationship between the members of the controller transfer matrix required to obtain noninteraction of the control channels;

iv) determination of the transfer functions of the controller matrix required to obtain the specified time domain behavior for $\frac{u}{u_c}$ and $\frac{w}{w_c}$;

v) determination of the transfer functions of the other members of the controller matrix according to the rules developed under iii; and

vi) substitution of the numerical values of the transfer functions of the controller matrix in the relationships obtained under ii for the purpose of closed loop dynamic response evaluations.

The controller matrix transfer functions developed in Appendix H to satisfy the operational specifications based on the heavy weight cruise condition (FC #4) are summarized in Table 6. It is seen that the elements of the controller matrix are all realizable with simple passive networks. Also shown in this table are the resultant closed loop transfer functions for this flight condition. The manner in which these transfer functions can be evaluated for the other five flight conditions and the required data necessary for this evaluation is included in Appendix H. Also included in this appendix are the relationships and data necessary to evaluate the transfer functions relating the aircraft manipulated variables δ_{RPM} and δ_F to the command inputs u_c and w_c.

TABLE 6. SUMMARY OF THE CONTROLLER MATRIX TRANSFER FUNCTIONS AND CLOSED LOOP TRANSFER FUNCTIONS FOR FLIGHT CONDITION 4

$$G_{11_s} = \frac{.105(s+.023)(s+5)}{s(s+5.5)} \qquad G_{21_s} = \frac{-.004(s+3.87)(s+5)}{s(s+5.5)}$$

$$G_{12_s} = \frac{-.00004(s+50)}{s(s+5.5)} \qquad G_{22_s} = \frac{-.00017(s+2.05)(s+50)}{s(s+5.5)}$$

$$\frac{u}{u_c}(s) = \frac{2.5}{(s+.5)(s+5)} \qquad \frac{u}{w_c}(s) = 0$$

$$\frac{w}{u_c}(s) = 0 \qquad \frac{w}{w_c}(s) = \frac{2.5}{(s+.5)(s+5)}$$

The time responses of the aircraft in u and w in response to step commands of 1 fps and 60 fpm in u_c and w_c respectively were evaluated by taking the inverse Laplace transform of the relations given in Table 6. These responses are shown in Figure 4c and 4d respestively. From these figures it can be seen that the design specifications have been met exceedingly well. These responses

achieve 95% of their final value 5 seconds after the application of the input and are essentially first order type behaviors with a slower rate of growth during the first second of the response interval. It is also seen that the crossfeed responses are zero as should be expected. It should be noted also that the close loop transfer functions for the other flight conditions obtained using the controller matrix given on Table 6 will not have exactly zero crossfeed responses. Preliminary tests indicate resultant closed loop transfer functions with 6th order numerators and 8th order denominators with, approximately, unity dc gain in the direct transfer functions and very small but finite dc gain in the crossfeed transfer functions.

The capability of the subsystem proposed to reject disturbances has been investigated by Smetana, et al.,(Ref. 9). It was found that the subsystem offers a very low compliance to gusty disturbances in angle of attack.

Summary and Conclusions

A control subsystem has been designed to introduce automobile type controls in a general aviation aircraft as a means of easing the piloting tasks in the longitudinal control. The approach consisted of a fly-by-wire technique which provides independent control of u and w through foot throttle depressions and yoke deflections respectively. Analytical studies indicate that these variables can be made to follow a step command with a typical first order system behavior having a time constant of 2 to 3 seconds while substantially eliminating the crossfeed responses $\frac{u}{w_c}$ and $\frac{w}{u_c}$.

Further a relatively complex control concept can be realized in a straight forward manner by using a controller matrix with passive elements only.

An important point to be made here is that the analysis carried out in Appendix H assumes that the fuselage leveler (subsystem 3) provides perfect suppression of the pitching motion. Obviously, this is a simplification whose consequences must be examined, particularly since the resulting pitching motions, while small, are not zero. The analysis carried out in Appendix H was viewed at the time as treating the most complex case which could be readily accommodated. Since that time another MIMO analysis which considered the pitching and plunging motions to be controlled but allowed u to be free was carried out in connection with studies of the gust response of the aircraft (Ref. 9). This study showed that some alterations in the controller matrix developed in Appendix H are necessary to achieve the desired dynamic responses. This is to be expected since the order of the transfer functions is higher in the three degree of freedom analysis. Thus it seems advisable to carry out the more

general analysis which includes the effects of operation of the fuselage leveler before settling on final values for the controller matrix components. The simpler analysis presented herein would seem to be adequate to demonstrate that the desired response can be achieved and that the crossfeed effects between channels can be suppressed in a fairly straight forward fashion.

SUBSYSTEM 2.

Conventionally, control of the pitch attitude of an aircraft is performed by a closed loop feedback system in which the pilot is the comparator and controller elements. As shown in Figure 5, the system consists of a cable and pulley arrangement which links the control column to the elevator. The artificial horizon flight instrument provides visual feedback to the pilot. The precise tracking requirements imposed by constant pitch attitude flying makes the use of a conventional control system incompatible with the goal of minimizing piloting tasks. Furthermore, the manner in which rate of climb and forward speed are to be controlled makes a conventional pitch angle control impractical. It may be recalled that in this aircraft rate of climb is controlled by fore and aft motions of the control column and forward speed is controlled by depression of the foot throttle. Both of these commands result in flap deflections and engine RPM changes which in turn act through the aircraft dynamics to produce changes in rate of climb and forward speed. Due to the inherent interaction exhibited by the aircraft as a plant, any control surface change affects not only the variable which is intended to control but all other longitudinal variables as well; this means that adjustments in flap position and engine RPM to obtain a desired value of rate of climb for example also create an undesired pitch angle. It is concluded therefore that an elevator to control column mechanical link would not be a practical manner of maintaining zero pitch attitude; even if this link were geared to produce, through the elevator, a pitch angle that opposes that created by the flaps, one cannot claim zero pitch capability at all times since the ratio degree of elevator per degree of flap does not remain constant with flight condition as seen in Table 7. One more disadvantage of a conventional pitch control for this airplane is that an attempt by the pilot to counteract external pitch disturbances would result in undesirable changes in rate of climb.

Accordingly, the function of the pitch control subsystem is to command elevator deflections to counteract sensed deviations from the zero pitch condition due to both internal and external disturbances. The Fuselage Leveler, a completely automatic control subsystem, was designed for this purpose.

Pitch autopilots have been used in aircrafts since 1912, their function being either as a stability augmentor or as a pilot relief system. A typical example is shown in Figure 6 and discussed in Blakelock (Ref. 10). The Fuselage Leveler is an extension of the pilot relief system differing from it in that it is operational throughout the flight mission and in that there is no mechanical connection between the elevator and the yoke. This is depicted conceptually in Figure 7.

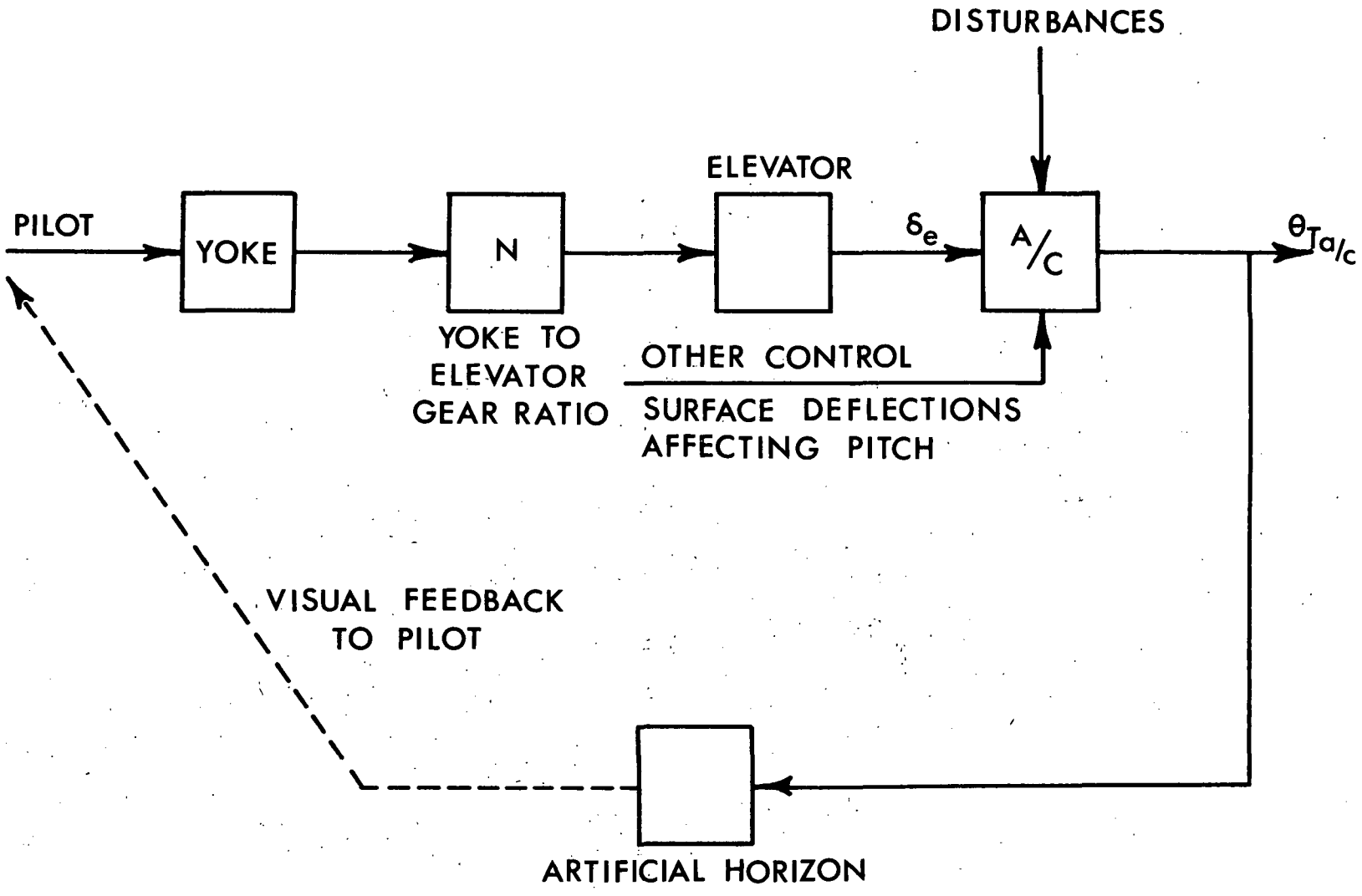

Figure 5. Conventional mechanical pitch control system.

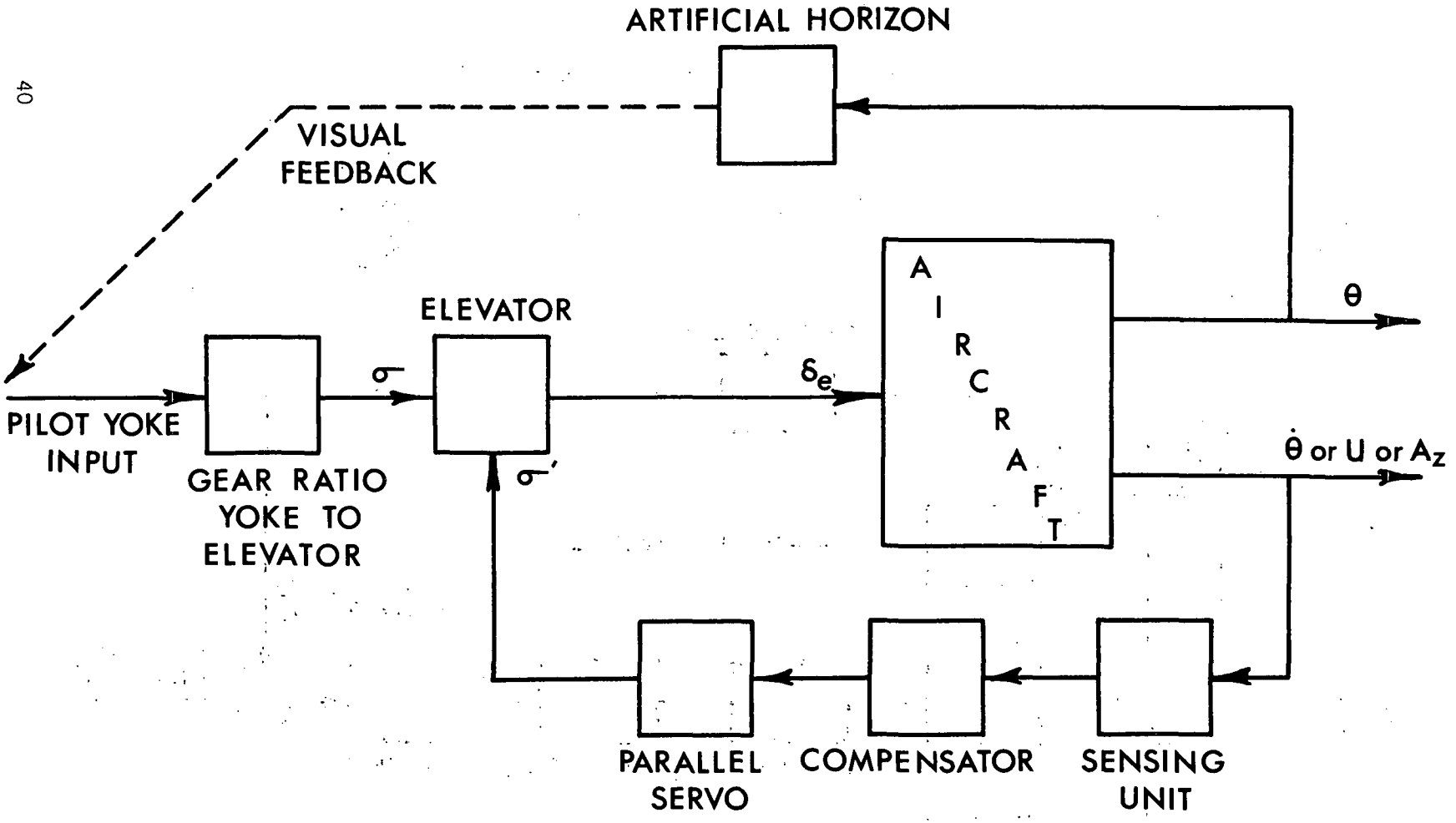

Figure 6. Typical pitch autopilot.

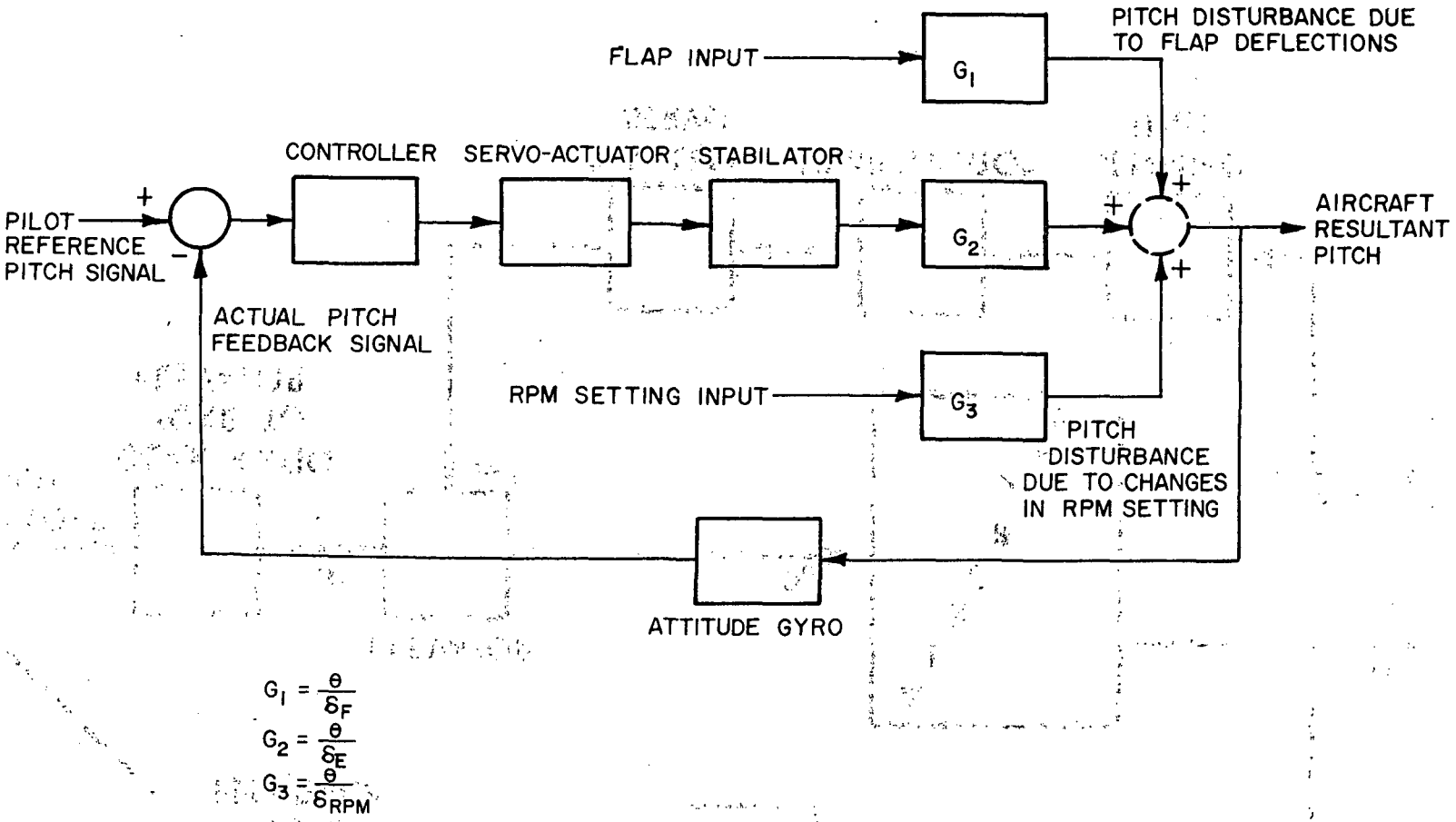

Figure 7. Fuselage leveller subsystem.

TABLE 7. AIRCRAFT PITCH ANGLE STEADY STATE CHARACTERISTICS

	Steady State pitch angle due to a one degree step			Maximum overshoot during transient Percent of Steady State value	
FC	Flap	Elevator	δ_E/δ_F	Flap	Elevator
1	- .867 deg.	13.480 deg.	.064	26.5%	55%
2	-1.900 deg.	12.600 deg.	.151	55.5%	79%
3	- .760 deg.	6.120 deg.	.124	8.0%	134%
4	-2.500 deg.	13.000 deg.	.192	147.0%	135%
5	-2.687 deg.	8.830 deg.	.305	106.0%	131%
6	-2.140 deg.	6.966 deg.	.307	37.5%	48%

The components of the subsystem in the forward loop are the controller, the servo actuator package, the control surface (stabilator), and the aircraft. The feedback loop consists of an attitude gyro. The disturbance channel is represented by the aircraft response to flap deflections.

The subsystem works as follows: A disturbance in pitch due to flap deflection (it is assumed that this is the major contribution to pitch disturbances) is sensed by the attitude gyro, which generates a voltage proportional to the amount of pitch deviation. This signal is subtracted from the input ($r = 0$) and the resultant error signal goes into the controller network where it is modified and shaped into a command signal to the servo actuator. The servo actuator deflects the stabilator to restore the attitude of the aircraft to its pre-disturbance value.

The design procedure can be outlined from Figure 7 as follows:

i) Determination of the plant dynamics and simplifications of the conceptual model based on evaluation of the aircraft dynamic responses.

ii) Closed loop subsystem specifications.

iii) Identification of the fixed components of the feedback subsystem.

iv) Determination of the controller transfer function by means of the root locus technique.

v) Investigation of the closed loop responses vs time at various points in the sybsystem for different type inputs.

vi) Comparison of these responses with the subsystem specifications.

System Equations of Motion

The steady state capability of the elevator to trim out the resultant pitch due to flap deflections is clearly established from Table 7. It remains to be seen whether or not the transient behavior of the aircraft is acceptable.

In order to analyze the longitudinal dynamics of the aircraft, the equations of motion must be first obtained. These equations are derived by applying Newton's laws of motion which relate the summation of the external forces and moments to the linear and angular accelerations of the aircraft. See for example McRuer et al. (Ref. 31). The linearized, decoupled, small perturbation, longitudinal equations of motion referred to stability axes in the Laplace domain are:

$$(s-X_u)\,u(s) - (sX_{\dot{w}}+X_w)w(s) - (sX_q-g)\theta(s) = X_{\delta_E}\,\delta_E(s) + X_{\delta_F}\,\delta_F(s) + T_{\delta_{RPM}}\,\delta_{RPM}(s)\cos\rho$$

$$-(z_u)\,u(s) + [s(1-z_{\dot{w}}) - z_w]w(s) - s(u_o+z_q)\,\theta(s) = z_{\delta_E}\,\delta_E(s) + z_{\delta_F}\,\delta_F(s) + T_{\delta_{RPM}}\sin\rho\,\delta_{RPM}(s)$$

$$-(M_u)\,u(s) - (sM_{\dot{w}}+M_w)w(s) + (s^2-M_q s)\,\theta(s) = M_{\delta_E}\,\delta_E(s) + M_{\delta_F}\,\delta_F(s) + T_{\delta_{RPM}}\,z_j\,\delta_{RPM}(s)$$

The notation used in these equations and throughout this work is that of McRuer et al. (Ref. 31).

The transfer functions of interest are those relating pitch angle θ to the control surface deflections δ_E, δ_F, and δ_{RPM}. These are obtained by applying Cramer's rule to this system of equations. They are

$$\frac{\theta}{\delta_E}(s) = \frac{(A_{\theta_E} s^2 + B_{\theta_E} + C_{\theta_E})}{\Delta(s)}$$

$$\frac{\theta}{\delta_F}(s) = \frac{(A_{\theta_F} s^2 + B_{\theta_F} s + C_{\theta_F})}{\Delta(s)} \qquad (1)$$

$$\frac{\theta}{\delta_{RPM}}(s) = \frac{(A_{\theta_{RPM}} s^2 + B_{\theta_{RPM}} s + C_{\theta_{RPM}})}{\Delta(s)}$$

where $\Delta(s)$ = longitudinal characteristic equation of the aircraft.

$$= (As^4 + Bs^3 + Cs^2 + Ds + E)$$

The coefficients of the polynomials making up these transfer functions are dependent on geometric parameters, airspeed, and non-dimensional stability derivatives. These coefficients were evaluated for representative conditions in the flight profile of the aircraft. These conditions are: light-weight (1) cruise, (2) climb, and (3) land; and heavy-weight (4) cruise, (5) climb, and (6) land. Appendices D and E list the required information to compute the coefficients of these transfer functions as well as the values of these coefficients for the unmodified and modified aircrafts respectively.

Substitution of these values for the light weight landing condition (FC#3) yields

Unmodified Aircraft

$$\frac{\theta}{\delta_E}(s) = \frac{12.3\ (s + 1.62)(s + .60)}{\Delta_3(s)}$$

$$\frac{\theta}{\delta_F}(s) = \frac{-\ 1.41\ (s - .22)(s + .18)}{\Delta_3(s)} \qquad (2)$$

$$\frac{\theta}{\delta_{RPM}}(s) = \frac{-\ .005\ (s + .6)(s + 8.44)}{\Delta_3(s)}$$

$$\Delta_3(s) = [(s + .269)^2 + (.434)^2][(s + 2.576)^2 + (3.73)^2]$$

Modified Aircraft

$$\frac{\theta}{\delta_E}(s) = \frac{17.5\ (s + 1.67)(s + .58)}{\Delta_3(s)}$$

$$\frac{\theta}{\delta_F}(s) = \frac{-\ 4.34\ [(s + .4)^2 + (.57)^2]}{\Delta_3(s)} \qquad (3)$$

$$\frac{\theta}{\delta_{RPM}}(s) = \frac{-\ .003\ [(s + .54)(s + 4.27)]}{\Delta_3(s)}$$

$$\Delta_3(s) = [(s + .241)^2 + (.356)^2][(s + 3.195)^2 + (2.197)^2].$$

The transfer functions for the other five flight conditions are obtained by substituting the values of the coefficients listed in Appendices D and E into the equations of set (1).

A step response test shows the behavior of the aircraft in pitch angle due to elevator and flap deflections and to changes in engine RPM. These transient responses were evaluated by a digital computer program which is based on the method of residues. Figures 8, 9, and 10 show the responses of the unmodified and modified aircrafts to elevator and flap deflections and to engine RPM change respectively. It is seen that in general the geometric modifications have improved the dynamics of the short period mode while the phugoid mode remains virtually unchanged. It is also seen that the elevator and flap power have increased substantially due to the geometric changes as evidenced by the difference in steady state value of the responses for the two aircrafts. While the dynamic improvement is advantageous for the design goal, the increased elevator and flap power is detrimental since it requires a more accurate positioning of the elevator for a given flap deflection.

Examination of these responses shows that the effect on pitch angle of a one degree step in flap deflection is many times more significant than a 50 RPM step change of the engine operating point. This has also been established by comparison of the Bode Plots of the transfer junctions $\frac{\theta}{\delta_E}$, $\frac{\theta}{\delta_F}$ and $\frac{\theta}{\delta_{RPM}}$. The small effect of changes in engine RPM on the total pitch angle of the aircraft can be explained physically as follows: For this aircraft the angle and distance between the thrust line and the x body axis are rather small, hence the resultant x and z-axis directed forces and the moment about the y-axis which are dependent on these two parameters are relatively small.

Based on these considerations, the conceptual block diagram of Figure (7) can be simplified by assuming that the only internal disturbance is that due to flap deflection. Since the objective of the subsystem is to counteract pitch angle deviations due to flap deflections with θ_{ref} set equal to zero degree, it is advantageous to modify the block diagram to show the flap deflection as a primary input. Thus, by means of block diagram algebra, the diagram shown in Figure 11 results.

where $G_1 = \theta/\delta_F$ $\quad G_2 = \theta/\delta_E$

G_{gyro} = transfer function of the gyroscopic device volts/degree

G_c = transfer function of the compensator volts/volts

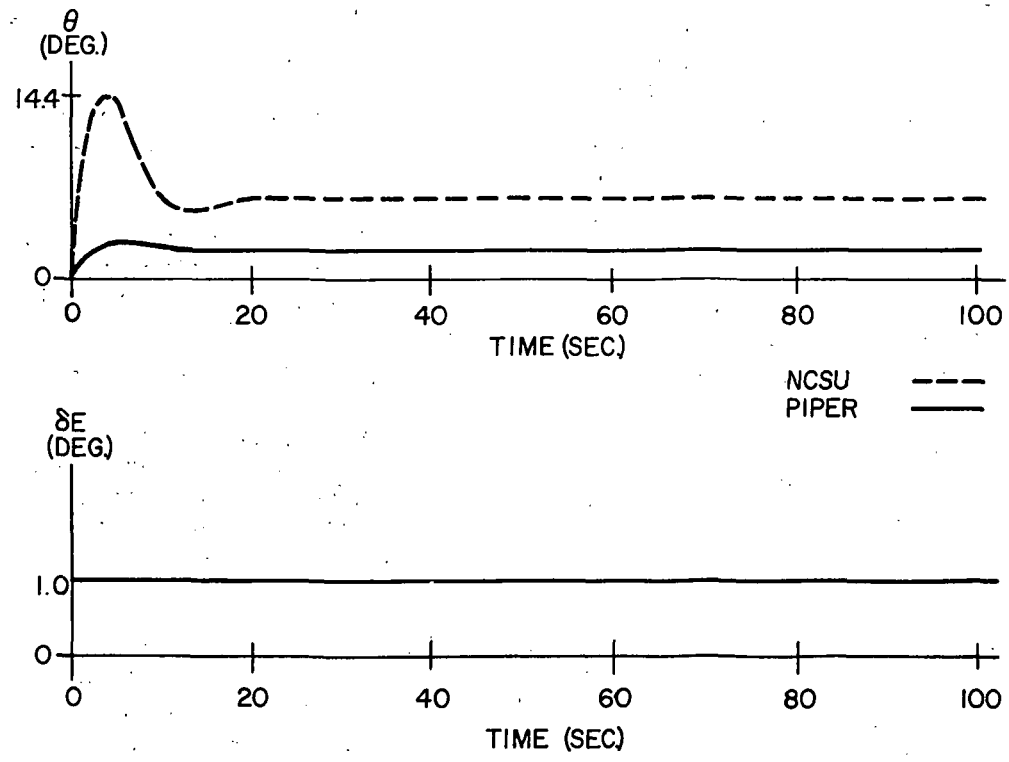

Figure 8. Pitch angle vs. time for a unit step in elevator deflection.

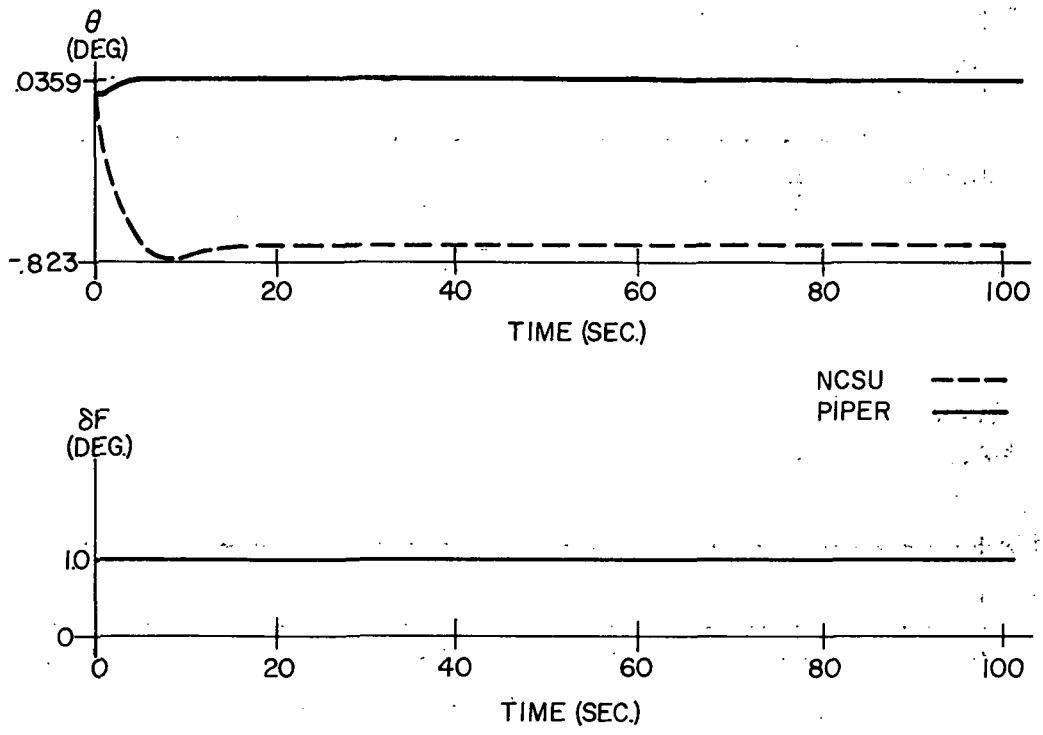

Figure 9. Pitch angle vs. time for a unit step in flap deflection.

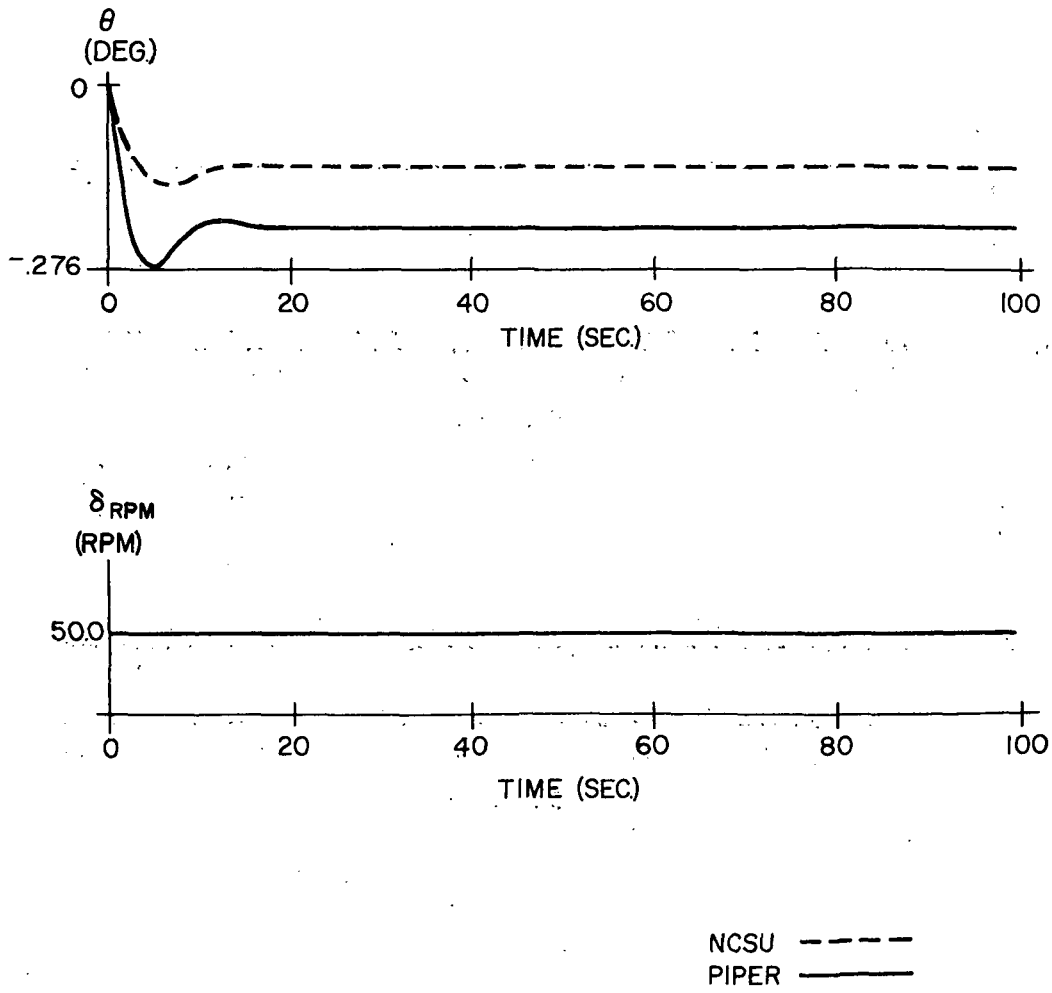

Figure 10. Pitch angle vs. time for a unit step in engine speed.

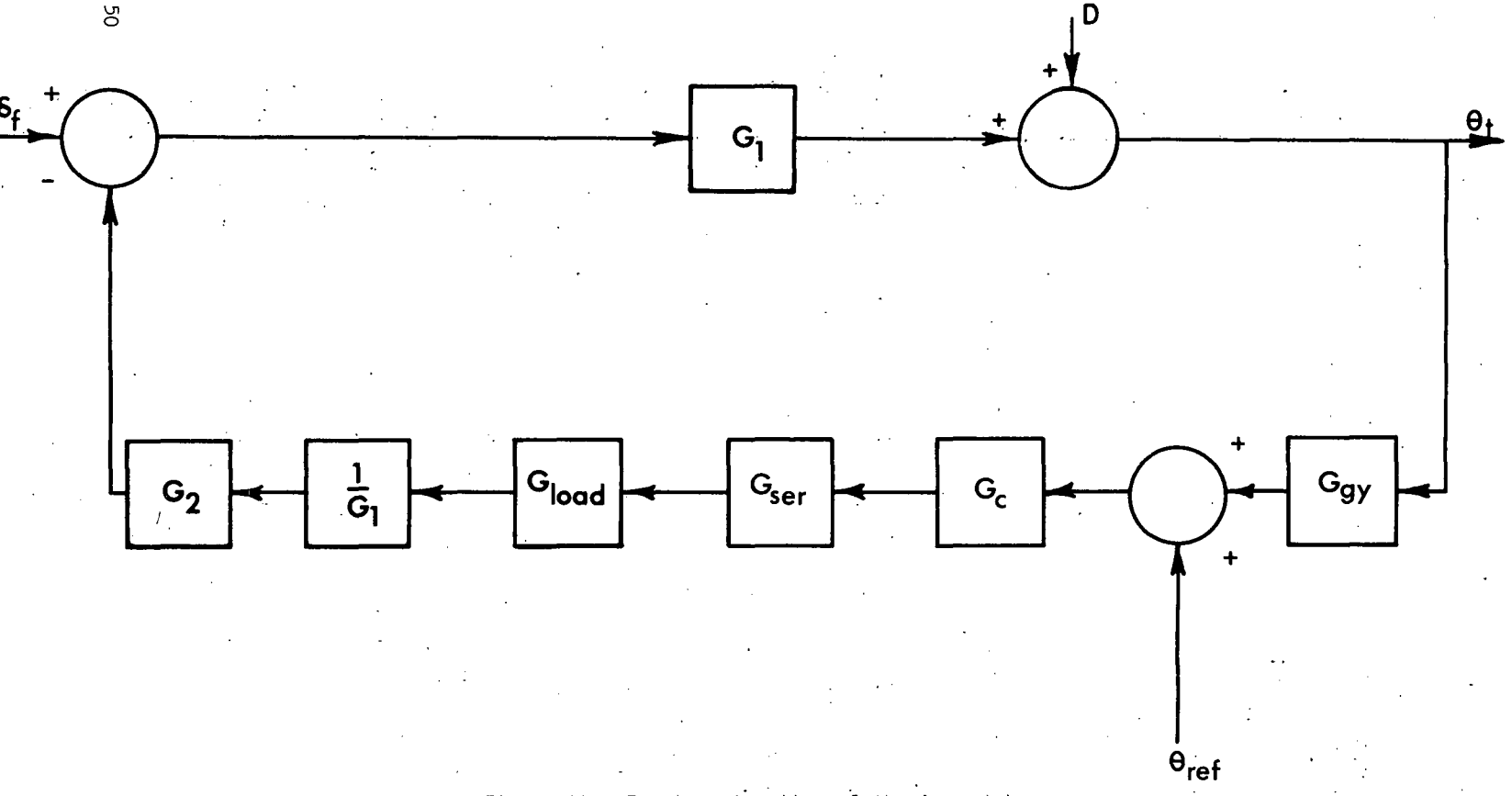

Figure 11. Fuselage leveller synthesis model.

G_{ser} = transfer function of the elevator actuator deg/volts

G_{load} = transfer function of the elevator deg/deg

Closed Loop Performance Specification

It is important to realize that the subsystem depicted in Figure 11 can behave as a regulator and a servomechanism. In the present design, the subsystem is intended to behave as a regulator; however, the pilot, with his capability of changing the reference value, can make the subsystem behave as a servomechanism. The subsystem will be designed as a regulator and the resultant configuration will then be evaluated for servomechanism behavior. Based on these considerations the following specifications are set

i) Final value of pitch angle to be within $\pm$ .5° of the set reference value.

ii) This value must be achieved in five seconds or less.

It would seem from these specifications that no restriction is placed on the amplitude of the subsystem transient response. However one can set a bound on this amplitude by referring to Figure 11 and considering the effect of a flap deflection as a command rather than as a 'disturbance'. A unit step in flap deflection with the subsystem inoperational would cause a steady state pitch angle as listed in Table 7; for the light weight landing condition (FC #3) this value is -.760 degrees of pitch per degree of flap. This flight condition is chosen as the basis for design because it is during this phase that the largest flap increment - 30 degrees - may be required and this deflection would cause a steady state pitch angle of - 22.2 degrees. In addition, examination of Figure 4a shows that this transient response exhibits a maximum overshoot of 8% of the steady state value and hence the aircraft would theoretically pitch approximately - 24 degrees in the process of settling down to the steady state value given above.

It is clear that with the subsystem operational this large transient pitch angle due to flap deflection will not occur since the resultant elevator deflection will counteract this resultant pitch angle. The airplane will have a transient behavior which will depend on the characteristic equation of the closed loop subsystem. This should have transient modes well damped so that the following specification is met

iii) For a worse case flap deflection (30 degrees) the maximum transient pitch angle should be less than - 30 degrees.

These are then the specialized specifications for the Fuselage Leveler Control subsystem.

Determination of the Characteristics of the Fixed Elements of the Subsystem

Examination of Figure II indicates that several components of the subsystem can be specified on a nominal basis prior to the synthesis phase. These are: the gyroscopic sensor, the comparator element, and the elevator actuator package. Two types of specifications must be made for these components; one static and one dynamic. The first type depends on the performance requirements at different points in the control subsystem loop; e.g., elevator actuator rate and position accuracy, gyro sensitivity and range, et al.; the second type depends on the relationship of the individual component dynamic response to that specified for the overall subsystem. The components specified thusly are then compared with the characteristics of available hardware. If these are not compatible, then the feasibility of a new design must be investigated.

The theory of operation and the representation of the hardware follows standard practice found in the literature and consequently they will not be discussed here. See for example Muzzey and Kidd (Ref. 38), Gibson and Tutuer (Ref. 39), Blakelock (Ref. 10).

The gyroscopic sensor is a stabilized vertical gyro with its rotor axis aligned with the positive y-axis of the aircraft. This device will put out, through a suitable pickoff, a voltage proportional to the aircraft pitch angle. The static specifications are:

i) Threshold = $.05^{\circ}$. This figure is based on 10% of the static accuracy of the closed loop subsystem.

ii) Range = $\pm 30^{\circ}$.

iii) Sensitivity = 1 volt/degree (nominal)

The dynamic specifications are:

iv) Erection system time constant less than 10% of subsystem time constant ($\leq .2$ sec).

v) Gyro transfer function representable as a pure gain device given by its sensitivity.

The comparator element is a simple operational amplifier with a nominal gain of unity and no significant dynamic characteristics relative to the rest of the system.

The elevator actuator package consists of a power amplifier supplying a reversible, field-controlled dc motor which, through a ball screw coupling, positions the elevator. The static specifications are:

vi) Position accuracy $\leq .04^{o}$.

vii) Actuation rate = 3.4 deg/sec.

The dynamic specification is that the actuator be representable by the following transfer function

$$\frac{\delta_E}{V_m}(s) = \frac{50}{(s + 50)} \tag{4}$$

where δ_E = elevator deflection and V_m = voltage input to the motor. This dynamic behavior is required to minimize the lag that is present between the application of a flap deflection and the reaction of the elevator. In general, a servoactuator is at least a second order system; but if properly compensated, it can be represented as a pure gain multiplied by a first order time lag for the operational frequencies of the aircraft. The additional degree of complication encountered in adjusting a servo to behave as desired above depends on the variations of the driven load with flight conditions and the required closed loop dc gain. Smetana, et al. (Ref. 13) provides a design example of such a system.

Controller Design

The simplest control law considered in the synthesis of the subsystem was the introduction of a controller with a transfer function given by a pure gain, i.e.,

$$G_c(s) = K_c \text{ (volts/volt)} \tag{5}$$

Physically this approach is based on the fact that a large value of feedback gain tends to decrease the magnitude of the closed loop transfer function. Note that while this approach may satisfy specification (i), the resultant dynamics may not be compatible with specifications (ii) and (iii).

The subsystem for this approach is that depicted in Figure II with the following component transfer functions

K_{AG} = 1 volt/degree

$G_c(s) = K_c$ volts/volt

$$G_{ser}(s) = \frac{50}{(s + 50)} \text{ degrees/volt}$$

$$G_1(s) = \frac{\theta}{\delta_F}(s) \text{ degree/degree}$$

$$G_2(s) = \frac{\theta}{\delta_E}(s) \text{ degree/degree.}$$

The closed loop transfer function can be written as

$$\frac{\theta_T}{\delta_F}(s) = \frac{G_1(s)}{1 + G_1(s)[\text{Gain} \cdot \frac{1}{(s + 50)} \cdot \frac{G_2(s)}{G_1(s)}]} \tag{6}$$

$$= \frac{G_1(s)}{1 + \text{Gain} \cdot [\frac{1}{(s + 50)} \cdot G_2(s)]} \tag{7}$$

where $\text{Gain} = K_c K_{AG} K_\sigma$.
The characteristic equation is given by

$$1 + \text{Gain} \cdot [\frac{1}{(s + 50)} \cdot G_2(s)] = 0 \tag{8}$$

A root locus diagram based on this equation is shown in Figure 12 for flight condition 3. This diagram shows how the subsystem poles seek the open loop zeroes as the gain is increased. From a dynamic point of view, in this subsystem gain is increased to improve the damping of the complex subsystem modes; since damping varies inversely with the angle between the line joining the origin of the s-plane with the complex roots and the negative real axis of the s-plane, it is seen that while the phugoid mode damping is improved, the short period mode damping deteriorates. Finally the subsystem becomes unstable at a gain value of 700. As indicated in the figure, the optimum gain value is 66 and the corresponding closed loop transfer function is

$$\frac{\theta_T}{\delta_F}(s) = \frac{-(4.34s^2 + 3.47s + 2.1)(s + 50)}{(s + .88s)(s + .905)[(s + 2.3)^2 + (5.03)^2](s + 50.5)} \tag{9}$$

and for this gain value $K_c = \frac{66}{50} = 1.32$ volts/degree.

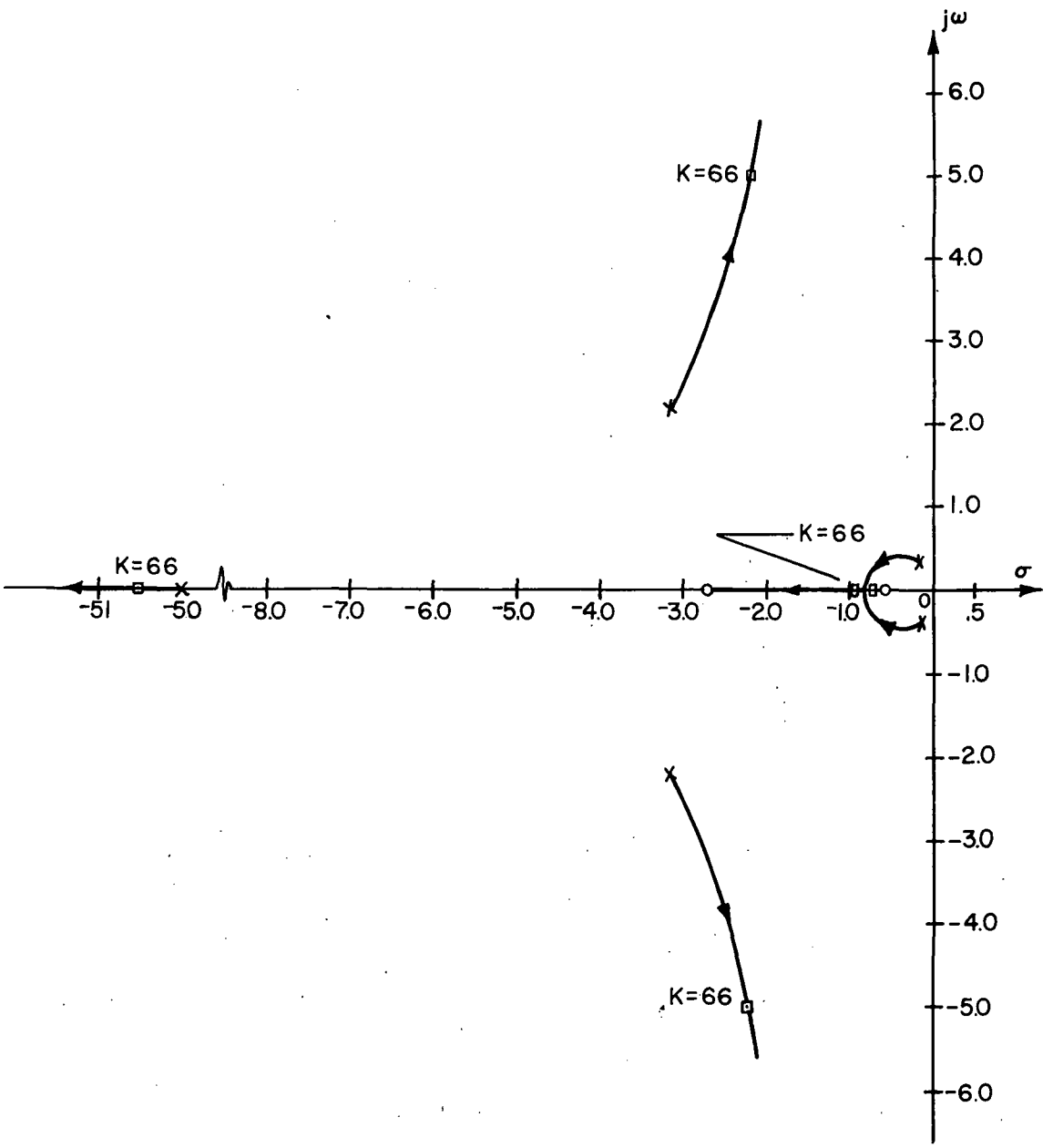

Figure 12. Root locus for gain compensator.

The most common criterion to show the physical limitations of a feedback control system is the relationship between the manipulated variable and the command input. In this case this requires the development of the transfer function relating elevator to flap deflection. From Figure 11 one gets

$$\frac{\delta_E}{\delta_F}(s) = \frac{G_1(s)\left(K_{AG}\, K_c \frac{K_\sigma}{(s+50)}\right)}{1 + \left[G_1(s)\, K_{AG}\, K_c \frac{K_\sigma}{(s+50)}\right]\left[\frac{G_2(s)}{G_1(s)}\right]} \tag{10}$$

$$= \frac{\text{Gain}\left(G_1(s)\, \frac{1}{(s+50)}\right)}{1 + \text{Gain}\left(\frac{1}{(s+50)}\, G_2(s)\right)} \tag{11}$$

For the value of gain given above this becomes

$$\frac{\delta_E}{\delta_F}(s) = \frac{-66\,(4.34s^2 + 3.47s + 2.1)}{(s+.885)(s+.905)[(s+2.3)^2 + (5.03)^2](s+50.5)} \tag{12}$$

The time responses of the aircraft in pitch angle and elevator deflection for a unit step input in flap deflection were evaluated by taking the inverse Laplace transform of equations (9) and (12) respectively. The results are shown in Figure 13. Time responses for the other five flight conditions with the same value of gain were evaluated and the results summarized in Table 8.

The time responses for pitch angle show that the pure gain controller approach is not acceptable because the steady state deviations from the reference value range from -.084 degree (Figure 13) to -.215 degree in the worst case. This is for a one degree flap deflection disturbance. Since the subsystem is linear, it is reasonable to expect that a 30 degree flap deflection will cause a steady state deviation ranging from - 2.4 degrees to - 6.3 degrees and this violates the maximum steady state pitch angle deviation specification. The settling time specification is met for the case shown in Figure 13 (T_s = 5.0 seconds) but it is unacceptable in other flight conditions (T_s = 10.0 seconds). The only specification that is met is that of maximum allowable transient pitch angle. This ranges from - .09 degrees (Figure 13) to - .232 in the worst case. Linear extrapolation for the 30 degree flap input shows that this parameter is within the bound specified.

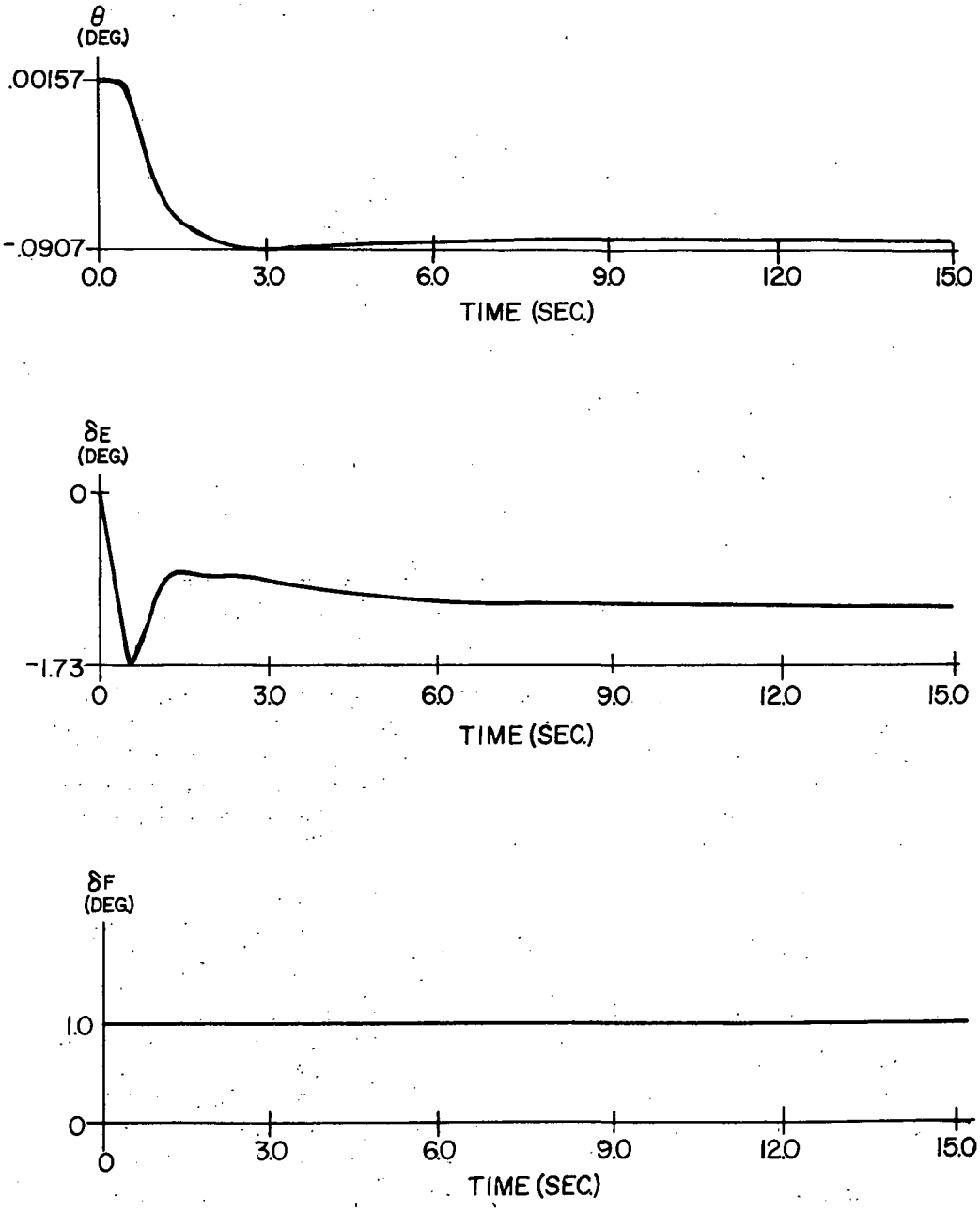

Figure 13. Aircraft pitch angle and elevator deflection vs. time for a one degree step in flap deflection in the pure gain compensator.

TABLE 8. SUMMARY OF PITCH ANGLE AND ELEVATOR TIME RESPONSE CHARACTERISTICS FOR THE FUSELAGE LEVELER WITH A PURE GAIN COMPENSATOR

FC	Gain	Subsystem Poles	$\theta_{T_{MAX}}$	$\theta_{T_{ss}}$	$\delta_{E_{MAX}}$	$\delta_{E_{ss}}$	δ_F
1	66	$(-.176 + j\,0.0)(-2.00 + j\,0.0)(-51.72 + j\,0.0)(-3.40 \pm j\,9.762)$	-.084	-.084	-.112	-.112	1°
2	66	$(-.170 + j\,0.0)(-2.47 + j\,0.0)(-51.56 + j\,0.0)(-3.76 \pm j\,8.71)$	-.110	-.110	-.146	-.146	1°
3	66	$(-.885 + j\,0.0)(-.905 + j\,0.0)(-50.48 + j\,0.0)(-2.3 \pm j\,5.03)$	-.090	-.080	-.112	-.112	1°
4	66	$(-.082 + j\,0.0)(-1.632 + j\,0.0)(-52.0 + j\,0.0)(-2.86 \pm j\,9.96)$	-.157	-.157	-.300	-.300	1°
5	66	$(-.163 + j\,0.0)(-1.50 + j\,0.0)(-.50.84 + j\,0.0)(-2.40 \pm j\,5.95)$	-.215	-.215	-.283	-.283	1°
6	66	$(-.545 + j\,0.0)(-.824 + j\,0.0)(-50.41 + j\,0.0)(-1.76 \pm j\,4.21)$	-.232	-.211	-.320	-.280	1°

$\theta_{T_{MAX}}$ = Maximum pitch angle during transient

$\theta_{T_{ss}}$ = Steady state pitch angle

$\delta_{E_{MAX}}$ = Maximum elevator deflection during transient

$\delta_{E_{ss}}$ = Steady state elevator deflection

It is important to note that further increase in gain would reduce the steady state deviation value but it would worsen the dynamic behavior since this is mostly due to the damping of the short period mode and the characteristics of this mode deteriorate with increased system gain.

The time responses of the elevator are within the physical limitations of the aircraft with nearly first order dynamic behavior. The steady state value ranges from - .112 degree (Figure 13) to - .32 degree in the worst case. The maximum elevator deflection during transient ranges from - .112 degree (Figure 13) to - .320 is the worst case. Linear extrapolation for the 30 degree flap deflection case shows that these parameters are within the 18 degree deflection capability of the elevator.

Lag Compensator Approach

The root locus of Figure 12 shows that the reason for the rapid migration of the short period roots towards the right of the s-plane with increase in gain is due to the presence of one of the open loop zeroes close to the origin. This zero location, which is contributed by the transfer function θ/δ_E, ranges from - .58 at the light weight landing condition to - .076 at the heavy-weight cruise condition. If a first order lag network is introduced as a compensator with a zero-pole ratio of 10:1 and with its pole and zero located at appropriate places on the s-plane, one can effectively retard the undesirable migration of the short period roots with the additional advantage that the phugoid roots migrate further into the left hand plane than in the pure gain case.

The subsystem block diagram for this approach is similar to the one shown in Figure 11 with the controller given by

$$G_c(s) = K_c \frac{(s + 10\ a)}{(s + a)} . \qquad (13)$$

The value of a is chosen to coincide with the innermost zero of the open loop transfer function for the design flight condition, i.e., the light-weight, landing condition. This value is a = .58 and hence the controller transfer function is

$$G_c(s) = K_c \frac{(s + 5.8)}{(s + 0.58)} . \qquad (14)$$

It should be noted that this is not a zero cancellation scheme in the general sense. In order to have zero cancellation, it is required to have an adaptive controller so that its pole coincides

with the zero of the open loop transfer function for all flight conditions. It is not the purpose of this design to introduce such a controller; rather the proposed compensator given by equation (14) will be tested for all flight conditions as the gain is increased.

The closed loop transfer function with this compensator can be written as

$$\frac{\theta_T}{\delta_F}(s) = \frac{G_1(s)}{1 + G_1(s)\left[K_{AG} \cdot \frac{K_c(s+5.8)}{(s+.58)} \cdot \frac{K_\sigma}{(s+50)} \cdot \frac{G_2(s)}{G_1(s)}\right]} \tag{15}$$

$$= \frac{G_1(s)}{1 + \text{Gain}\left[\frac{(s+5.8)}{(s+.58)} \cdot \frac{1}{(s+50)} \cdot G_2(s)\right]} \tag{16}$$

where $\text{Gain} = K_c K_{AG} K_\sigma$.

The characteristic equation is given by

$$1 + \text{Gain}\left[\frac{(s+5.8)}{(s+.58)} \cdot \frac{1}{(s+50)} \cdot G_2(s)\right] = 0. \tag{17}$$

A root locus diagram based on this equation is shown in Figure 14. As indicated, the optimal value of gain is 52 and the value for which the system becomes unstable is 82. The root loci for all other flight conditions were analyzed and it was found that flight condition 6 - the heavy weight landing condition - was unstable at the optimal value of gain mentioned above. The marginal stability gain for this flight condition is 26. Hence a gain of 24 was chosen. For this value the closed loop transfer function becomes

$$\frac{\theta_T}{\delta_F}(s) = \frac{-(4.34s^2 + 3.47s + 2.1)(s+50)(s+.58)}{(s+.58)(s+50.16)[(s+2.72)^2+(.48)^2][(s+.63)^2+(3.21)^2]} \tag{18}$$

and $K_c = \frac{\text{Gain}}{K_{AG} K_\sigma} = \frac{24}{50} = .480$ volts/volt. Note that this requires the use of an attenuator in conjunction with the compensator.

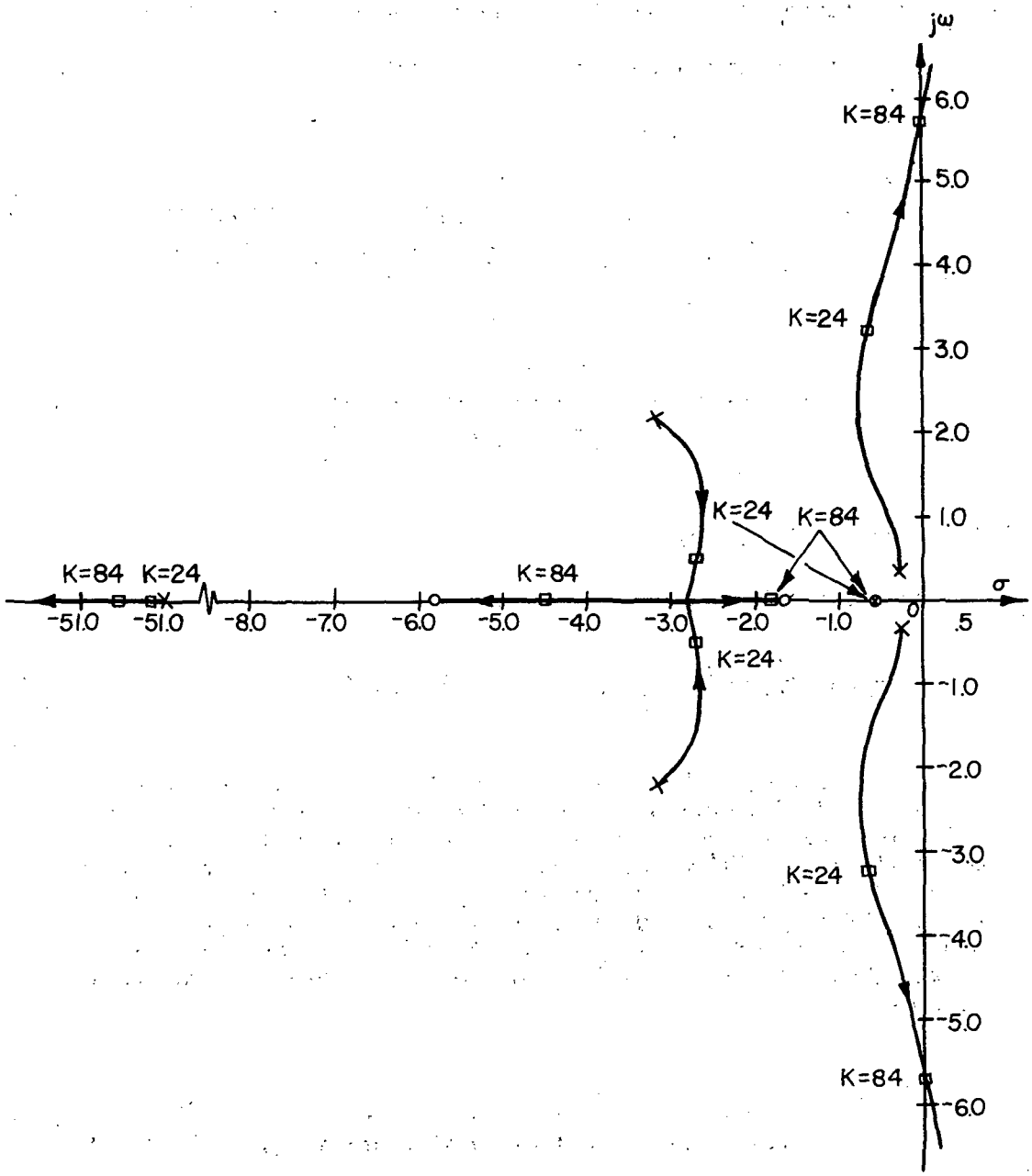

Figure 14. Root locus for lag compensator.

The transfer function δ_E/δ_F for the subsystem with the lag compensator becomes

$$\frac{\delta_E}{\delta_F}(s) = \frac{G_1(s) \cdot \left(K_{AG} \frac{K_c(s+5.8)}{(s+.58)} \cdot \frac{K_\sigma}{(s+50)}\right)}{1 + G_1(s) \cdot \left[K_{AG} \cdot \frac{K_c(s+5.8)}{(s+.58)} \cdot \frac{K_\sigma}{(s+50)} \cdot \frac{G_2(s)}{G_1(s)}\right]} \quad (19)$$

$$= \frac{\text{Gain} \cdot \left[G_1(s) \cdot \frac{(s+5.8)}{(s+.58)} \cdot \frac{1}{(s+50)}\right]}{1 + \text{Gain} \cdot \left[\frac{(s+5.8)}{(s+.58)} \cdot \frac{1}{(s+50)} \cdot G_2(s)\right]} \cdot \quad (20)$$

For the value of gain chosen above this becomes

$$\frac{\delta_E}{\delta_F}(s) = \frac{-24 \cdot [(4.34s^2 + 3.47s + 2.1)(s+5.8)}{(s+.58)(s+50.16)[(s+2.72)^2+(.48)^2][(s+.63)^2+(3.21)^2]} \quad (21)$$

The time responses of the pitch angle and the elevator of the aircraft were evaluated from equations (18) and (21) respectively. These are shown in Figure 15. Time responses for the other five flight conditions with the same compensator and value of the gain were evaluated and the results are summarized in Table 9.

Figure 15 shows that the pitch angle steady state deviation has been drastically reduced from that of the pure gain case. These deviations range from - .025 degree (Figure 15) to - .090 degree for the worse case condition. Extrapolation for a worse case flap deflection disturbance indicates that the steady state deviations would range from - .75 degree to - 2.7 degree. While this represents an improvement over the pure gain case, it does not meet the steady state deviation specification. The values for $\theta_{T_{MAX}}$ range from - .160 degree (Figure 15) to - .332 degree for the worse case condition. These are somewhat higher values than those obtained for the pure gain case but they meet the specification for the maximum allowable transient pitch angle. These increased values are due to the fact that, for the chosen subsystem gain, both the phugoid and short period modes are complex. The values for settling time range from 6 seconds (Figure 15) to 15 seconds in the worse case condition. This

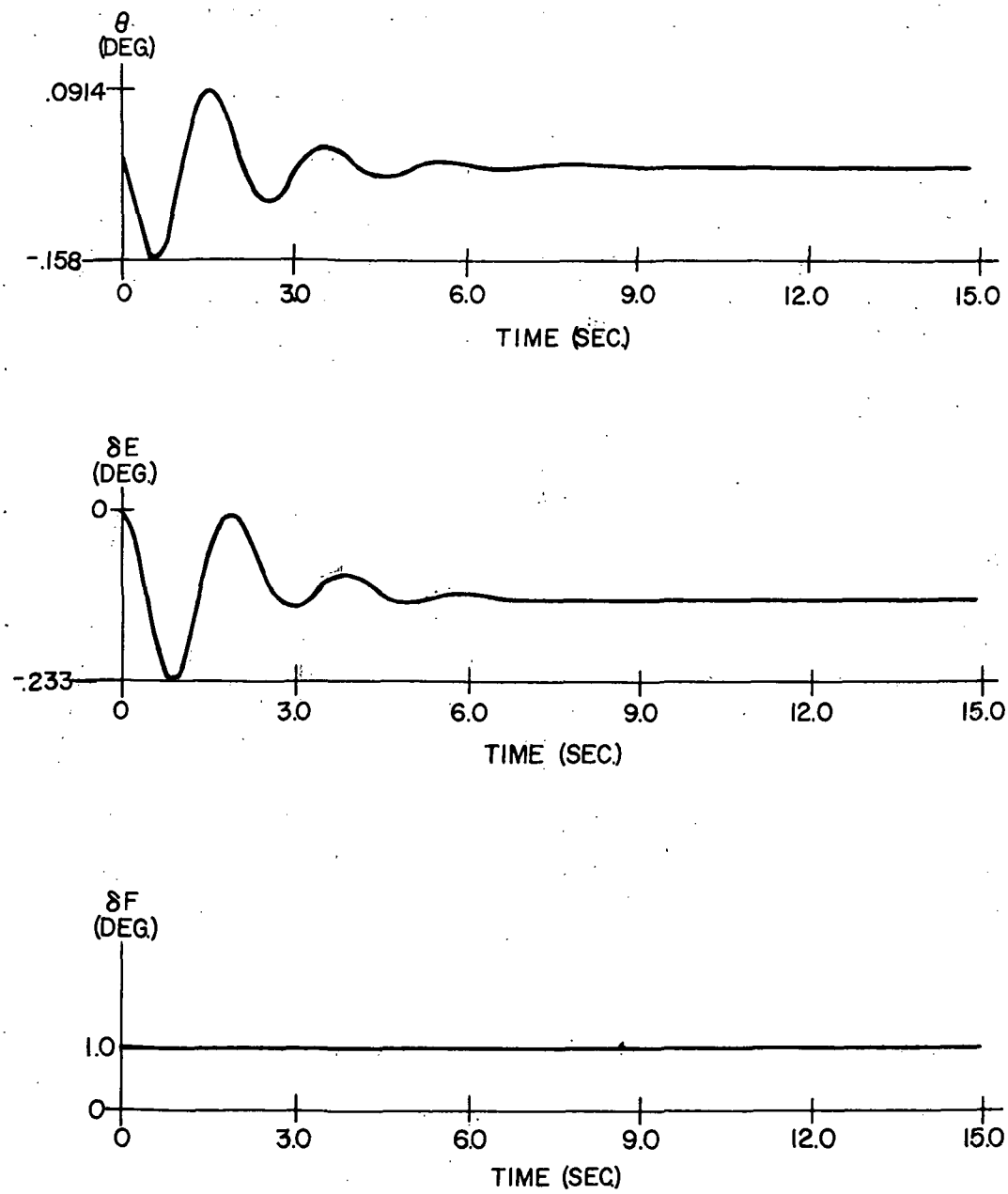

Figure 15. Aircraft pitch angle and elevator deflection vs. time for a one degree step in flap deflection in the lag compensator subsystem.

TABLE 9. SUMMARY OF PITCH ANGLE AND ELEVATOR TIME RESPONSE CHARACTERISTICS FOR THE FUSELAGE LEVELER WITH A LAG COMPENSATOR

FC	Gain	Subsystem Poles	$\theta_{T_{MAX}}$	$\theta_{T_{ss}}$	$\delta_{E_{MAX}}$	$\delta_{E_{ss}}$	δ_F
1	24	$(-.167+j0.0)(-50.60+j0.0)(-2.552\pm j2.29)(-2.705\pm j5.65)$	-.166	-.012	-.194	-.060	1°
2	24	$(-.164+j0.0)(-50.53+j0.0)(-4.00\pm j2.94)(-1.81\pm j4.05)$	-.185	-.030	-.242	-.143	1°
3	24	$(-.580+j0.0)(-50.16+j0.0)(-2.72\pm j.482)(-.631\pm j3.21)$	-.160	-.025	-.233	-.122	1°
4	24	$(-.078+j0.0)(-2.55+j0.0(-4.05+j0.0)(-50.7+j0.0)(-1.324\pm j5.93)$	-.177	-.041	-.375	-.200	1°
5	24	$(-.151+j0.0)(-1.70+j0.0)(-5.23+j0.0)(-50.28+j0.0)(-.256\pm j3.87)$	-.328	-.060	-.475	-.300	1°
6	24	$(-.44+j0.0)(-1.06+j0.0)(-4.10+j0.0)(-50.1+j0.0)(-.084\pm j2.83)$	-.332	-.090	-.580	-.385	1°

$\theta_{T_{MAX}}$ = Maximum pitch angle during transient

$\theta_{T_{ss}}$ = Steady State pitch angle

$\delta_{E_{MAX}}$ = Maximum elevator deflection during transient

$\delta_{E_{ss}}$ = Steady State elevator deflection

indicates a deterioration from the values obtained for the pure gain case and it is due to the suboptimal value of gain chosen as discussed above.

The time responses for the elevator have also deteriorated from those of the pure gain case but they are still within the physical limitations of the aircraft. In this case, $\delta_{E_{MAX}}$ and $\delta_{E_{ss}}$ range from - .233 degree and - .122 degree (Figure 15) to - .580 degree and - .385 degree for the worse case condition. This implies that a flap deflection of 30 degrees would cause these values to range from - 7 degree and - 3.66 degree to - 17.4 degree and - 11.55 degree.

Angle, Rate, and Acceleration Feedback Plus Lead Compensator Approach

At this juncture in the design, it became obvious that in order to obtain the specified settling time and dynamic response a way had to be found whereby the damping of the short period poles would be improved. This can be accomplished by feeding back rate and acceleration signals in addition to the position signal which had been used up to this point. For the subsystem under consideration, this is equivalent to placing a pair of zeroes on the negative real axis provided by a compensator of the form

$$G_c(s) = K_c \frac{(s+5.8)}{(s+.58)} (s+b)(s+c) \quad . \tag{22}$$

Examination of Figure 14 points out the need for both rate and acceleration feedback; rate feedback alone would create a zero on the negative real axis which, if located to the left of the outermost open loop transfer function zero, for example at - 7, would affect only the migration of the actuator pole. Rate plus acceleration feedback would create two zeroes on the negative real axis of the s-plane so that the open loop poles, after migrating due to the increase in system gain, would end up on or near the real axis. Several trial runs were made for different values of b and c and these were finally chosen as b = 7 and c = 8. The resultant compensator transfer function was

$$G_c(s) = \frac{K_c(s+5.8)}{(s+.58)} (s+7)(s+8) \quad . \tag{23}$$

The closed loop transfer function with the compensator given by equation (23) is derived from Figure 11 as

$$\frac{\theta_T}{\delta_F}(s) = \frac{G_1(s)}{1 + G_1(s)\cdot[K_{AG}\cdot(s+7)(s+8)\cdot\frac{K_c(s+5.8)}{(s+.58)}\cdot\frac{K_\sigma}{(s+50)}\cdot\frac{G_2(s)}{G_1(s)}]} \quad (24)$$

$$= \frac{G_1(s)}{1 + \text{Gain}\cdot[\frac{(s+7)(s+8)(s+5.8)}{(s+.58)}\cdot\frac{1}{(s+50)}\cdot G_2(s)]} \quad (25)$$

The characteristic equation is given by

$$1 + \text{Gain}\cdot[\frac{(s+7)(s+8)(s+5.8)}{(s+.58)}\cdot\frac{1}{(s+50)}\cdot G_2(s)] = 0 \quad (26)$$

A root locus diagram based on this equation is shown in Figure 16. It can be seen that the system is stable for all values of gain and that the complex modes can be made overdamped for values of gain higher than 200. Because of the limitations imposed by this very high value of gain, it was decided to operate the system at a gain value of 52 as shown in the figure. At this point the subsystem closed loop transfer function is

$$\frac{\theta_T}{\delta_F}(s) = \frac{-(4.34s^2 + 3.47s + 2.10)(s+50)(s+.58)}{(s+.58)(s+1.67)(s+5.2)[(s+7.48)^2 + (2.01)^2](s+928.8)} \quad (27)$$

and $K_c = \text{Gain}/50 = \frac{52}{50} = 1.04$ volts/volt.

The transfer function δ_E/δ_F becomes

$$\frac{\delta_E}{\delta_F}(s) = \frac{G_1(s)\cdot(K_{AG}(s+8)(s+7)\cdot\frac{K_c(s+5.8)}{(s+.58)}\cdot\frac{K_\sigma}{(s+50)}}{1+G_1(s)\cdot[K_{AG}(s+8)(s+7)\frac{K_c(s+5.8)}{(s+.58)}\cdot\frac{K_\sigma}{(s+50)}]\cdot\frac{G_2(s)}{G_1(s)}} \quad (28)$$

$$= \frac{\text{Gain}\cdot[G_1(s)\cdot\frac{(s+8)(s+7)(s+5.8)}{(s+.58)(s+50)}]}{1+\text{Gain}\cdot[\frac{(s+8)(s+7)(s+5.8)}{(s+.58)(s+50)}\cdot G_2(s)]} \quad (29)$$

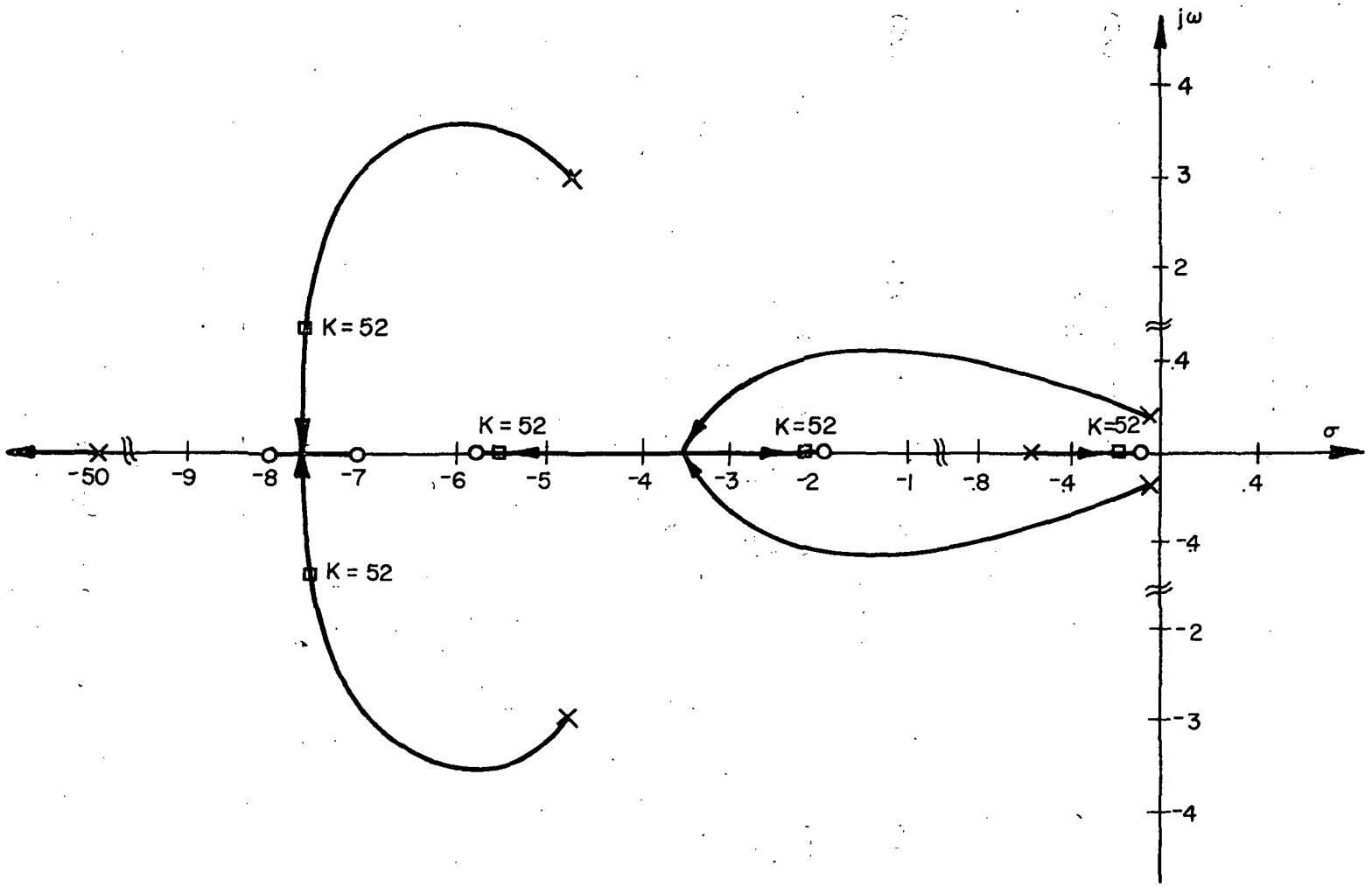

Figure 16. Root locus for lag plus double zero compensator.

For the value of gain chosen above this becomes

$$\frac{\delta_E}{\delta_F}(s) = \frac{-52\,[(4.34s^2 + 3.47s + 2.1)(s+8)(s+7)(s+5.8)]}{(s+.58)(s+1.67)(s+5.2)[(s+7.48)^2+(s.01)^2](s+928.8)} \quad (30)$$

The time responses of pitch angle and elevator deflection of the aircraft based on equations (27) and (30) are shown in Figure 17. The time responses for the other five flight conditions with the compensator given by equation (23) and the value of gain chosen above were evaluated and the results are summarized in Table 10. It can be seen from these figures that the three design specifications have been met. The steady state deviation ranges from - .0002 degree (Figure 17) to - .0005 degree in the worst case; the maximum pitch angle ranges from - .001 (Figure 17) to - .002 in the worse case; and the settling time is of the order of two to five seconds. Linear extrapolation for a 30 degree flap input indicates that $\theta_{T_{ss}}$ ranges from - .006 degree to - .015 degree and that $\theta_{T_{MAX}}$ ranges from - .03 degree to - .06 degree. A similar consideration of the required elevator deflection indicates that these are well within the capabilities of the aircraft; $\delta_{E_{MAX}}$ ranges from - .165 degree (Figure 17) to - .255 degree in the worst case and $\delta_{E_{ss}}$ ranges from - .088 degree (Figure 17) to - .212 in the worst case. Thus for a 30 degree flap deflection these parameters range from - 4.95 degrees to - 7.65 degrees and from - 2.64 degrees to - 6.36 degrees respectively.

Subsystem Responses for a Change in Reference Value

The subsystem, with the elements proposed in the last section, has been shown to perform well within the bounds established by the performance specifications. Its behavior due to a change in reference value remains to be investigated. The closed loop transfer function relating θ_T to θ_{ref} is obtained from Figure 7 as

$$\frac{\theta_T}{\theta_{ref}}(s) = \frac{G_c(s) \cdot \frac{K_\sigma}{(s+50)} \cdot G_2(s)}{1+G_c(s) \cdot \frac{K_\sigma}{(s+50)} \cdot G_2(s) \cdot K_{AG}(s+7)(s+8)} \quad . \quad (31)$$

Note that in order to develop this transfer function is necessary to set δ_F, δ_{RPM}, and external disturbances equal to zero.

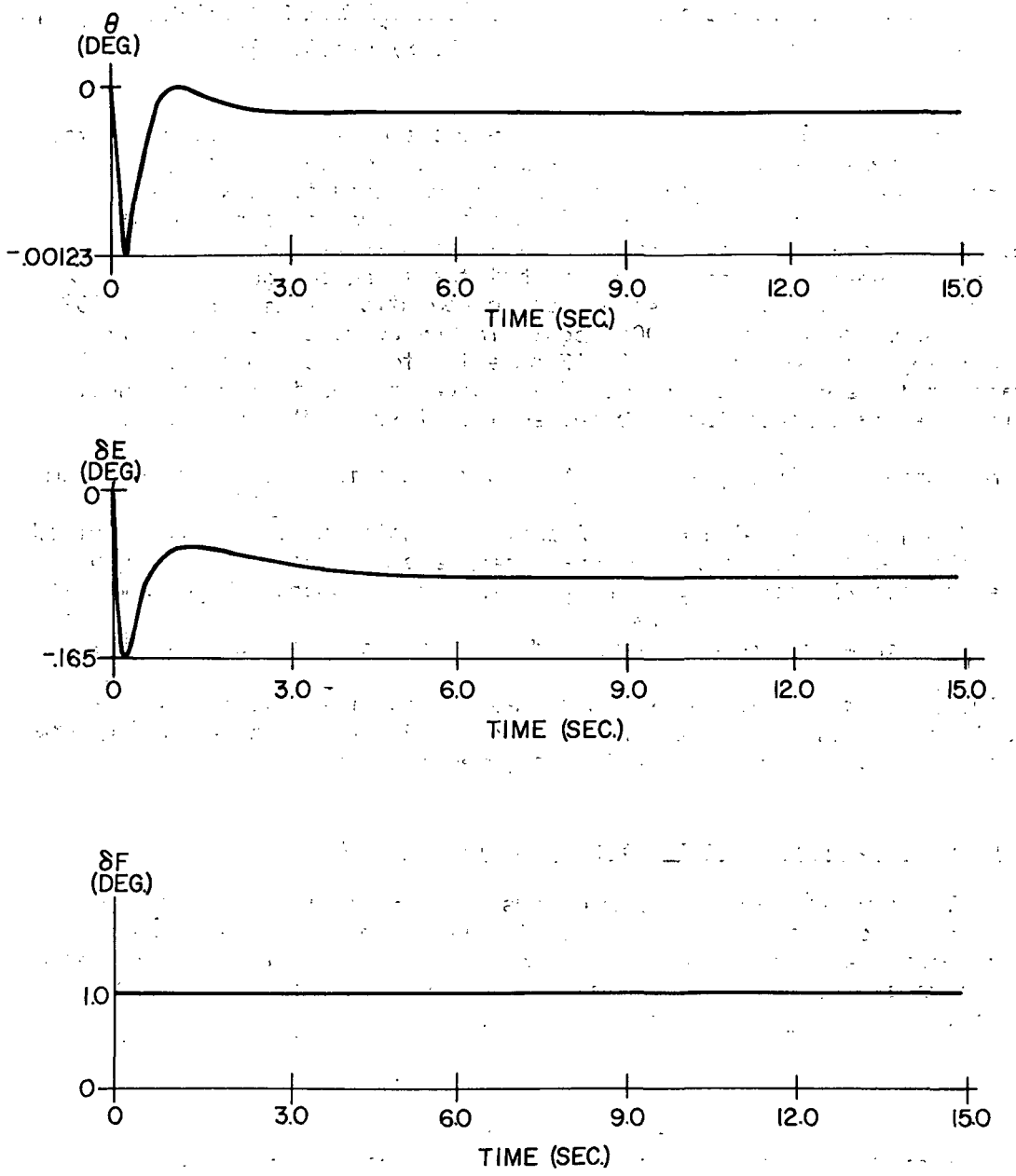

Figure 17. Aircraft pitch angle and elevator deflection vs. time for a one degree step in flap deflection in the lag plus double zero compensator system.

TABLE 10. SUMMARY OF PITCH ANGLE AND ELEVATOR TIME RESPONSE CHARACTERISTICS FOR THE FUSELAGE LEVELER WITH A LAG PLUS DOUBLE ZERO COMPENSATOR

FC	Gain	Subsystem Poles	$\theta_{T_{MAX}}$	$\theta_{T_{ss}}$	$\delta_{E_{MAX}}$	$\delta_{E_{ss}}$	δ_F
1	52	$(-.165+j0.0)(-2.820+j0.0)(-5.193+j0.0)(-7.708\pm j1.222)(-3173.97\pm j0.0)$	-.00013	-.00010	-.042	-.042	1°
2	52	$(-.160+j0.0)(-3.341+j0.0)(-5251+j0.0)(-7.655\pm j1.053)(-28.7.91+j0.0)$	-.00026	-.00026	-.106	-.106	1°
3	52	$(-.580+j0.0)(-1.674+j0.0)(-5.192+j0.0)(-7.490\pm 1.947)(-997.50+j0.0)$	-.001	-.0002	-.165	-.088	1°
4	52	$(-.076+j0.0)(-1.956+j0.0)(-5.54+j0.0)(-7.56\pm j.847)(-3734.07+j0.0)$	-.00038	-.00038	-.154	-.154	1°
5	52	$(-.148+j0.0)(-1.626+j0.0)(-5.625+j0.0(-7.405\pm j1.245)(-1578.45+j0.0)$	-.00053	-.00053	-.213	-.213	1°
6	52	$(-.432+j0.0)(-1.020+j0.0)(-5.260+j0.0)(-7.374\pm j2.160)(-794.02+j0.0)$	-.002	-.0005	-.255	-.212	1°

$\theta_{T_{MAX}}$ = Maximum pitch angle during transient

$\theta_{T_{ss}}$ = Steady State pitch angle

$\delta_{E_{MAX}}$ = Maximum elevator deflection during transient

$\delta_{E_{ss}}$ = Steady State elevator deflection

Simplification of this equation results in

$$\frac{\theta_T}{\theta_{ref}} = \frac{(\frac{1}{K_{AG}})(K_c\ K_\sigma\ K_{AG}) \cdot (\frac{(s+5.8)}{(s+.58)}) \cdot (\frac{1}{s+50}) \cdot G_2(s)}{1+\text{Gain}\ \frac{(s+5.8)}{(s+.58)} \cdot \frac{1}{(s+50)} \cdot G_2(s) \cdot (s+7)(s+8)} \quad . \tag{32}$$

It is important to note that the characteristic equation of this transfer function is the same as that given by equation (26). Accordingly for the value of gain chosen in the previous section equation (33) becomes

$$\frac{\theta_T}{\theta_{ref}}(s) = \frac{52[(s+5.8)(17.5s^2+39.4s+16.9)]}{(s+.58)(s+1.67)(s+5.2)[(s+7.48)^2+(2.01)^2](s+128.8)} \tag{33}$$

Similarly, the transfer function relating elevator deflection of θ_{ref} is

$$\frac{\delta_E}{\theta_{ref}}(s) = \frac{G_c(s)\ \frac{K_\sigma}{(s+50)}}{1+G_c(s)\ \frac{K_\sigma}{(s+50)} \cdot G_1(s) \cdot K_{AG} \cdot (s+7)(s+8)} \tag{34}$$

which for the value of gain chosen becomes

$$\frac{\delta_E}{\theta_{ref}}(s) = \frac{52[(s+5.8)(s^4+7.01s^3+18.67s^2+8.60s+2.84)]}{(s+.58)(s+1.67)(s+5.20)[(s+7.48)^2+(2.01)^2](s+928.8)} \cdot \tag{35}$$

The time responses of the pitch angle and elevator of the aircraft to a unit step change in pitch reference value are shown in Figure 18.

Although no specifications were set for this type of performance, it can be seen from these figures that the transition from one reference pitch value to another causes aircraft pitch angle and elevator

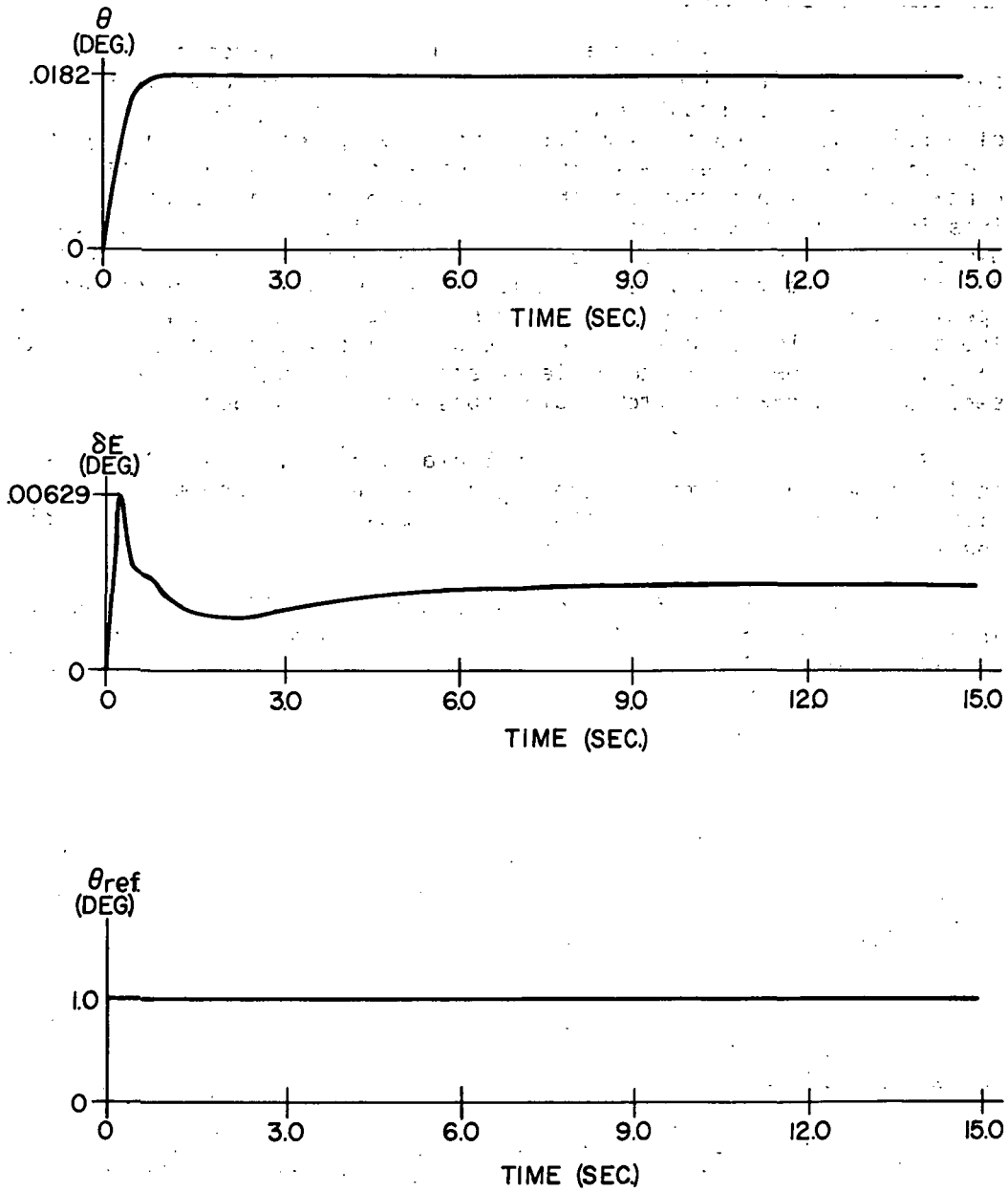

Figure 18. Total pitch angle and elevator deflection vs. time for a one degree step in reference pitch angle.

deflection responses which are well damped and within the physical limitations of the aircraft.*

Summary and Conclusions

This study has shown that the pitch angle attitude of a general aviation aircraft using flap deflections for lift modulation can be maintained at a constant reference value of zero degree by means of a relatively simple automatic control subsystem shown in Figure 19. The controller and feedback elements were derived based on the dynamics of the aircraft for the light-weight landing condition. This is the worst case condition insofar as flap deflection-pitch disturbance is concerned. The aircraft pitch angle responses for all flight conditions were found to be well within the performance specifications. The elevator responses were found to be well within the physical limitations of the aircraft. The values for the design flight condition were: zero steady state pitch angle within two seconds and a maximum pitch angle transient of .01 degree.

A separate study performed by Smetana, et al., (Ref. 9) shows that the response of the aircraft pitch angle to an angle of attack disturbance due to a vertical gust is completely attenuated rendering the subsystem as an excellent SAS.

This radically different but simple system fulfills the requirement of constant attitude flying as part of the goal of overall minimization of piloting tasks.

---

*Figure 18 also indicates that, because of the low dc gain of the subsystem when it is operational as a regulator, it will be necessary to augment the θ_{ref} input when it is desirable to operate the system as a servomechanism. This augmenting factor is of the order of 55.55 volts/volt for all flight conditions.

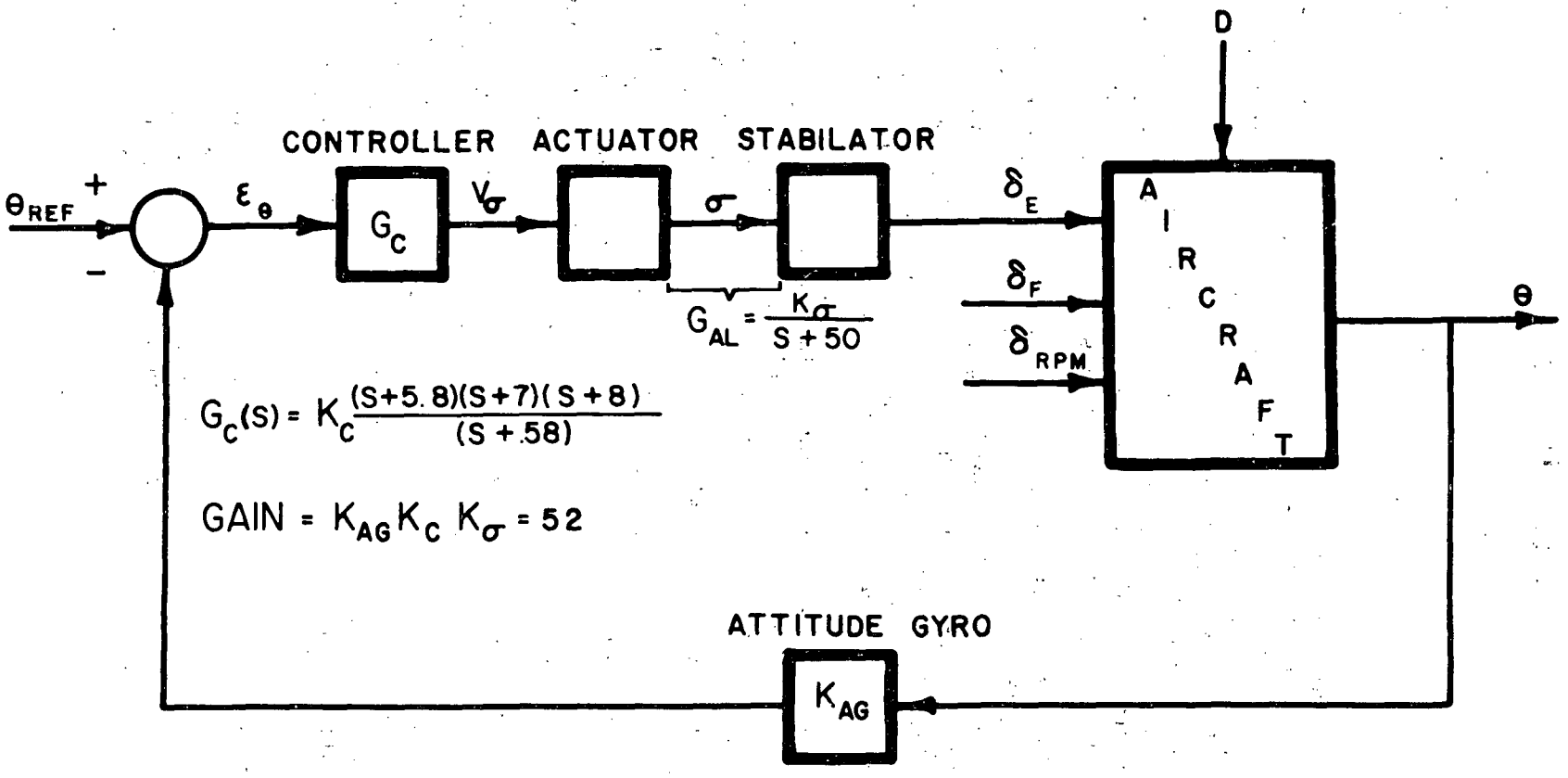

Figure 19. Final form fuselage leveller.

SUBSYSTEM 3.

This subsystem obtains coordinated turns with one pilot command, twisting the yoke. Note that the rudder pedals are not present in this mechanization, rudder deflection being controlled by twist of the yoke.

Initially a simple mechanical interconnect between rudder and ailerons was considered. The rudder-to-aileron deflection ratio would be chosen to optimize the lateral dynamics and ameliorate the adverse yaw produced by aileron deflection. Initial thinking also tended to consider the wings leveler an optional feature; however, the lateral dynamics of the airplane showed a need for stability augmentation, making it desirable to employ a more elaborate feedback-type turn coordinator. The function of the wings leveler portion of this system is to counteract the usual spiral instability.

Calculation of the effects of geometric modifications to the PA28-235C showed that there was little difference in the response due to rudder inputs, but that there were significant changes in the magnitude of the response due to aileron inputs; damping ratios and frequencies remained virtually unchanged. These dynamic characteristics can be improved substantially, however, through the use of stability augmentation systems.

The most common stability augmentor in use today is the yaw damper [Blakelock (Ref. 10); Jarvis, et al. (Ref. 11)]. This concept has been in use for over twenty years and has been included on all U. S. fighter aircraft since the F-100. Since the Dutch roll is a combination of yawing and sideslipping motions, the most direct yawing method of controlling this motion is to measure the yaw rate, r, with a rate gyro and use this signal to position the rudder to eliminate the yaw rate. A washout circuit is required for this system to eliminate the response of the actuator to steady-state yaw rate during steady turns.

To achieve the design goals of coordinated turns and bank angle steering, two additional loops must be added to a stability augmentation system employing a damper. Figure 20 shows a conceptual block diagram for such a system. Sideslip feedback provides turn coordination by nulling the sideslip angle through the positioning of the rudder. Feeding back bank angle position provides bank angle steering as well as spiral stability for wings level flight (wings leveler function).

The representation of the hardware in this system follows standard practice found in the literature. The aileron and rudder servos are, in general, at least second order, but if properly designed, their natural frequencies are much higher than that of the aircraft. If the damping ratio is high enough, the servos can

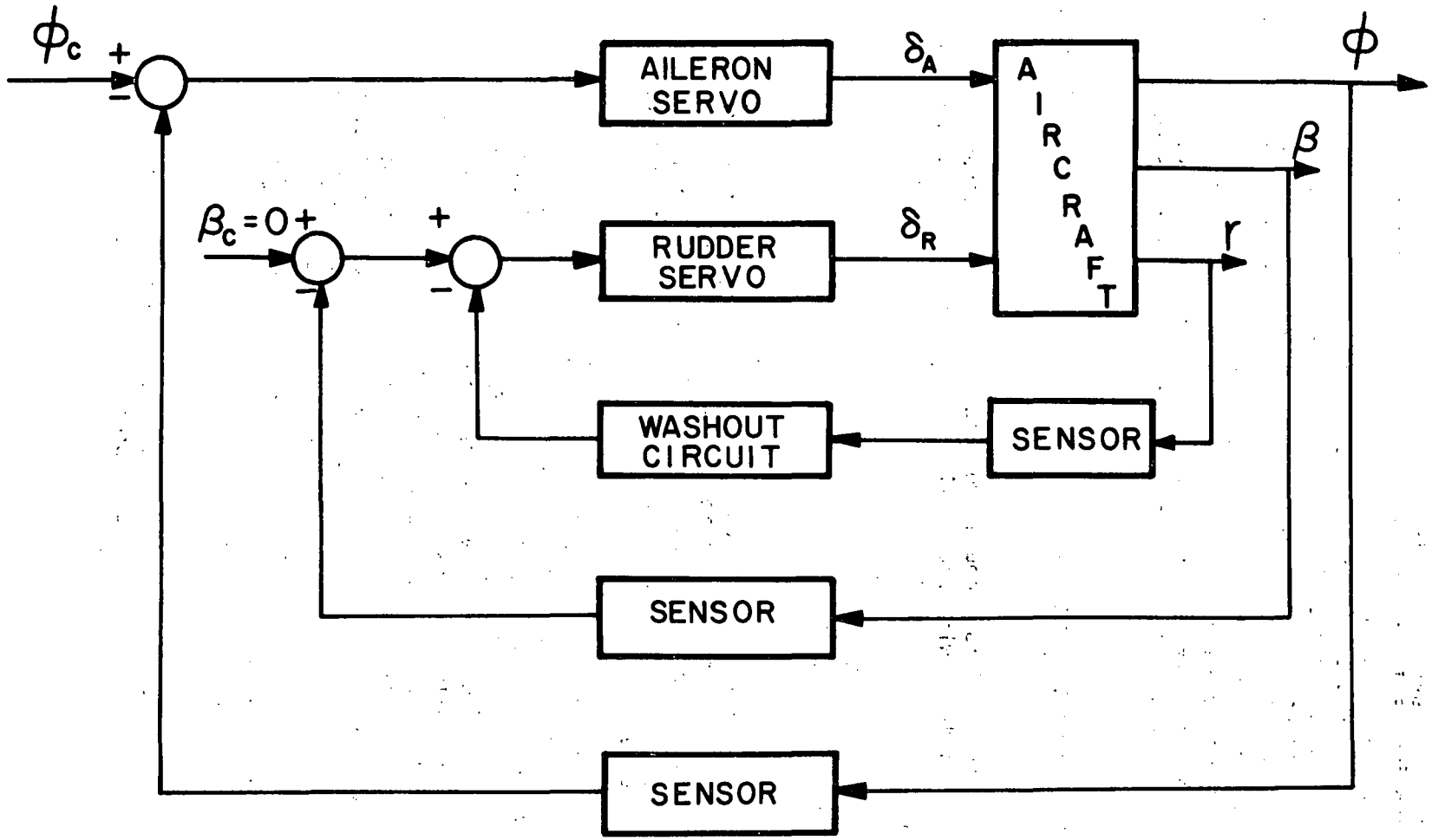

Figure 20. Block diagram of yaw damper system.

be represented by a gain multiplied by a first order time lag. This approximation is justified when the frequency responses of the two servos are compared on a Bode plot. The system response for a well-damped second order system is nearly identical to a first order system at frequencies below the corner frequency. Since the aircraft operates at frequencies less than 5 rad/sec, this approximation will be sufficiently accurate for servos having time constants of 0.1 second or less. Because the ailerons must have quick response characteristics to eliminate any lag between the pilot command and the initiation of the roll maneuver, a very fast acting servo was chosen. Its transfer function was taken to be

$$\text{Aileron servo} = \frac{50}{(S + 50)} \quad . \tag{36}$$

The rudder was not at first thought to need such rapid response in order to damp out the yawing oscillations; therefore, its servo was taken to be

$$\text{Rudder servo} = \frac{10}{(S + 10)} \quad . \tag{37}$$

The sideslip angle was assumed initially to be measured by a β-vane* mounted on a wingtip boom to insure that the vane measures the flow relative to the undisturbed wind. For the measurement of the bank angle, a vertical gyro is used. Both of these sensors are modeled by pure gains.

A brief examination of this basic system will give some insight as to how the system characteristics can be improved using angle feedback and electrical shaping networks. A root locus diagram for the r/δ_r transfer function is shown in Figure 21. Since the heavy-weight landing condition represents the worst case of the six flight conditions analyzed, this condition will be used throughout this section with only the end results given for the other five conditions. If the yaw rate is fed back to position the rudder as shown in Figure 20, the roots of the aircraft plus the control system will move toward their respective zeros with changes in system gain. The optimum gain value for this system is realized when the Dutch roll damping ratio is at a maximum, as indicated on the root locus diagram. The damping ratio in this case is approximately .34.

---

*Suitable gust response characteristics, however, dictate the use of inertial type (integrating accelerometer) β sensor for frequencies above about 0.1 rad/sec.

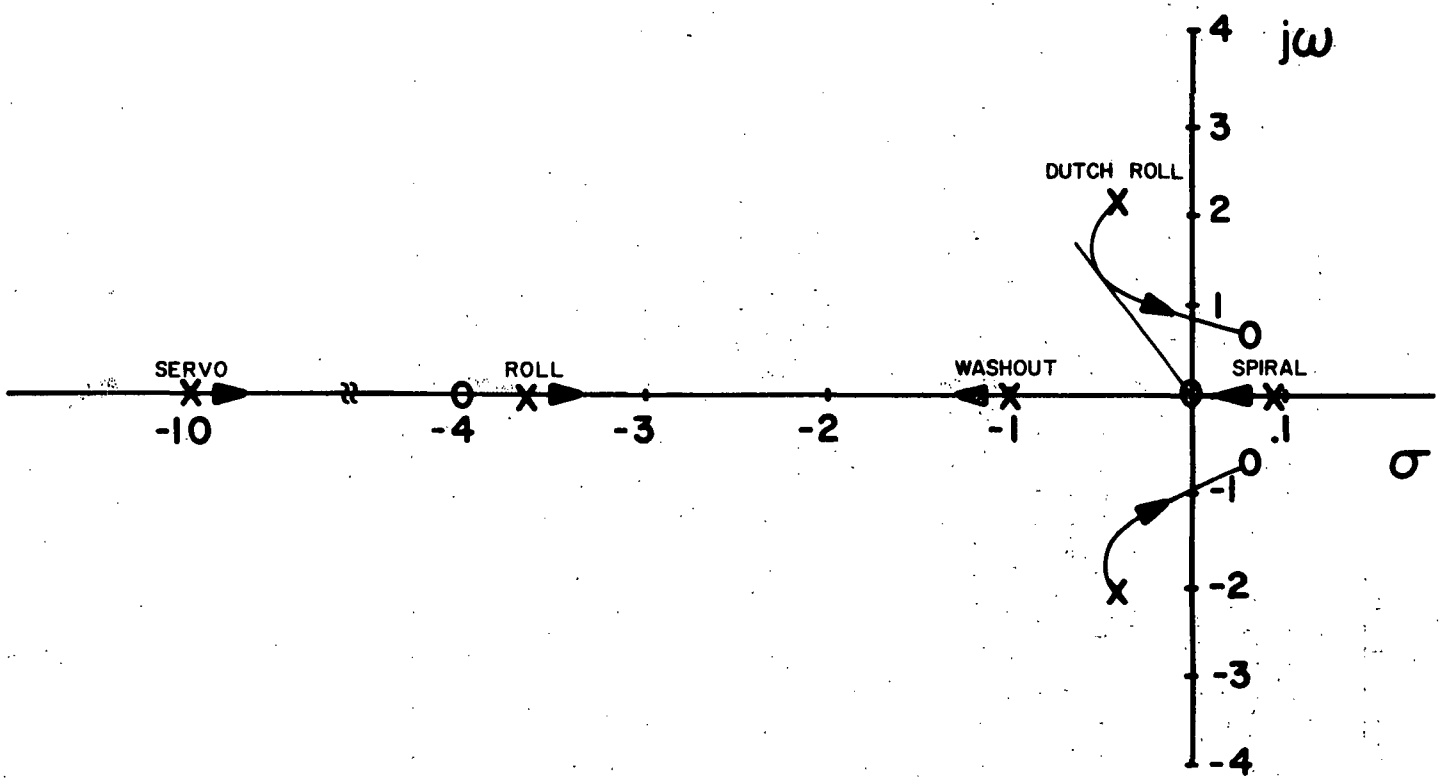

Figure 21. Root locus for yaw damper system.

The β and φ loops have likewise been analyzed, but the Dutch roll damping ratio could not be improved without the addition of several compensator networks. This concept was discarded in favor of a simpler system that eliminated the need for a washout circuit and required only two feedback loops.

Turn Coordinator--Inner Loop

Recalling that the Dutch roll consists of yawing and sideslip motions, the next choice for damping this oscillation is to feed back the sideslip angle, as shown in Figure 22. Note that only two angles, β and φ, are fed back in this system. The yaw rate loop has been eliminated in this concept. The inner loop is much the same as the β-loop in the first system with the addition of the compensator network. Here, the β-loop serves to coordinate turns and to increase Dutch roll damping. The outer loop is also similar to the first concept, with the addition of the compensator in the feedback loop. Again, the φ-loop acts as the command loop. Finally, a lag element has been added as a command-shaping network to reduce the magnitude of the aileron deflection and to increase the total time in which the aileron is deflected from its equilibrium position.

A complete analysis of this system requires the use of multi-loop analysis techniques. The details of this technique are not generally available in most textbooks. Therefore, a general control system with two inputs, three outputs, and two-loop closures is developed in Appendix C. McRuer, et al., (Ref. 12) should be consulted for additional details concerning this method.

In order to compare the turn coordinator with the general multiloop system shown in Appendix C, the turn coordinator must be reduced to a unity feedback system. This is accomplished by using block-diagram algebra. Figure 23 shows the unity feedback form of the system. Comparing the general system shown in Figure 75 in Appendix C to the turn coordinator system shown in Figure 23, it is seen that

$$
\begin{aligned}
q_{1c} &= \phi_c & q_{2c} &= \frac{\beta_c}{K\,(s+a)(s+b)} \\
q_1 &= \phi & \delta_2 &= \delta_A \\
q_2 &= \beta & \delta_1 &= \delta_r \\
q_3 &= r
\end{aligned}
\qquad (38)
$$

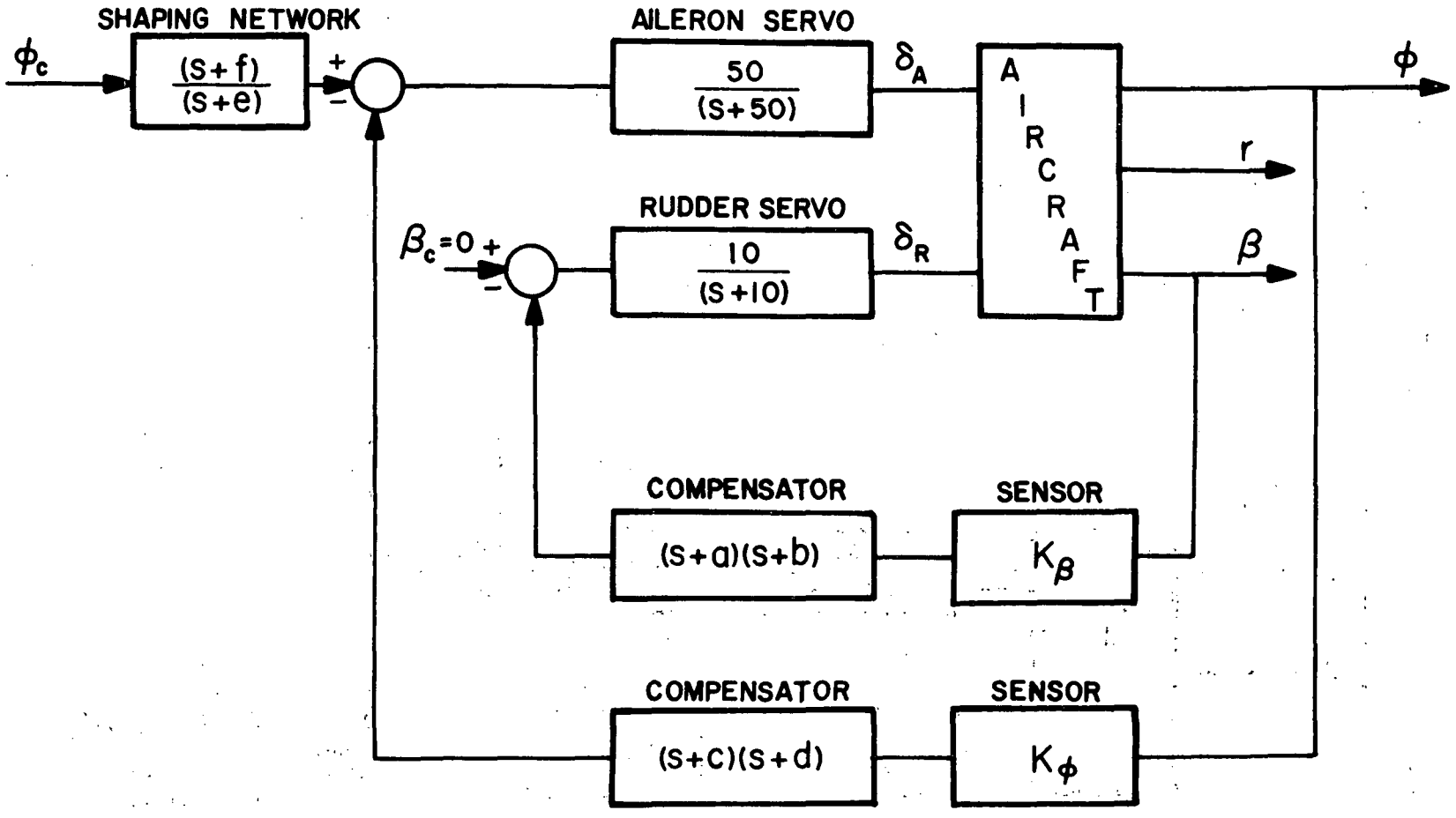

Figure 22. Block diagram of turn coordinator system.

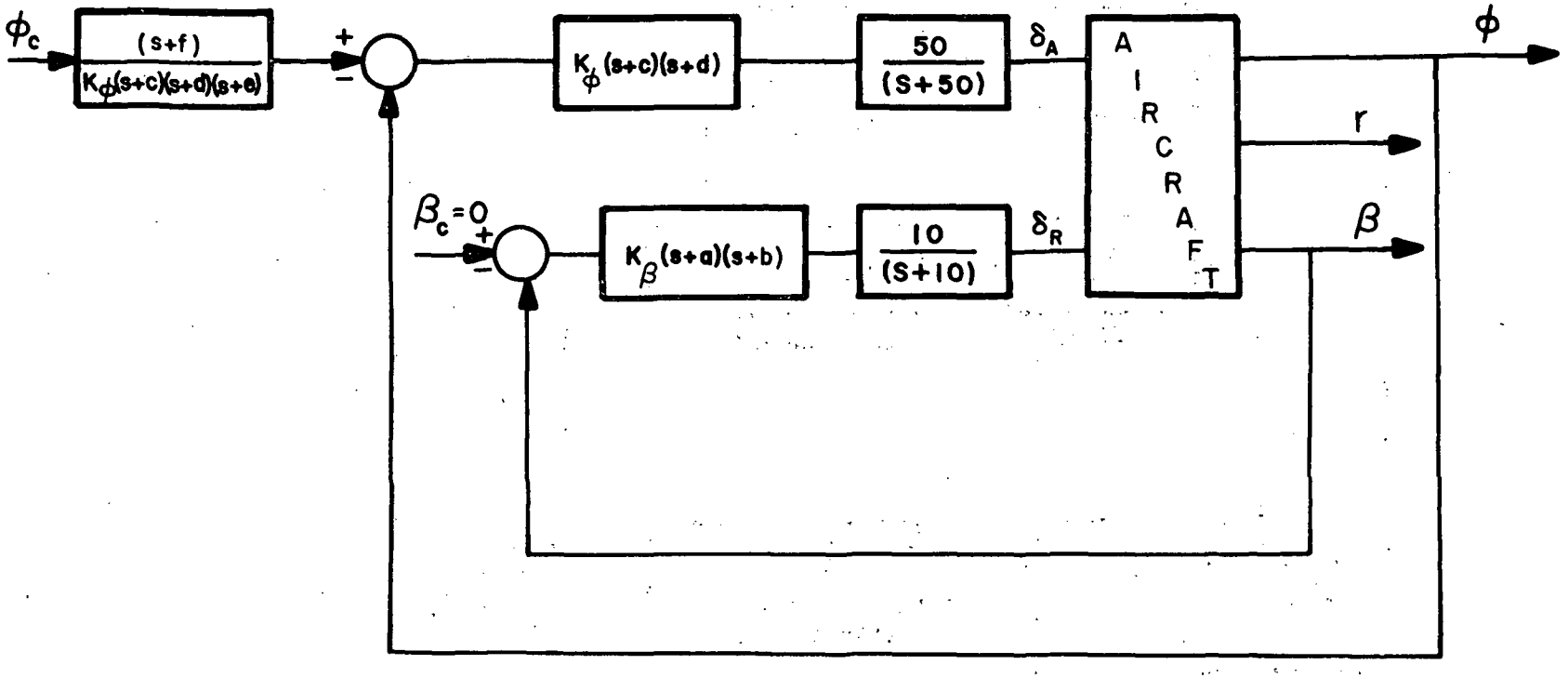

Figure 23. Turn coordinator in unity feedback form.

$$G_{12} = (\text{Rudder Servo})\ K_\beta\ (S + a)(S + b)$$

$$G_{21} = (\text{Aileron Servo})\ K_\phi\ (S + c)(S + d)$$

$$J_1 = \frac{(S + f)}{K_\phi (S + c)(S + d)(S + e)}$$

From Figure 76 the aircraft with the inner-loop closed can be represented by ϕ'_{δ_A}. Thus,

$$\phi'_{\delta_A} = \frac{\frac{N^\phi_{\delta_A}}{\Delta}\left(1 + \frac{G_{12} N^{\beta\ \phi}_{\delta_r \delta_A}}{N^\phi_{\delta_A}}\right)}{1 + \frac{G_{12} N^\beta_{\delta_r}}{\Delta}} \tag{39}$$

From McRuer (Ref. 12), the cross coupling term $N^{\beta\ \phi}_{\delta_r \delta_A}$ is evaluated as

$$N^{\beta\ \phi}_{\delta_r \delta_A} = (AS + B) \tag{40}$$

where $A = L_{\delta_A} Y^*_{\delta_r} - Y^*_{\delta_A} L_{\delta_r}$

$$B = -N_r (L_{\delta_A} Y^*_{\delta_r} - Y^*_{\delta_A} L_{\delta_r}) + L_r (N_{\delta_A} Y^*_{\delta_r} - Y^*_{\delta_A} N_{\delta_r}) + (N_{\delta_A} L_{\delta_r} - L_{\delta_A} N_{\delta_r}).$$

Thus, equation (39) can be rewritten as

$$\phi'_{\delta_A} = \frac{\frac{1}{\Delta} N^\phi_{\delta_A} + \frac{10K_\beta}{(S + 10)}(S + a)(S + b)(AS + B)}{1 + \frac{10K_\beta}{(S + 10)} \frac{(S + a)(S + b) N^\beta_{\delta_r}}{\Delta}} \tag{41}$$

Since ϕ'_{δ_A} is written in a form convenient for root-locus analysis, it is readily seen that

$$\text{open-loop zeros} = (S + a)(S + b)\, N^{\beta}_{\delta_r} \qquad (42)$$

$$\text{open-loop poles} = \Delta\,(S + 10)\ .$$

Thus, a root locus can be constructed to determine the movement of the open-loop poles as the gain K_β is increased. Figure 24 shows the open-loop placement of the aircraft roots, plus the servo root at (S + 10). The zeros at (S - .29) and (S + 3.9) represent the numerator of β/δ_r transfer function. There is one additional zero for this transfer function at (S + 102) which is not shown on the root-locus plot.

The two zeros at (S + 3.4) represent the compensator network placed in the feedback loop to achieve the proper system performance. The process that led to the selection of this type of compensator involved the trial and error analysis of different feedback combinations.

The use of only position feedback was not feasible here, since it caused the Dutch roll roots to go unstable. By feeding back position plus rate, the desired damping ratio could be obtained, but at the cost of an extremely high gain in the feedback loop (K_β = 35 for critical damping). Gain values of this magnitude would require system voltages in excess of the 28 volt supply. Finally, by adding acceleration feedback*, the desired performance was achieved with low system gains. Rather than use a separate feedback loop for each quantity, it is possible to obtain the same effect by feeding back only the output of a position sensor through a special circuit that performs single and double differentiation in the proper amounts and sums them with a signal proportional to position** The result can be described as a pair of electrical zeros, (S + a)(S + b). When these two zeros are placed on the

---

*It is relatively easy to adapt a β-vane to measure β directly (see Ref. 13).

**Standard control system practice does not favor such operations. Recent improvements in solid-state operational amplifiers, however, give indication of permitting these taboos against signal differentiation to be lifted.

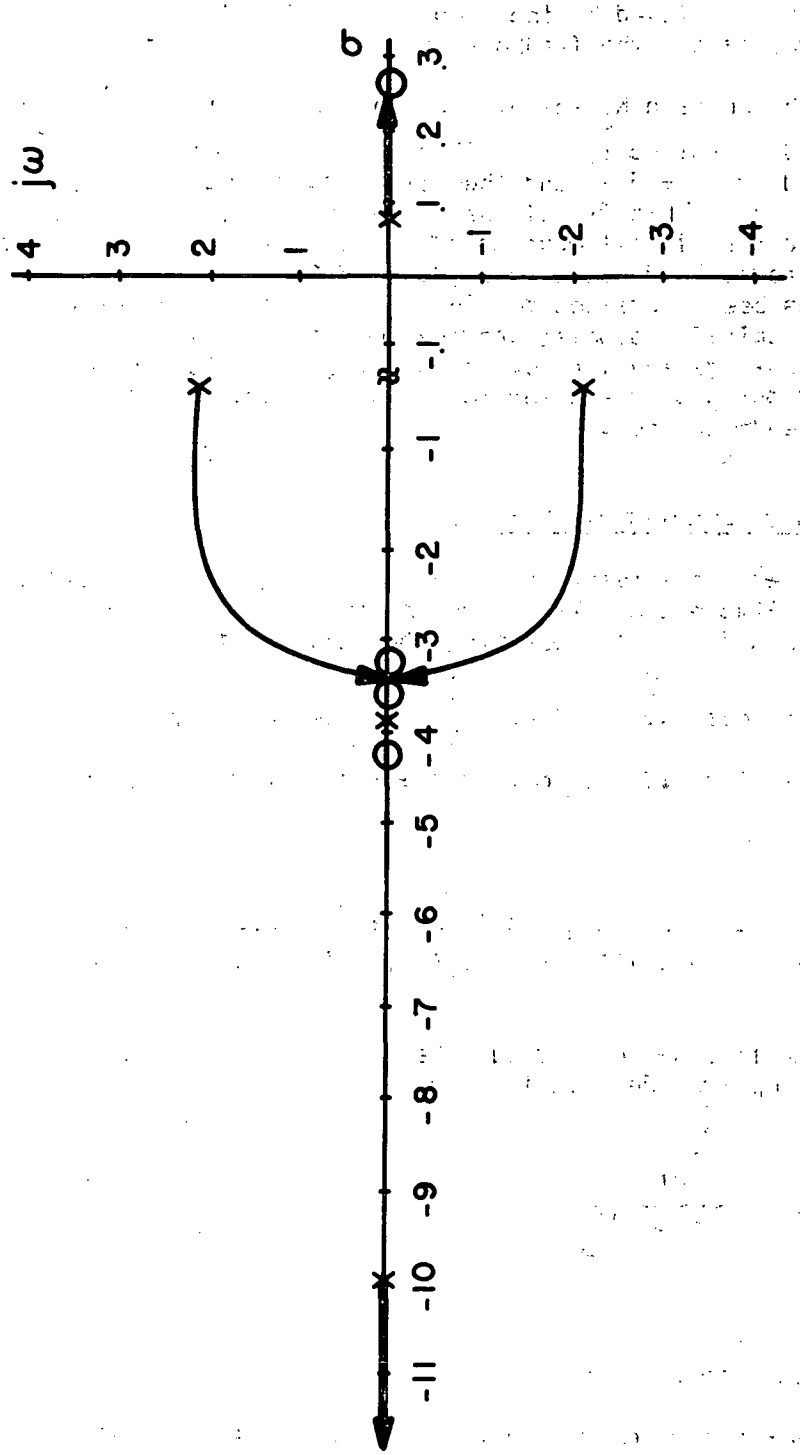

Figure 24. Root locus for turn coordinator inner loop.

β/δ_r root locus, it is immediately apparent that their placement on the real axis between the roll root and the origin causes the Dutch roll roots to move in the desired direction. Several compensators of this type were tried, with the best system performance achieved by the compensator $(S + 3.4)(S + 3.4)$. With this compensator, the feedback gain was set at $K_\beta = 1.0$.

With the gain K_β set at 1.0, the Dutch roll damping ratio is increased dramatically from .12 to .89. The roll root remains unchanged at $(S + 3.7)$ and the spiral root moves from $(S - .086)$ to $(S - .27)$. Thus two of the design goals have been met: (1) the aircraft will make coordinated turns at all times due to the feedback of sideslip angle, and (2) the Dutch roll damping ratio has been increased to .89. It remains now to make the aircraft spirally stable, provide for commands in roll, and to provide a wings leveler for cruise flight. This can be accomplished by the closing of the outer loop plus the addition of a compensator in the feedback loop.

Turn Coordinator--Outer Loop

The aircraft system roots with the inner loop closed are shown in Figure 25a. The system block diagram is redrawn in Figure 26 with ϕ'_{δ_A} representing the equivalent aircraft system with the inner loop closed (i.e., $\frac{N^{\phi}_{\delta_A}}{\Delta}$ represents the aircraft with no control system, ϕ'_{δ_A} represents the aircraft with one loop closed. That is,

$$\phi'_{\delta_A} = \frac{(S + 94)(S^2 + 6.34S + 10.8)}{(S - .27)(S^2 + 6.8S + 12.4)(S + 3.7)(S + 93)} \tag{43}$$

Examining this system without the compensator, it is seen that the closed-loop transfer function is

$$\phi/\phi_1 = \frac{G_{21}\phi'_{\delta_A}}{1 + G_{21}\phi'_{\delta_A}} \tag{44}$$

and

$$\begin{aligned} \text{open-loop zeros} &= (S+94)(S^2+6.34S+10.8) \\ \text{open-loop poles} &= (S - .27)(S^2+6.8S+12.4)(S+3.7)(S+93)(S+50). \end{aligned} \tag{45}$$

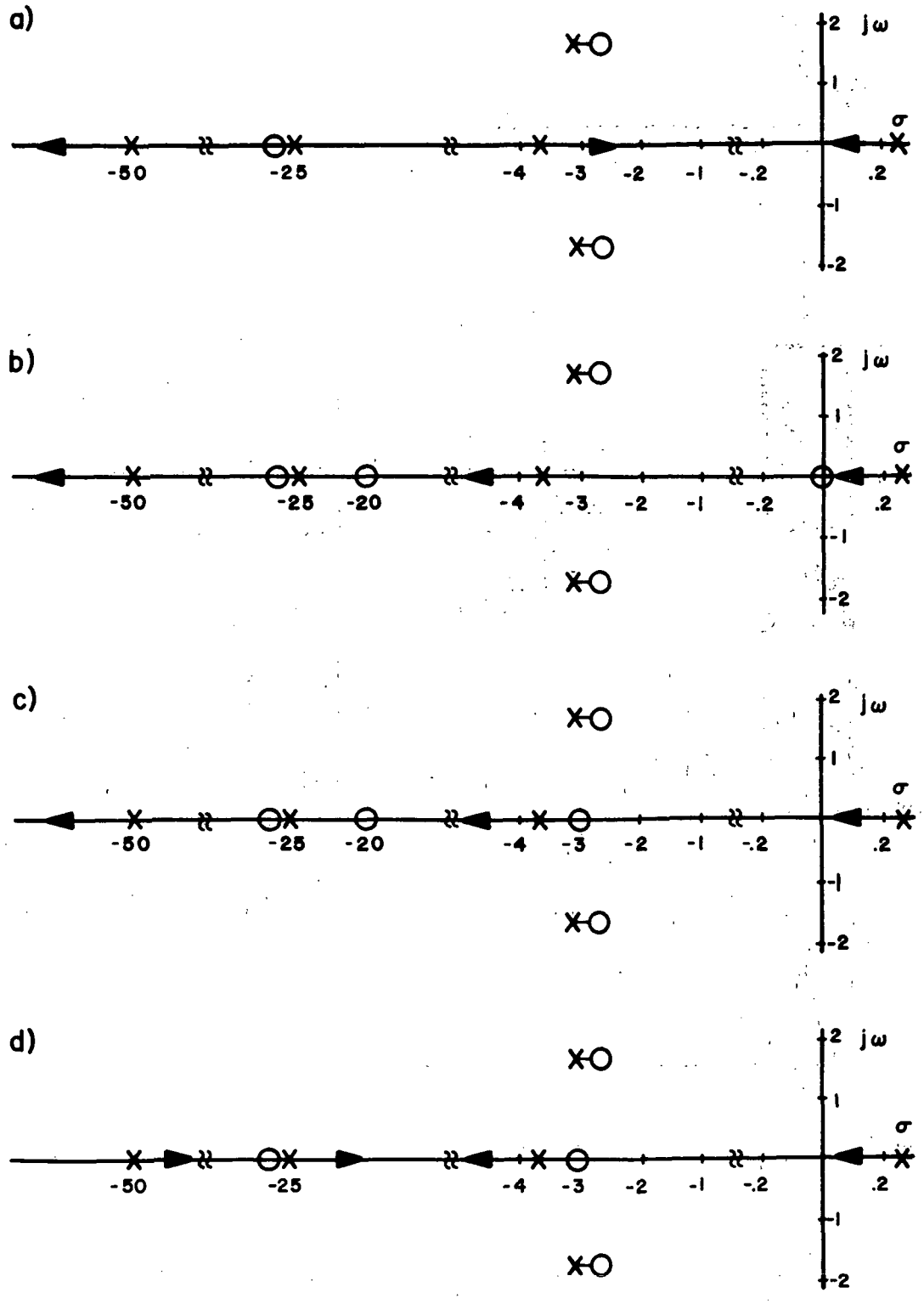

Figure 25. Root locus comparisons for the turn coordinator outer loop with different compensators in the feedback loop.

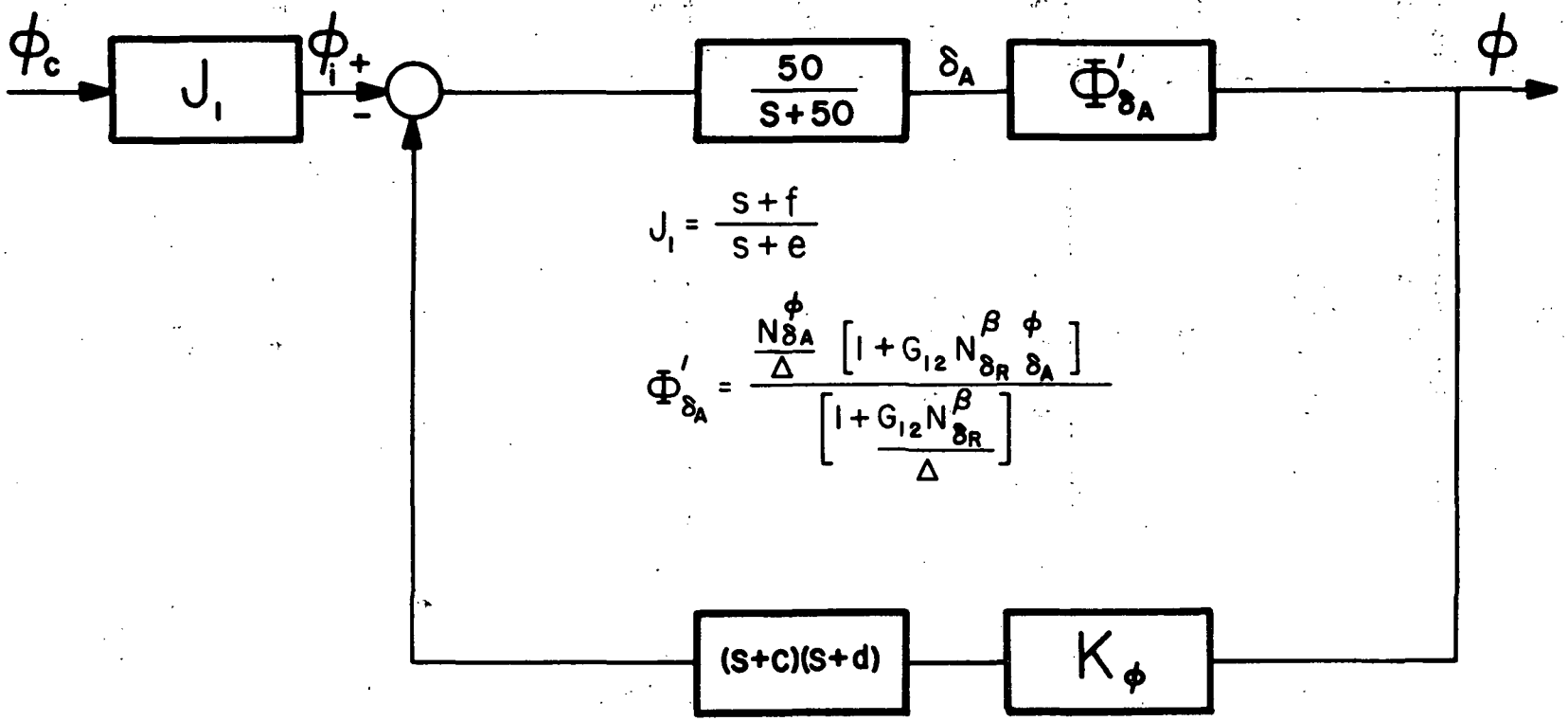

Figure 26. Simplified block diagram of turn coordinator.

Increasing the gain in the feedback loop will make the aircraft spirally stable. However, the roll response is degraded. Many attempts were made to correct this problem by adding compensation networks.

Four of the systems examined are worthy of discussion. From the root-locus diagram, it is evident that, in order to bring the spiral root into the left-hand plane and not degrade the roll performance, a compensator zero must be placed on the real axis between the two roots. In terms of block-diagram algebra, this means putting a (S + C) compensator in the feedback loop. Physically, this causes the position signal ϕ to be fed back along with its first derivative. Based on the experience gained in the analysis of the inner loop, acceleration feedback was also included in this loop. The second zero in the compensator was placed between the roll root and the aileron servo root on the real axis. A value of d = 20 was chosen to give a very rapid roll response. For the compensator root, c, a value of c = .001 was chosen to make the aircraft neutrally stable in the spiral mode. The root locus is shown in Figure 25b. The time responses for control inputs were excellent with a roll time constant of .05 seconds giving a very rapid bank angle response and the neutrally stable spiral root holding the bank angle at the desired value. However, the responses to gust inputs were found to be extremely poor for this system. This is seen from an analysis of the gust transfer function. From Onsott and Salmon (Ref. 14), the gust transfer function is given as

$$\beta/\beta_g = \frac{N_{\beta_{\beta_g}} + G_{21} N^{\beta\ \phi}_{\beta_g \delta_A}}{\Delta''} \tag{46}$$

where $\Delta'' = \Delta + G_{21} N_{\phi_{\delta_A}} + G_{12} N_{\beta_{\delta_r}} + G_{12} G_{21} N^{\phi\ \beta}_{\delta_A \delta_r}$.

For the basic aircraft with no control system, $G_{12} = G_{21} = 0$, which reduces the gust transfer function to

$$\beta/\beta_g = \frac{N_{\beta_{\beta_g}}}{\Delta} \tag{47}$$

where $N_{\beta_{\beta_g}}$ is the third order, having one zero in the right-hand plane that very nearly cancels the spiral root. When the control system is added and the gain is increased, this zero will move into

the left-hand plane, leaving no zeros in the numerator to cancel the effect of the spiral root. Thus, for a step in sideslip gust, the system acts as an integrator, increasing the value of β with time. Two solutions to this problem are apparent. The first is to reduce the system gain so that the numerator zero will not move out of the general region of the spiral root. The second is to move the compensator at (S + .001) away from the origin. The first solution is not feasible since the required reduction of system gain will decrease the Dutch roll damping ratio to an undesirable value. The second solution gives the desired Dutch roll damping and gust response. This root locus is shown in Figure 25c, where c = 3. This solution, however, presented another problem--the steady-state gain was too low. A simple analysis of the steady-state system gain for a step input demonstrates the reason for this. The approximate form of the steady-state value of bank angle is given as

$$\phi_{ss} \simeq \frac{f \cdot DD}{K_\phi \cdot DD \cdot c \cdot d \cdot e} = \frac{f}{K_\phi \cdot c \cdot d \cdot e} \tag{48}$$

where DD is a coefficient that contains stability derivatives, and c, d, e, and f are the root locations of the shaping network and compensators that were shown in Figure 23. When the compensator was changed from c = .001 and d = 20 to c = 3 and d = 20, the steady-state gain was reduced by 3000. The steady-state gain can be increased by reducing K_ϕ or by increasing the gain in the command-shaping network. Increasing the gain in the shaping network caused the voltage in the system to exceed 28 volts. Reducing the gain in the feedback loop decreased system performance substantially. The solution was found by eliminating one of the compensators in the feedback loop. This yielded the desired value for steady-state gain, while maintaining excellent roll response and response to sidegusts. Its root locus is shown in Figure 25d.

A detailed analysis of the aileron servo system caused minor changes to be made in the command-shaping network and the servo gain. The steady-state gain of the servo transfer function was increased from 1.0 to 1.43, and the command-shaping network was changed to

$$\frac{14.7\ (S + 2.74)}{(S + 10)(S + 13)} \tag{49}$$

The value of the numerator root in the shaping network was set to reduce the influence of the spiral root on the system response. The denominator roots were chosen to yield the desired response from the aileron servo. This essentially acts like a band-pass filter.

With the values for the command-shaping network set, K_ϕ was then chosen to give $\phi_{ss} = 1$ for unity inputs. This is seen from equation (48), which, after rearranging and substituting the proper values for the system components, gives

$$K_\phi = \frac{14.7\ (2.74)}{(130)(3)} = .103 \qquad (50)$$

Since this relation is only approximate, the final value chosen for K_ϕ was .117. This value yielded the desired position for the spiral root and a very rapid bank angle response.

The time histories for the system are shown in Figure 27. Note the initial adverse yawing of the aircraft. The adverse yaw for this aircraft is roughly 3-1/2 times greater than conventional aircraft due to the full-span Fowler ailerons. Since the rudder servo is slower than the aileron servo, the rudder will lag the positioning of the ailerons. This caused an initial yaw rate in a direction opposite the intended one. In rough turbulent air, this lag effect could cause a stability problem. In an effort to reduce this initial adverse yaw, a faster servo was put in the inner loop to drive the rudder. Since considerable engineering effort was required to produce the first order aileron servo with a time constant of .02 seconds,* this same servo was chosen for the rudder actuator. Figure 28 shows the time response for the system with the faster rudder servo. The adverse yaw rate has been reduced from 1.2 deg/sec to .2 deg/sec. The Dutch roll damping ratio has been increased from .89 to .96. This resulting increase, albeit small, eliminates the overshoot in yaw rate. The increase in damping ratio comes from the higher system gain allowed in the inner loop. With the slower servo, the maximum excursion in sideslip was approximately 1.5 degrees. With the faster servo, the maximum excursion was reduced to .4 degrees. This reduction in sideslip angle allowed a change in scaling that provided a higher feedback gain.

The block diagram for the final design is given in Figure 29. The dynamic performance specifications for each of the six flight conditions are shown in Table II. The roll root is located at -25 on the real axis. The response rate for the system is governed by the smallest root in the command-shaping network (which is located at -10), the relative nearness of the spiral root to the zero in the command-shaping network, and the rate of the command input (for a command rate of 80 deg/sec, the response time for a pure gain system would be .25 seconds).

---

*These studies are reported in detail in Ref. 13.

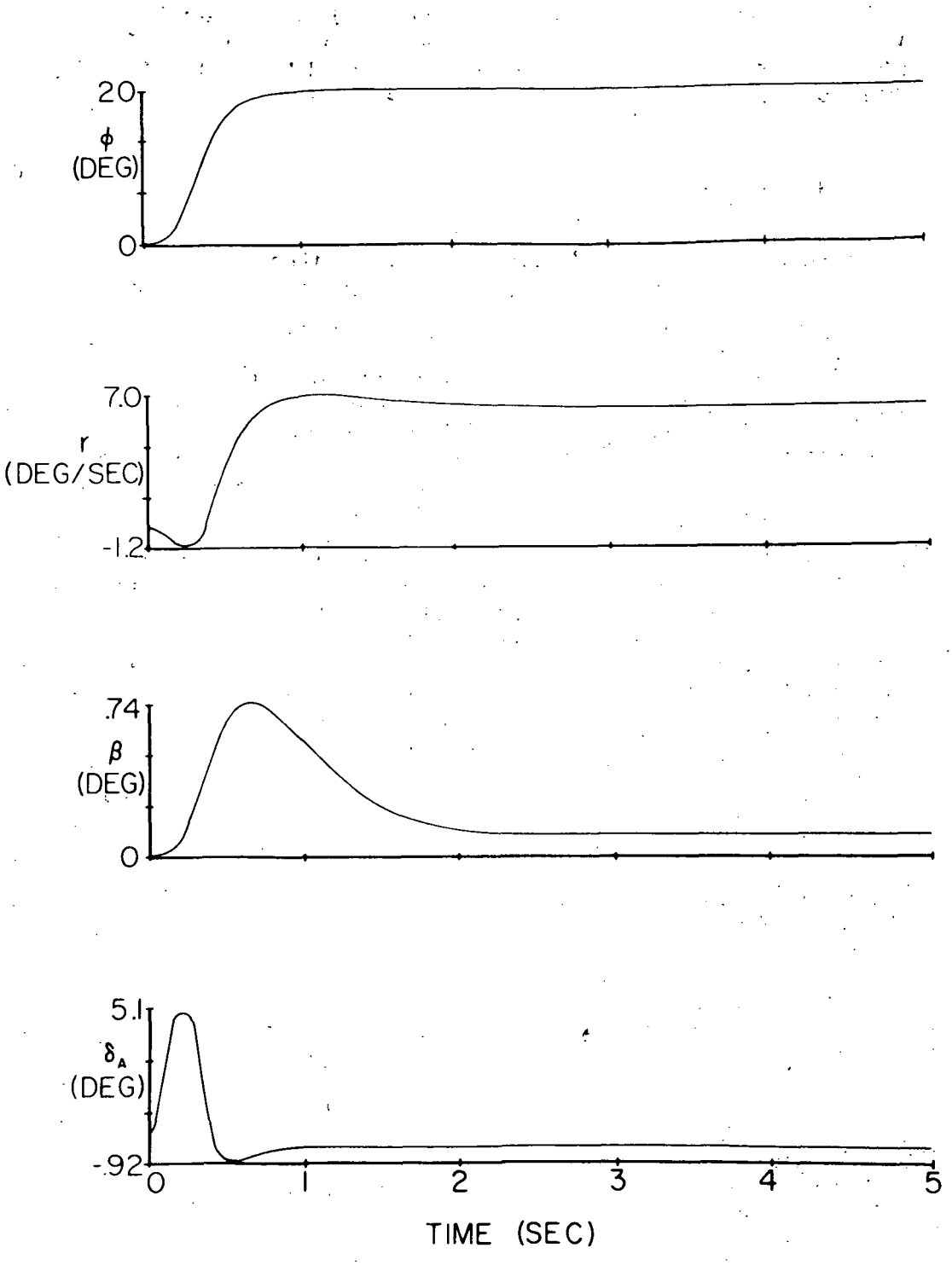

Figure 27. Turn coordinator transient response for a 20 degree ramp step in bank angle command, rudder servo = 10/(S + 10).

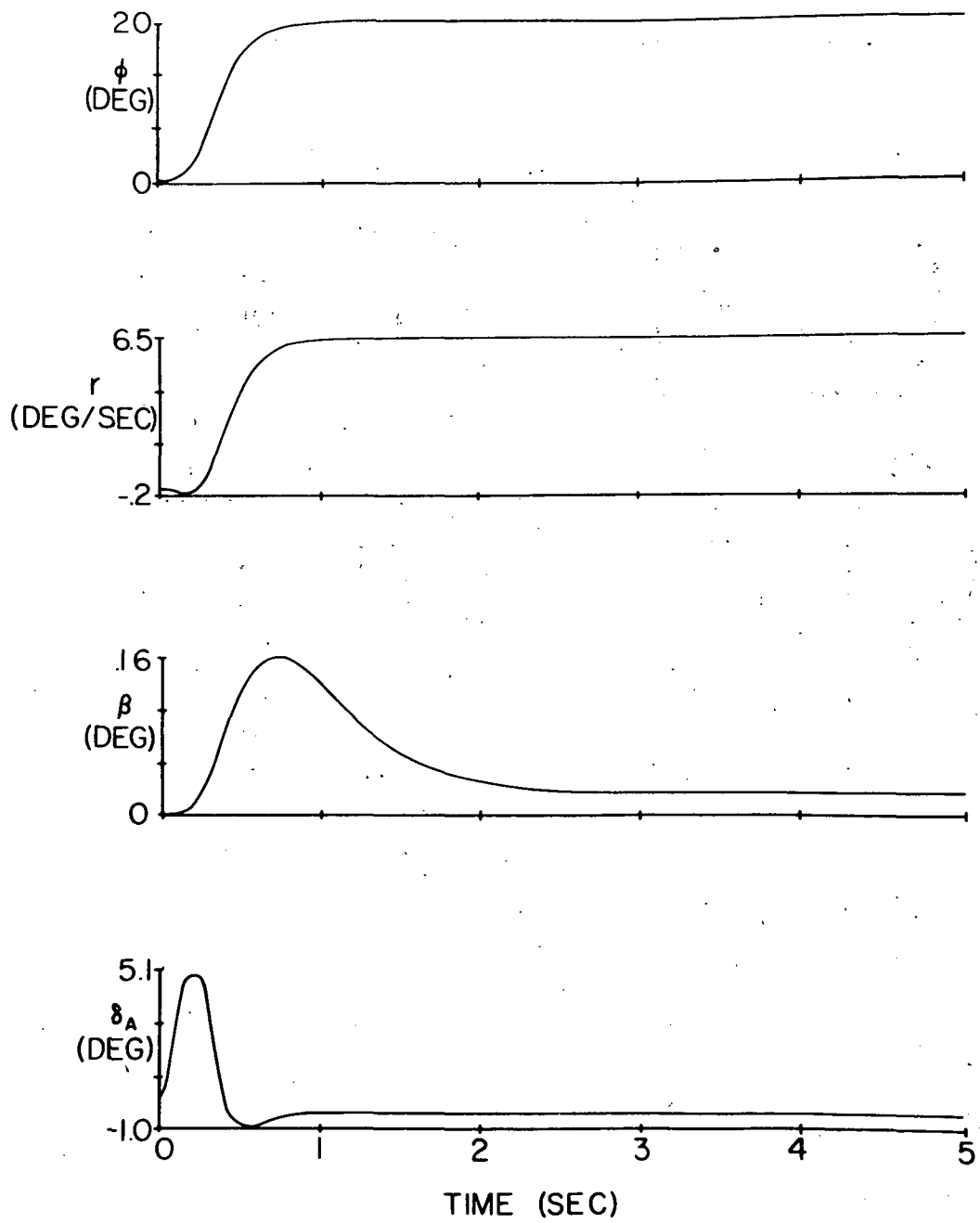

Figure 28. Turn coordinator response for a 20 degree ramp step in bank angle command, rudder servo = 71.4/(S + 50).

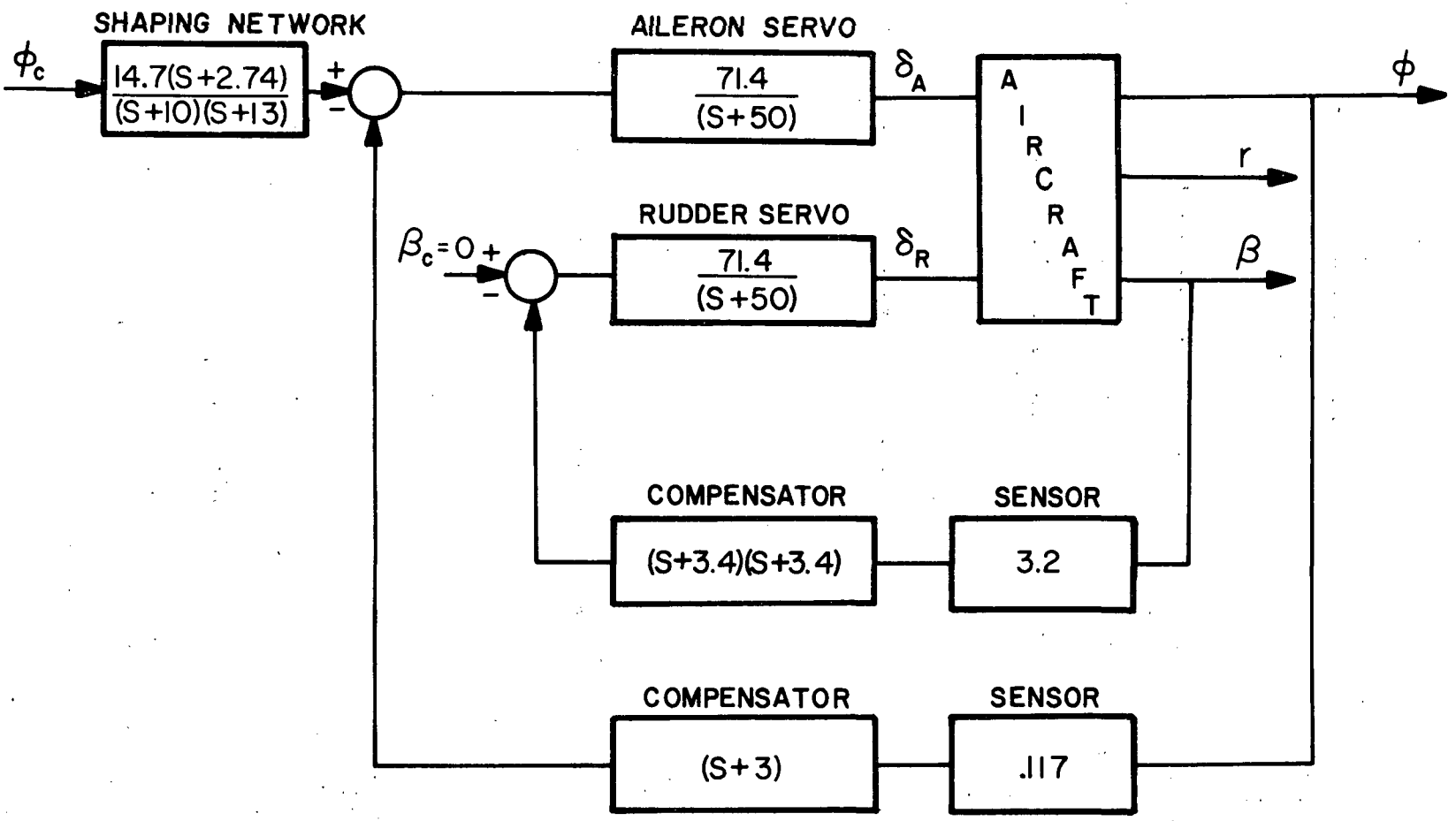

Figure 29. Final block diagram of turn coordinator system.

TABLE II. DYNAMIC PERFORMANCE SPECIFICATIONS FOR THE TURN COORDINATOR SYSTEM SHOWN IN FIGURE 29 (BANK ANGLE COMMAND EQUALS 20 DEGREES, BANK ANGLE COMMAND RATE EQUALS 80 DEGREES/SECOND)

	FLIGHT CONDITION					
	1	2	3	4	5	6
Spiral root location	2.77	2.69	2.77	2.78	2.65	2.69
Dutch roll damping ratio	.98	.98	.97	.98	.98	.97
Maximum aileron deflection (deg)	2.3	2.5	5.3	1.8	3.4	5.1
Maximum sideslip (deg)	.02	.03	.10	.01	.07	.16
Steady-state sideslip (deg)	.005	.007	.024	.004	.010	.023
Bank angle response time (to 95 percent steady state) (sec)	.60	.63	.68	.59	.66	.72
Steady-state bank angle (deg)	19.4	19.4	19.8	19.4	19.6	20.0
Maximum sideslip for a 20 degree step in gust disturbance (deg)	.03	.03	.05	.03	.04	.06
Maximum bank angle for a 20 degree step in gust disturbance (deg)	.007	.008	.04	.007	.02	.06

From Figure 29 and Table II, it is apparent that the lateral-directional response has been greatly improved. The oscillatory response characteristics of the original aircraft have been eliminated. Turn coordination is achieved with a single input. The spiral mode is stable, the roll response time has been decreased, and the overshoot from the Dutch roll mode has been eliminated. These dynamic characteristics greatly exceed all handling quality specifications for smooth air. In addition, Table I2 shows that the response to disturbances from steady sidegusts* are negligible for bank angle. For sideslip, the response to disturbances are generally on the same order as the excursions due to control surface inputs.

One final point must be attended to before the design of the lateral control system is complete: control during crosswind landings. Two solutions to this problem are seen to be feasible. The first is the sideslipping approach. An intentional sideslip is produced by the pilot by crossing the aileron and rudder controls. This intentional sideslip feature could be provided in the system by using a rudder override. This, however, does not appear practical at this point since it requires the pilot to make a complicated maneuver with a control surface that will only be used occasionally. The second, and more practical solution, is the drift approach. The aircraft is flown with zero sideslip in a wings level attitude. In this configuration, the aircraft will be yawed with respect to the runway. Therefore, in order to make a safe touchdown, castering gears will be needed. This is in keeping with the simple-to-fly concept since it does not require additional action on the part of the pilot. (See table I2).

TABLE I2. METHODS OF CONTROL DURING A CROSSWIND LANDING

METHOD	SIDESLIP ANGLE	BANK ANGLE	ADDITIONAL PILOT DUTIES
Sideslipping	unknown	held to zero by aileron deflection	rudder and aileron control
Drifting	0	0	visual lineup

*See Ref. 9 for a more complete study of gust response.

INSTRUMENT DISPLAY

As part of reducing pilot workload through the simplification of the control system, it was necessary to rearrange and redesign the PA28-235C standard instrument panel in keeping with the human factors requirements already discussed and FAA regulations listed in FAR, Part 23, and presented here in Table 13. Table 14 lists the instruments, controls, etc. presently available on the PA28-235C. Those instruments and controls necessary and desirable in the modified aircraft are contained in Table 15.

Table 16 lists groupings by function of the instruments, controls, and indicators for the modified aircraft. These functional groups are illustrated in Figure 30. The standard Piper panel is shown in Figure 31.

The yoke would physically remain as it is in the standard aircraft. There are at least two feasible ways to implement the speed monitor: dialed input, as on military aircraft; or a pointer on the airspeed indicator, as for the speed control autopilots on cars (Figure 32). The foot throttle would necessitate the removal or restructuring of the rudder pedals and their function. Sufficient data are available regarding optimum size, location, and angle of the foot throttle. The omni, gyrocompass, rate-of-climb indicator, airspeed indicator, altitude indicator, glideslope, distance-measuring equipment and all other related indicating and control equipment would be tied into a unified control system. However, there must be a capability to disconnect faulty subsystems to avoid a total system failure.

TABLE 13. FAR 23 REQUIREMENTS

CONTROLS

Master switch	Flaps	Mixture if controllable
Gear	Full tank selector	Pitch, yaw, bank
Ignition	Throttle	Prop speed/ pitch if controllable

INSTRUMENTS

Airspeed	Altitude	Mag. compass

GAUGES

Cyl. head temp. if cowl flaps or $V>V_Y$	Fuel quan.
MAP for blown engines	Oil press.
Ammeter	Oil temp.
Oil quantity in tank	Tach
Fuel pressure when pumped	

INDICATORS

Stall warning $V_{stall} + 5 < V_{warning} < V_{stall} + 10$
Flap position
Gear position

DEVICES

Voltage regulator	Circuit breakers or fuses	Seat belts

DROP HEIGHT = $3.6\sqrt{W/S} \simeq 16$ ins.
Gyro inst. must signal state "off or on"

TABLE 14. PIPER EQUIPMENT

CONTROLS

Mag switches	Carb. heat
Starter	Rudder trim with indicator
Primer	Flap control
Throttle & friction	Toe brakes
Parking brakes	Steerable nosewheel
Stab. trim with indicator	

INSTRUMENTS

Turn & bank	Altimeter	ADF
Airspeed	Marker beacon	DME
Gyro compass	Omni	Autopilot
Gyro horizon	Glideslope	Mag compass
R/C indicator	2 transducers	

GAUGES

Vacuum gauge	Exhaust temp.	Oil temp.
MAP	Ammeter	Fuel pres.
Recording tack	Oil pres.	4 fuel quan.

INDICATORS

Stall warning light	Rudder trim	Stab. trim

DEVICES

Clock	Ash tray
Cigar. lighter	Fresh air
Heat & defrost contr.	Exhaust
Check lists	External tiedowns
Circuit breakers	Wing jack points
Switches--master, lights, fuel pump	Tow bar

TABLE 15. EQUIPMENT NECESSARY OR DESIRABLE ON MODIFIED AIRCRAFT

	NECESSARY	DESIRABLE
CONTROLS	Throttle Carb. heat Pitch Mixture Primer Tank selector Stab. trim Mag-master-starter Friction control Flap Brakes Yoke	Rudder trim
INSTRUMENTS	Airspeed R/C indicator Mag & gyro compass Gyro horizon Turn & bank Altimeter VOR (omni) transceiver	ADF DME Autopilot Glideslope Marker beacon
GAUGES	MAP Tach Oil pres. Fuel quan. Oil temp. Fuel pres. Ammeter	Cyl. head temp.
INDICATORS	Flap position Stab. trim Stall warning	Rudder trim
DEVICES	Circuit breakers Switches (lights) Clock Cigar. lighter Ash tray Heat & defrost Check list Flight manual	Tow bar Level points Tiedowns Jack points Check lists

TABLE 16. FUNCTIONAL GROUPS FOR THE MODIFIED AIRCRAFT

FLIGHT	EXTRAS	SWITCHES
Airspeed	Fuel selector - in floor	Cabin
Rate-of-climb	Clock - in yoke	Panel
Magnetic compass	Yoke	Fuel pump
Directional gyro	Rudder pedals - toe brakes	Rotating beacon
Gyro horizon	Stabilator trim control & indicator - floor	Marker
Turn & bank indicator	Rudder trim control & indicator	Landing beam
Altimeter	Flap position	Flap switch & indicator
Stall warning	Phone jack - overhead	Dimmer pot
Flap position indicator	Mike button - on yoke	

NAVIGATION	POWER	FUEL	ENGINE
Dual Transceivers	Throttle - MAP gauge	4 fuel quan.	Oil temp.
Omni & glideslope display	Prop speed - tachometer	1 fuel pres.	Oil pres.
Marker beacon receiver & indicator	Mixture - exh. temp.	Primer	Ammeter
DME control & indicator	Carb heat		
ADF receiver & indicator	Friction control		
Autopilot			

MAIN GROUP	CIRCUIT BREAKERS
Comb. master-mags- starter	Circuit breakers
Check lists	

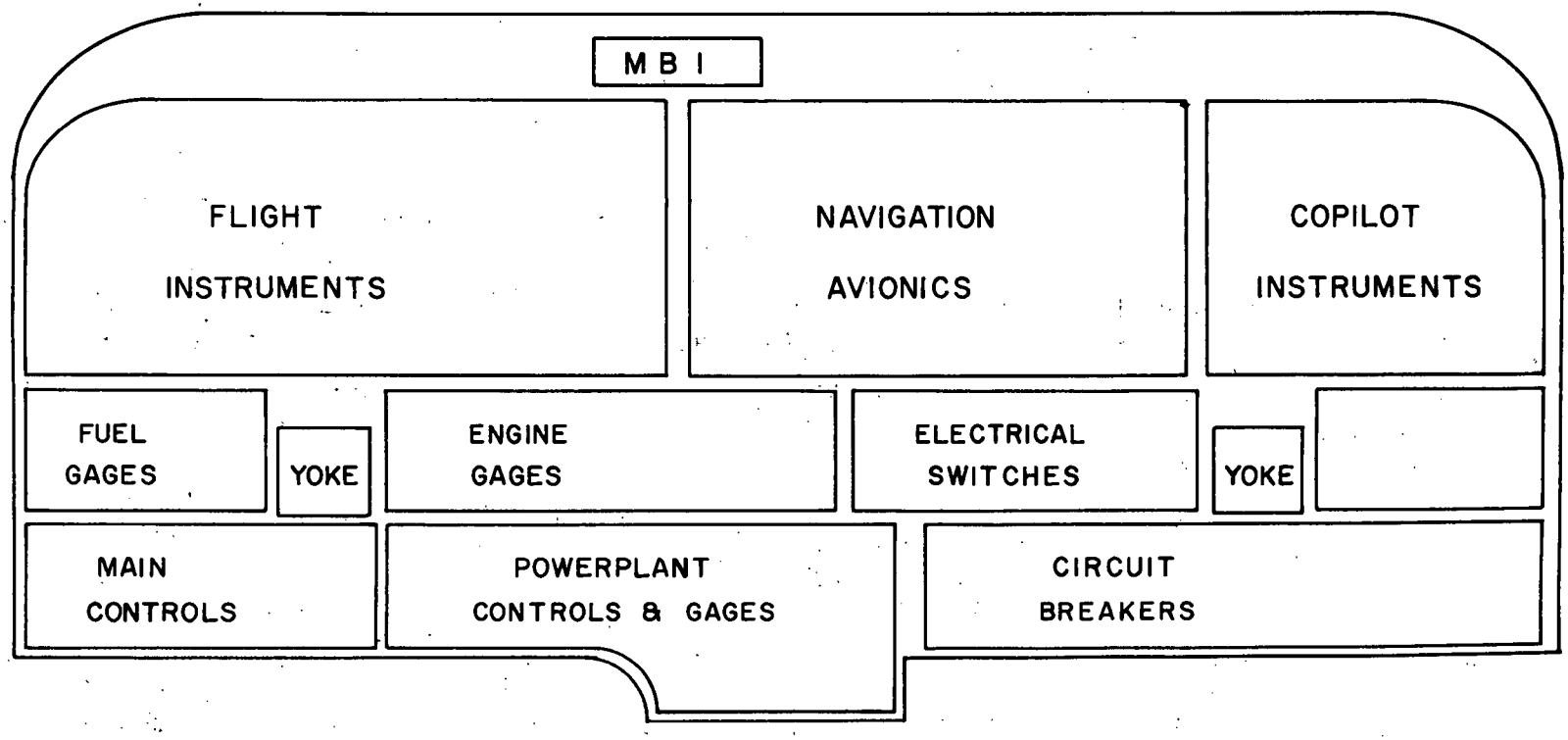

Figure 30. Layout of groups.

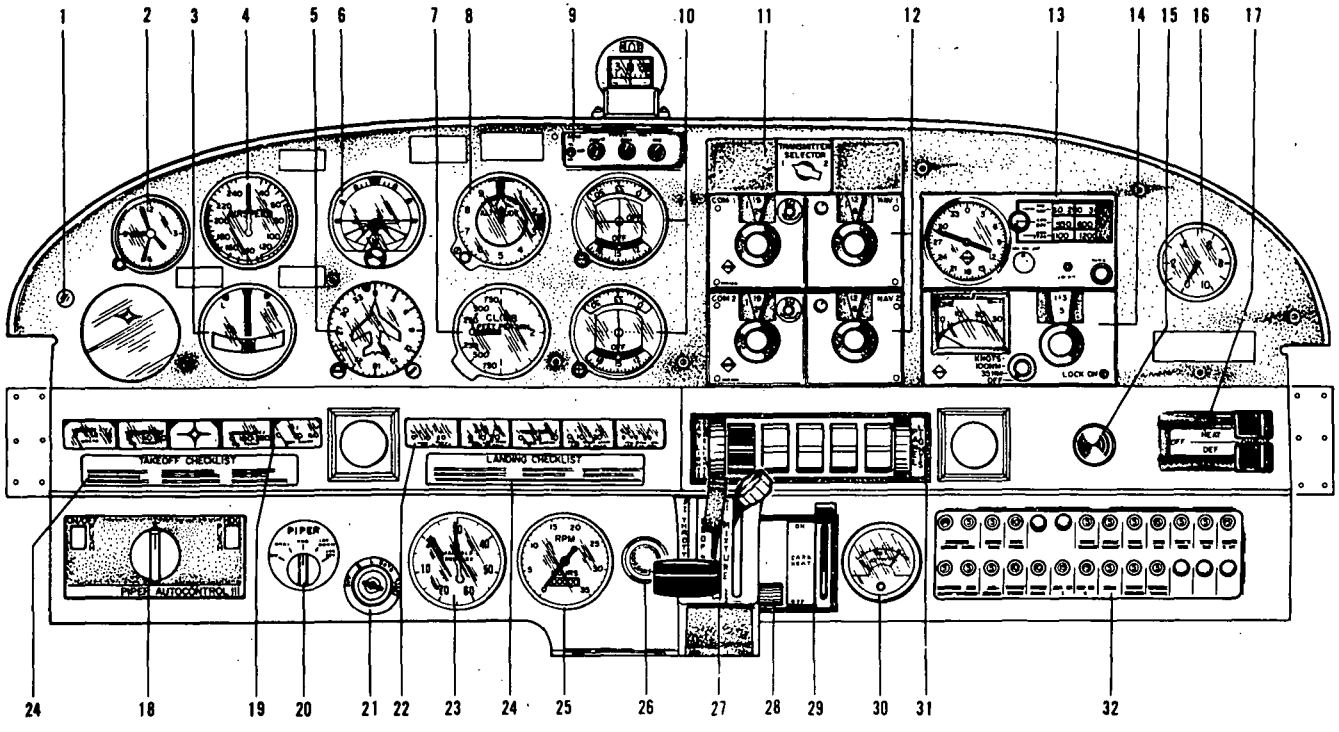

1. STALL WARNING LIGHT
2. CLOCK
3. TURN AND BANK INDICATOR
4. AIRSPEED INDICATOR
5. DIRECTIONAL GYRO
6. GYRO HORIZON
7. VERTICAL SPEED INDICATOR
8. ALTIMETER
9. MARKER BEACON RECEIVER CONTROL
10. OMNI AND GLIDESLOPE INDICATORS
11. TRANSMITTER SELECTOR SWITCH
12. COMMUNICATIONS AND NAVIGATION TRANSCEIVERS
13. ADF RECEIVER AND INDICATOR
14. DME CONTROL AND INDICATOR
15. CIGAR LIGHTER
16. VACUUM SUCTION INDICATOR
17. HEAT AND DEFROST CONTROLS
18. AUTOCONTROL III AUTOPILOT
19. ENGINE INSTRUMENT CLUSTER
20. OMNI-COUPLER
21. MAGNETO SWITCHES AND STARTER
22. FUEL SYSTEM CLUSTER
23. MANIFOLD PRESSURE
24. TAKEOFF AND LANDING CHECK LISTS
25. TACHOMETER
26. ENGINE PRIMER
27. THROTTLE QUADRANT
28. THROTTLE QUADRANT FRICTION KNOB
29. CARBURETOR HEAT CONTROL
30. EXHAUST GAS TEMPERATURE GAUGE
31. SWITCH PANEL
32. CIRCUIT BREAKER PANEL

Figure 31. Standard piper panel.

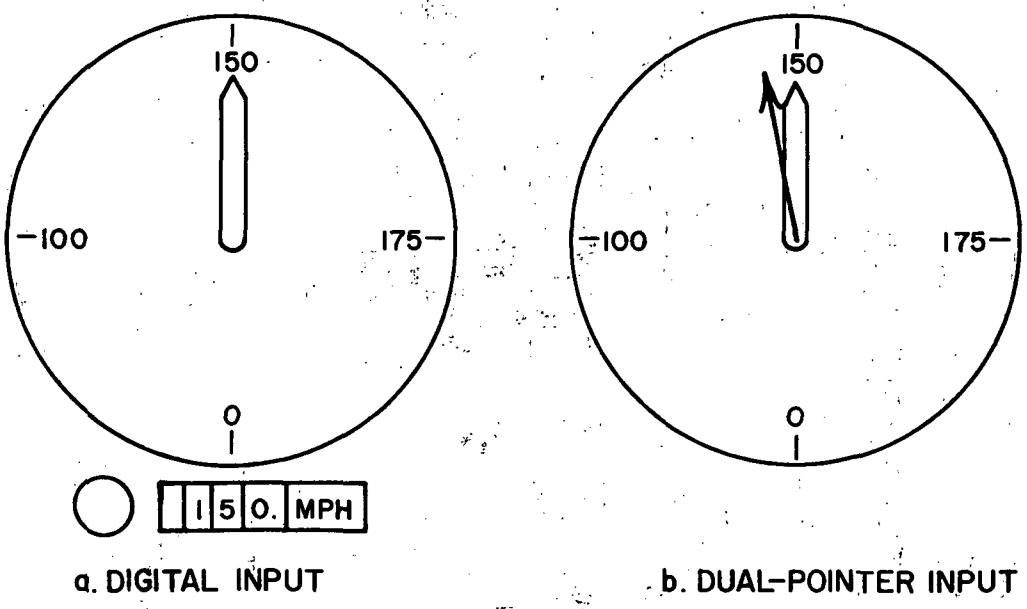

Figure 32. Speed monitor.

MISSION PROFILE

It is assumed that the modified aircraft has the original powerplant (235HP), a constant-speed propeller (85% maximum efficiency), and is equipped with a supercharger to maintain constant output at various altitudes. The wing planform has been changed from a 12% thick airfoil with partial-span, single-slotted flaps to an 18% thick airfoil with a full-span, single-slotted .30c Fowler type flap.

There are four variables, two independent and two dependent. The two independent variables that are controlled by the pilot are rate-of-climb and airspeed. In order to minimize the effects of weight and altitude changes, the airspeed is replaced by a ratio of dynamic pressure to gross weight. The air density changes by 21% from zero to 15,000 feet. However density appears as a square root term in the dynamic pressure-velocity relation, thereby giving a maximum of 4.5% error over the entire range of altitudes. The worst error that would occur by normalizing the relation with respect to weight would be 12% (12% higher velocity reading). This is for sea level conditions. At altitude, the actual velocity would increase, thereby closing the gap between calculated velocity and actual velocity. At the maximum altitude, the error caused by weight normalization would be reduced by 4.5%.

Once the rate of climb and airspeed are specified, then the flap position and throttle setting values are uniquely determined.

The flight profile is broken down into three categories: takeoff (including climb to altitude), cruise, and landing. The control settings for each of these configurations are detailed below.

Takeoff

For takeoff, the aircraft starts at the end of the runway with the flaps retracted (stick pushed all the way forward), full throttle, and brakes on. After the brakes are released, the aircraft rolls down the runway, building up speed, until it reaches 85% of the takeoff velocity. Takeoff velocity is defined as the velocity for level flight at zero angle of attack with the flaps set at 30°. At this point, the pilot pulls back on the yoke, causing the flaps to deflect to 30°. The aircraft will be airborne when the velocity reaches 95 ft/sec. for gross weight and standard sea level conditions. Calculations show that the takeoff roll should take 650 feet with a time of 12.5 seconds. At takeoff, the control settings will be

Rate of climb - ft/min.	950
Throttle	100%
Speed - ft/sec	95
Flaps	30°

Assuming a "straight out" pattern with no maneuvers, the aircraft continues in the configuration until the desired altitude is reached.

Cruise

When the desired altitude is reached, the rate of climb is reduced to zero and the velocity is set at cruise velocity. The various control settings are given below for 100%, 75% and 60% cruise power.

Rate of climb - ft/min.	0	0	0
Throttle	100%	75%	60%
Speed - ft/sec.	215	188	164
Flap setting	10% ret	1.4°	4.3°

Landing

For landing, the pilot enters the pattern at 800 feet. He then sets up his speed and desired rate of descent. The rate of descent will depend on how large a traffic pattern the pilot chooses to fly. The aircraft will continue in the configuration until he reaches the end of the runway, at which time he applies power to bring his rate of descent to zero just as he contacts the runway. Some sample control settings are shown below.

Throttle	20%	30%	40%
Speed - ft/sec.	81	82	85
Rate of climb - ft/min.	-543	-443	-308
Flap setting	30°	34°	36°
L/D	5.94	5.77	5.85

Just before touchdown, the rate of climb should approach zero. This can be accomplished in a number of combinations of flap and throttle settings. One example is shown below.

Throttle	60%
Speed - ft/sec.	95
Rate of climb - ft/min.	0
Flap setting	33°

AERODYNAMICS

INTRODUCTION

In order to achieve constant attitude flight during all modes, it is necessary to change the normal method of operation during takeoff, climb, and landing. The solution to the problem lies in the ability to vary the lift without changing the fuselage pitch angle. The aerodynamic considerations which would effect the modification of an existing aircraft to meet this requirement will be presented here in some detail. In the order considered, they are

1. Lift augmentation at constant fuselage attitude
2. Static balance
3. Direct lift control
4. Lateral control
5. L/D ratios for landing.

Static performance calculations are also presented for the aircraft, with the geometric modifications needed to meet these aerodynamic requirements.

A comparison of the aerodynamic characteristics of conventional aircraft with those of the constant attitude aircraft shows that one major difference exists between the two. This difference is the angle of attack variations with airspeed.

For conventional aircraft, changes in flight speed are accomplished by moving along curve 1 on the plot of life coefficient versus angle of attack as shown in Figure 33. If the flap deflection is increased, the aircraft will operate along curve 2

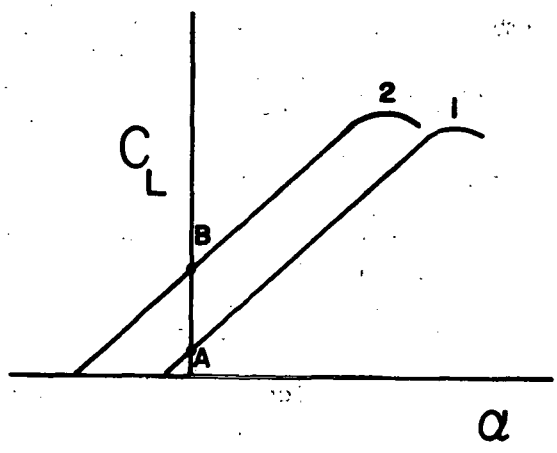

Figure 33. Lift coefficient changes with variation in angle of attack and flap deflection.

with changes in speed. For the constant attitude case, speed changes made at a zero rate of climb occur at a constant angle of attack, i.e., move from point A to B in Figure 33 to decrease speed. This concept of speed changes at constant angle of attack during cruise is easily seen from the following analysis. Assume that the wing is mounted to the fuselage at zero incidence angle. The relationship between flight path angle, angle of attack, and pitch angle is given by

$$\gamma = \theta - \alpha. \tag{51}$$

But for constant attitude flight at $\theta = 0^{\circ}$, this reduces to

$$\gamma = -\alpha. \tag{52}$$

Since the flight path angle is defined as

$$\tan \gamma = \frac{R/C}{U_o} , \tag{53}$$

$$\gamma = -\alpha = \tan^{-1} \frac{R/C}{U_o} ; \tag{54}$$

for small flight path angles this becomes

$$\alpha = \frac{(-R/C)}{U_o} . \tag{55}$$

Thus when rate of climb is zero, changes in forward speed will occur at a constant angle of attack. Another interesting observation can be made from equation (55). The angle of attack is always zero during level flight, positive during descent, and negative during climb. This immediately presents a problem for takeoff at constant attitude. Just prior to lifting off the runway, the aircraft is at zero angle of attack (i.e., rate of climb is zero). As soon as enough lift is generated, the aircraft will leave the runway at a finite rate of climb, causing the angle of attack to decrease. This in turn will reduce the lift and cause the aircraft to fall back to the runway unless enough additional lift is applied by some other means. Hence, it is seen that the takeoff condition is a critical design point; more attention will be given to it later.

Equation (55) also demonstrates the conditions under which the aircraft could be stalled. In order for α to reach a value high enough for stall to occur, the aircraft must be climbing or descending at a very high rate at slow speed. The maximum rate of climb is limited in this case by the engine power, and calculations show that a stall will not occur under climb conditions. The maximum descent rate is limited by the fuselage drag, and for this aircraft, it never exceeds - 1000 ft/min., thereby preventing the aircraft from stalling during descents. The maximum positive angle of attack achieved is 11° with the wing stalling at 16°. The maximum negative angle of attack is 10° with the wing stalling at -14°. Thus, it is seen that as long as the aircraft remains in constant attitude flight, it cannot be stalled. Since it cannot be stalled, it will never go into a spin. From this steady state analysis, this design concept appears to be stall proof and spin proof. Only eventual flight tests can demonstrate whether the pilot will be able to get the aircraft into a stall condition during some transient phase of flight.

A final point pertaining to equation (55): it allows for the determination of the instantaneous value of rate of climb through the measurements of angle of attack and airspeed. Precise tracking by means of rate of climb is not currently possible due to the lack of low cost instruments with sufficient response rates to indicate the rate of climb. Currently, two basic types of instruments are available for rate of climb measurement. The first is a low cost pneumatic device which is standard equipment on general aviation aircraft. However, it has a long response time, making it impractical for precise tracking. The second instrument gives an improved response time by using an integrating accelerometer, but it is too costly for most general aviation applications. Constant attitude flight provides a fast response, low cost rate-of-climb indicator through the measurements of angle of attack and airspeed. This means of tracking can be very important just prior to touchdown during the landing maneuver.

LIFT AUGMENTATION

It is apparent that the major design problem aerodynamically is to achieve enough lift at the negative angles of attack at which the aircraft will be operating. It was originally thought that very high values of C_L at $\alpha = 0^o$ would be needed to take off within the same distance as the original aircraft. A study was undertaken to determine the relation between aircraft C_L and takeoff distance in order to ascertain the size of the lift coefficient needed to make constant attitude flight feasible with current high lift technology. Equation 56, taken from Sanders (Ref. 17), was used to calculate the total takeoff distance over a 50-foot obstacle.

$$S_{T.O.} = S_{roll} + S_{climb\ 50\ ft}$$

$$= \frac{13\ (W/S)}{\sigma\ (C_D - \mu C_L)_{roll}}\ \ell n\ \ 1 + \frac{(C_D - \mu C_L)_{roll}}{(T/W - \mu)\ C_{L_{TO}}} \qquad (56)$$

$$+ \frac{87\ (W/S)\ \ T/W - (C_D/C_L)_{T.O.}}{\sigma\ C_{L_{max}}}\ \ (ft)$$

The distance for takeoff and climb to 50 feet was plotted against lift coefficient with power, wing area, and aspect ratio remaining constant while varying the aircraft weight from 2000 to 2900 lbs. The lower limit was chosen as the minimum take-off weight anticipated for the selected aircraft with pilot, fuel, and radio equipment; the upper weight limit is the maximum at which the FAA has certified the selected aircraft. The power and wing area used is that of the current configuration, with AR = 7.5.

The results of these calculations are shown in Figure 34. From this figure it is seen that under no circumstances would a lift coefficient greater than 3.25 be required for this aircraft; greater lift coefficients would actually increase the takeoff distance because of the increased induced drag in the climb configuration. In order to maintain the takeoff distance for the existing unmodified aircraft, C_L values of around 1.80 can be tolerated. This simple check demonstrates that the lift augmentation required for constant attitude flight is feasible with current high-lift technology.

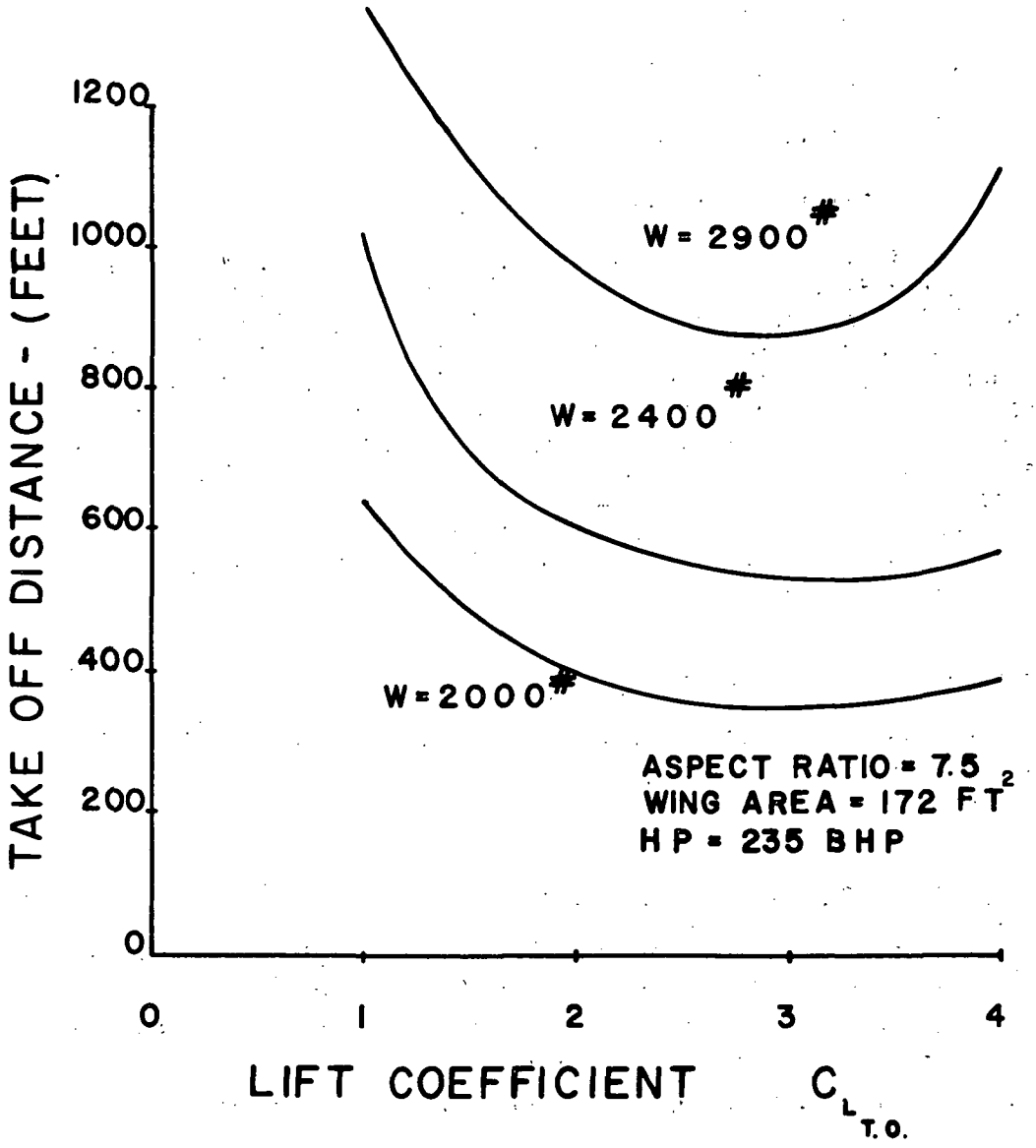

Figure 34. Variation of total takeoff distance with lift coefficient and weight.

A number of methods for achieving the required lift augmentation were examined in relation to the following requirements:

(1) Lift coefficient at zero angle of attack equal to approximately 3.25

(2) Low drag at high lift

(3) Low minimum drag coefficient

(4) Simplicity of structure.

As part of this study, the effects of drag and weight changes on the aircraft were considered. A 20% reduction in weight results in a 40% increase in rate of climb. This same reduction in weight increases the maximum speed by only 2%. Maximum speed is affected primarily by power and drag; varying the drag coefficient by 20% causes a change of 7% in the maximum speed. Changing the aspect ratio from 7.5 to 6.0 reduces the horsepower required for a maximum speed by 10%. A decrease in drag coefficient of 10% reduces the horsepower required for a maximum speed of 200 ft/sec. by 9%. Major emphasis should be placed on "cleaning up" the drag and holding down the weight wherever possible, if performance is to be kept at a high level.

Ducted Propellers to Increase Static Thrust

The ducted propeller was eliminated early in the study because its large size limited its use to a pusher configuration, entailing vast modification to the existing aircraft.

Added Lift from Propeller Slipstream

Additional lift from the propeller slipstream would yield only a $\Delta C_L \simeq .4$. To increase this to a usable quantity for takeoff would require at least a doubling of engine power; because the high thrust is not needed for landing, the ΔC_L resulting from the propeller slipstream would not be available during landing.

Tilting the Wing to Provide Proper Wing Angle of Attack

The lift can be modulated by changes in the wing angle of attack, its camber, its area, or its circulation. The wing angle of attack can only be changed by rotating the wing relative to the fuselage. After some analysis, this approach was discarded due to the weight penalty or the mechanism required to rotate the wing at high aerodynamic load conditions.

Boundary Layer Control by Suction and Blowing

Suction and blowing over trailing-edge flaps were investigated as a means of bleeding off the boundary layer and increasing the circulation around the wing, respectively. The boundary layer control device best suited for light aircraft was found to be the ARADO system [Fisher (Ref. 18)]. Preliminary calculations indicated that this system would require a 20 horsepower auxiliary power unit (APU) and would weigh 150 lbs. The APU would be needed to supply the required air flow throughout the flight profile. This idea was discarded in favor of the simpler and less costly mechanical-flap system.

A Purely Mechanical Flap Configuration

The final configuration examined was full-span, slotted flaps. Slotted flaps increase the lift of an airfoil by an increase in camber and, in some cases, by an increase in chord. The slotted flap delays separation of the flow from the flap by ducting high-energy air from the lower surface and utilizing it to energize the boundary layer on the upper surface of the flap. The important design parameters are flap deflection, flap size, chordwise position of the slot lip, and shape of the passage through which the air must flow.

The full-span, trailing edge, Fowler flap is well suited to this particular design because it can increase the wing's camber as well as its area. Not to be overlooked are the many years of flight experience with these mechanical systems, their reliability, acceptance by the flying population, and the multitude of wind tunnel data and analytical techniques available for specifying their performance. Modulating the lift by means of full-span Fowler flaps was therefore chosen as the basis of this design study.

AIRFOIL SELECTION

With the selection of the means for augmenting the lift during constant attitude flight, the next step was to consider the selection of an airfoil section that would generate the required lift in addition to improving the aircraft performance during cruise. Since the lift coefficient at takeoff condition must be between 1.80 and 3.25, appropriate airfoils equipped with full-span flaps were examined. In addition to the lift requirement, it was felt that the wing section should exhibit good stall characteristics to insure that the aircraft would give adequate stall warning in the event of a system failure.

Full-span flaps could be expected to yield lift coefficient increments between 1.5 and 2.0 for a 30° flap deflection. Abbott and von Doenhoff (Ref. 19) was consulted to find all airfoils that could give section lift coefficients of .3 or greater at $\alpha = 0^{\circ}$ as well as exhibiting good stall characteristics. This selection criteria yielded 42 airfoils for further detailed examination.

Young (Ref. 20) and Hoak and Ellison (Ref. 2) were used to convert the 2-D section data as listed in Abbott and von Doenhoff to data for 3-D wings equipped with full-span flaps. This method is outlined below.

For 2-D data, the increment in C_{ℓ} for flap deflection is shown in Hoak and Ellison to be

$$\Delta C_{\ell} = -C_{\ell_{\alpha}} \alpha_{\delta} \delta_f \tag{57}$$

where $C_{\ell_{\alpha}}$ = 2-D lift curve slope per degree

α_{δ} = lift effectiveness parameter found in Figure 35

δ_f = flap deflection in degrees.

This is converted to 3-D data by use of the relation

$$\Delta C_L = \Delta C_{\ell} \frac{C_{L_{\alpha}}}{C_{\ell_{\alpha}}} \frac{(\alpha\delta)C_L}{(\alpha\delta)C_{\ell}} K_b \tag{58}$$

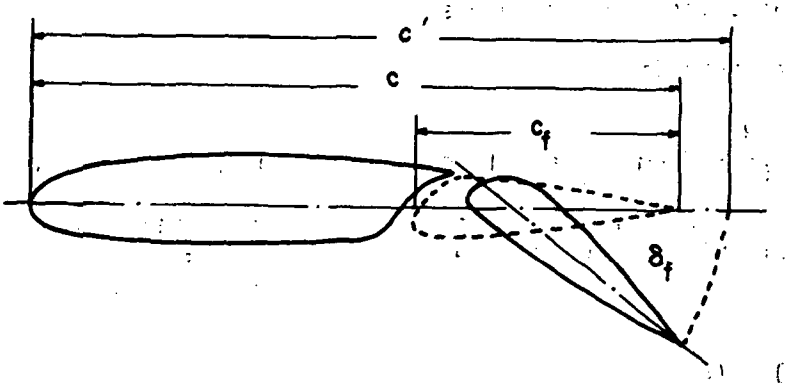

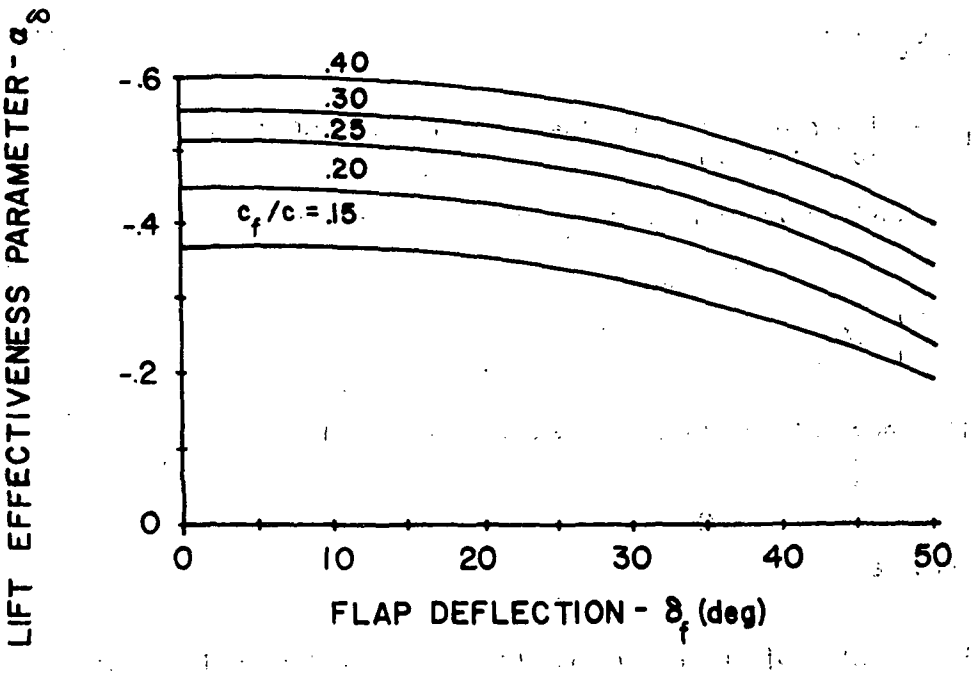

Figure 35. Section lift effectiveness parameter of single-slotted flaps (Ref. 21).

where C_{L_α} = 3-D lift curve slope per degree

$\frac{(\alpha\delta)C_L}{(\alpha\delta)C_\ell}$ = ratio of 3-D flap effectiveness parameter to the 2-D flap effectiveness parameter

K_b = flap span factor.

The terms $\frac{(\alpha\delta)C_L}{(\alpha\delta)C_\ell}$ and K_b are found in Hoak and Ellison (1970) and have the value of 1.035 and 1.0 respectively. Therefore, the complete equation for determining the increment in C_L for a flapped airfoil is,

$$\Delta C_L = -1.035\ (\alpha_\delta)(\delta_f)(C_{L_\alpha})\ . \tag{59}$$

Young suggests that a correction be made to the lift curve slope in the above relation when using flaps that extend the chord such as Fowler flaps. For nonextending chord flaps, the total C_L is

$$C_L = C_{L_w} + \Delta C_L \tag{60}$$

where C_{L_w} = life coefficient of the basic wing based on C_{L_α} of the basic wing.

Taking the derivative with respect to α on both sides,

$$\frac{dC_L}{d\alpha} = \frac{d}{d\alpha}(C_{L_w} + \Delta C_L). \tag{61}$$

For a flap that extends the chord such as the Fowler flap, Young shows

$$\frac{dC_L}{d\alpha}_{\text{Fowler}} = c'/c \frac{dC_L}{d\alpha} \tag{62}$$

where c'/c = ratio of the effective wing chord to the chord of the basic airfoil section as shown in Figure 35.

Integration yields

$$C_{L_{Fowler}} = c'/c\ C_L + k. \tag{63}$$

In order to evaluate the constant k, it is helpful to look at a C_L vs. α curve for Fowler flaps and non-extending chord flaps (Figure 36).

From this figure, it is evident that when $C_L = 0$ for the non-extending chord flaps, then $C_{L_{Fowler}} = 0$. Thus, $k = 0$. Hence,

$$C_{L_{Fowler}} = c'/c\ C_L = c'/c\ (C_{L_w} + \Delta C_L)$$

$$C_{L_{Fowler}} = c'/c\ \left(C_{L_\alpha} \frac{(\alpha - \alpha_{ZL})}{57.3} + \frac{1.035 \cdot \alpha\delta \cdot \delta_F \cdot C_{L_\alpha}}{57.3}\right)$$

$$C_{L_{Fowler}} = c'/c\ C_{L_\alpha} \left(\frac{\alpha - \alpha_{ZL}}{57.3} + \frac{1.035 \cdot \alpha\delta \cdot \delta_F}{57.3}\right) \tag{64}$$

where α_{ZL} = angle of zero lift.

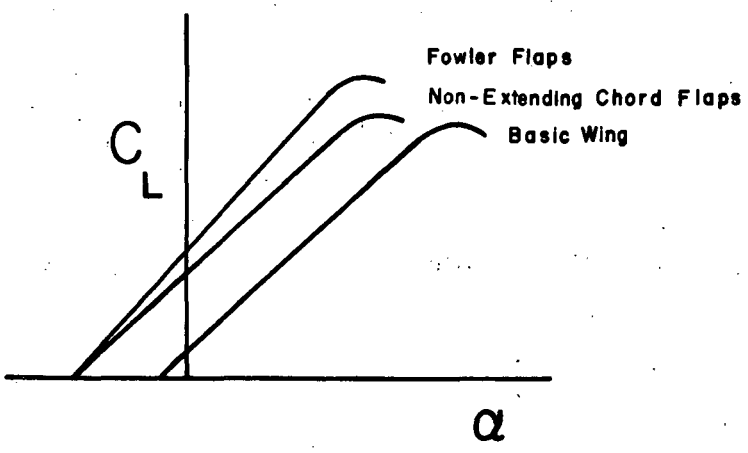

Figure 36. Lift curve slope variation with flap devices.

Thus, if C_{L_α} is corrected by c'/c, the lift coefficient due to flaps that extend the chord, such as Fowler flaps, will be obtained.

In order to be conservative and to provide a better fit to known wind tunnel data, such as that found in Cahill (Ref. 22) and Lowry (Ref. 23), the value of the constant in the above equation has been decreased from 1.035 to .960. Thus,

$$C_{L_{Fowler}} = c'/c \; C_{L_\alpha} \frac{\alpha - \alpha_{ZL}}{57.3} + \frac{.960 \cdot \alpha_\delta \cdot \delta_F}{57.3} \tag{65}$$

For an airfoil with a .30C Fowler flap, c'/c is approximately 1.28 (see Table 2 in Young). In terms of flap deflection, c'/c can be expressed as

$$c'/c = 1 + (.007)(\delta_F). \tag{66}$$

For the single-slotted flap, a c'/c = 1 is normally used since it extends the chord only slightly over a 40^o deflection range.

To determine the increment in profile drag coefficient, the method found in Young was used. This relation is

$$\Delta C_{d_o} = \delta_1(c_f/c) \; \delta_2(\delta_F) \tag{67}$$

where δ_1 and δ_2 are functions determined from experimental data and are shown in Figure 37.

For the pitching moment coefficient, Young suggests that a good approximation is

$$\Delta C_m = -.34 \; (\Delta C_L) \text{ single-slotted flaps}$$
$$\Delta C_m = -.43 \; (\Delta C_L) \text{ Fowler flaps.} \tag{68}$$

This difference in pitching moment coefficient increment suggests that the severe pitching moments common with Fowler flaps may cause undue static stability requirements. Therefore, single-slotted flaps were analyzed along with the Fowler flaps such that a trade-off study could be made based on the advantages and disadvantages of the two.

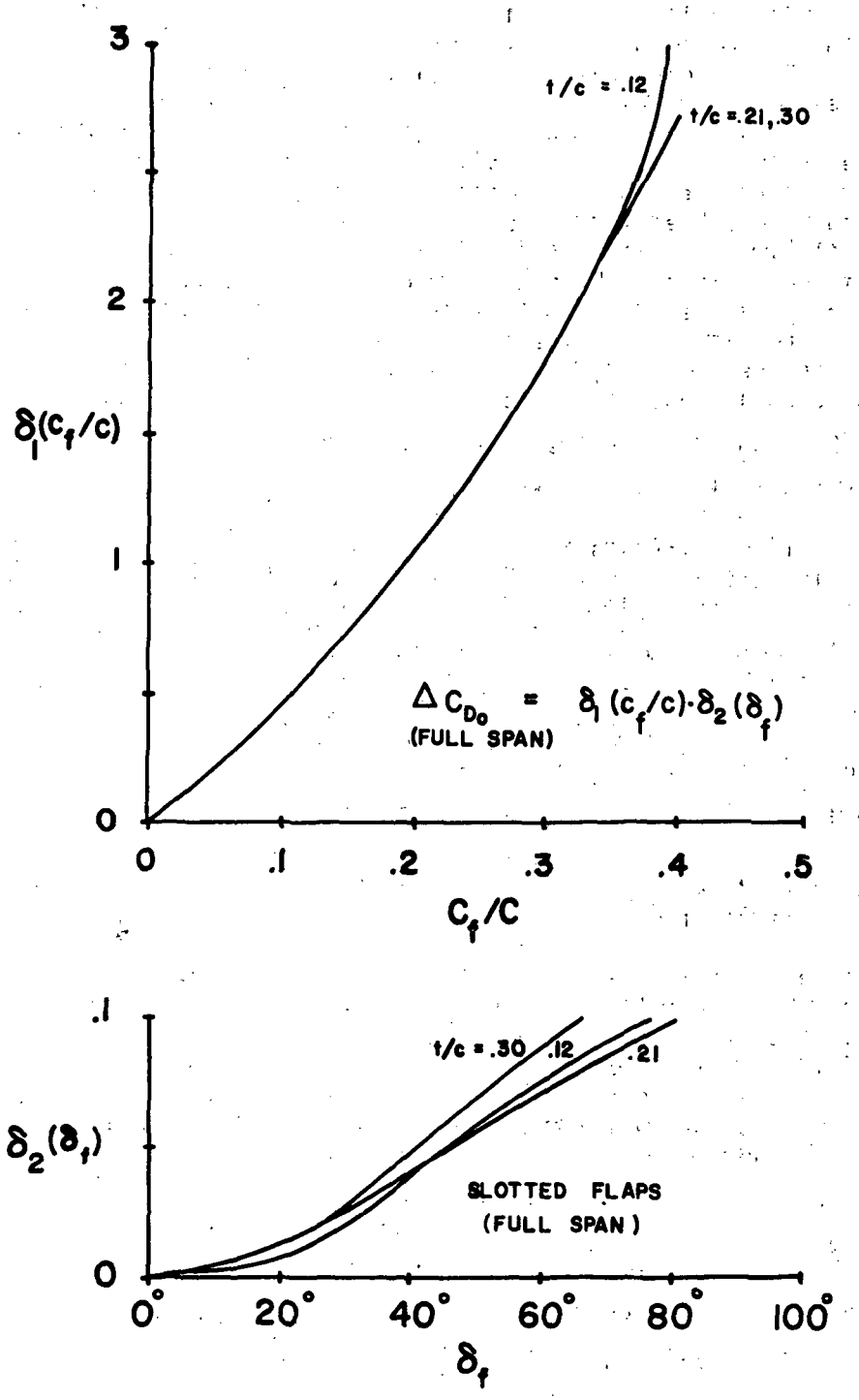

Figure 37. The function $\delta_1(c_f/c)$ and $\delta_2(\delta_f)$ for slotted flaps (Ref. 20)

With these analytical expressions for converting section data into flapped-wing data established, each of the 42 airfoils was examined for its lift and drag characteristics with a single-slotted flap applied, then with a Fowler flap applied to the wing. When the section data were taken from Reference 19, standard roughness at Reynolds number six million was assumed. Standard roughness was assumed in order to give a worst case analysis in performance. This will also ease the tolerances to which the wing must be built and should give better performance than the analysis predicts since the drag on production aircraft is rarely as high as standard roughness predicts. After the production routine has been established, tolerances can then be tightened to improve the performance further. The mechanism of the flap track for the Fowler flap is assumed to deflect the flap as it extends it, in much the same way as for the NACA single-slotted flap, except that it extends the chord by 28%. The criteria used to select the desired airfoil were (1) cruise C_L = .42, (2) takeoff value of C_LS = 290, and (3) minimize the cruise value of C_DS. The reason for criterion (1) will become apparent later.

Ten of the airfoils examined are listed in Table 17. Included in this list are the 23012, which had at one time been considered for this application, the 65_2-415, which is currently on the PA28-235C, two of the more commonly used airfoils, the 2412 and the 4412, along with six of the best airfoils examined. Two observations are readily made from Table 17. First, the Fowler flap gives a substantial reduction in the wing area required for takeoff, leading to a smaller value of C_DS and hence increasing performance; secondly, the smallest wing area and C_DS value is obtained for the 63_3-618 airfoil. Therefore, this airfoil with a full-span Fowler flap was selected to replace the existing wing on the PA28-235. The lift and drag coefficients for the 63_3-618 at AR = 8 are given in Figure 38.

Table 17 shows that the wing area may be reduced to 152.3 sq. ft. For these calculations, the wing area was reduced by decreasing the chord to 4.76 ft. The wing span was left at its original value of 32 ft. in order to preserve the necessary storage space for fuel tanks, flap actuators, and aileron actuators. This changed the aspect ratio to 6.7 which would increase the lift curve slope, giving a higher value of C_L at takeoff, and thereby allow a further reduction in wing area in order to keep the takeoff value of C_LS at 290. However, this wing area proved to be too large for the desired cruise performance (minimum C_LS too large). The cruise value of C_L for the PA28-235C is equal to .31. Because of the downlift of the tail, a wing C_L = .42 is required in order to generate a total airplane C_L of .31. For this reason, all of the

TABLE 17. COMPARISON OF DIFFERENT AIRFOILS EQUIPPED WITH SINGLE-SLOTTED AND FOWLER FLAPS

	SINGLE-SLOTTED FLAPS				FOWLER FLAPS			
SECTION	$C_{D_{cruise}}$	$\delta_{F_{cruise}}$	$C_D S_{cruise}$	S	$C_{D_{cruise}}$	$\delta_{F_{cruise}}$	$C_D S_{cruise}$	S
63_3-618	.02279	2.0	4.20	184.3	.02278	1.9	3.47	152.3
23012	.02397	7.2	5.48	228.6	.02392	6.8	4.52	188.9
65_2-415	.02274	4.7	4.70	206.6	.02261	4.4	3.86	170.7
63_4-421	.02516	3.8	4.85	192.7	.02506	3.6	3.99	159.2
64_3-618	.02305	2.1	4.30	186.6	.02304	2.0	3.56	154.2
65_3-618	.02354	2.1	4.52	192.0	.02350	2.0	3.73	158.7
2412	.02322	6.2	5.19	223.3	.02302	5.8	4.25	184.6
4412	.02181	2.8	4.39	201.1	.02175	2.7	3.65	166.2
63_1-412	.02200	3.9	4.32	196.3	.02198	3.7	3.57	162.2
63_2-615	.02357	2.4	4.42	187.5	.02355	2.3	3.66	155.0

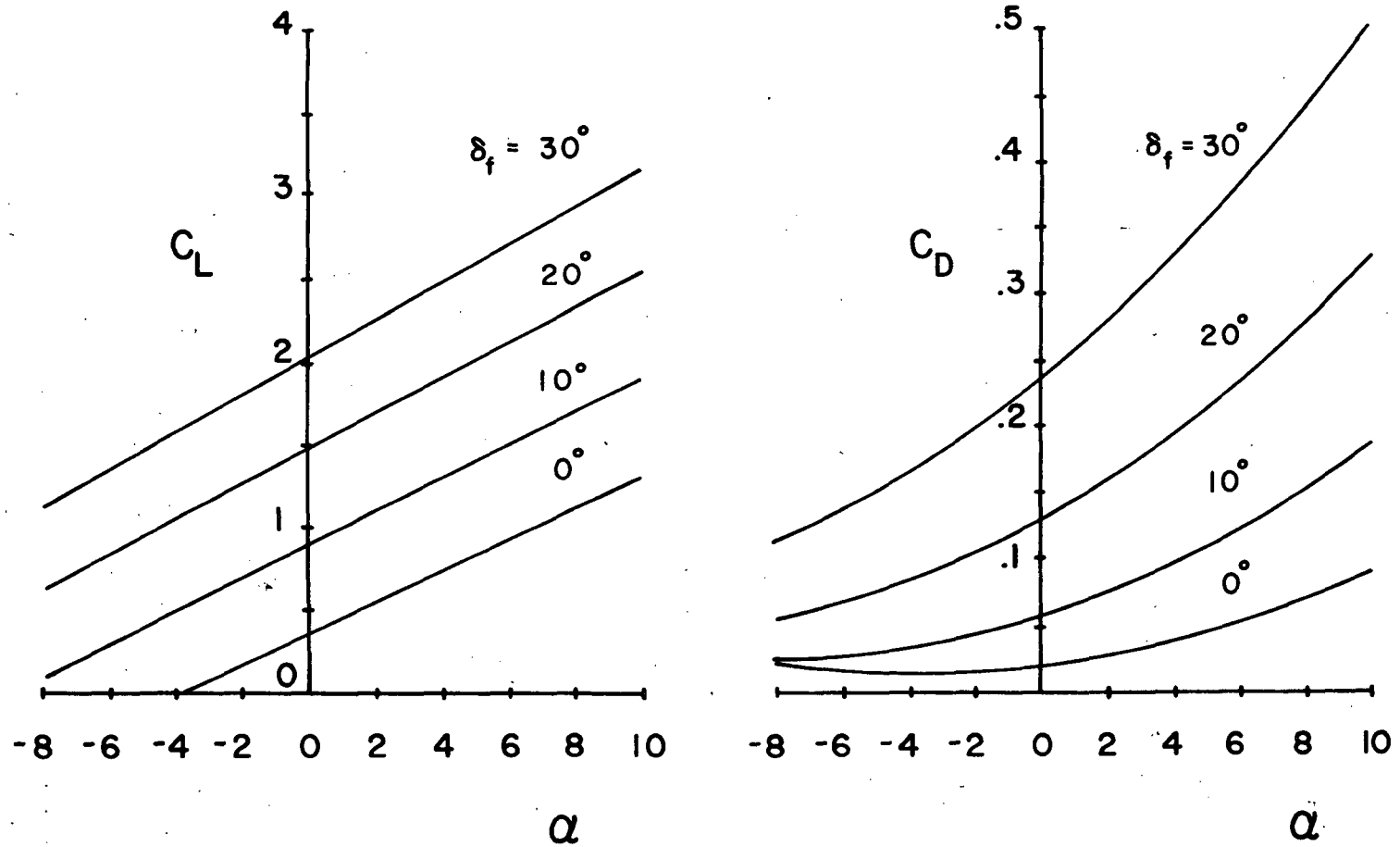

Figure 38. Aerodynamic characterisitcs for the 63_3-618 wing with full-span Fowler flap, AR = 8, Re = 6 x 10^6, standard roughness assumed.

airfoils were compared at a cruise value of C_L = .42. However, with the modification contemplated, a wing C_L = .42 gives a total airplane C_L = .417 (because of the reduced static margin). Therefore, in order to attain the desired cruise performance,* the wing area was reduced to 128 sq ft. at a slight penalty in takeoff performance. The increase in takeoff speed was from 63.6 to 67 mph. Since the current PA28-235C takes off at approximately 65 mph, this increase in takeoff speed was not considered significant.

---

*Minimum wing C_L is that C_L obtained for $\alpha = 0$, $\delta_F = 0$. There is thus a maximum speed for a given S and W above which the aircraft will begin a pullup. Higher speeds can therefore be obtained with a particular airfoil and incidence angle only by reducing wing area.

STATIC PERFORMANCE

The selection of full-span Fowler flaps for the high lift devices greatly increases the pitching moment, causing static stability problems. The major cause for this increased pitching moment was due to changing the flap span from a partial span (.45b/2) on the unmodified aircraft to full span on the modified version. This one factor caused a doubling of the pitching moment, since the wing planform is rectangular. The selection of Fowler flaps over single-slotted flaps also contributed to increased moments. In addition to these two geometric modifications, the original aircraft had a minimum static margin of 30% and was placarded for weights less than 2100 lbs. Since it was felt that the aircraft should be able to fly at dry weight plus a light female pilot, the minimum weight for this design was taken at 1625 lbs, further complicating the static stability problem. These three contributions to pitching moment require the tail effectiveness to be increased by 240% over the original aircraft.

Since it is not desirable to make the tail area too large because of high drag and down lift at the forward CG location, it was decided that the best approach would be to make moderate increases in the tail area as well as the tail length and tail airfoil section. The wing position on the fuselage was also changed to give a better static balance. The criteria for determining the wing-to-fuselage mounting position are shown below.

1. Structural Consideration

   a. Preferred location of wing L.E. from datum (taken from the propeller tip) 85.6 in. to 98.7 in., most desirable 90.4 in. This position would allow the use of the existing spar mount.

   b. Less desirable location from datum 55.6 in. to 73.6 in., most desirable in this range 64.6 in.

2. Aerodynamic and Stability considerations

   a. Minimum static margin $\geq$ 5%

   b. Incidence angle of horizontal tail within $\pm$ 18°

   c. Tail angle of attack $\leq$ 14°

d. V_{cruise} at gross weight $\geq$ 145 mph

e. $S_{horizontal\ tail} \leq 31$ sq ft.

An acceptable combination was finally arrived at after a lengthy trial and error process. The wing was moved forward by 14 in. and the tail length was increased by 3.3 ft. The horizontal tail airfoil section was changed from 0009 to 0012, increasing the angle of attack range from 13° to 16°. Finally, the horizontal tail area was increased by 4.5 sq ft to 31.0 sq ft.

These geometric changes developed one additional problem--the location of the landing gear. In order to make the aircraft rotate onto the nose gear after touchdown, the gear position would have to be located in the flap tracks due to the decrease in wing chord and the new wing position on the fuselage. Since this was certainly not a feasible solution, the landing gear design was changed, mounting it on the fuselage. The final geometric configuration is shown in Figure 39. Table 18 lists the geometric details required for aerodynamic performance and stability derivative calculations. Table 19 shows the final weight and balance distribution.

The concept for the lift augmentation system requires very fast flaps positioned by power servos. These fast acting flap servos are ideally suited to move the flaps differentially as ailerons, yielding extremely high amounts of aileron control power. This approach will simplify the wing structure, since spoilers would have been the most logical choice for a separate lateral control system. This will also eliminate the requirement for a separate actuation device. These full-span Fowler ailerons yield 3-1/2 times the aileron power normally found on aircraft in this class, in addition to large amounts of adverse yaw. However, adverse yaw is not a major problem, since the aircraft is equipped with a turn coordinator which can also be made to act as a yaw damper to augment the dynamic stability.

The propeller on the original PA28-235C is 80 in. in diameter, 2-blades, with constant speed control. Data from Hartman and Biermann (Ref. 24) were used to calculate the power available from the 235 bhp engine-propeller combination. From these calculations, it appeared that the propeller diameter on the original aircraft was selected to maximize available horsepower at maximum cruise speed. Since V_{max} is rarely flown, a more suitable criterion would be to maximize the available horsepower over the widest ranges of useful speeds, i.e., in the range of maximum climb speed and 75% cruise speed. Figure 40, representing the 75% cruise power

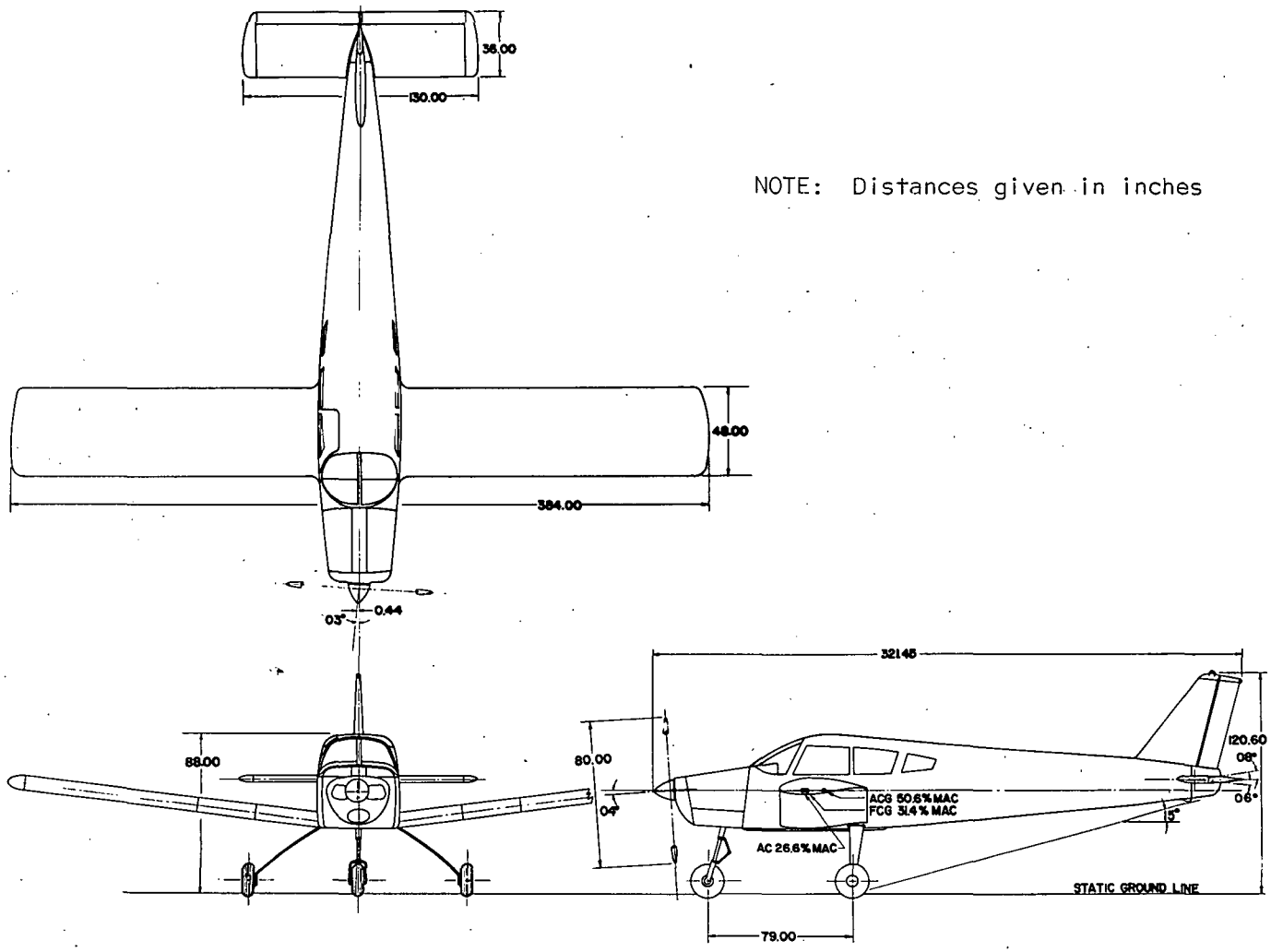

NOTE: Distances given in inches

Figure 39. Three-view of modified PA28-235C.

TABLE 18. GEOMETRIC DESCRIPTION OF THE MODIFIED PA28-235C

Wing section	63_3-618
Wing area (ft^2)	128.0
Wing span (ft)	32.0
Wing Chord (ft)	4.0
Wing aspect ratio	8.0
Wing taper ratio	1.0
Wing incidence angle (deg)	0.0
Wing dihedral (deg)	7.0
Flap Span (one side) (ft)	13.5
Flap chord (ft)	1.2
Aileron span (one side) (ft)	13.5
Aileron chord (ft)	1.2
Rudder section	0009
Vertical tail area (ft^2)	11.6
Rudder area (ft^2)	4.1
Fin area (ft^2)	7.5
Vertical tail span (ft)	4.3
Horizontal tail section	0012
Horizontal tail area (ft^2)	31.0
Horizontal tail span (ft)	10.8
Horizontal tail chord (ft)	3.0
Horizontal tail aspect ratio	3.6
Horizontal tail taper ratio	1.0
Efficiency factor for horizontal tail and vertical tail	.9
C_{L_α} (1/rad): Wing ($\delta_f = 0^o$)	5.4
Horizontal tail	4.3
Vertical tail	2.8
Fuselage volume (ft^3)	226.0
Fuselage length (ft)	24.9
Fuselage width (ft)	4.3
Fuselage body side area (ft^2)	72.4
Fuselage height: at 1/4 fuselage length from nose (ft)	4.17
at 3/4 fuselage length from nose (ft)	3.54
at wing body intersection (ft)	4.33
Fuselage radius in vicinity of vertical tail (ft)	.7
Length from CG to tail quarter chord (ft)	17.9 FOR, 17.2 AFT
Length from CG to wing AC (ft)	.2 FOR, 1.0 AFT
Length from CG to vertical tail AC (ft)	17.2 FOR, 16.5 AFT
Length from nose to wing AC (ft)	6.86
Height from body centerline to vertical tail AC (ft)	2.8

TABLE 19. WEIGHT AND BALANCE FOR THE MODIFIED PA28-235C

Item #	Weight	Designation	In. Aft of Datum	Moment # in.
1	383.8	Engine	28.4	10,900
2	299.0	Fuselage	114.0	34,086
3	504.0	Wing	88.8	44,755
4	55.0	Horizontal Tail	289.6	15,928
5	30.0	Vertical Tail	305.6	9,168
6	19.4	Engine Acces.	32.6	633
7	3.5	Prop. Spinner	8.0	28
8	56.0	Prop	8.7	486
9 a	12.5	Nose Gear	35.4	443
9 b	33.9	Main Gear	93.6	3,173
10	22.2	Elec. Equip.	164.7	3,657
11	4.2	Std. Inst.	66.4	279
12	7.0	Prop. Access	24.7	173
13	10.5	Engine Access	48.5	510
14	7.7	Opt. Elec. Equip.	162.3	1,250
15	14.7	Opt. Inst.	64.8	953
16	5.1	Radio	150.4	767
17	23.3	Misc. Equip.	80.4	1,873
18	22.5	Oil	34.1	767
19	340.0	Pilot & Front Pssg.	85.5	29,070
20	340.0	Rear Pssg's.	118.1	40,154
21	492.0	Fuel - 84 Gal.	88.8	43,690
22	200.0	Baggage	142.8	28,560
TOTALS;	2,886.3			271,303

condition, shows that the power available curves fall off rapidly at speeds less than design speed and fall off slowly at speeds higher than design speed. A careful analysis of these curves shows that the maximum rate of climb can be increased by 70 ft/min. by the proper selection of design speed. Several design speeds were tried for two and three-blade propellers with 85 in., two-blade propeller and the 79 in., three-blade propeller giving the best climb and cruise performance. Since ground clearance is critical for this aircraft, the shorter three-blade propeller was chosen for the modified aircraft.

Performance calculations do not require a detailed knowledge of component drag, just the total drag and its variation with angle of attack. In order to determine the drag polar for this configuration, the basic performance data published in the Piper owner's manual were used.

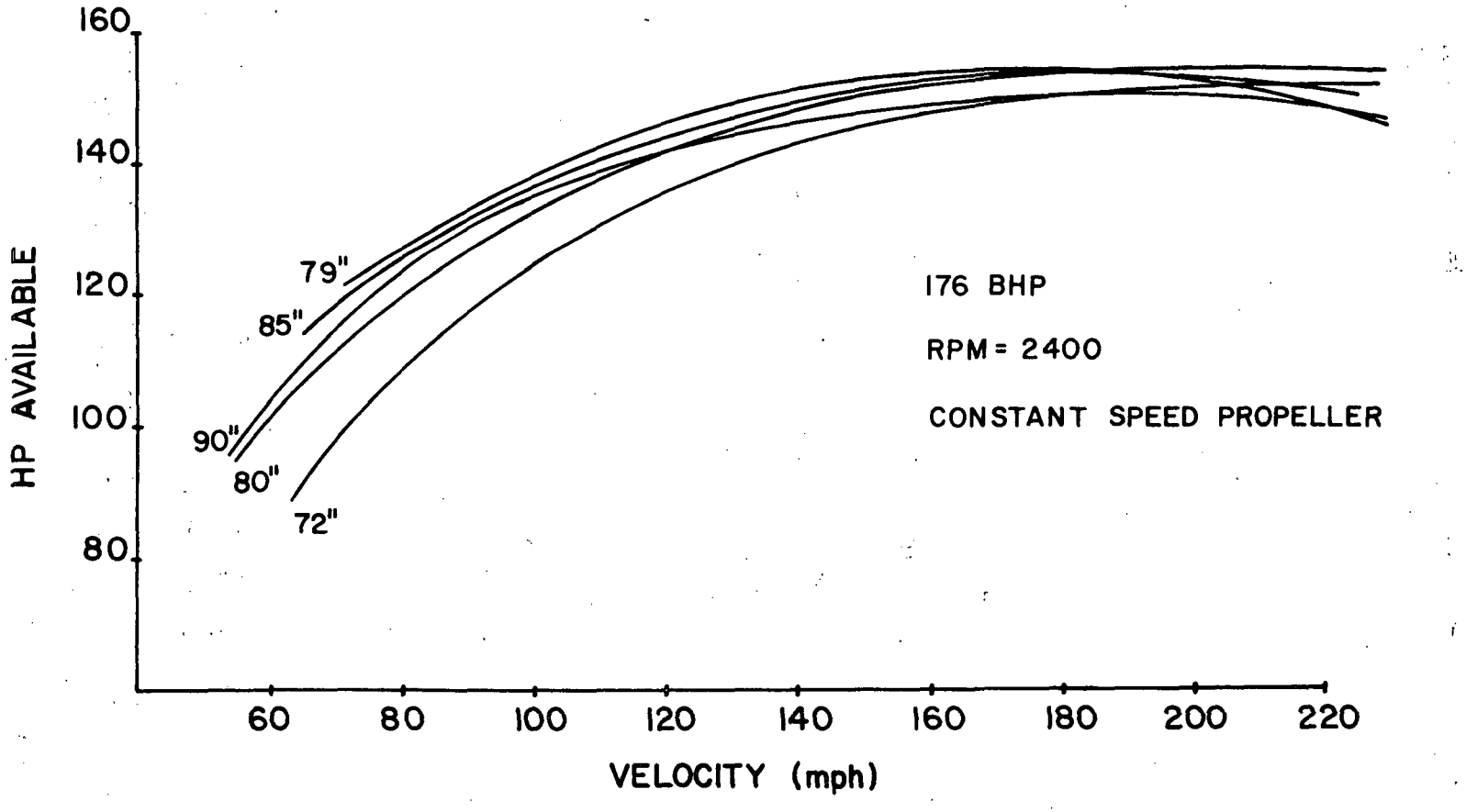

Figure 40. Comparison of power available with variation in propeller diameter (79 in. propeller has 3 blades, all others have 2 blades).

The speed at 75% cruise power is 214 ft/sec. Since required power equals available power at this zero rate of climb condition,

$$HP_{req} = \frac{DU_o}{550} = HP_{av} = 146 \tag{69}$$

$$D = 375.9 \text{ lbs} \tag{70}$$

$$C_D = \frac{2D}{\rho U_o^2 S} = .04009 \tag{71}$$

where S = wing area = 172 ft^2

D = total aircraft drag

$$C_D = (C_D)_{wing} + (C_D)_{parasite} \tag{72}$$

For the 65_2-415 airfoil* at cruise

$$(C_D)_{wing} = C_{d_o} + \frac{C_L^2}{\pi ARe} \tag{73}$$

$$(C_D)_{wing} = .01050 + \frac{(.31)^2}{6\pi(.9)} = .01616 \tag{74}$$

$$(C_D)_{parasite} = .02393 \tag{75}$$

where e = span efficiency factor

AR = aspect ratio.

For conventional aircraft, only the fuselage frontal area is moving into the wind during climbs. However, for constant attitude flight, the entire planform area is seen by the wind and must be accounted for in the drag analysis.

The parasite drag coefficient is primarily made up of the fuselage, landing gear, and empennage components. That is

---

* See Reference 19.

$$(C_D S)_{parasite} = (C_{D_\pi})_{FLG} \cdot F + (C_{D_\pi})_E \cdot S = 4.11596 \quad (76)$$

where $(C_{D_\pi})_{FLG} = .18$ = drag coefficient of fuselage and landing gear based on fuselage cross section,

$(C_{D_\pi})_E = .0025$ = drag coefficient of empennage based on wing area,

$F = 20.4\ ft^2$ = fuselage cross sectional area.

To account for the planform drag due to the fuselage during climb and descent, the product of $(C_{D_\pi})_{FLG} F$ is corrected by the following relation

$$(C_{D_\pi})_{FLG} \cdot (F \cos \alpha + A \mid \sin \alpha \mid) \quad (77)$$

where A = planform area of the fuselage = $60\ ft^2$.

Since for small angles $\cos \alpha \simeq 1$ and $\sin \alpha \simeq \alpha$, equation (77) reduces to

$$(C_{D_\pi})_{FLG} \cdot (F + A \mid \alpha \mid) . \quad (78)$$

After referencing this to wing area, the parasite drag coefficient is seen to be

$$(C_D)_{parasite} = \frac{(C_{D_\pi})_{FLG}}{172} (20.4 + 60 \mid \alpha \mid) + (C_{D_\pi})_E \quad (79)$$

$$(C_D S)_{parasite} = .06302 \mid \alpha \mid + .02394 \quad (80)$$

To base this relation on the new wing area of $128\ ft^2$, multiply equation (80) by the ratio 172/128, which yields

$$(C_D)_{parasite} = .06302 \mid \alpha \mid \frac{172}{128} + .02394 \frac{172}{128} . \quad (81)$$

Finally, the total aircraft drag coefficient based on a wing area of 128 ft^2 is

$$C_D = .08469 \mid \alpha \mid + .03215 + (C_D)_{wing} \qquad (82)$$

which is the drag polar used for the aircraft.

The usual performance calculations were performed utilizing standard methods such as those found in Dommasch (Ref. 25). Calculations were made to specify the aircraft performance over its entire flight profile for use in structural and dynamic stability analysis. In order to present the results of this multitude of data in a compact form, a performance map was drawn by plotting flap deflection, speed, rate of climb, and percent of maximum horsepower on the same graph. This plot yielded the performance for one weight and altitude. An attempt was made to normalize the curves such that one curve could be used to represent the performance over all weight and altitude conditions. The results of this effort are presented in Figure 2. This normalization was not completely successful, however, causing large errors in percent hp at low weights, but it does give a reasonable representation throughout the most useful payloads range (2300-2900 lbs). In any event, it demonstrates the trends well and proved useful in conceptual analysis of the control system.

The usual performance specifications found in the aircraft owner's manual are presented in Table 20 for the maximum weight condition (2900 lbs). In addition to the calculations for the modified aircraft, these same calculations were made for the original aircraft and compared to the published data. The close agreement between the calculated and published figures for the original aircraft lends credence to the accuracy of the calculations for the modified version.

TABLE 20. PERFORMANCE COMPARISON BETWEEN THE PA28-235C AIRCRAFT AND THE MODIFIED PA28-235C

	PIPER		NCSU
	Published	Calculated	63_3-618 Section
Cruising Speed (75% power, sea level, mph)	145	144	151
Cruising Speed (75% sea level power, 7000 ft, mph)	154	150	161
Maximum Speed (sea level, mph)	164	165	158
Maximum Speed (7000 ft, mph, sea level power)	-	174	176
Rate of Climb (fpm, sea level)	900	917	829
Takeoff Speed (mph, sea level)	65	65	67
Landing Speed (mph, sea level)	65	65	60
Takeoff Run (ft, sea level)	810	-	562
Takeoff Distance over a 50 ft obstacle (ft, sea level)	1350	-	1288
Landing run (ft, sea level)	680	-	756
Landing Distance over a 50 ft obstacle (ft, sea level)	1300	-	1381

DIRECT LIFT CONTROL

Elimination of the pitch degree of freedom is analogous to the use of direct lift control. Because the constant attitude aircraft was to operate in this fashion the literature was reviewed for indications of the special characteristics of this type of flight control. DLC has the potential to greatly increase the visibility from the cockpit during the landing and takeoff phases of flight, to eliminate the need to flare, to simplify the landing task, and to eliminate the possibility of stalls. If these advantages can be realized, DLC not only simplifies the task of piloting, but also greatly enhances the operational safety of the aircraft, assuming, of course, that the automatic systems are reliable.

Work in the field of direct lift control (DLC) historically has concerned itself with rapid and precise adjustments of altitude during the landing mode. This capability can be extended, perhaps, to the entire flight regime to allow the aircraft to make all maneuvers by using DLC while keeping the fuselage pitch angle level with the horizon at all times.

Direct lift control is a method whereby the pilot has direct control of the lift on the airplane through the control of flaps, spoilers, ailerons, boundary layer control devices, or thrust deflection or vectoring devices, instead of depending on rotating the entire airplane in pitch to change lift. Wind tunnel and flight testing in this area has been devoted primarily to research on partial-span, trailing-edge flaps as a means of achieving DLC. For the modified aircraft under consideration, implementation of DLC would be achieved by use of full-span, trailing-edge flaps.

For the constant attitude aircraft, all variations in lift should be made by changing the flap setting of the wing while maintaining a constant fuselage pitch angle. In order to accomplish constant attitude flight while changing the lift vector, some means of activating the stabilator must be installed in order to compensate for the changes in pitching moment for each subsequent change in lift. Two means of accomplishing this result are readily apparent. The first consists of a single degree of freedom gyro which would detect any variation of pitch from the zero reference position. Once the deviation is sensed, a servo would be actuated that would position the stabilator so that the fuselage pitch angle returns to zero. The second method involves a horizontal, tail-to-flap interconnect that would cancel the pitching moment caused by any changes in lift. This interconnect would cause a signal to be sent to the stabilator when the flap-position control is moved. This system would require a shaping of the signal so that a given amount of flap deflection would require a particular setting for the stabilator.

Several tests conducted by NASA and LTV have used the second method. In these tests, the horizontal, tail-to-flap interconnect utilized direct current so that the signal could be properly shaped, as determined from wind tunnel tests. These tests, however, were conducted during landing only, with the aircraft speed varying only $\pm$ 5 ft/sec. This wide range of speeds could possibly cause some difficulty in shaping a proper signal for a range of CG locations and varying altitudes.

Testing of a DLC configuration on the F-8 pointed out another possible problem in this area. The F-8 utilizes partial-span flaps and drooped ailerons with the DLC idea being applied to the drooped ailerons. The first wind tunnel test determined that the incremental effect of aileron droop position on airplane pitching moment coefficient was non-linear, with the inboard flap deflected 20°. To build an interconnect of horizontal tail with aileron droop position that would exactly cancel the non-linear pitching moment increment with the inboard flap at 20° would be too complex and costly for the airplane under consideration. Analysis indicated that the non-linearity could be reduced by repositioning the inboard flap so that the deflections of the inboard flap and the aileron would not coincide with the DLC authority range. A second wind tunnel test confirmed that, by repositioning the inboard flap to 40°, the incremental effect was more compatible to the programming of a horizontal tail interconnect. Figure 41 shows the comparison of the interconnect requirements for the 20° and 40° inboard flap positions with an airplane CG location of 27% of the wing mean geometric chord. More forward CG locations would require more horizontal tail interconnect and vice versa. Interconnect can be achieved by optimizing for the most forward CG expected during landing. Analyses indicate that, if this is done, interconnect may be satisfactory for the other CG locations encountered. This is based on pilot reports that slightly overcompensating the pitching moment is better than undercompensating it.

Of the above-mentioned methods, the second system seems to have more disadvantages than the first; however, it must be noted that the second system has been tested and flown, and the pitfalls are now known, whereas the first system has not been tested. Thus, a thorough analysis of the gyrostabilizer system needs to be conducted.

Tests on DLC aircraft currently being flown indicate a need for rapid deflection rates of DLC surfaces during landing, so that quick and precise altitude changes can be made. Flap actuator rates for the aircraft tested are on the order of 40 deg/sec over a range of 30° deflection angle. Likewise, the horizontal tail actuation rates must be rapid to prevent any lag in the positioning of the elevator to cancel any pitching moments. In tests of the F-8, the horizontal tail had an original trim actuator maximum rate of 1.9 deg/sec, which caused it to lag behind the flap

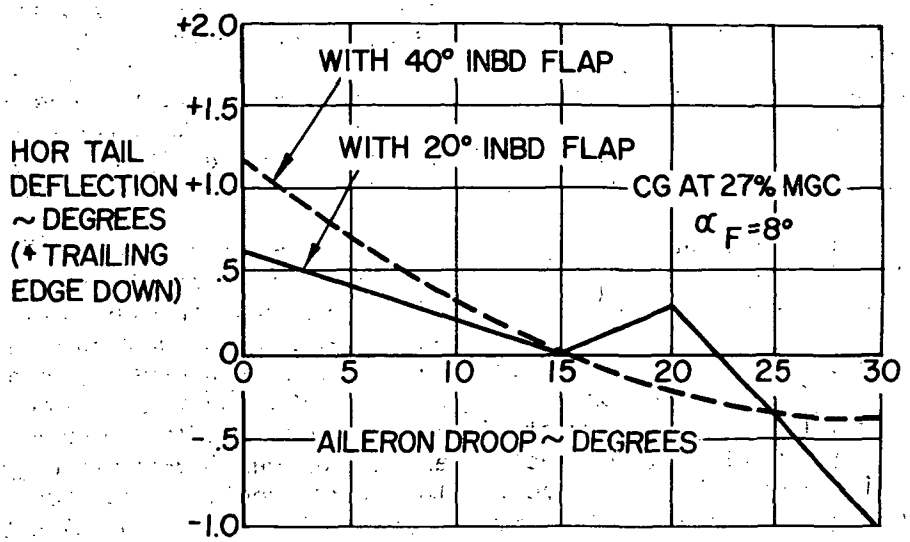

Figure 41. Interconnect requirements for inboard flap positions with a CG at 27% MGC.

deflection during DLC operation by .5 seconds. The trim actuator servo motor was replaced with one that could provide an actuator rate of 3.8 deg/sec with a lag time of .16 sec. Pilots found this to be a satisfactory arrangement.

Figure 42 indicates how, for the transport aircraft described in Ref. 22, the time histories of the flaps and elevator progressed when a step input was applied to the flap control surface. The aircraft autopilot system counteracted the aircraft's nose-down pitching moment, which had been caused by the auxiliary flap motion, so as to maintain a nearly constant aircraft attitude. The corresponding changes in elevator angle are shown in this figure. Unfortunately, the elevator angle for flap moment compensation was programmed by the flap command voltage and not by flap position, which resulted in an initial nose-up pitch of the airplane.

Several other important factors were noted during the tests. The control wheel-to-flap relation could be made linear by using a shaping network in the DLC servo amplifier to compensate for the non-linearities of the control linkages. The second important

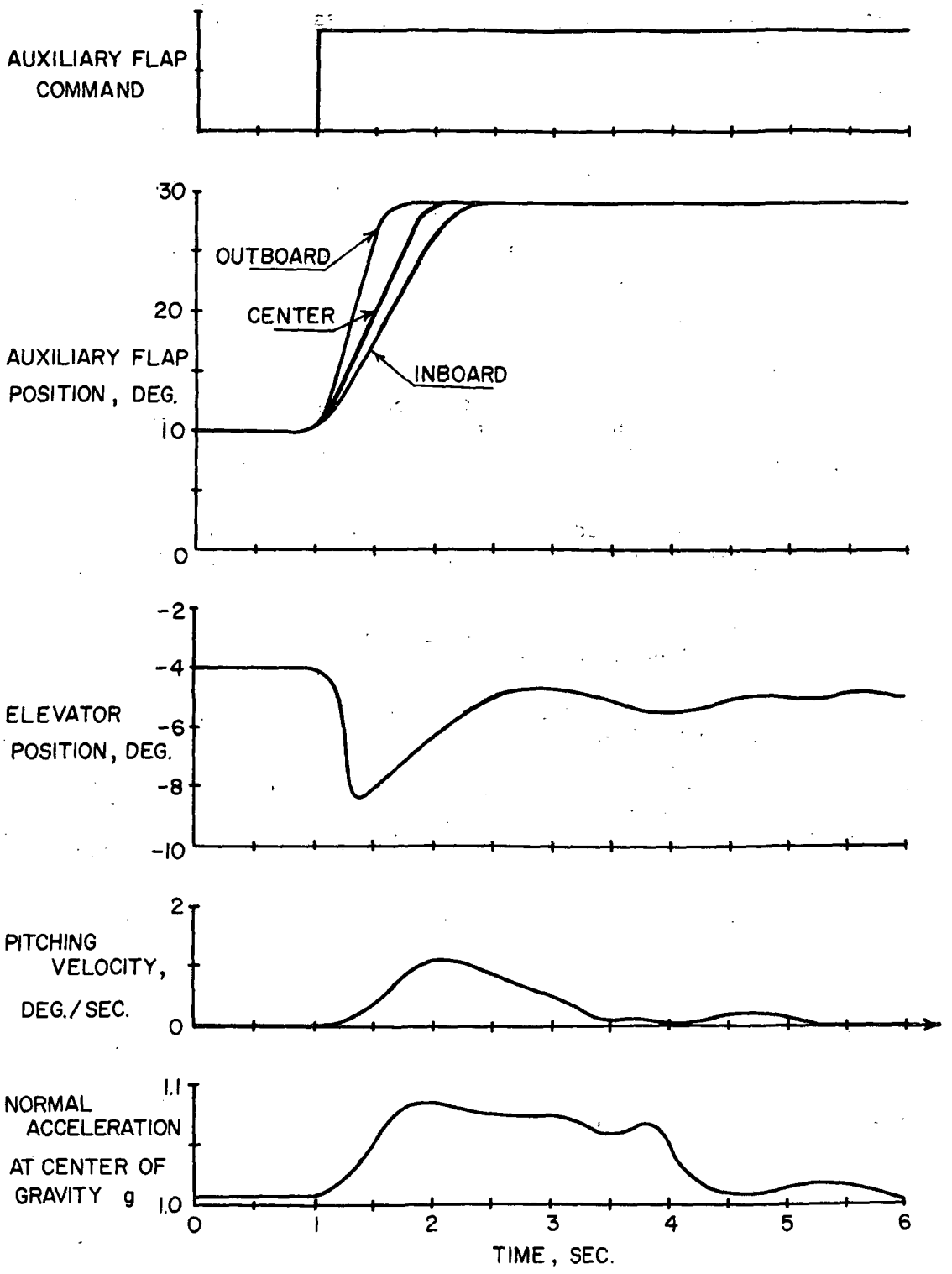

Figure 42. Response of aircraft to an auxiliary flap step; main flap at 40°.

factor is that the F-8 experiences a 40% loss in lateral control authority on its drooped positions. If droop ailerons are used on the constant attitude aircraft, this loss of aileron control authority must be examined closely to determine whether the ailerons will give sufficient roll power during all modes of flight.

An automatic throttle system has been tested in conjunction with DLC. Two types of sensing systems are available to operate the autothrottle. These are the angle-of-attack sensing system and the airspeed sensing system. The airspeed sensing system can be operated without additional development. Because it has not been tested, further development will undoubtedly be required to adapt the angle-of-attack, automatic throttle control to DLC.

In summary, many of the pitfalls of DLC have been discovered through extensive flight testing of operational aircraft. An evaluation of DLC with its accompanying restrictions indicates that it <u>is</u> feasible to adapt the concept to the constant attitude aircraft. Three questions, however, require additional consideration:

1. Can an uncoupled single degree of freedom gyro be used to maintain the fuselage level during all flight modes?

2. What are deflection rates required for the flaps and horizontal tail?

3. What system would provide lateral control adequate for aircraft equipped with DLC?

As the reader will note, these questions were studied extensively during the development of the simple-to-fly, constant attitude control system. (See section on CONTROL SYSTEM SIMPLIFICATION.)

LATERAL CONTROL AERODYNAMICS

To obtain the required lift during takeoff and climb, full-span, trailing-edge flaps are used on the modified airplane. This introduces the problem of generating sufficient lateral control, particularly during low speed flight when the flaps are deflected. Conventional aileron arrangements cannot be used, since the flaps cover the full span of the wings. Before deciding to operate the flaps differentially to provide lateral control, a study was made of other possible means of obtaining the necessary rolling moments. The common lateral control devices used with full-span, trailing-edge flaps are of two basic types: devices located forward of the trailing-edge, commonly referred to as spoilers; and adaptations of conventional ailerons generally located at the wing trailing-edge.

Spoilers

Almost all spoiler-type devices have certain common characteristics that are dependent on the wing, aileron, and flap configuration. When spoilers are located near the wing leading-edge, their effectiveness is roughly proportional to the lift coefficient; large rolling moments are provided at large angles of attack. As these devices are moved toward the wing trailing-edge, their effectiveness becomes more nearly independent of lift coefficient, i.e., remains almost constant or increases slightly at small angles of attack and decreases at large angles of attack, becoming more nearly linear with respect to spoiler projection. Data obtained from wind tunnel and flight tests indicate that small spoiler deflection or projections on the order of .01 c or less generally have little or no effect in producing roll, unless the wing is slotted in the spoiler vicinity. Slotting the wing from the lower to the upper surfaces to the rear of the spoiler improves the rolling effectiveness, particularly at large angles of attack, and the linearity with respect to projection, as flaps are retracted or deflected. Spoiler controls, especially those located far forward on the wing, are quite effective in the low-speed-flight range slightly beyond stall because of their pronounced influence in reducing lift or reducing the effective angle of attack over the wing section affected by their action.

Tests of spoilers at various chordwise locations indicate a perceptible time lag in the rolling response for forward spoiler locations; this time lag decreases as the spoiler is moved rearward. Slotting the wing behind the spoiler further reduces the lag in the response of the airplane to control deflections. At spoiler locations to the rear of about .60c, this time lag becomes imperceptible to pilots and hence unobjectionable at low and moderate values of Mach and Reynolds number.

Spoilers provide less pitching moment than conventional ailerons and hence would be expected to produce lower wing stresses and to have higher reversal speeds. In addition, spoilers provide favorable yawing moments over most of the flight range, except possibly at high angles of attack or lift, where the adverse yaw produced is less than that obtained with conventional ailerons.

The hinge-moment characteristics of spoilers are very unusual over the spoiler deflection range and require special treatment to provide acceptable control forces.

Since spoiler control is obtained through a loss of lift on one wing, whereas almost no effect is produced on the other wing, some difficulty may be encountered in raising a wing that has dropped. This problem is not serious, however, since the axis of rotation with spoiler control is seldom farther outboard than .20b/2 from the plane of symmetry.

There are four main types of spoilers. The first is the retractable, circular-arc spoiler that usually emerges only from the upper surface of the wing. This is sometimes referred to as a retractable-arc spoiler (Figure 43-b). The second type is the plug aileron, which fits into a slot in the wing in the neutral position and leaves this slot open when deflected upward (Figure 43-e). The third type of spoiler is the hinged-flap spoiler or upper-surface aileron, which lies along and forms part of the wing contour in the neutral position (Figure 43-a). The fourth and last type is the slot-lip aileron, which consists essentially of a small flap hinged near the front of a slot through the wing (Figures 43-c and 45-d).

Retractable-arc Spoilers. With retractable-arc spoilers, the lag characteristics and effectiveness for small spoiler projections generally are satisfactory with flaps retracted. With slotted flaps deflected, spoiler projections as large as .02c may be ineffective in producing rolling moments. However, the effectiveness of the spoiler controls, when located between .6c and .7c, usually increase rapidly for projections between .02c and .07c and increase less rapidly for larger projections. The effectiveness can also be improved by opening a slot just behind the spoiler (they become, in effect, plug-type spoilers).

The hinge-moment characteristics of retractable-arc spoilers can be varied considerably by changing the width of the spoiler plate, the angle of the upper surface of the spoiler, the distance between the spoiler pivot axis, or the center of curvature of the spoiler plate; they can also be changed by installing a plate on top of and normal to the spoiler arc or by venting or beveling the spoiler. In most cases, however, the type of variation of hinge moment with spoiler projection that results in the most desirable stick feel can be obtained only through the use of some auxiliary

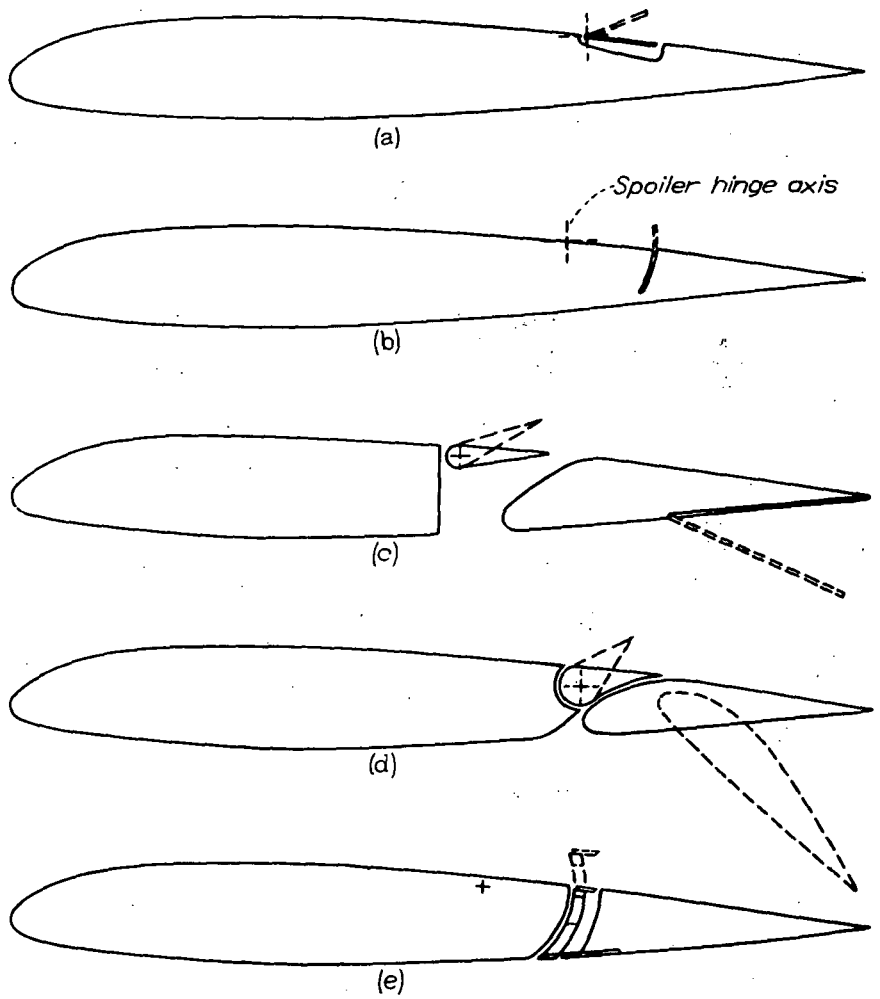

(a) Hinged-flap spoiler.
(b) Retractable-arc spoiler.
(c) Slot-lip aileron (type A).
(d) Slot-lip aileron (type B).
(e) Plug aileron.

Figure 43. Spoiler types.

device such as guide ailerons, which are conventional ailerons covering 5% to 10% of the wing span located near the wing tips.

Flight tests show that the wheel forces are very small, but the force variation with wheel deflection does not seem unsatisfactory for the tested airplane. Wind-tunnel tests indicate, however, that for spoilers that are thicker than those used during the flight test, undesirable control-force characteristics may result from a tendency for the spoilers to be pulled small distances out of the wing and from large forces required to hold large spoiler deflections. The minimum thickness of a spoiler may be limited by the rigidity required to prevent flexural vibrations.

The rolling velocities obtained with spoilers alone during flight tests generally are only about one-third less than the rolling velocities obtainable with spoilers and guide ailerons. At small wheel deflections, the use of guide ailerons results in greater improvements in the lateral control characteristics, particularly at low speeds. The yawing characteristics of the flight-tested airplane with spoilers and guide ailerons are favorable at high and moderate speeds and are only slightly unfavorable at landing speeds.

Plug-type Spoilers. Some of the disadvantages of the retractable-arc spoiler are overcome with the plug-type spoiler. Wind tunnel data indicate that plug spoilers, when used with slotted flaps, have hinge-moment characteristics that result in satisfactory stick feel. For some airplanes, however, the plug may have to be quite narrow or some alternative means may have to be provided in order to avoid excessive stick forces.

Hinged-flap Spoilers. An investigation of hinged-flap spoilers indicated that, although the effectiveness of such spoilers is about the same as the effectiveness of some other spoiler devices, the hinge-moment characteristics generally are unsatisfactory unless a balancing device is provided. Some degree of balance may be obtained with a small plate that projects into the airstream below the wing as the spoiler is deflected.

Slot-lip Spoilers. Both wind tunnel and flight tests of slot-lip spoilers at various chordwise positions have indicated that the most satisfactory position of the slot-lip spoiler, from both aerodynamic and structural considerations, is between .7c and .8c. When slot-lip spoilers are used in conjunction with a slotted flap, a convenient arrangement with satisfactory characteristics consists of a slot-lip spoiler located on the lip of the wing slot, ahead of the flap (Figure 43-d). Of course, this arrangement could not be used with a Fowler-type flap arrangement. Because of the physical impossibility of obtaining positive aileron deflections in this position with the flaps retracted, a high differential stick linkage, (probably a cam) would be required in the control system.

The greatest advantage of spoiler devices results from their adaptability to arrangements that involve full-span lift flaps. Also, the yawing moments caused by spoiler control may be favorable over a large part of the lift coefficient range. The pitching moment characteristics of spoilers are less adverse from considerations of wing twist than the pitching moment characteristics of conventional flap-type ailerons; the rolling effectiveness usually increases with lift coefficient, and some lateral control may be retained beyond stall. Finally, spoilers can be linked to act as drag brakes on "clean" airplanes to provide the necessary L/D ratios during landing.

Conventional Ailerons

Three types of ailerons were considered: the flap-trailing-edge aileron, drooped aileron, and aileron with retractable flaps.

Flap-trailing-edge Ailerons. The flap-trailing-edge aileron consists of a conventional aileron installed in the rear part of the lift flap. For such arrangements, conventional aileron balancing devices can be used, although the aileron chord may have to be limited to about .10c because of structural considerations. In order to obtain a reasonable amount of lateral control, the aileron span must be long, although only a small increase in lateral control is obtained by extending the ailerons inboard of station .2b/2.

When the flap is deflected, the aileron maintains most of its effectiveness for negative deflections but is relatively ineffective for positive deflections. These characteristics are such that, in order to obtain the best rolling performance, a differential aileron motion should be used when the flap is deflected, but not necessarily when the flap is retracted.

The yawing characteristics of this type of aileron may be expected to be unfavorable when the lift flaps are deflected, because the adverse induced aileron yawing-moment coefficient varies directly with the lift coefficient and because the variations in profile drag caused by aileron deflection also contribute an adverse yawing moment.

Considerations of overall characteristics indicate that when full-span flaps are fully deflected, lateral control should be obtained from some device other than conventional ailerons at the trailing edge.

Drooped Ailerons. Ailerons outboard of partial-span flaps sometimes are drooped and operated differentially when the flaps are deflected. In other arrangements, a single flap or the rear flap of a double-slotted-flap combination is used to provide lateral

control as well as lift. The lateral control characteristics for all of these arrangements are similar to the lateral control characteristics for flap-trailing-edge ailerons; when the ailerons are drooped, the aileron effectiveness for positive deflections is low, and the adverse yawing moments for either positive or negative deflections are high. The problem of providing aerodynamic balance for lateral control, while maintaining an efficient high-lift device, may be more difficult for drooped ailerons than for flap-trailing-edge ailerons.

Ailerons with Retractable Flaps. When ailerons are used with retractable, duplex flap arrangements, the rolling effectiveness obtained with the partial-span, inboard flap deflected is increased slightly for negative aileron deflections, compared with that obtained with flaps retracted. The characteristics of ailerons spanning the same part of the wing as the flaps are affected by the position, contour, and deflection of the flaps. In an early adaptation of this arrangement, the flap moved rearward as it was deflected, but no gap was left between the flap nose and the lower surface of the wing. The lower surface of the aileron was therefore completely shielded by the deflected flap. In spite of this shielding effect, flight tests indicated that the ailerons were nearly as effective with flaps deflected as with flaps retracted. The yawing characteristics at a given lift coefficient were less unfavorable with the flaps deflected than with the flaps retracted. Wind tunnel tests indicate that this shielding effect can be corrected if a gap is left between the nose of the deflected flap and the lower surface of the wing. An arrangement of this kind may consist either of an approximately full-span, narrow-chord aileron in combination with a full-span flap or a partial-span aileron in combination with full-span duplex flaps.

Conclusions of Lateral Control Type Study

A careful analysis of each of these seven lateral control devices indicated that the plug spoiler offered the most advantages, and it was subsequently selected for further investigation to determine if it could give adequate performance in roll. Its advantages accrued from its simplicity of structure and overall effectiveness during flap-retracted as well as flap-deflected mode of operation. Another important factor in its selection was the availability of wind tunnel data using the 23012 Fowler-type flap equipped with a plug spoiler.

Preliminary reports suggested that the maximum value of Pb/2V should be between .07 and .08. Also a roll rate between 18 and 23 degrees/sec is required during takeoff and landing conditions (AFFDL-TR-69-72). Calculations using the wind tunnel data from WR-L-376 give a Pb/2V equal to .076 and a roll rate for landing conditions equal to 22.3 degrees/sec. These calculations are for

plug spoilers located at .65c from the leading edge and covering 37% of the span. The maximum control force required to move the ailerons was calculated to be 28 lbs.

The vertical tail size was found to satisfy directional stability requirements. Using the existing vertical tail section and rudder, the aircraft requires approximately .75 degrees of rudder for each degree of sideslip. Therefore, no changes were considered necessary in the vertical tail section.

The results of this study led to the specification of spoilers for use with the manually-operated backup lateral control system.

LIFT TO DRAG RATIOS FOR LANDING

One of the requirements for satisfactory handling characteristics of aircraft is a proper L/D ratio during landing. If the L/D ratio is too small, the aircraft will sink too fast during final approach, causing a hard landing. If the L/D ratio is too high, the aircraft has a tendency to float, and the pilot will have difficulty touching down.

An examination of current literature and pilot opinions indicates that the value of L/D during landing should be between 5.5:1 and 6.0:1. A study was undertaken to see if the Piper PA 235C, with its proposed modifications, could achieve satisfactory values of L/D. The flight profile of the 235C, equipped with a full-span, Fowler-type flap, was examined for various combinations of power and flap settings. The results show that the proper L/D values between power settings of zero and 40% could be achieved with the aircraft in its current configuration. There is no need to equip the aircraft with any type of spoilers or aerodynamic brakes to bring the L/D ratio to the desired value.

Some examples of how the proper L/D ratio can be achieved are given below.

Power	Flaps-deg	R/C-fpm	V-fps	L/D
0%	22	-827	81	5.77
10%	24	-682	82	5.99
20%	30	-543	81	5.94
30%	34	-443	82	5.77
40%	36	-308	85	5.85

Thus, the pilot has a wide range of settings from which to choose, depending on his desired rate of sink while maintaining L/D and forward speed virtually constant.

SYSTEM DYNAMIC CONSIDERATIONS

INTRODUCTION

In order to achieve the control system and aerodynamic requirements previously detailed in this study, it is necessary to establish criteria for optimum dynamic behavior of the aircraft to insure that all systems respond quickly, with minimum pilot effort and maximum pilot comfort. Human tracking capability depends on the function being tracked, the presentation method of the tracked and tracking functions, and the dynamic response of the tracking system-to-operator inputs; all these factors must be considered in determining the overall system dynamic response.

Basic legal requirements, as stated in the Federal Aviation Regulations, Part 23, include bank angles up to 60^{o} and limit maneuvering load factor to 3.8. These are structural considerations. The human factors are somewhat more stringent, as the aircraft should be able to withstand much more buffeting than the pilot finds comfortable. Also, there is the requirement that the pilot must track, or control, certain of the dynamic modes of the aircraft as they are excited by his inputs or random disturbances. Another case is the modes which must be tracked by automatic systems, such as pitch angle and bank angle.

The aerodynamic calculations have demonstrated the feasibility of constant attitude flight utilizing direct lift control throughout the flight profile. This has been accomplished while at the same time improving the overall performance of the aircraft. This concept eliminates the pitch degree of freedom, thereby materially reducing the pilot's workload. Stalls and spins do not appear possible with this aircraft.

HUMAN PILOT DYNAMICS

There are various models for the human operator, all similar, but each including gain, time delay, and time periods which vary according to individual and task. Jex (Ref. 26) and McRuer (ref. 27) present data on a highly refined human operator transfer function which includes terms for gain, pure time delay, equalization (operator latencies), and neuromuscular subsystem dynamics, compared with an approximate model. McRuer's results are for what he calls a "subcritical task," in which the operator must manipulate a given element, consisting of a first-order divergence. Jex's results are for what he calls a "critical task," in which the operator must stabilize (compensatory tracking) an increasingly unstable element up to loss of control. McRuer's equations are shown in Figure 44, and the Bode plot of his results are in Figure 45. Tables 21, 22, and 23 from Damon illustrate the speed with which a human pilot can move his limbs and activate a control in response to a command.

Precision Model

Equalization and Gain | Basic Latencies | Neuromuscular System

$$Y_p = K_p\left(\frac{T_L j\omega + 1}{T_I j\omega + 1}\right) e^{-j\omega\tau} \left\{ \underbrace{\left(\frac{\pm T_K j\omega + 1}{T_K' j\omega + 1}\right)}_{e^{-j\alpha/\omega}} \underbrace{\frac{1}{(T_{N_1} j\omega + 1)\left[\left(\frac{j\omega}{\omega_N}\right)^2 + \frac{2\zeta_N j\omega}{\omega_N} + 1\right]}}_{(T_N j\omega + 1)^{-1} \text{ or } e^{-j\omega T_N}} \right\}$$

where

$$\alpha \doteq \frac{1}{T_K'} \pm \frac{1}{T_K}$$

where

$$T_N \doteq T_{N_1} + \frac{2\zeta_N}{\omega_N}$$

Approximate Model

$$Y_p = K_p\left(\frac{T_L j\omega + 1}{T_I j\omega + 1}\right) e^{-j\omega\tau} \quad \frac{e^{-j\alpha/\omega}}{T_N j\omega + 1}$$

$$\doteq K_p\left(\frac{T_L j\omega + 1}{T_I j\omega + 1}\right) e^{-j[\omega(\tau + T_N) + (\alpha/\omega)]} \quad ; \; \tau_{eq} = \tau + T_N$$

Figure 44. Describing function models.

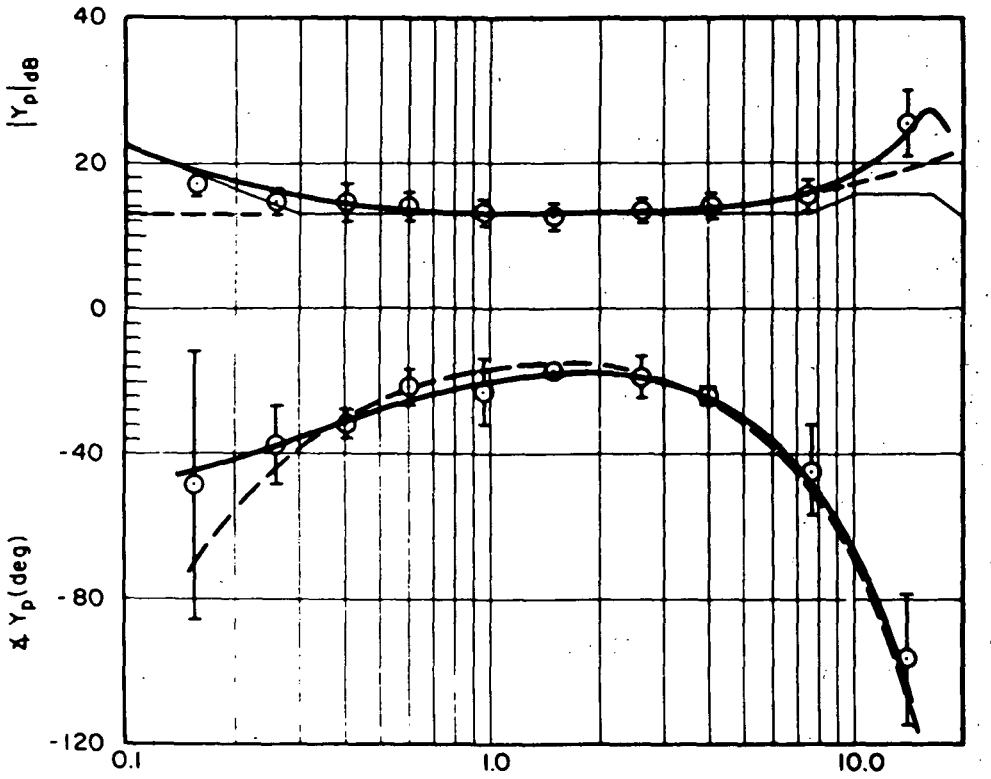

Precision Model (———)

$$Y_p = (25.1)\left(\frac{j\omega}{7.8}+1\right)e^{-0.09\,j\omega}\left\{\left(\frac{\frac{j\omega}{0.3}+1}{\frac{j\omega}{0.05}+1}\right)\frac{1}{\left(\frac{j\omega}{10}+1\right)\left[\left(\frac{j\omega}{16.5}\right)^2+\frac{2(0.12)}{16.5}\,j\omega+1\right]}\right\}$$

Approximate Model (— — —)

$$Y_p = (4.2)\,\frac{j\omega}{7.8}+1\;e^{-j[0.21\omega+(0.19/\omega)]}$$

$$(Y_C = K_C/(j\omega - 2);\ \omega_j = 4.0\ \text{rad/sec})$$

Figure 45. Typical pilot describing function data and models.

TABLE 21. SPEED OF ARMS AND HANDS IN VARIOUS MOVEMENTS

Test Conditions: The subjects moved their hands from one position to another as fast as possible consistent with task requirements. Time was measured from the beginning to the end of the physical movement. The number of subjects varied between 5 and 18. Differences in test conditions are noted.

Distance Moved (Inches	Direction Moved	Force Applied or Weight Moved	Accuracy of Primary Importance?	Velocity (In/ sec)
1.0	Right	Negligible	Yes-positioning	3.2
1.0	Left		movements	3.6
3.9	Right			7.4
3.7	Left			8.1
15.7	Right			20.6
15.7	Left			21.8
			(Brown and Slater-Hammel, 1949)	
2 3/4	Left	Negligible	Yes-positioning	8.9[a]
2 3/4	Right		movements	9.2[a]
2 3/4	Up			9.4[a]
2 3/4	Down			9.4[a]
2 3/4	In			9.2[a]
			(Herbert, 1957)	
1	Varied	Negligible	No	8.4
6	(little difference)			52.8
11				89.0
16				115.0
			(Peters and Wenborne, 1936)	
Varied	Varied	6 lbs	No	175
		9		150
		12		140
		15		130
		18		120
		21		110
			(Koepke and Whitson, 1940)	
45° arc	Elbow flexion	Negligible	No	441 degrees/sec.
			(Brozek et al., 1952)	
45° arc	Elbow flexion	Negligible	No	425 degrees/sec.
45° arc	Elbow flexion			448 degrees/sec.
			(Glanville and Kreezer, 1937)	

[a] Includes auditory reaction time, averaging 0.2 second.

TABLE 22. SPEED OF ARM AND HAND MOVEMENTS WITH CONTROL STICK

Test Conditions: The subjects moved an aircraft control stick as fast as possible against varying resistance. These data summarize the results of four studies: Advisory Committee for Aeronautics, 1916; Hertel, 1930; Beeler, 1944; Oriansky, 1948.

Distance Moved (In Inches)	Direction of Movement	Resistance to Movement (Pounds)	Velocity (In/sec)
± 6	Pull[a]	< 20	75 +
± 6		20 - 100	50 - 75
± 6		100-200	25 - 50

[a]Push is about 25% faster (Oriansky, 1948).

Studies of sine wave tracking show that errors increase with mounting frequency of the tracked element. Pew (Ref. 28) shows that there is a slight decrease in error at 1 to 2 cps, with extended practice. No tracking data were found in the frequency range of airplane natural frequencies like the phugoid. It does not seem likely that manipulation of the phugoid would result in any marked improvement in tracking accuracy for the pilot. A decrease in time from 40 seconds to 20 seconds would not bring the phugoid into the range where the pilot can track it as a continuous function. If the short period oscillation can be manipulated, it should be slowed down to allow better pilot control or speeded up and heavily damped to remove it from the pilot's control for quick completion.

The effect of a pure time lag on tracking performance is not documented here, but it appears that, as response lags input, tracking errors increase. For tasks in which the operator must track a displayed variable, control lags must be kept small. If the pilot is attempting a maneuver, he can easily adapt to control lags. For example, roll-out from a turn in a Cessna 150 must begin 10^{o} to 15^{o} before the desired heading is reached, a task quickly mastered by student pilots.

Consideration of human factors requires that displacements, velocities, and accelerations of aircraft motions excited by standard maneuvers be within the limits of pilot and passenger

TABLE 23. SPEED OF REACHING FOR AND OPERATING TOGGLE SWITCHES--

WITH PRECEDING CUE

Test Conditions: The subjects were 10 adult males, 5 being U. S. Air Force pilots on flying status. Each subject, seated in a fighter cockpit mockup, had to reach and operate 9 toggle switches located in different cockpit positions. The subject was first alerted by a 10-second cue light indicating the approximate location of the ensuing stimulus light adjacent to the toggle switch to be activated. Upon perceiving the stimulus light, the subject removed his right or left hand, whichever was closer, from a sidestick control grip located in front of each armrest, and operated the designated switch. Response time was measured from the onset of the stimulus to the activation of the switch.

Hand Used	General Direction of Hand Movement	Toggle Distance From Hand Starting Point (Inches)	Mean Speed of Movement (Seconds)
Right	Forward	6	0.76
Left	Forward	6	.80
Right	Forward	9	.65
Left	Forward	9	.78
Right	Forward	15	.84
Left	Forward	15	.90
Right	Forward	18 1/4	.77
Left	Forward	18	.78
Either	Forward	23	.86

comfort. Also, modes which must be controlled should be in a frequency range which the pilot can easily track. Modes which are not to be tracked by the pilot or the automatic system should be of high frequency and damping, so as to disappear rapidly, but still not violate the pilot comfort requirements.

The human acceleration limit dictated by comfort is about 1.5g, which corresponds to a bank angle of 48°. A 60° bank results in 2g's for flight with no vertical acceleration except gravity. Thus, a 60° bank is unacceptable. A logical limit is taken to be $\phi = 45^{\circ}$, or 1.41g. Therefore, the vertical load factor is 1g in unaccelerated flight, the side acceleration is 1g and the total load factor is 1.414g. The lower limit for comfort is very close to 1g, as the human body is much more sensitive to negative accelerations than to positive accelerations.

The only limits on frequency are that frequencies of all modes must be below the lowest natural structural frequency and that the frequencies not be high enough to generate unacceptable acceleration. Table 24 summarizes the frequencies and damping ratio requirements.

TABLE 24. FREQUENCY AND DAMPING RATIO REQUIREMENTS

Mode	τ (sec.)	ω (rad/sec)	ζ
Tracked	1.5 - 6	1 - 4	.4 - .6
Untracked	1 - 6	1 - 6	.5 or greater
Dutch Roll	1 - 6	1 - 6	.08 - .12
Phugoid	15 - 30	.2 - .4	.6 or greater

RESPONSE RATES OF CONTROL SURFACES

At this point in the design cycle, some idea of the response rates of the various control surfaces was needed so that sizing of the actuators could be made. Response rates for individual control surfaces describe the hardware to be selected for the various controllers. Because contract funds were not available to complete specific controller design, quantitative analysis was not possible. An attempt was made, however, to obtain some qualitative estimates of these response rates based on the literature. Although some of the estimates are a bit subjective, it is felt that they will assist materially in determining actuator requirements.

It is desirable that control surface deflections occur within twice the longitudinal short-period mode of the aircraft. For the 235C in its present configuration, this short-period mode is 1.2 cycles per second. For a unit step input to the control surface, this gives a rise time of .416 seconds. There are two ways in which the system can be designed using this rise time.

The first method is to let the rise time remain constant, regardless of input. For example, if it is desired to obtain a flap deflection of 13.4 degrees in .416 seconds, an actuation rate of 32.2 deg/sec would be needed. Thus, it is seen that the system would require a variable actuation rate depending on the magnitude of the deflection. Since the magnitude of flap deflection is determined by the yoke position, the rate of flap deflection would also be determined from the position of the yoke. This arrangement would cause serious human factors problems. For example, if a sudden gust were to disturb the aircraft, the pilot could be startled into making an inadvertant rapid movement of the yoke, causing the flaps to extend rapidly and subsequently slow down the aircraft.

The second method, and the one that seems most promising, is to maintain a constant deflection rate. This would allow the yoke to control the magnitude of flap displacement only. The critical condition for deflection rates would be during low-speed, low-powered flight. The worst case would require moving the flaps 13.4 degrees in order to achieve a high rate of climb. This would necessitate moving the flaps at a rate of 32.2 deg/sec.

Another factor to be considered is the lag time for the power plant. The lag time for turbine engines is currently on the order of .23 seconds for a power change of 37% with reciprocating-propeller engines taking somewhat less time to respond (RPM of constant-speed propeller remains the same, hence the only change is in fuel flow and propeller blade angle setting). Thus, to change power by 30% would require a time of less than .2 seconds.

Horizontal Tail

Since the elevator will be tied either directly or indirectly to the movement of the flaps, it is important to establish the response rates of the elevator based on the deflection rates of the flaps. Two methods of coupling these two control surfaces are considered feasible. The first method consists of correcting the pitching moment by using a gyro directly connected to the horizontal tail which senses any changes in the pitch of the aircraft and corrects it to zero pitch by re-positioning the horizontal tail. This system would require the horizontal tail to change position as quickly as possible without undue overshoot. The second method consists of a mechanical or electrical linkage between the flaps and the horizontal tail. This linkage would be geared to deflect the horizontal tail by the required amount to keep the pitch angle at zero at all times. It is obvious that a stabilator deflection rate which is too fast would cause the aircraft to pitch up until the flaps caught up with the stabilator and then level off. If the stabilator response were too slow, the aircraft would initially pitch down, then level off as the stabilator caught up with the flaps. This leading or lagging effect would occur only if the stabilator were programmed by flap command. This can be eliminated if the stabilator position is programmed by actual flap position.

Flight tests of an F-8 using a stabilator-to-flap interconnect with flap deflection rates of 40 deg/sec, found an actuation rate of 3.8 deg/sec to be satisfactory.

Ailerons and Spoilers

Wind tunnel data from Ref. 29 shows that the time for ailerons and spoilers to move to 100% deflection (or roll angle $\phi = 4.6^{o}$) is .22 seconds. Full deflection of the spoiler is .10c and for the aileron, 35^{o}. The time for the wing to make a roll angle of $\phi = 4.6^{o}$ for the aileron was found to be .48 seconds. The time for the spoiler to make the same roll angle was found to be .57 seconds for the spoiler located at .83c. Ref. 30 showed that the actual time required for the deflection of an aileron to 35^{o} was equal to .15 seconds, which was considered instantaneous.

Thus it is seen that there is no perceivable lag in the actual movement of any of the control surfaces. The time it takes the control surfaces to move to the maximum deflection is

Ailerons and spoilers	.22 seconds
Engine power ($\Delta\rho$ = 30%)	.20 seconds
Flap deflection ($\Delta\delta_f = 13.4^{o}$)	.416 seconds

These are seen to be within the one-half cycle range of the short-period mode. Once the controls are deflected, response time is immediate, with response time for maximum deflections being

Ailerons ($\phi = 4.6^{o}$)	.48 seconds
Spoilers ($\phi = 4.6^{o}$)	.57 seconds
Flaps ($\Delta\delta_f = 13.4^{o}$)	.70 seconds
Power ($\Delta\rho = 30\%$)	.40 seconds.

SYSTEM EQUATIONS OF MOTION

A rigid body stability and control analysis was performed using essentially those methods and programs reported in NASA CR-1975; however, the derivation of the equations of motion for all flight modes is presented here in some detail. These equations are derived by applying Newton's laws of motion which relate the summation of the external forces and moments to the linear and angular accelerations of the aircraft. These equations may be found in any standard text on the subject such as McRuer, et al., (Ref. 31). The linearized, small perturbation equations of motion referred to the stability axis are

$$(S-X_u)u - (SX_{\dot{w}}+X_w)w - (SX_q-g)\theta = X_{\delta_e}\delta_e + X_{\delta_f}\delta_f + T_{\delta_{RPM}}\cos\zeta$$

$$-(Z_u)u + [S(1-Z_{\dot{w}})-Z_w]w - S(U_o+Z_q)\theta = Z_{\delta_e}\delta_e + Z_{\delta_f}\delta_f + T_{\delta_{RPM}}\sin\zeta$$

$$-(M_u)u - (SM_{\dot{w}}+M_w)w + (S^2-M_qS)\theta = M_{\delta_e}\delta_e + M_{\delta_f}\delta_f + (ZjM)/(Iyy)T_{\delta_{RPM}}\delta_{RPM} \quad (83)$$

$$(S-Y_v) - (SY_p^* + g/U_o)\phi + S(1 - Y_r^*)\psi = Y_{\delta_A}^*\delta_A + Y_{\delta_r}^*\delta_r$$

$$-(L_\beta)\beta + (S^2 - SL_p)\phi - SL_r\psi = L_{\delta_A}\delta_A + L_{\delta_r}\delta_r$$

$$-(N_{\dot{\beta}})\beta - SN_p\phi + (S^2 - SN_r)\psi = N_{\delta_A}\delta_A + N_{\delta_r}\delta_r .$$

The notation used in these equations and throughout this work is that of McRuer, et al., (Ref. 31). The reader is referred to that reference for details.

The first three equations describe the airplane motion in the longitudinal mode, whereas the last three describe the motions in the lateral-directional mode. Note that the lateral mode has been decoupled from the longitudinal mode by the linearization of the equations of motion. Therefore, the longitudinal dynamics can be analyzed by use of the first three equations only; and the lateral dynamics by use of the last three only.

By applying Cramer's rule to these equations, the transfer functions can be obtained for both lateral and longitudinal dynamics. The longitudinal transfer functions derived were U/δ_e, α/δ_e, θ/δ_e, W/δ_e, U/δ_f, α/δ_f, θ/δ_f, W/δ_f, U/δ_{RPM}, α/δ_{RPM}, θ/δ_{RPM}, and W/δ_{RPM}.

The transfer functions are

$$\frac{U}{\delta_e} = \frac{A_u S^3 + B_u S^2 + C_u S + D_u}{\Delta_l}$$

$$\frac{U}{\delta_f} = \frac{A_u S^3 + B_u S^2 + C_u S + D_u}{\Delta_l}$$

$$\frac{U}{\delta_{RPM}} = \frac{A_u S^3 + B_u S^2 + C_u S + D_u}{\Delta_l} \qquad (84)$$

$$\frac{W}{\delta_e} = \frac{A_w S^3 + B_w S^2 + C_w S + D_w}{\Delta_l}$$

$$\frac{W}{\delta_f} = \frac{A_w S^3 + B_w S^2 + C_w S + D_w}{\Delta_l}$$

and

$$\frac{W}{\delta_{RPM}} = \frac{A_w S^3 + B_w S^2 + C_w S + D_w}{\Delta_l}$$

where Δ_l = characteristic equation of the longitudinal dynamics

$$= (AS^4 + BS^3 + CS^2 + DS + E)$$

and $A = 1$

The following quantities were neglected in the equations:

T_u and $T_{\delta_{RPM}}$

I_{xz}

γ_o (changes order of lateral equations) .

The lateral transfer functions derived were ϕ/δ_A, β/δ_A, r/δ_A, ϕ/δ_r, β/δ_r and r/δ_r. These transfer functions are

$$\phi/\delta_A \quad \frac{(A_\phi S^2 + B_\phi S + C_\phi)}{\Delta_2}$$

$$\beta/\delta_A = \frac{(B_\beta S^2 + C_\beta S + D_\beta)}{\Delta_2}$$

$$r/\delta_A = \frac{(A_\psi S^3 + B_\psi S^2 + C_\psi S + D_\psi)}{\Delta_2} \qquad (85)$$

$$\phi/\delta_r = \frac{(A_\phi S^2 + B_\phi S + C_\phi)}{\Delta_2}$$

$$\beta/\delta_r = \frac{(A_\beta S^3 + B_\beta S^2 + C_\beta S + D_\beta)}{\Delta_2}$$

$$r/\delta_r = \frac{(A_\psi S^3 + B_\psi S^2 + C_\psi S + D_\psi)}{\Delta_2}$$

where Δ_2 = characteristic equation of the lateral dynamics

$$= (AS^4 + BS^3 + CS^2 + DS + E)$$

and $A \equiv 1$.

The coefficients in these transfer functions are functions of geometric parameters, airspeed, and non-dimensional stability derivatives (Ref. 31). These coefficients were evaluated for representative conditions in the flight profile of the aircraft. These conditions are light-weight cruise, climb and landing; and heavy-weight cruise, climb and landing. The dimensional and non-dimensional stability derivatives as well as the numerator and denominator coefficients for each of the six flight conditions are listed in Appendices D and E for the unmodified and modified aircraft, respectively.

Substituting these values into the above equations yields the numerical values for the transfer functions. Evaluating the transfer functions for the heavy weight landing conditions yields

UNMODIFIED AIRCRAFT

$$\frac{U}{\delta_e} = \frac{K_u(S + 1.5)(S - 185)}{\Delta_1}$$

$$\frac{U}{\delta_f} = \frac{K_u(S + 1.14)(S + 6.55)(S - 3.25)}{\Delta_1}$$

$$\frac{U}{\delta_{RPM}} = \frac{K_u(S^2 + 5.55S + 3.84)(S - 3.78)}{\Delta_1}$$

$$\frac{W}{\delta_e} = \frac{K_w(S^2 + 0.36S + 0.28)(S + 79)}{\Delta_1}$$

$$\frac{W}{\delta_f} = \frac{K_w(S^2 + 0.34S + 0.28)(S + 11.6)}{\Delta_1}$$

$$\frac{W}{\delta_{RPM}} = \frac{K_w(S^2 + 0.58S + 0.36)(S - 1.5)}{\Delta_1}$$

$$\frac{\theta}{\delta_e} = \frac{K_\theta(S + 0.92)(S + 0.48)}{\Delta_1}$$

$$\frac{\theta}{\delta_f} = \frac{K_\theta(S^2 + S + 0.36)}{\Delta_1}$$

$$\frac{\theta}{\delta_{RPM}} = \frac{K_\theta(S + 0.4)(S + 2.4)}{\Delta_1} \qquad (86)$$

$$\phi/\delta_A = \frac{(S - .12)(S - .71)}{\Delta_2} \qquad \phi/\delta_r = \frac{(S + 1.5)(S - 23)}{\Delta_2}$$

$$\beta/\delta_A = \frac{(S + 6.8)(S - .1)}{\Delta_2} \qquad \beta/\delta_r = \frac{(S + 3.9)(S + 80.7)(S - .35)}{\Delta_2}$$

$$r/\delta_A = \frac{(S + .16)(S + 5.9)(S - .11)}{\Delta_2} \qquad r/\delta_r = \frac{(S^2 - .16S + .61)(S + 4)}{\Delta_2}$$

$$\Delta_2 = (S + 3.5)(S - .099)(S^2 + .925 + 5.3)$$

MODIFIED AIRCRAFT

$$\frac{U}{\delta_e} = \frac{K_u(S + 1.98)(S - 130)}{\Delta_1}$$

$$\frac{U}{\delta_f} = \frac{K_u(S + 1.98)(S + 4.95)(S - 1.15)}{\Delta_1}$$

$$\frac{U}{\delta_{RPM}} = \frac{K_u(S + 1.96)(S + 4.41)(S - 3.39)}{\Delta_1}$$

$$\frac{W}{\delta_e} = \frac{K_w(S^2 + 0.32S + 0.24)(S + 9.72)}{\Delta_1}$$

$$\frac{W}{\delta_f} = \frac{K_w(S^2 + 0.32S + 0.20)(S + 10)}{\Delta_1}$$

$$\frac{W}{\delta_{RPM}} = \frac{K_w(S^2 + 0.98S + 0.65)(S - 0.68)}{\Delta_1}$$

$$\frac{\theta}{\delta_e} = \frac{K_\theta(S + 1.02)(S + 0.43)}{\Delta_1}$$

$$\frac{\theta}{\delta_f} = \frac{K_\theta(S^2 + 1.28S + 0.483)}{\Delta_1}$$

$$\frac{\theta}{\delta_{RPM}} = \frac{K_\theta(S + 0.37)(S + 1.51)}{\Delta_1} \qquad (87)$$

$$\Delta_1 = K_{D_1}(S^2 + 0.29S + 0.16)(S + 3.07)(S + 1.94)$$

$$\frac{\phi}{\delta_A} = \frac{K_\phi(S^2 + .48S + 2.31)}{\Delta_2}$$

$$\frac{\beta}{\delta_A} = \frac{K_\beta(S + 23)(S + .17)}{\Delta_2}$$

$$\frac{r}{\delta_A} = \frac{K_r(S - .94)(S + 1.1)(S + 15.5)}{\Delta_2}$$

$$\frac{\phi}{\delta_r} = \frac{K_\phi(S + 1.6)(S - 29.5)}{\Delta_2}$$

$$\frac{\beta}{\delta_r} = \frac{K_\beta(S + 3.9)(S + 102)(S - .29)}{\Delta_2}$$

$$\frac{r}{\delta_r} = \frac{K_r(S^2 - .12S \pm .55)(S + 4)}{\Delta_2}$$

$$\Delta_2 = K_{D_2}(S + 3.7)(S - .086)(S^2 + 92S + 4.8).$$

The transfer functions for the other five flight conditions are similarly evaluated and are shown in Appendices D and E.

With the development of the transfer functions and evaluation of the numerator and denominator coefficients, the transient responses of the aircraft can now be obtained. The transient responses were evaluated on a digital computer by employing the method of residues. Figures 46 and 47 show the responses of the unmodified and modified aircraft for rudder and aileron pulse inputs, respectively.

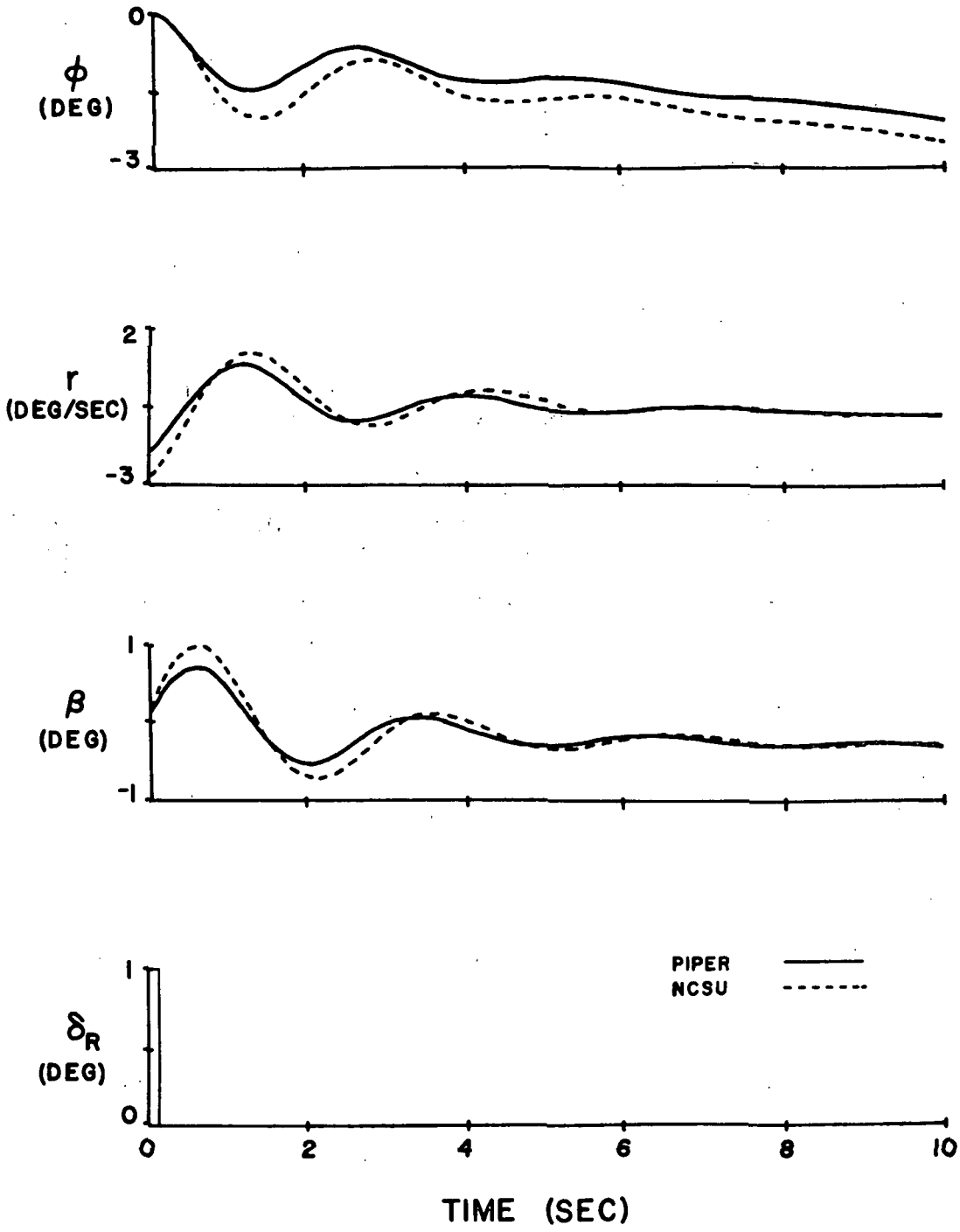

Figure 46. Transient response for a pulse rudder deflection.

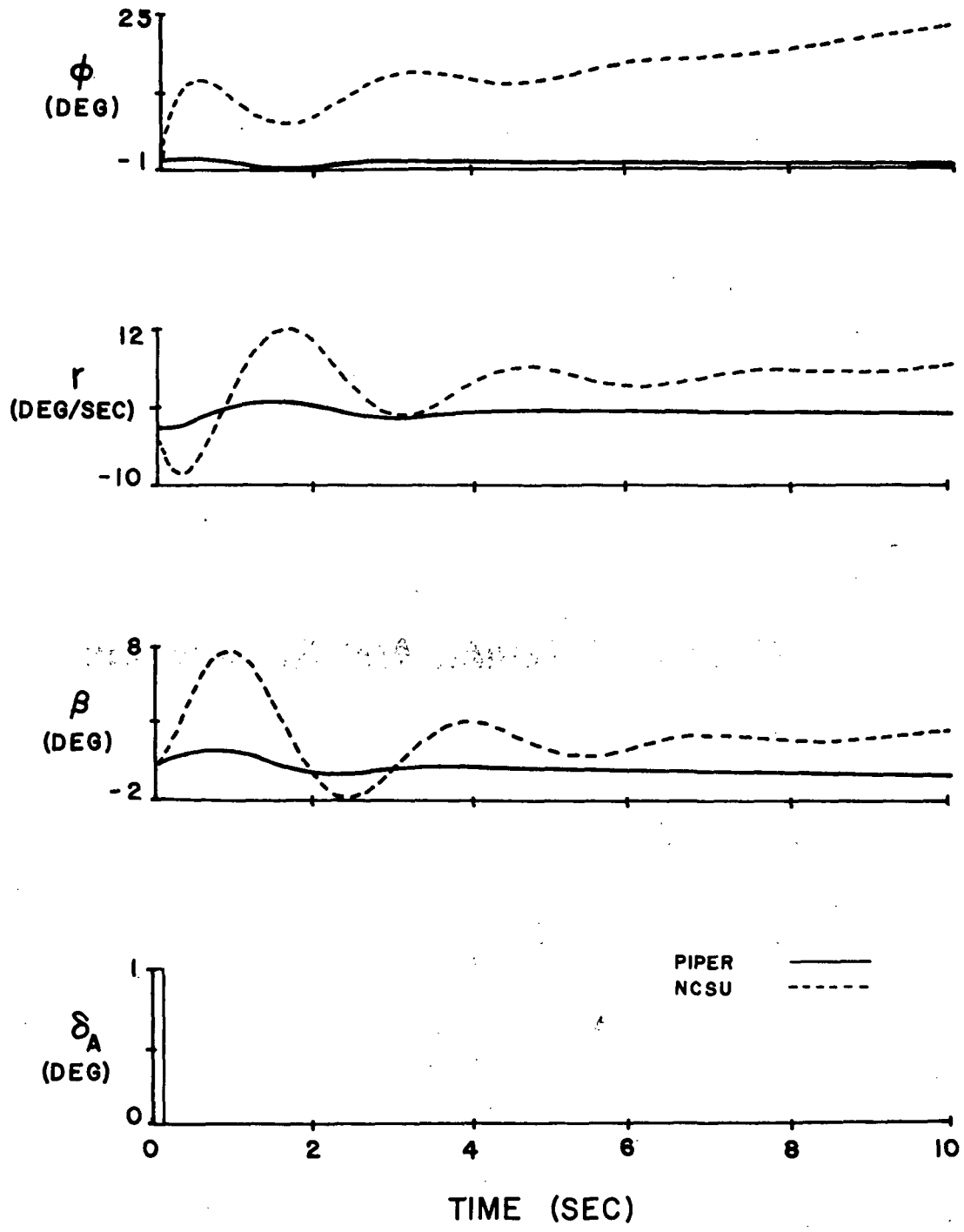

Figure 47. Transient response for a pulse aileron deflection.

AIRCRAFT MATERIAL AND FABRICATION

INTRODUCTION

In the beginning, the problem of airframe material and fabrication for the modified aircraft was approached from the standpoint of reducing the structural weight required in conventional riveted construction. As the program progressed, it became apparent that the area of manufacturing cost was at least as sensitive and possibly more so than the area of structural weight. With current construction practices, structural components represent approximately 40% of total light airplane weight. The cost of structural material represents approximately 4% of the market value of the light airplane, with structural labor representing another 8%. Therefore, any attempts at weight savings in new materials and manufacturing methods must be coupled with a close regard for material and manufacturing costs.

In order to determine true fabrication requirements, it was necessary to obtain weight estimates for the modified wing and tail, perform an aeroelastic analysis, and compute design and loading parameters. Since the modified PA-235C was to represent a complete departure from conventional light aircraft in control system and aerodynamic design, it was decided that perhaps completely new construction types and fabrication methods might be used to enhance the innovative nature of the aircraft.

STRUCTURAL WEIGHT ESTIMATES

Early in the design of any aircraft, it is desirable to obtain estimates of potential structural weight requirements. All performance evaluations depend to some degree on the various weight parameters of the proposed aircraft. Thus, the accuracy with which the aircraft meets performance expectations depends to a great extent on the accuracy of the weight estimates. Unfortunately, the true structural weight can only be realized after design completion and sometimes only after field testing and modification. It is possible, however, to predict optimum structural proportions early in the design study and thus obtain an optimum weight prediction. The optimum predicted may not be realized in the actual design because of cost and manufacturing requirements; it does, however, offer a starting point.

The modifications needed to adapt the Piper 235C for constant attitude flight include the redesign and construction of a new wing. In addition, the empennage is to be increased in size and the fuselage lengthened by approximately three feet using standard construction techniques.

Wing Weight

The structural weight of the wing can be divided into several classes for analysis. The weight breakdown in terms of material is given below for the proposed wing.

1. Primary structure: Material required to resist shear, bending, and torsion loads

2. Secondary structure: Material required for the leading and trailing edges and control surfaces

3. Miscellaneous: Material required for joint inefficiency, minimum gage materials, and non-tapered sections.

Primary Structure. Figure 48 illustrates the airfoil under consideration and the equivalent primary structure which is used in the analysis. For the purpose of this analysis, the airfoil is considered as typical two spar, rib, stringer panel construction.

The bending moment at the root of the wing is given by $M = Vb$, where $V = V_L - V_I$. Since there are no wing engines, it can be assumed, for purposes of calculating an ideal structure, that the lift distribution equals the inertia distribution. Since wing

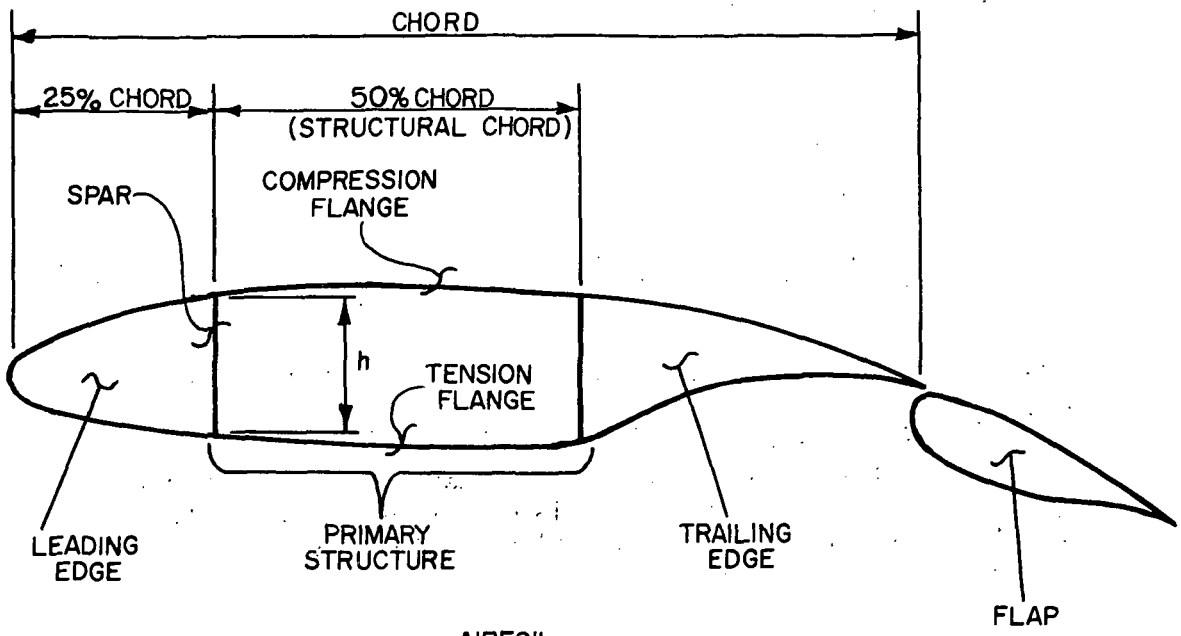

a. AIRFOIL

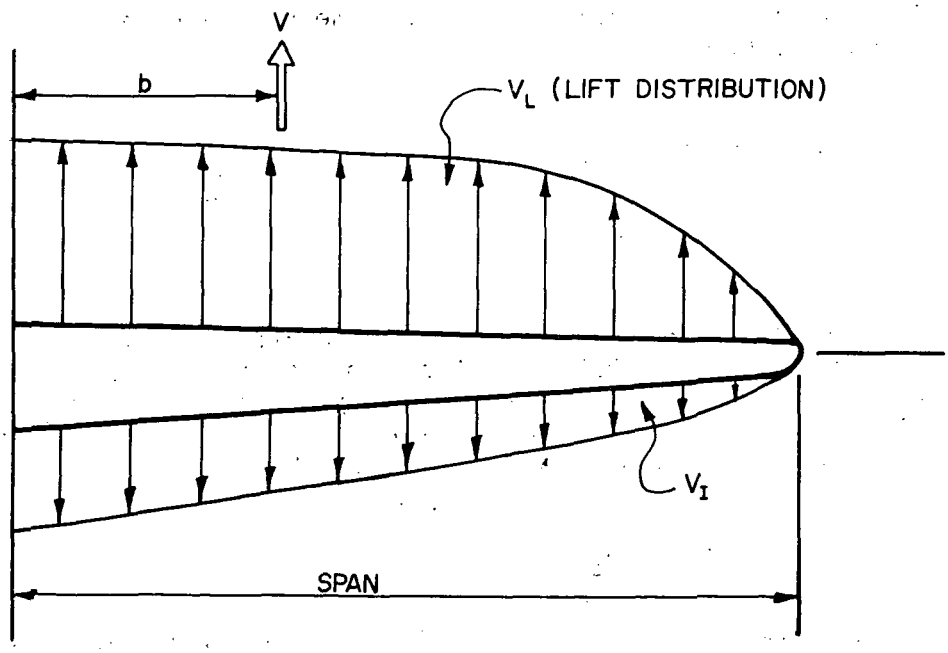

b. LOAD DISTRIBUTION

Figure 48. Weight analysis model.

inertia is a function of wing weight, V_I can be calculated by a reduction factor I_b, where

$$I_b = (W_g - W_w)/W_g \tag{88}$$

The total bending load is then

$$M = nI_bVb \quad \text{where } n = \text{load factor and } V = V_L \tag{89}$$

Finding the unknown wing weight as a function of wing weight requires an iteration process; however, the wing weight should be small compared to gross weight. I_b is then approximately equal to one. Once a wing weight is determined, the process can be repeated if additional accuracy is desired. This moment can be considered as a couple and resolved into forces acting in the flange plane. The flange force P becomes

$$P = M/h = nVb/h \tag{90}$$

The stress in the tension flange and the required area in the tension flange are given as

$$s_{bt} = P/A_{tf} = P/\bar{t}Cs \tag{91}$$

$$A_{tf} = P/S_t \tag{92}$$

The relationship for the compression flange is not so straightforward. Assuming that the failure mode is by wide column buckling and that the axial compression is evenly distributed, $q = P/C_s$. Using q and L as parameters and Figure 49a, the compression relationship for $\bar{t}$ is

$$\bar{t} = .0012L + z/S_c \quad . \tag{93}$$

Multiplying by C_s gives the required compression flange area

$$A_{cf} = .0012LC_s + P/S_c \quad . \tag{94}$$

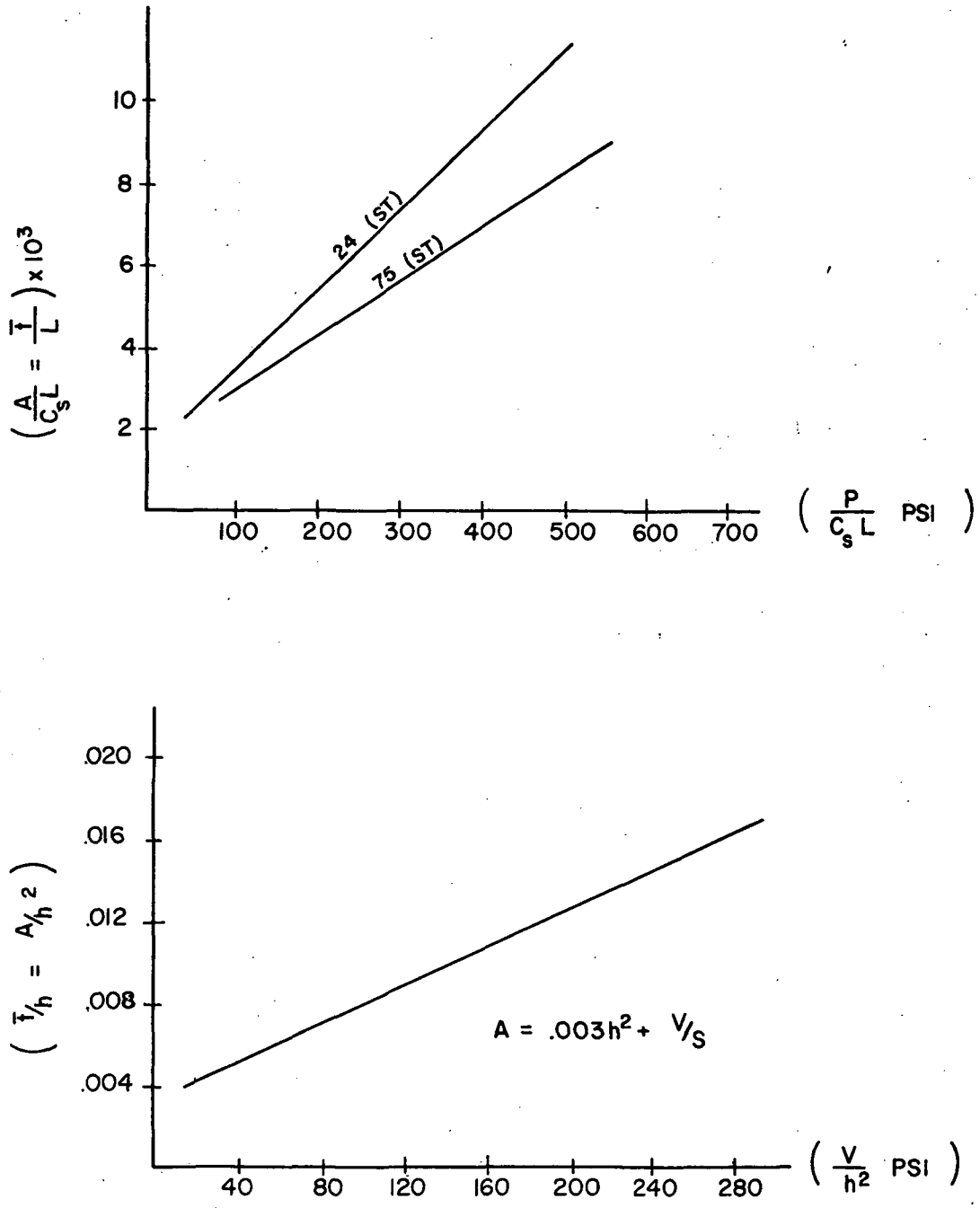

Figure 49. Optimum weight of shear and compression panels.

The total flange area is given by combining equations (92) and (94).

The development of the shear area follows much the same pattern as that of bending. As with bending, the main problem is determining the appropriate stress factor for the failure mode. If the web height and shear load are known at a particular section, the minimum area can be determined from these parameters. Figure 49b shows the optimum design envelope for a shear web with beaded holes. This curve can be approximated by $A_s/h^2 = .003 + V/h^2S_s$. Multiplying this equation by h^2 gives the required shear web area.

$$A_{sw} = .003h^2 + V/S_s. \tag{95}$$

The last section to be considered for primary loading is the shear ribs which transmit shear loads normal to the tension and compression flanges. The rib model is illustrated in Figures 50a and 50b. The total shear load across L is given by $V = (W_g/S_w)nLC$, and $Ra = V/2$. From the symmetry of Figure 50c, it is obvious that the maximum moment occurs at the center. Taking moments with $x = C_s/2$ gives

$$M' = 1/2(W_g/S_w)nLC(C_s/2) - n(W_g/S_w)L(C/2)(C_s/4)$$

$$= n(W_g/S_w)LCC_s(1/4 - 1/8)$$

$$= n/8(W_g/S_w)LCC_s \ . \tag{96}$$

This moment is resisted by the rib flange material. Reducing M' to an equivalent couple gives the resulting flange force P' which equals M'/h. The flange stress is then given by $s_f = P'A'_{rf} = M'/A'_{rf}h$. The total flange material is

$$A_{rf} = n/4(W_g/S_w)LCC_s/S_t(C_s/L)(1/h) \quad \text{area/unit span} \tag{97}$$

Equation (95), given for spar web shear, can be modified to describe the area required to resist rib shear. This modification results in

$$A_{rs} = .003h^2 + nLC/S_s(W_g/S_w) \ . \tag{98}$$

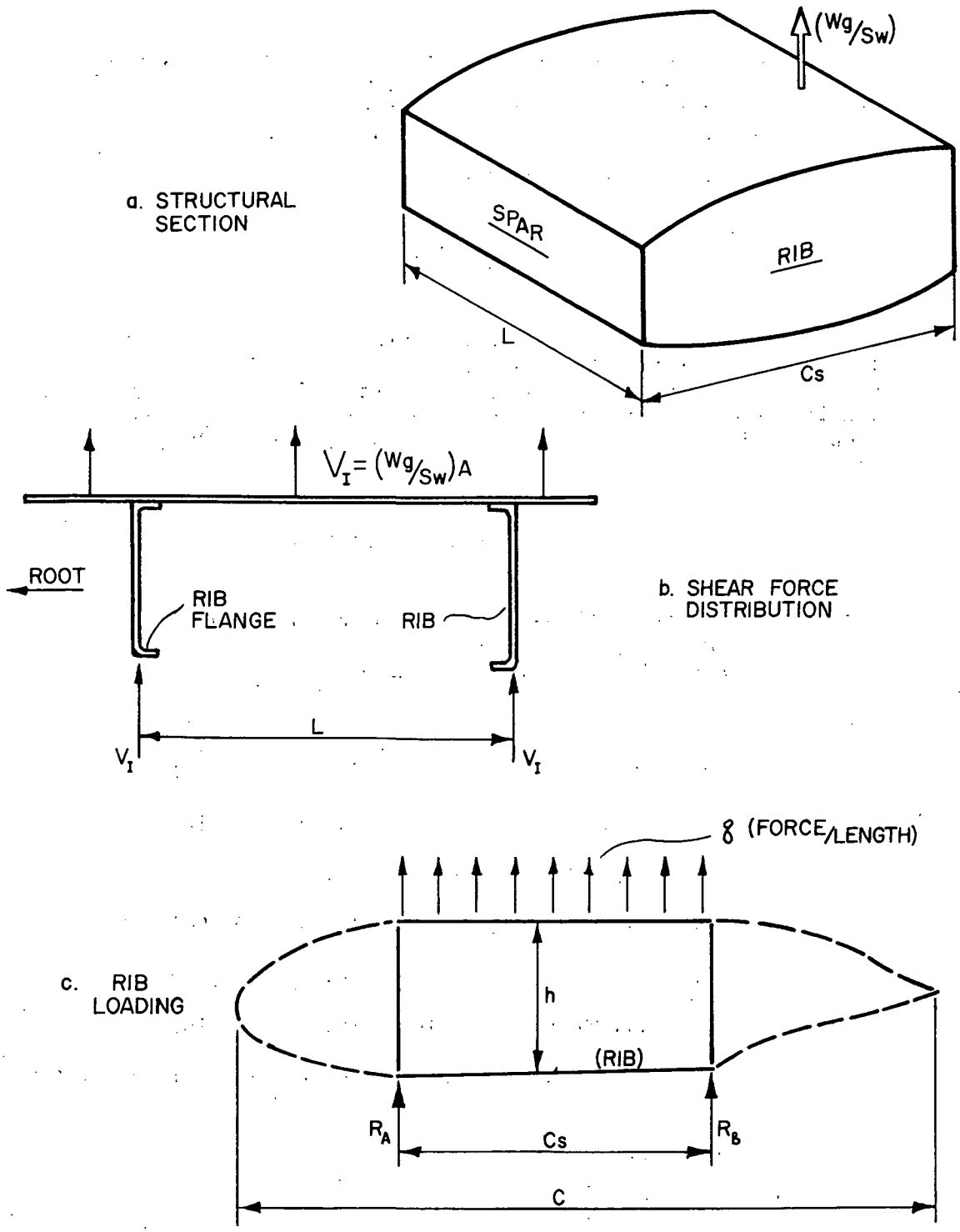

Figure 50. Rib analysis model.

An applied, equation (98) assumes that the load is evenly distributed over the entire area. For the case under consideration, this is only approximately true for the area of the structural chord C_s. If the area of C_s is assumed constant, multiplying (98) by C_s/L gives the required area/unit span

$$A_{rs} = .003h^2C_s/L + nCC_s(W_g/S_w)/S_s \quad . \tag{99}$$

The total volume of material required for the primary structure is obtained by integrating equations (92), (94), (95), (97), and (99) over the span and adding the results. Table 25 lists the geometry, loading, and material parameters necessary to determine the area required for primary root material. These areas have been calculated as follows:

TABLE 25. MATERIAL PARAMETERS

Basis: a. Airfoil, NACA series 23012 with Fowler flap
b. Material, 24TS aluminum
c. Aircraft, Piper Cherokee 235-C

Parameters:

1. W_g = 2900 lbs.	9. C_s = 48 in.
2. V = 1450 lbs.	10. b = 37.8 in.
3. n = 3.8	11. h = 9.2 in.
4. safety factor = 1.5	12. S_t = 65,000 psi
5. P = 33,958 lbs.	13. S_c = 38,000 psi
6. span = 15 ft.	14. S_s = 21,500 psi
7. mean chord = 67.2 in.	15. L = 9.2 in.
8. root chord = 96 in.	16. (W_g/S_w) = 17.2 lbs/ft^2

a. $A_{ft} = .5225$ in^2

b. $A_{fc} = 1.424$ in^2

c. $A_{sw} = .638$ in^2

d. $A_{rf} + A_{rs} = 1.5345$ in^2

The primary structure is also subjected to torsional loads. It is difficult to estimate the sectional areas required to resist torsional shear without a detailed analysis of shear flows and structure geometry; however, the ratio of $t_s/\bar{t}$ can be predicted. Assuming this value is approximately 0.5, then 50% of the compression and tension panels is skin, which is capable of resisting shear loads. A further assumption is that the material required to resist only torsion loads is approximately 2/3 of the available shear material. The total material to resist torsional shear is then given as

$$A_s = 2/3[.5(A_{ft} + A_{fc}) + A_{sw} + A_{rf} + A_{rs}] \quad (100)$$

The total primary root material is the sum of equations (92), (94), (95), (97), (99), and (100), which, for the areas given, equals 6.22 in^2. The next step is to integrate this area over the span. If a parabolic shape of the form $A = ax^2 + bx + c$ is assumed, integration of this area shape over the span gives the complete volume of material. Applying boundary conditions that A = 6.22 at x = 0, and A = 0 at $x = L_x$ and integrating yields

$$\text{Vol.} = 6.22L_w - (6.22/3)L_w. \quad (101)$$

Substituting L_w = 180 inches into equation (101) and multiplying this value by the value of aluminum density, .100 lb/in^3, gives the total primary wing weight of 74.59 lbs.

Secondary Structure. The treatment of secondary structures is not as straightforward as that of the primary structures. In most cases, these are determined by material construction requirements instead of load requirements. Shanley (Ref. 32) indicates that secondary structures such as flaps should be treated by experience in the early development of the structure. He has suggested a value of .0243 lb/in^2 as the weight-per-unit area required for metal Fowler flaps. This value has been experimentally determined from a large number of aircraft and includes the weight of the trailing-edge support structure and extension tracks. For full-span flaps which are 30% chord, the flap weight is

$$W_{ff} = (.0243)(.3)(67.2)(180) = 88.3 \text{ lbs.} \quad (102)$$

In the case of the leading edge, it can be assumed that the skin and any reinforcement used can be represented by the

equivalent skin thickness, of the wide column compression flange. This is based on the assumption that the leading edge will be dictated by material continuity instead of load requirements. For a leading edge of 25% chord, the curved path of the leading edge equals 37.6 inches at the mean chord. For a compression skin thickness of .0164 inches, the weight of the leading edge is

$$W_{le} = .100[(.0164)(37.6)(180)] = 11.196 \text{ lbs.} \tag{103}$$

Non-Optimum Weight. There are generally four sources of weight increase from non-optimum proportions:

1. Joint inefficiency
2. Doubler or splice effects
3. Non-tapered members
4. Necessity to use standard gauge materials

The effects of these parameters have been widely considered in aircraft construction. It has been found in most cases that these effects represent a certain portion of the minimum structural weight. The non-optimum structural weight can then be expressed as

$$W_{act} = W_{opt} + W_{opt}\,(\text{Sum}.k_i) \tag{104}$$

where k_i represents the percentage increase in the optimum weight caused by the various parameters. These values have been experimentally determined from a large number of commercial aircraft. Average values taken for typical construction are given below.

a. $k_1 = .30$ (joint inefficiency)
b. $k_2 = .15$ (doubler effect)
c. $k_3 = .31$ (non-tapered members)
d. $k_4 = .30$ (standard gauge requirements)

Recognizing that the flap weight calculated above is statistically correct, all other weights must be corrected using the non-optimum factors listed above. The resulting wing weight is given as

$$W_{wing} = W_{ff} = (1 + k_1 + k_2 + k_3 + k_4)(A_{ft} + A_{fc} + A_{sw} + A_{rf} + A_{rs} + A_s + A_{le}) \tag{105}$$

$$W_{wing} = 252.16 \text{ pounds.}$$

As previously noted, the above estimate neglects the load-reducing effect of wing inertia. This area could be pursued by continuing the process until the estimates converged.

Horizontal Tail Weight

Figure 51 illustrates horizontal tail loading based on the recommendations of Reference 32. The resulting bending moment at the span root becomes

$$M_r = (12.63/4)(6.32)(50) = 12{,}000 \text{ in-lb} \quad (106)$$

and the shear load at the root is

$$V_r = 6.32\ (50) + 316 \text{ lb.} \quad (107)$$

Semi-monocoque construction with a single spar located at 50% chord is assumed. If it is further assumed that the spar web carries the complete shear load, the area of the shear web becomes, from Figure 49.

$$A_{sw} + .003h^2 + (V_r/S_s)sf \quad (108)$$

$$A_{sw} = .003(2.86)^2 + (316/21{,}500)1.5 + .0468 \text{ in}^2/\text{in.} \quad (109)$$

If the tension and compression flanges carry only axial loads, the load becomes

$$P_f = M_r/h = 12{,}000/2.86 = 4{,}200 \text{ lb.} \quad (110)$$

The area required for the tension flange will be

$$A_{tf} = 4{,}200(1.5)/65{,}000 = .097 \text{ in}^2/\text{in.} \quad (111)$$

The compression area becomes, from Figure 49

$$A_{cf} = .0012(6.32)12 + 4{,}200(1.5)/38{,}000 = .257 \text{ in}^2. \quad (112)$$

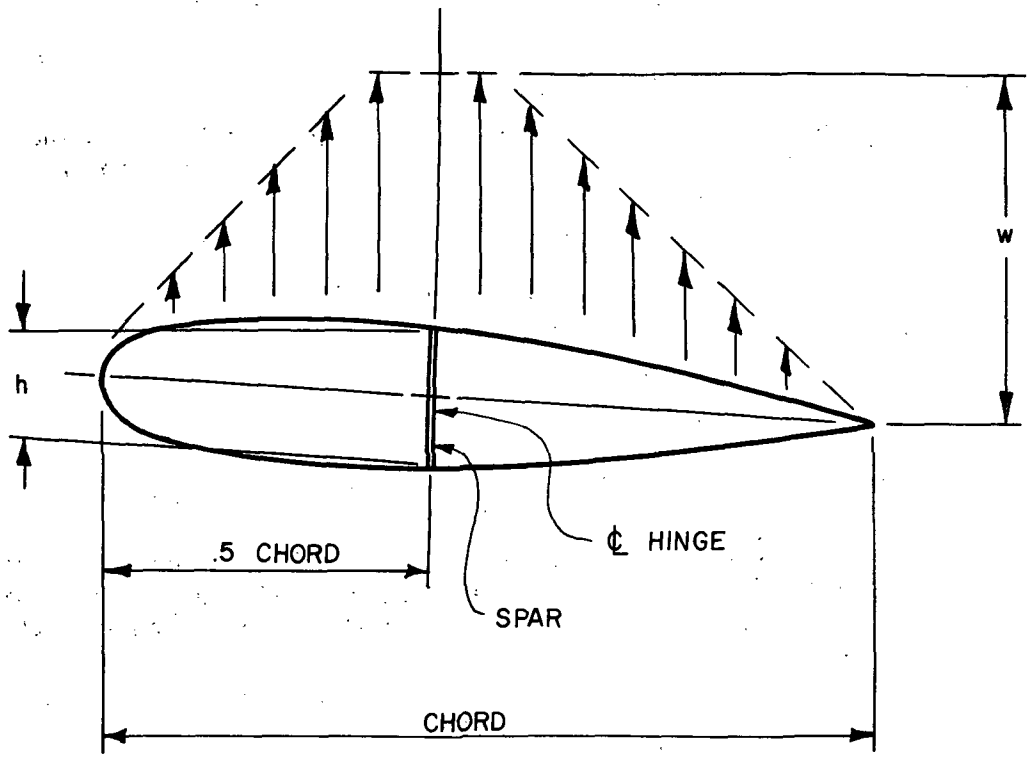

MEAN CHORD = 2.5 ft.

SPAN = 12.63 ft.

h = 2.86 inches (average)

t = .020 inches (minimum guage)

n = 3.8

w = 34.5 lbs./ft^2 (corrected for load factor)

Figure 51. Horizontal tail, geometry and loading, reference 23012 airfoil.

The material required for the leading and trailing edges will equal the average skin thickness multiplied by the equivalent length of material. Assuming that the flange equals 1.5 ft, the remaining length for the edges is 34.5 in. The skin area then becomes

$$A_{skin} = 34.5t = .69 \text{ in}^2 . \quad (113)$$

Assuming the same proportion of torsional shear material as used in the wing,

$$A_{ts} = .667(1.09) = .727 \text{ in}^2 . \quad (114)$$

The total root area will be the sum of equations (109), (111), (112), (113), and (114), which gives

$$A_t = 1.818 \text{ in}^2. \quad (115)$$

For a material density of .100 lb/in^3, the weight of the horizontal tail becomes

$$W_{ht} = (1 + k_1 + k_2 + k_3 + k_4)(.100)(1.818)(151.6) \quad (116)$$

$$W_{ht} = 52.1 \text{ lb.}$$

Vertical Tail Weight

The vertical tail and its theoretical load distribution are shown in Figure 52. Based on this loading, the root bending moment and shear are respectively 5170 in-lb and 172 lb. Based on the same assumptions used for the horizontal tail, the area of the shear web becomes

$$A_{sw} = .003(3.42)^2 + 172(1.5)/21,500 = .0472 \text{ in}^2 \quad (117)$$

For a flange loading of 1510 lb the area of the tension flange is

$$A_{tf} = 1,510(1.5)/65,000 = .035 \text{ in}^2 \quad (118)$$

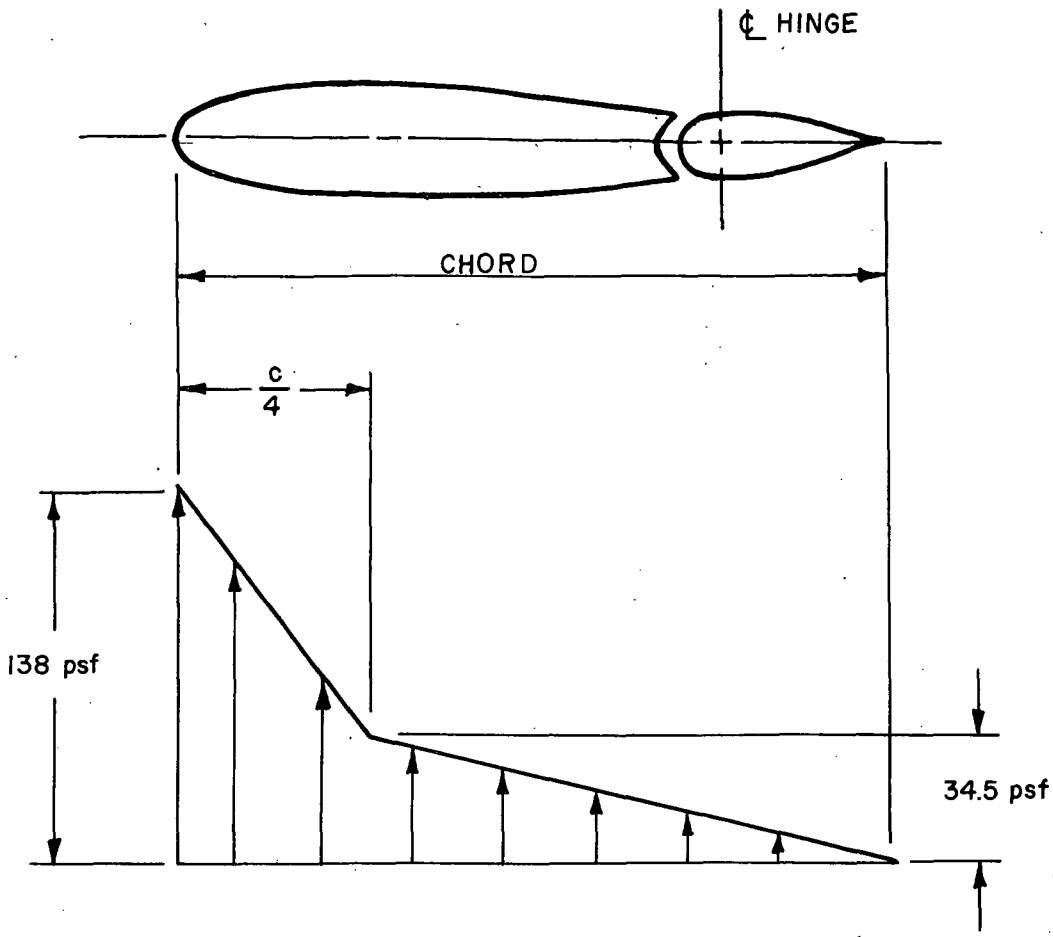

MEAN CHORD = 3.03 ft.

SPAN = 5 ft.

h = 3.42 in.

t = .020 in. (minimum gage)

n = 3.8

Figure 52. Vertical tail, geometry and loading.

and the compression flange area becomes

$$A_{cf} = 1{,}510(1.5)/38{,}000 + .0012(5) = .1317 \text{ in}^2 \quad . \tag{119}$$

For a flange length of 16.3 inches, the remaining length for the leading and trailing edges is 41.4 inches, and the skin area is

$$A_{skin} = 41.4t = .828 \text{ in}^2 \quad . \tag{120}$$

For the torsional shear material,

$$A_{ts} = .667(1.04) = .7938 \text{ in}^2 \quad . \tag{121}$$

The total root area then becomes

$$A_t = 1.834 \text{ in}^2. \tag{122}$$

Therefore, the total material required at the root is 1.834 in^2. For a material density of .100 lb/in^3, the weight of the vertical tail becomes

$$W_{vt} = (1 = k_1 + k_2 + k_3 + k_4)(.100)(1.834)(60) \tag{123}$$

$$W_{vt} = 21 \text{ lb}.$$

Thus, the weight estimate for the new empennage section recommended for aerodynamic purposes is 73.1 lb.

AEROELASTIC ANALYSIS

Aeroelastic behavior can be characterized as structural response to aerodynamic forces. This response is normally described in terms of structural deflections resulting from aerodynamic forces or, more commonly, as the effect of structural deflections on aerodynamic performance. Since any structure must be designed to withstand the maximum expected loads, a major consideration is determining what modes and magnitudes of deflection are acceptable from a performance standpoint. This may be restated as a consideration of the effect which lift and control surface deformation have on aerodynamic performance. These deformations can be considered in two classes.

1. Flutter, which may be classified as aerodynamically-forced, unsteady, divergent vibration

2. Stable deformation, which may be described as deformations which assume and maintain a deformed shape particular to a given flight mode.

In studying the aerodynamic requirements for a simple-to-fly aircraft, it is necessary to determine the interaction of structural geometry, inertia, and elastic properties and the relationship of these parameters to lift and control surface deformation.

Flutter

Early in the analysis of any aircraft structure, it is desirable to examine its in-flight stability. This is emphasized by the need to predict the level of flight parameters which must not be exceeded if safe, structurally stable flight is to be maintained. From the structural viewpoint, the parameter of most importance is the flutter velocity or, more directly, the flutter frequency. The problem can be approached from either of two paths. First an aircraft can be analyzed to determine whether or not the critical velocity lies outside the range of projected operations. Second, if the critical velocity lies inside the desired range, the structure can be examined to determine what modifications will make the aircraft structure stable at the desired velocity. In either case, the net results and procedure are the same:

1. Determine the critical flutter velocity and critical frequency

2. Determine the effects of the various structural parameters on the critical frequency

3. Modify the structure to increase the flutter velocity above the operating range.

A large amount of previous work has been directed toward determining the effect of various parameters or properties on the critical velocity. Attempts have also been made to offer a simplified flutter analysis. Most are based on the theory that control surface flutter can be prevented in airplanes with dive speeds less than 300 mph, if the control surfaces are dynamically balanced. Scanlan (Ref. 33) suggests the following formula for the maximum permissible unbalance:

$$K/1 = 0.20[6 - (V_d/150)^2] \quad . \tag{124}$$

This formula is applicable only for cases where perpendicular axis dynamic balance is important, such as wing bending and aileron or flap vibration.

Detailed flutter analysis does not normally play an important role in the design of light aircraft. Experience has shown that the critical velocities are usually sufficiently greater than the maximum design velocities. The proposed modification of the Piper Cherokee does not fall into this area of existing experience. Since the aircraft may be operated at the maximum design speeds with extended flaps, careful attention must be given to flutter analysis in determining the effect of flap extensions on the critical velocity.

Figure 53-a shows the flutter model for the wing under consideration. The mathematical model can be formulated using an energy analysis and applying the Lagrange equations of motion. From Figure 53-b, the velocity of a wing mass particle subjected to translational and rotational motion is given as

$$V_w^2 = \dot{h}^2 + R^2\dot{\alpha}^2 - 2\dot{h}R\cos\theta. \tag{125}$$

Assuming small angles of rotation, α will approximately equal 180° and the particle velocity becomes

$$V_w^2 = (\dot{h} + R\dot{\alpha})^2 \quad . \tag{126}$$

The kinetic energy for the wing then becomes

$$\bar{V}_w = 1/2 \int (\dot{h} + R\dot{\alpha})^2 dm_w \tag{127}$$

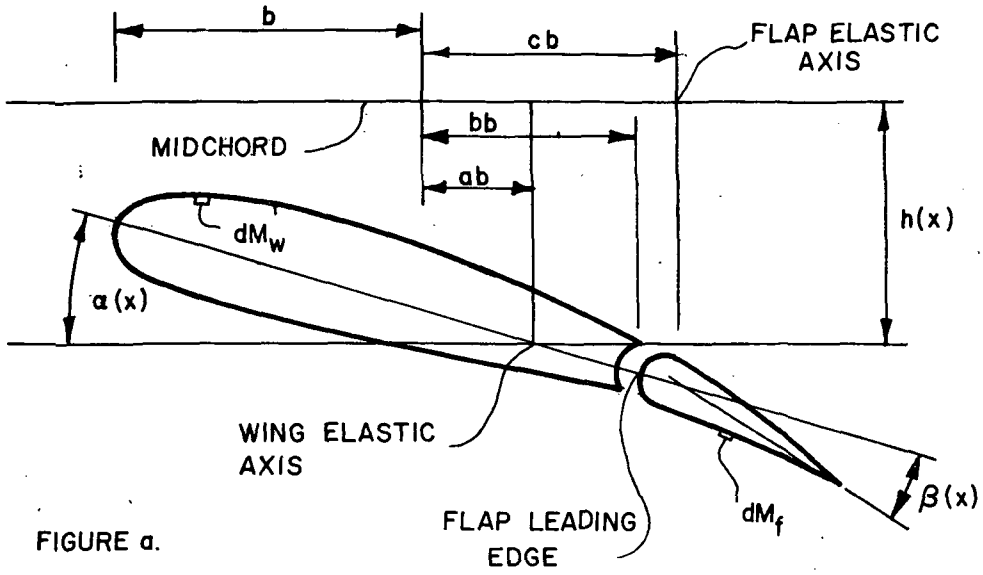

FIGURE a.

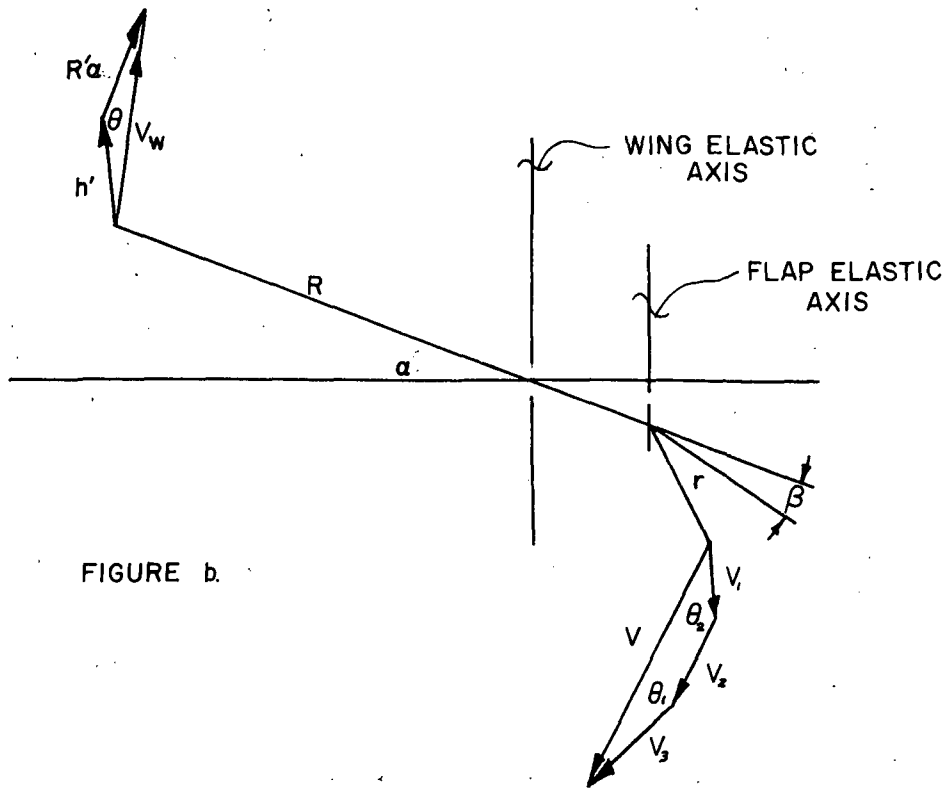

FIGURE b.

Figure 53. Flutter model.

$$\bar{V}_w = 1/2\int \dot{h}^2\, dm_w + 1/2\, R^2\dot{\alpha}^2 dm_w + 1/2\int 2R\dot{\alpha}h\cdot dm_w \qquad (128)$$

Expressing equation (128) in terms of station mass and the static and inertia moments gives

$$\bar{V}_w = 1/2\, \bar{m}_w \dot{h}^2 + 1/2\, \bar{I}_w \dot{\alpha}^2 + \bar{S}_w \dot{\alpha}\dot{h} \qquad (129)$$

Likewise, an expression for the velocity of a flap mass particle can be written. With α and β small θ_1 and θ_2 approaching 180^o giving

$$V_f^2 = [\dot{h} + (c - a)b\dot{\alpha} + r\dot{\beta}]^2 \qquad (130)$$

and the kinetic energy of the flaps becomes

$$\bar{V}_f = 1/2\int \dot{h}^2\, dm_f + 1/2\int (c-a)^2 b^2 \dot{\alpha}^2 dm_f + 1/2\int r^2\dot{\beta}^2 dm_f$$
$$+ \int rh\ddot{\beta} dm_f + \int [(c-a)b + r]\dot{\alpha}\dot{h}\, dm_f$$
$$+ \int [(c-a)br + r^2]\dot{\alpha}\dot{\beta} dm_f \quad . \qquad (131)$$

Expressing equation (131) in terms of station mass and static and inertia moments gives

$$\bar{V}_f = 1/2\, \bar{m}_f \dot{h}^2 + 1/2\, \bar{I}_f \dot{\alpha}^2 + 1/2\, \bar{I}_\beta \dot{\beta}^2 + \bar{S}_f \dot{h}\, \dot{\alpha}$$
$$+ \bar{S}_\beta \dot{h}\, \dot{\beta} + [(c-a)b\bar{S}_\beta + \bar{I}_\beta]\dot{\alpha}\dot{\beta} \qquad (132)$$

The total kinetic energy of the wing-flap combination per unit span becomes

$$\bar{V}_k = \bar{V}_w + \bar{V}_f \qquad (133)$$

If

$$\bar{m} = \bar{m}_w + \bar{m}_f \tag{134}$$

$$\bar{S}_\sigma = \bar{S}_w + \bar{S}_p \tag{135}$$

$$\bar{I}_\sigma = \bar{I}_w + \bar{I}_f \tag{136}$$

Equation (133) becomes

$$\bar{V}_k = 1/2\bar{m}\dot{h}^2 + 1/2\ \bar{I}_\alpha\ \dot{\alpha}^2 + \bar{I}_\beta\ \dot{\beta}^2 + \bar{S}_\alpha \dot{h}\dot{\alpha} \quad \bar{S}_\beta \ddot{h}\beta + [(c-a)b\bar{S}_\beta + \bar{I}_\beta]\dot{\alpha}\dot{\beta} \tag{137}$$

Likewise, an expression for the potential energy of the wing-flap combination in terms of combined mass, mass moments of inertia, and the uncoupled natural frequencies can be written. The equation for the potential energy is then given as

$$\bar{V}_p = 1/2\ \bar{m}w_h^2\ h^2 + 1/2\ \bar{I}_\alpha w_\alpha^2\ \alpha^2 + \bar{I}_\beta w_\beta^2\ \beta^2 \tag{138}$$

It has been shown that structural damping is a function of the amplitude of an elastic system and not its frequency. It has been found experimentally that damping can be described by a force whose magnitude is proportional to the elastic restoring force and in phase with the velocity of oscillation. If the proportionality constant is taken as g, and $i = \sqrt{-1}$, simple harmonic motion can be defined as

$$x = x_o e^{i\omega t} \tag{139}$$

Then an expression for the dissipation energy of the wing-flap system can be written. Taking ω as the coupled natural frequency of the wing-flap combination, Scalian suggests the following relationship for the dissipation energy:

$$\bar{D} = 1/2\ \frac{\bar{m}g_h\omega_h^2\ h^2}{\omega} + 1/2\ \bar{I}\alpha\ \frac{g_\alpha\omega_\alpha^2\ \alpha^2}{\omega} + 1/2\ \frac{1_\beta g_\beta \omega_\beta^2\ \beta^2}{\omega} \tag{140}$$

The Lagrangean equation of motion is given as

$$\frac{d(\delta V_k)}{d+(\delta q^{\cdot})} + \frac{\delta V_p}{\delta q} + \frac{\delta D}{\delta q^{\cdot}} = Q \tag{141}$$

where q represents the variable under consideration and Q the forcing function. Applying the Lagrange equation to the energy expressions of the wing-flap combination results in three simultaneous equations.

$$\bar{m}\ddot{h} + \bar{S}_\alpha \ddot{\alpha} + \bar{S}_\beta \ddot{\beta} + \frac{\bar{m}\omega_h^2 g_h \dot{h}}{\omega} + \bar{m}\omega_h^2 = \bar{Q}_h \tag{142}$$

$$\cdot\bar{S}_\alpha \ddot{h} + \bar{I}_\alpha \ddot{\alpha} + [(c-a)b\bar{S}_\beta + \bar{I}_\beta]\ddot{\beta} + \frac{\bar{I}_\alpha \omega_\alpha^2 g_\alpha \alpha^{\cdot}}{\omega} + \bar{I}_\alpha \omega_\alpha^2 \alpha = \bar{Q}_\alpha \tag{143}$$

$$\bar{S}_\beta \ddot{h} + [(c-a)b\bar{S}_\beta + \bar{I}_\beta]\ddot{} + \bar{I}_\beta \ddot{\beta} + \frac{\bar{I}_\beta \omega_\beta^2 g_\beta}{\omega} \beta^{\cdot} + 1_\beta \omega_\beta^2 \beta = \bar{Q}_\beta \tag{144}$$

The analysis of the aerodynamic forcing functions of the wing-flap combination moving in simple harmonic motion is quite detailed. The analysis of these forces for a three-dimensional airfoil was first accomplished by Theodorsen (Ref. 34). Any change in the shape of an airfoil is accompanied by a change in the circulation about it. Any change in circulation is further accompanied by a vortex shed from the trailing edge of the airfoil. For the case of simple harmonic motion, a continuous set of shed vortices develop behind the airfoil section. These vortices in turn produce vertical velocities on the airfoil. The lift of an oscillating airfoil moving at constant forward velocity is a function of the deflection motion as well as deflection shape. The aerodynamic moments are likewise functions of the oscillating motion and shape. Therefore, the airfoil lift and the aerodynamic moments about the elastic and flap axes are functions of h, $\dot{h}$, $\ddot{h}$, α, $\dot{\alpha}$, $\ddot{\alpha}$, β, $\dot{\beta}$, $\ddot{\beta}$, ν, ω, and airfoil geometry. Theodorsen developed the following expressions for the aerodynamic lift and moment forcing functions for the full span:

$$Qh = \int_0^{\ell} Lp(x)dx \tag{145}$$

$$Q_{\alpha} = \int_0^{\ell} MF(x)dx \tag{146}$$

$$Q\beta = \int_0^{\ell} Tdx \tag{147}$$

where

$$L = \pi\ell b^2\omega^2 f(x)L_h h + \pi\ell b^3\omega^2([L_{\alpha} - (1/2 + a)L_h]F(x)\alpha + [L_{\beta} - (c-e)L_z]\beta) \tag{148}$$

$$M = \pi\ell b^3\omega^2[M_h - (1/2 + a)L_h]f(x)h + \pi\ell b^4\omega^2([M_{\alpha} - (1/2+a)(L_{\alpha}+M_h) + (1/2 + a)^2 L_h]F(x)\alpha + M_{\beta} - (1/2 + a)L_{\beta} - (c-e)M_z + (c - e)(1/2 + a)L_z]\beta \tag{149}$$

$$T = \pi\ell b^3\omega^2[T_h - (c - e)P_h]f(x)h + \pi\ell b^4\omega^2([T_{\alpha} - (c - e)P_{\alpha} - (1/2 + a)T_h + (1/2 + a)(c - e)P_h]F(x)\alpha + [T_{\beta} - (c - e)(P_{\beta} + T_z) + (c - e)^2 P_z]\beta) \tag{150}$$

The terms L_h, L_{α}, L_{β}, L_z, M_h, M_{α}, M_{β}, M_z, T_h, T_{α}, T_{β}, T_z, P_h, P_{α}, P_{β}, and P_z are mathematically complex. Their detailed treatment is extremely complicated and beyond the scope of this study. These functions have been evaluated using the T functions of Theodorsen and the ϕ functions of Küssner (Ref. 33). Experience has shown that these terms, which are functions of $\nu/b\omega$, with the exception of L_h, L_{α}, and M_{α}, which are functions of $\nu/b\omega$ and $(\nu/b\omega)^2$, do not vary rapidly with $\nu/b\omega$ and can be assumed constant along the span as functions of $1/k = \nu/b_r\omega$. The terms L_h, L_{α}, and M_{α} can be rewritten as

$$L_h = C_1(L_h) + \frac{br}{b} C_2(L_h) \tag{151}$$

$$L\alpha = C_1(L\alpha) + \frac{br}{b} C_2(L\alpha) + \frac{br}{b}^2 C_3(L\alpha) \tag{152}$$

$$M\alpha = C_1(M\alpha) + \frac{br}{b} C_2(M\alpha) \tag{153}$$

where $C_1(L_h)$ is the constant part of L_h; $C_2(L_h)$ is the part of L_h which is a function of $\nu/b_r\omega$; $C_3(L_\alpha)$ is the part of L_α which is a function of $(\nu/b_r\omega)^2$. Values for all terms have been tabulated as functions of geometry and 1/k. Reference 33 has a complete set of the tabulated values for these terms.

Based on equations (148) through (153), a new set of functions can be defined which will lead to more clearly defined forcing functions. These relationships are given as follows:

$$A_{hh} = {}_o\int^{\ell} b^2[f(x)]^2 + brC_2(L_h)\ {}_o\int^{\ell} b[f(x)]^2dx \tag{154}$$

$$A_{h\alpha} = -{}_o\int^{\ell} ab^3 f(x)F(x)dx + brC_2(L\alpha){}_o\int^{\ell} b^2 f(x)F(x)dx$$

$$+ br^2C_3(L\alpha){}_o\int^{\ell} bf(x)F(x)dx - brC_2(L_h)$$

$${}_o\int^{\ell} (1/2 + a)b^2 f(x)F(x)dx \tag{155}$$

$$A_{\alpha h} = -{}_o\int^{\ell} ab^3 f(x)F(x)dx - brC_2(L_h){}_o\int^{\ell} (1/2 + a)b^2 f(x)F(x)dx \tag{156}$$

$$A_{\alpha\alpha} = {}_o\int^{\ell} (1/8 + a^2)b^4[F(x)]^2dx + brC_2(M_{\alpha o}\int^{\ell} b^3[F(x)]^2dx$$

$$+ brC_2(L_h){}_o\int^{\ell} (1/2 + a)^2b^3[F(x)]^2dx$$

$$- br^2C_3(L_\alpha)_o\int^{\ell}(1/2 + a)b^2[F(x)]^2dx$$

$$- br^2C_2(L_\alpha)_o\int^{\ell}(1/2 + a)b^3[F(x)]^2dx \qquad (157)$$

$$A_{h\beta} = \ell_1\int^{\ell}b^3f(x)[L - (c-e)L_z]dx \qquad (158)$$

$$A_{\alpha\beta} = \ell_1\int^{\ell}b^4F(x)[M_\beta - (1/2 + a)L_\beta - (c-e)M_z$$

$$+ (c - e)(1/2 + a)L_z]dx \qquad (159)$$

$$A_{\beta h} = \ell_1\int^{\ell}b^3f(x)[Th - (c - e)P_h]dx \qquad (160)$$

$$A_{\beta\alpha} = \ell_1\int^{\ell}b^4f(x)[T_\alpha - (c - e)P_\alpha - (1/2 + a)\ T_h$$

$$+ (1/2 + a)(c - e)P_h]dx \qquad (161)$$

$$A_{\beta\beta} = \ell_1\int^{\ell}b^4[T \ - (c - e)(P \ + T_z) + (c - e)^2P_z]dx \qquad (162)$$

Using equations (154) through (162), the forcing functions Q_h, Q_α, and Q_β can be redefined as

$$Q_h = \pi\ell\omega^2(A_{hh}h + A_{h\alpha}\alpha + A_{h\beta}\beta) \qquad (163)$$

$$Q_\alpha = \pi\ell\delta^2(A_{\alpha h}h + A_{\alpha\alpha}\alpha + A_{\alpha\beta}\beta) \qquad (164)$$

$$Q_\beta = \pi\ell\omega^2(A_{\beta h}h + A_{\beta\alpha}\alpha + A_{\beta\beta}\beta) \qquad (165)$$

A complete set of expressions now exists for the lift force and aerodynamic moments of the oscillating airfoil for its complete span. The next step in the analysis is to change the Lagrange equations from

unit span expressions to full span equations. This can be accomplished by using the following relationships:

$$M = \int_0^{\ell} \bar{m}(x)[f(x)]^2 dx \tag{166}$$

$$1_\alpha = \int_0^{\ell} \bar{1}_\alpha(x)[F(x)]^2 dx \tag{167}$$

$$1_\beta = \int_{\ell_1}^{\ell} \bar{1}_\beta(x) dx \tag{168}$$

$$S_\alpha = \int_0^{\ell} \bar{S}_\alpha(x) f(x) F(x) dx \tag{169}$$

$$S_\beta = \int_{\ell}^{\ell} \bar{S}_\beta(x) f(x) dx \tag{170}$$

$$P_{\alpha\beta} = \int_{\ell_1}^{\ell} [\bar{S}_\beta(x)(c - a)b + \bar{1}_\beta(x)] F(x) dx \tag{171}$$

Replacing the unit span terms in equations (142), (143), and (144) with the integrated functions above and equating the results to equations (163), (164), and (165) results in the dynamic equations for the full span airfoil.

$$M\ddot{h} + S_\alpha\ddot{\alpha} + S_\beta\ddot{\beta} + M\omega_h^2 h + \frac{g_h\omega_h^2 M}{\omega} h \quad .$$

$$= \pi\ell\omega^2[A_{hh}h + A_{h\alpha}\alpha + A_{h\beta}\beta] \tag{172}$$

$$S_\alpha\ddot{h} + 1_\alpha\ddot{\alpha} + P_{\alpha\beta}\ddot{\beta} + 1_\alpha\omega_\alpha{}^2\alpha + \frac{g_\alpha\omega_\alpha^2 1_\alpha}{\omega} \&$$

$$= \pi\ell\omega^2[A_{\alpha h}h + A_{\alpha\alpha}\alpha + A_{\alpha\beta}\beta] \tag{173}$$

$$S_\beta\ddot{h} + P_{\alpha\beta}\ddot{\alpha} + 1_\beta\ddot{\beta} + 1_\beta\omega_\beta^2\beta + \frac{g_\beta\omega_\beta^2 1_\beta}{\omega} \beta$$

$$= \pi\ell\omega^2[A_{\beta h}h + A_{\beta\alpha}\alpha + A_{\beta\beta}\beta] \tag{174}$$

Since the system vibrates in simple harmonic motion with frequency ω at the flutter speed,

$$h'' = -\omega^2 h \tag{175}$$

$$\alpha'' = -\omega^2 \alpha \tag{176}$$

$$\beta'' = -\omega^2 \beta \tag{177}$$

$$h' = i\omega h \tag{178}$$

$$\alpha' = i\omega \alpha \tag{179}$$

$$\beta' = i\omega \beta \tag{180}$$

Substituting equations (175) through (180) into (172), (173), and (174) and simplifying yields the final set of dynamic equations.

$$[M + \pi\ell A_{hh} - M(1 + ig_h)(\frac{\omega_h}{\omega})^2]h + (S_\alpha + \pi\ell A_{h\alpha})\alpha + (S_\beta + \pi\ell A_{h\beta})\beta = 0 \tag{181}$$

$$(S_\alpha + \pi\ell A_{\alpha h})h + [I_\alpha + \pi\ell A_{\alpha\alpha} - I_\alpha(1 + g_\alpha)(\frac{\omega_\alpha}{\omega})^2] + (P_{\alpha\beta} + \pi\ell A_{\alpha\beta})\beta = 0 \tag{182}$$

$$(S_\beta + \pi\ell A_{\beta h})h + (P_{\alpha\beta} + \pi\ell A_{\beta\alpha})\alpha + [I_\beta + \pi\ell A_{\beta\beta} - I_\beta(1+ig_\beta)(\frac{\omega_\beta}{\omega})^2]\beta = 0 \tag{183}$$

This could be re-expressed in determinate form as

$$\begin{matrix} a_{11} & a_{12} & a_{13} \\ a_{21} & a_{22} & a_{23} \\ a_{31} & a_{32} & a_{33} \end{matrix} \begin{matrix} h \\ \alpha \\ \beta \end{matrix} = 0 \qquad (184)$$

For a solution other than $h = \alpha = \beta = 0$ to exist, the determinant of coefficients must vanish: $|A| = 0$. If a function X is defined as

$$X = (\omega_\alpha/\omega)^2, \qquad (185)$$

expanding the determinant will result in a third order equation of the form

$$AX^3 + BX^2 + CX + D = 0 \qquad (186)$$

where A, B, C, and D are complex coefficients of the form $A_{real} + A_{imaginary}$. Equation (186) can then be expressed as two simultaneous equations of the form

$$A_r X^3 + B_r X^2 + C_r X + D_r = 0 \qquad (187)$$

$$A_i X^3 + B_i X^2 + C_i X + D_i = 0. \qquad (188)$$

The critical value of ω will occur when equations (187) and (188) vanish simultaneously. Then with k and ω known, the equation can be solved for the critical flutter velocity.

The flutter analysis as given is based on two underlying assumptions:

1. Air flow is incompressible.
2. The aspect ratio of the wing is infinite.

These assumptions have been experimentally verified for low-speed aircraft. It is generally recognized that the compressibility factor can be ignored for Mach numbers less than or equal to 0.5. No mathematical treatment has been devised to give a completely reliable account of the effect of very low aspect ratio wings. Experience has shown that the

effect of low aspect ratios is a small increase in flutter speed over the theoretical prediction. This then leads to the conclusion that the effect of these two assumptions will be a slightly conservative flutter velocity estimate.

The natural torsional frequency, torsional rigidity, and mass distribution of the wing are the most important inputs to the flutter determinant. It is generally agreed that the wing should have enough torsional rigidity to limit deflections to 3^{o} at the design loads. Wings with uniform taper would have a greater concentration of wing mass at the root. This would be desirable from the standpoint of mass distribution, but it would increase the percentage of tip deflection. In all cases, it is desirable to concentrate mass close to the elastic axis to reduce static and inertia moments. It is also highly desirable to balance the control surfaces dynamically so that they move with the structure as if rigidly attached, although the span-wise distribution of mass is of much greater importance.

Thus, the flutter problem is essentially one of solving for the characteristic root of a third order determinant. The problem is somewhat complicated in that the coefficients of the expanded third order polynomial have both real and imaginary parts. The technique employed here is one of separating the expanded determinant into two equations, one real and one imaginary. The characteristic roots $(\omega_{\alpha}\ \omega)^2$ of these independent equations are then plotted as functions of 1/k. The equations will intersect at the critical frequency of the original third order polynomial. The critical flutter velocity of the wing is then found from the relationship

$$1/k = v/b\omega \quad . \tag{189}$$

Table 26 contains the properties and terms which were used in evaluating the flutter velocity for the proposed wing modification. These estimated properties were obtained using the material requirements and distribution specified in the preliminary wing weight estimate. Using these values, the wing has been analyzed for flutter resulting from the following coupled modes of vibration:

1. Vertical wing bending, wing torsion, flap torsion
2. Vertical wing bending, wing torsion
3. Vertical wing bending, flap torsion
4. Wing torsion, flap torsion.

The root locus plots for these modes are given respectively in Figure 54 through 57 for the uniform wing being considered. Careful consideration was also given to the possible use of a tapered wing. Figure 58 shows the characteristic root plot for a uniformly tapered wing of 2.5 taper ratio. As shown in Figures

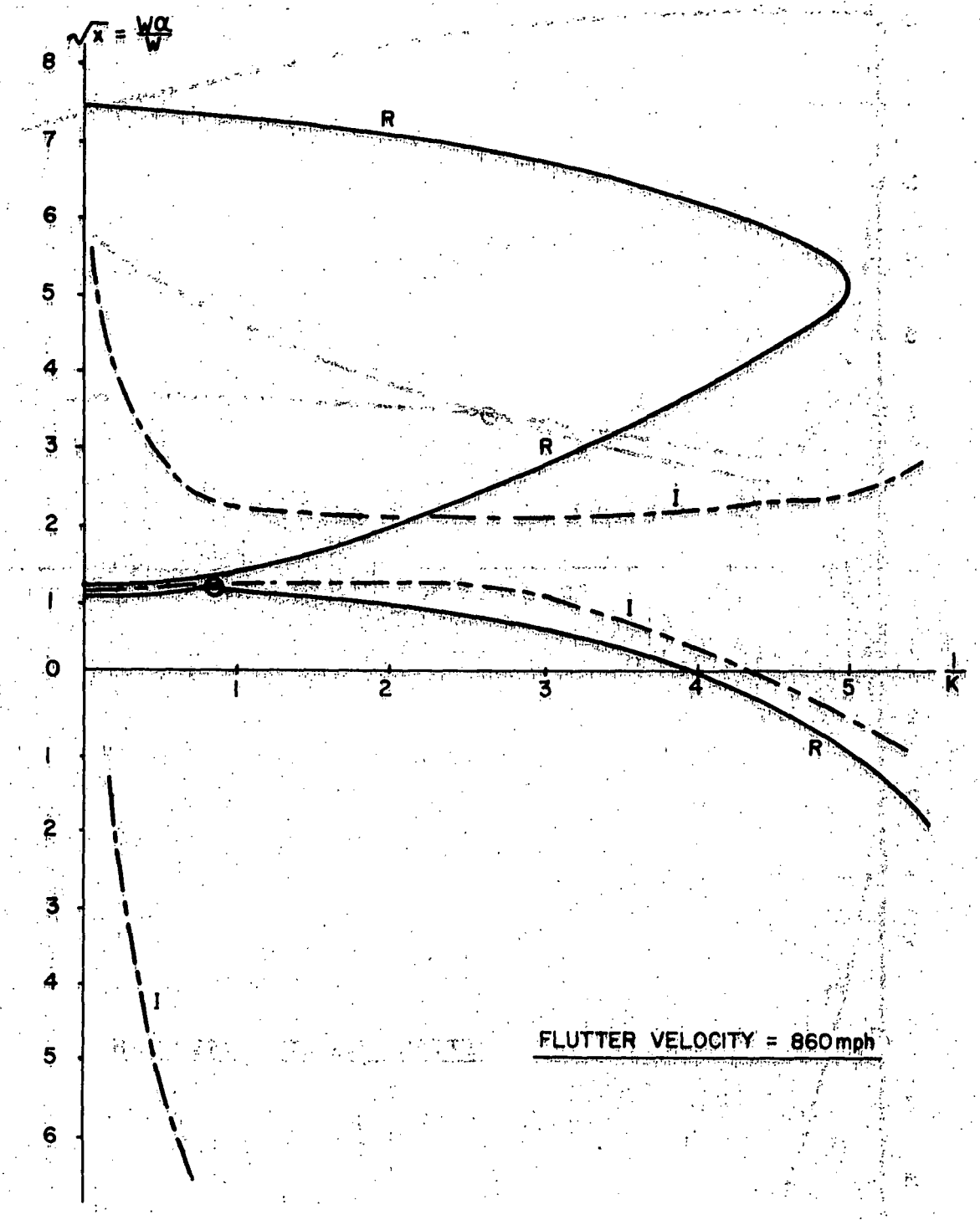

Figure 54. Characteristic flutter roots, three degrees of freedom, Case I: Bending, wing and flap torsion (uniform fixed free wing).

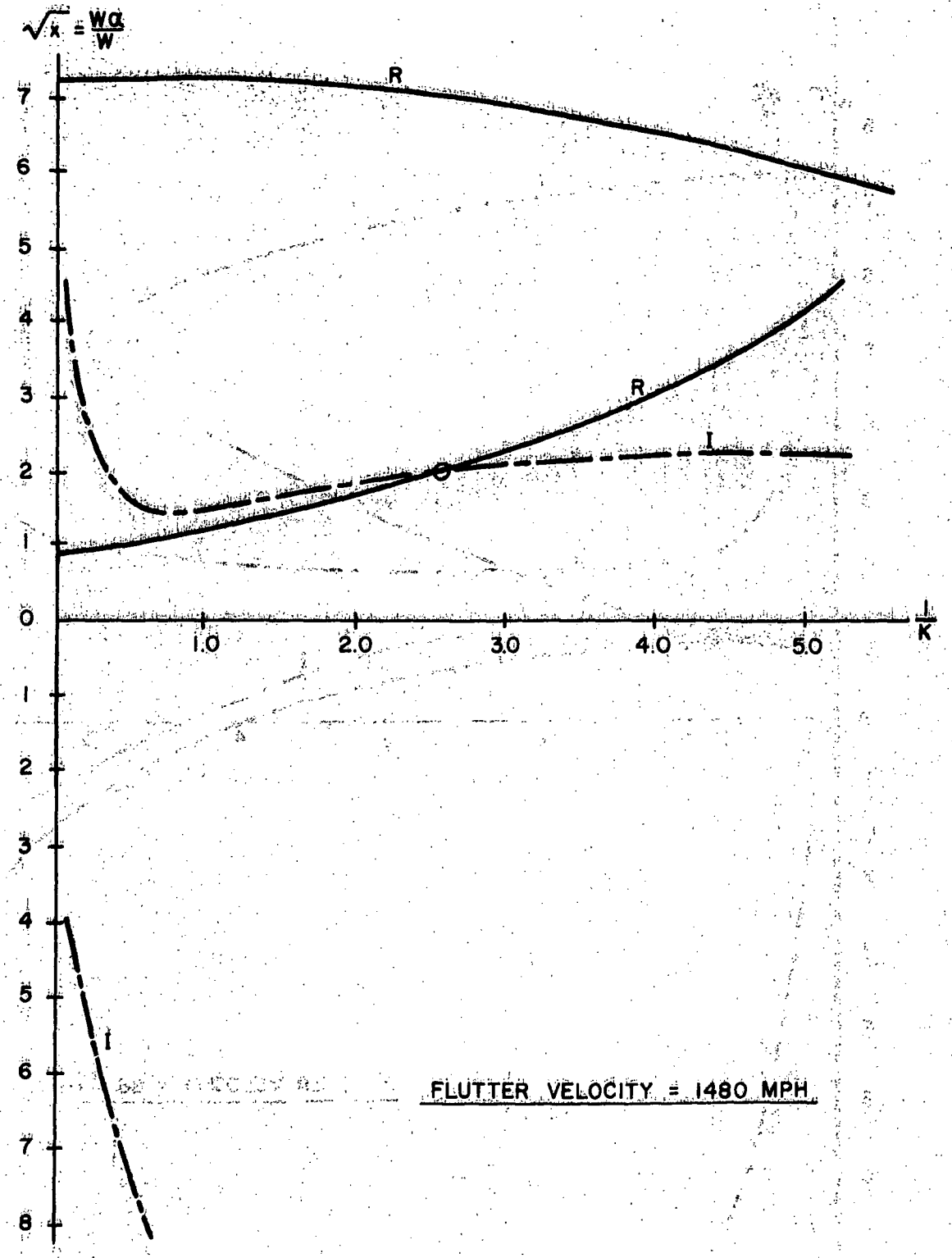

Figure 55. Characteristic flutter roots, two degrees of freedom. Case 2: Bending and wing torsion (uniform fixed free wing).

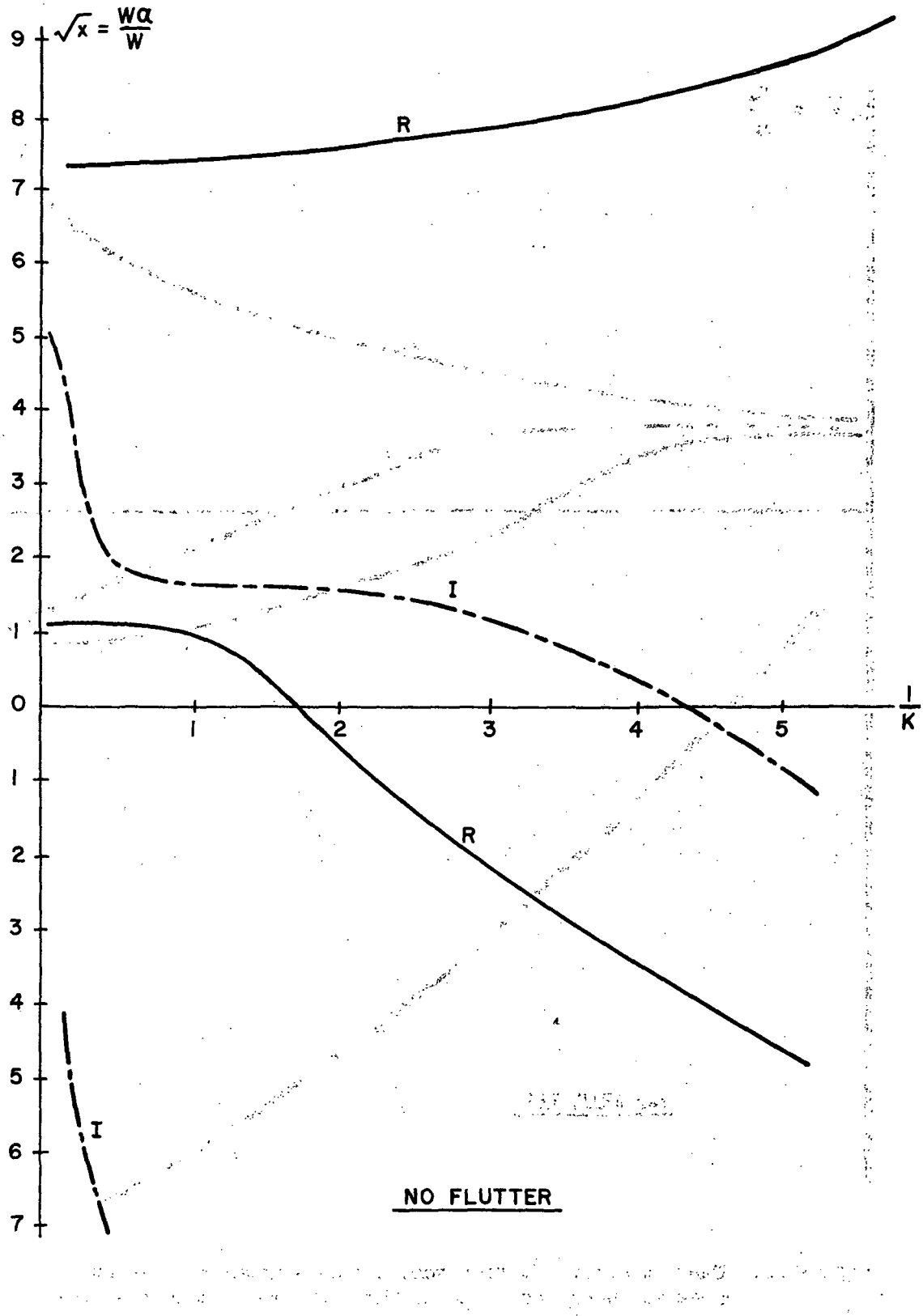

Figure 56. Characteristic flutter roots, two degrees of freedom. Case 3: Bending and flap torsion (uniform fixed free wing).

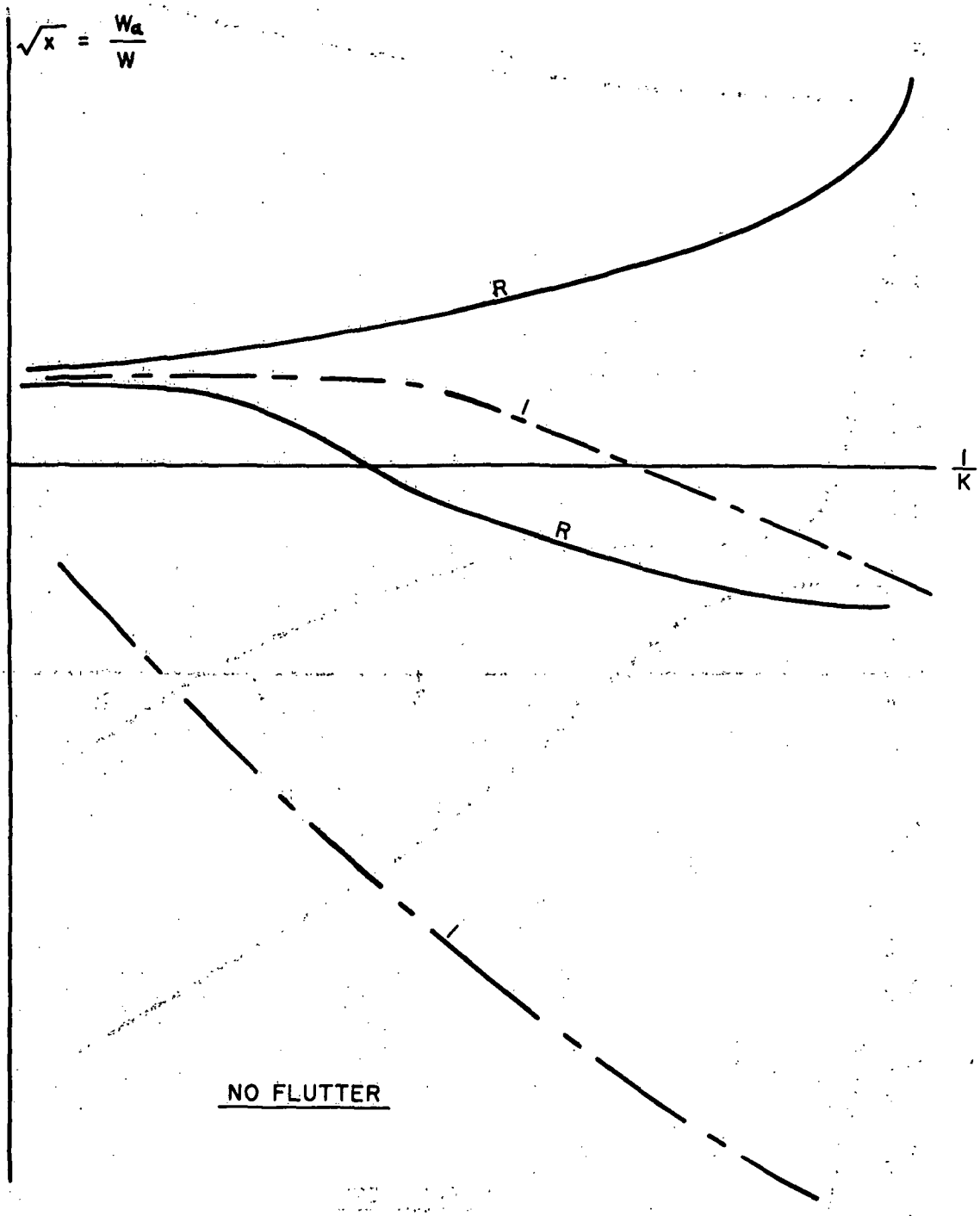

Figure 57. Characteristic flutter roots, two degrees of freedom. Case 4: Wing and flap torsion (uniform fixed free wing).

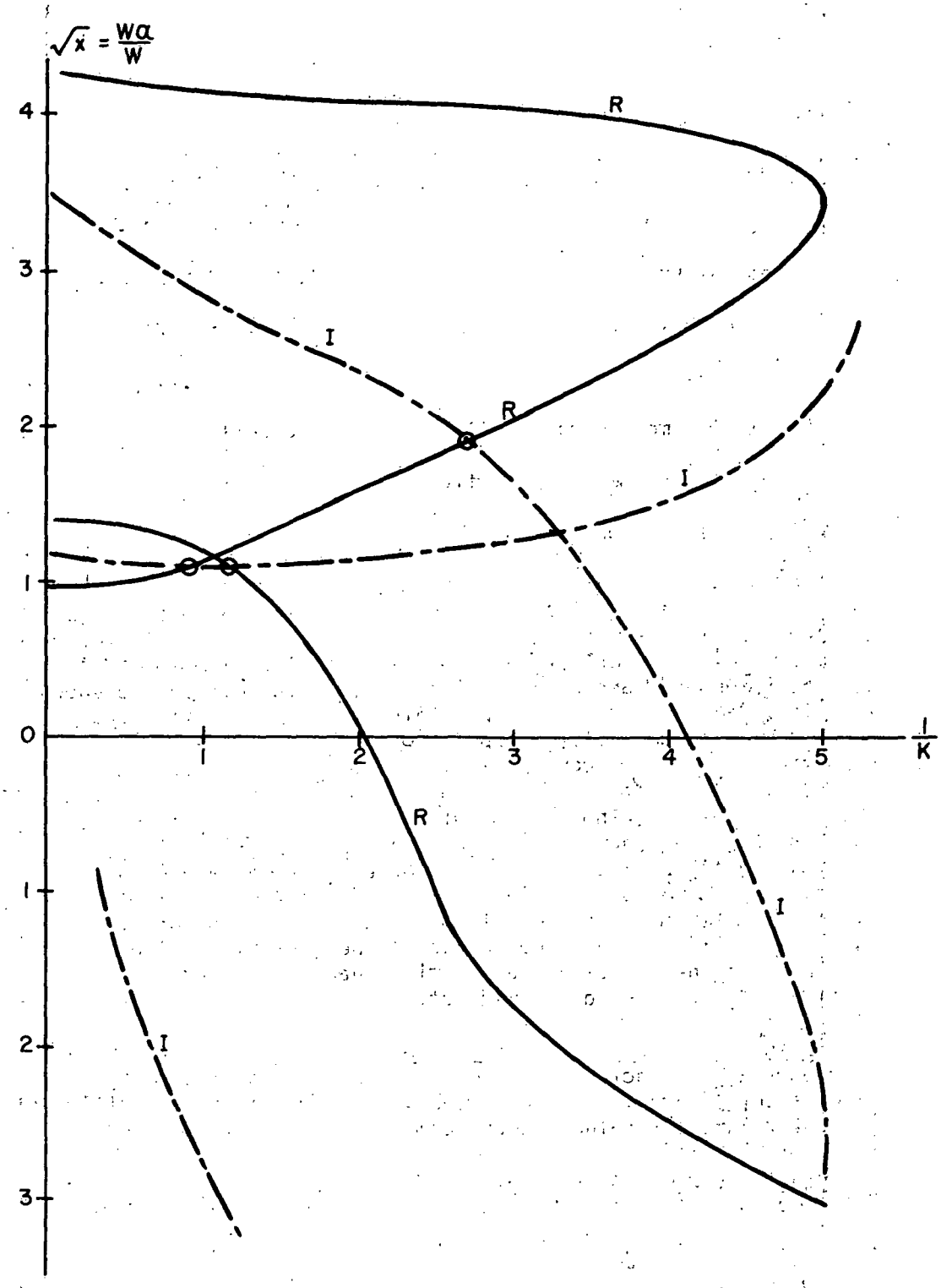

Figure 58. Characteristic flutter roots, three degrees of freedom. Case I: Wing bending, wing and flap torsion (uniform tapered wing, taper ratio = 2.5).

TABLE 26. ROOT PARAMETERS (23012 NACA SERIES AIRFOIL)

Wing weight	11.4 lbs./ft.
Wing static moment	6.0 ft.lb./ft.
Wing mass moment of inertia	29.49 lb.ft.^{2}/ft.
Flap weight	4.25 lb./ft.
Flap moment of inertia	8.81 lb.ft.^{2}/ft.
Flap static moment	4.93 lb.ft./ft.
Wing area moment of inertia	.0106 ft.^{4}
Wing polar moment of inertia	.015 ft.^{4}
Flap polar moment of inertia	.0075 ft.^{4}

56 and 57 the real and imaginary roots do not converge and hence no flutter exists for the cases of bending and flap torsion or wing and flap torsion. For the three degrees of freedom case and two degrees of bending and wing torsion, flutter velocities are shown to exist at 860 mph and 1480 mph. Since these velocities are well above the speed generally accepted for incompressible flow, they cannot be accepted as completely accurate without including compressibility effects in the analysis. Garrick (Ref. 36) suggests that, for ordinary wings of normal density and low ratio of bending to torsional frequency, the compressibility correction to the critical flutter velocity is in the order of a 3% reduction in speed. This gives a predicted flutter velocity of 834.2 mph. Since the maximum design velocity is 219 mph, it can safely be assumed that flutter does not appear to be a problem. Figure 59 is a plot of the normalized deflection shapes for bending and torsion which were used in the flutter analysis.

Natural Frequency and Airfoil Deflection Shapes. The natural frequency and deflection modes of the airfoil are of primary importance in the evaluation of the flutter determinant coefficients. These parameters for the non-uniform airfoil need to be examined.

The uncoupled natural bending frequency is the first factor. Figure 60 shows that the deflection y_i at any station i along the span due to loads F_j, can be written as

$$y_i = ci_1F_1 + ci_2F_2 \ldots\ldots + ci_nF_n \qquad (190)$$

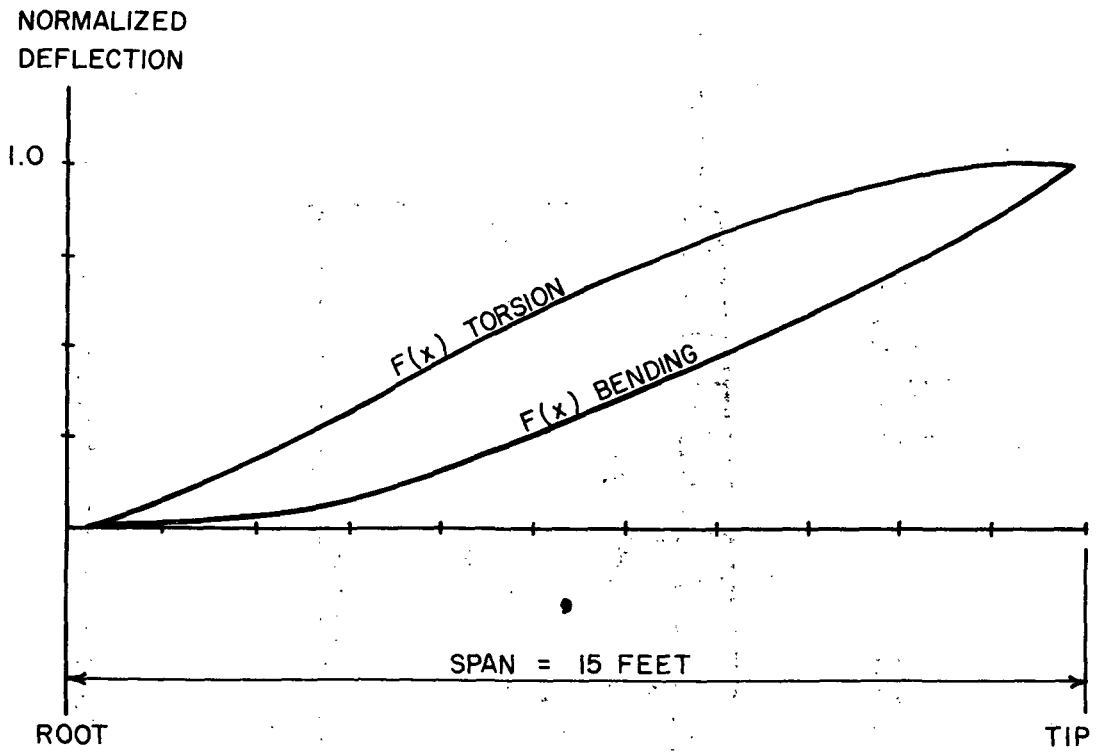

Figure 59. Normalized deflection shapes for bending and torsion (uniform fixed free wing).

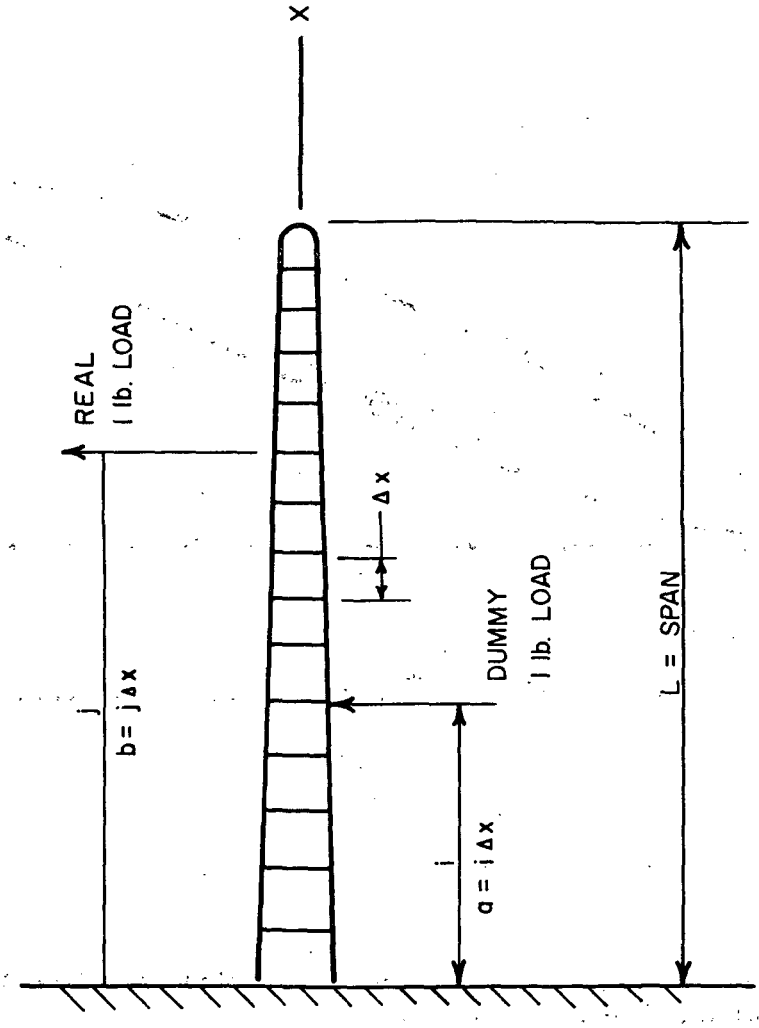

Figure 60. Influence coefficient model.

where c_{ij} are influence coefficients, to be defined later. Expressions for the complete span result in n equations, which can be expressed in matrix form as

$$[Y] = [c][F] \tag{191}$$

If the system is vibrating in one of its natural modes with frequency ω, the forces F_j are the inertia forces

$$F_j = m_j y_j \omega^2 \tag{192}$$

which gives

$$[Y] = \omega^2[c][M][Y] \tag{193}$$

where [Y] is the column modal matrix, [C] is a square symmetric matrix of influence coefficients, and [M] is the diagonal square mass matrix. The solutions to this equation take the form of assuming a deflection shape and iterating until the desired accuracy is obtained. For pure bending only, $\omega = \omega_h$, and [Y], when normalized, equals f(x).

A similar expression for the torsional mode can be written

$$[\alpha] = \omega^2[B][I][\alpha] \tag{194}$$

where [B] is a square matrix of torsion influence coefficients, [I] is a square diagonal matrix of mass inertia, and [α] is the deflection shape. For pure torsion, $\omega = \omega_\alpha$, and [α], when normalized, equals F(x).

The bending influence coefficients, using Figure 60 and applying dummy load criteria, can be evaluated

$$S = \int_0^{\ell} \frac{1}{EI} M(m dx) \tag{195}$$

where m is a dummy one pound load, and M is a real one pound load. The resulting deflection is given by

$$S = \int_0^a \frac{(a-x)(b-x)dx}{EI} \qquad o \leq a \leq b \tag{196}$$

$$S = \int_0^b \frac{(a-x)(b-x)dx}{EI} \qquad o \leq b \leq a \tag{197}$$

For the given loads, S is equal to the bending influence coefficient. Since the wing geometry is variable from station to station, I will be a function of the station. The best approach to solving equations (196) and (197) will be by numerical integration. The final solution takes the form

$$C_{ij} = \left(\frac{a^2 b}{2} - \frac{a^3}{6}\right) \frac{1}{EI_i} + \sum_{n=1}^{i} \left[(n-1)ab\Delta x - \frac{(n-1)^2 a\Delta x^2}{2}\right.$$

$$\left. - \frac{(n-1)^2 b\Delta x^2}{2} + \frac{(n-1)^3 \Delta x^3}{3}\right] \frac{1}{E(I_{i-1} - I_i)} \tag{198}$$

for $a \leq b$ where $a = i\Delta x$ and $b = j\Delta x$. Since the matrix is symmetrical, $c_{ij} = c_{ji}$ can also be written.

The torsion influence coefficients can be found by a similar process from the relations

$$\alpha_{ij} = \int_0^a \frac{T(\tau dx)}{Gj} \qquad a \leq b \tag{199}$$

$$\alpha_{ij} = \int_0^a \frac{T(\tau dx)}{Gj} \qquad b \leq a \tag{200}$$

"Fluta". Since the solution to the flutter determinant requires many long and tedious calculations, a digital computer program, "Fluta," was written to form and evaluate the determinant. The output from this evaluation contains the coefficients of the real and imaginary cubic equations described above. The analysis can proceed either of two ways.

1. If the wing has no discontinuities and uniform taper, the designer supplies the root geometry, mass, and static and inertia terms.

2. If the wing has discontinuities, the designer supplies the geometry, mass, and static and inertia terms at incremental stations of the wing.

Figure 61 is a flow diagram which indicates the calculating procedure for Fluta.

Wing Divergence

Wing divergence may be described generally as the static instability of an airfoil in torsion. This will occur when the torsional rigidity of the structure is exceeded by the aerodynamic twisting moments. The problem may be studied further by considering that for most wings the aerodynamic lift center lies forward of the elastic axis. From Figure 62 it is seen that as the wing is twisted through α_i the angle of attack increases, causing an increase in lift. This increase in lift will, in turn, further increase the twist. This process will continue until the twisting torque equals or exceeds the wing resistance, or torsional stiffness. At this point the wing will no longer be able to find an equilibrium between the applied torque and torsional stiffness. The speed at which the applied torque just equals the wing resistance is referred to as the torsional divergence speed.

From Figure 62 the torque per interval ΔTi is

$$\Delta Ti = \pi \ell v^2 bi(1 + 2ai)\Delta xi\alpha i, \tag{201}$$

setting

$$\lambda = \pi \ell v^2 \tag{202}$$

and

$$A_i = (1 + 2ai)bi^2 \Delta xi. \tag{203}$$

Equation (203) can be rewritten in matrix form as

$$[\Delta T] = \lambda [A][\alpha] \tag{204}$$

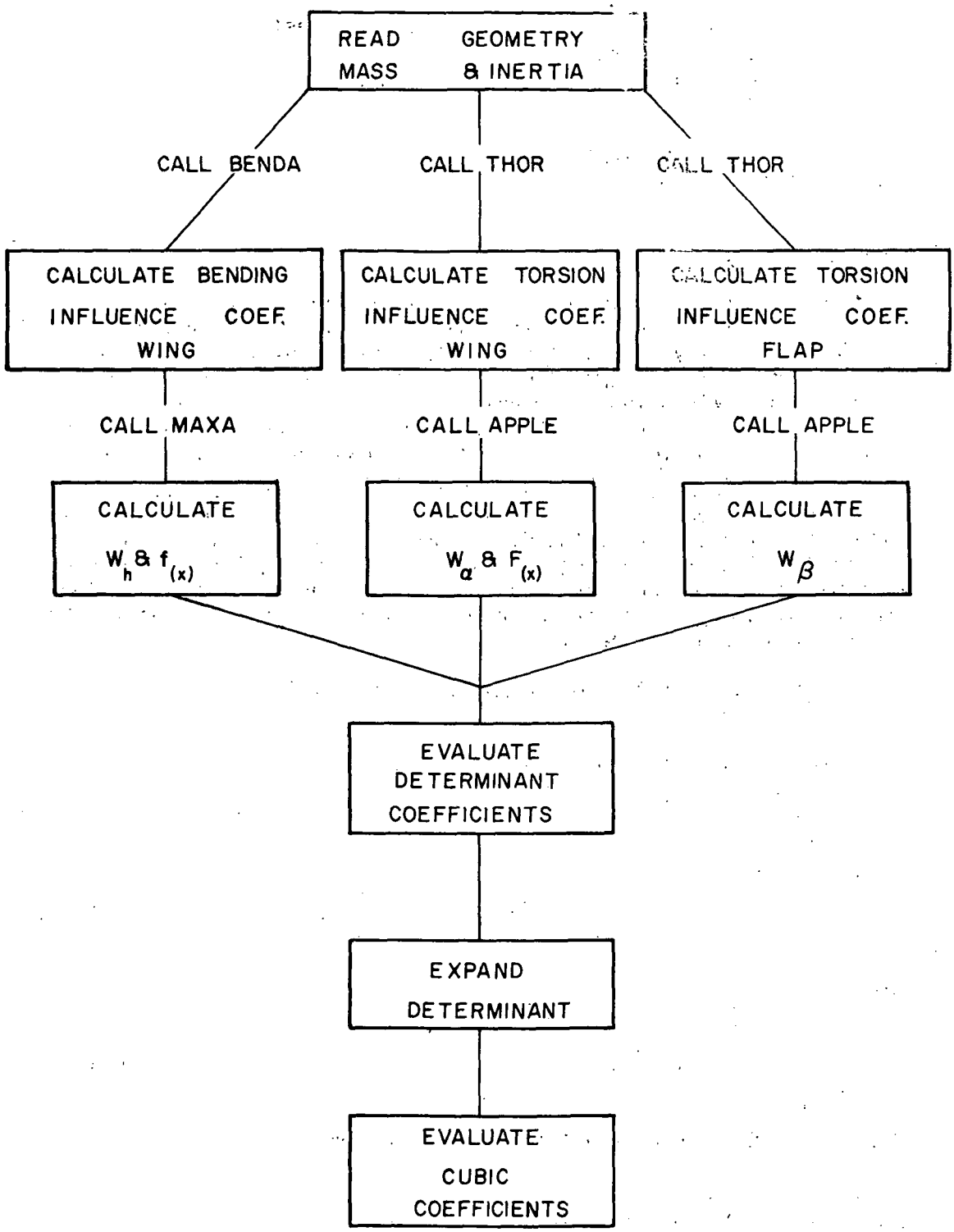

Figure 61. Calculation flow.

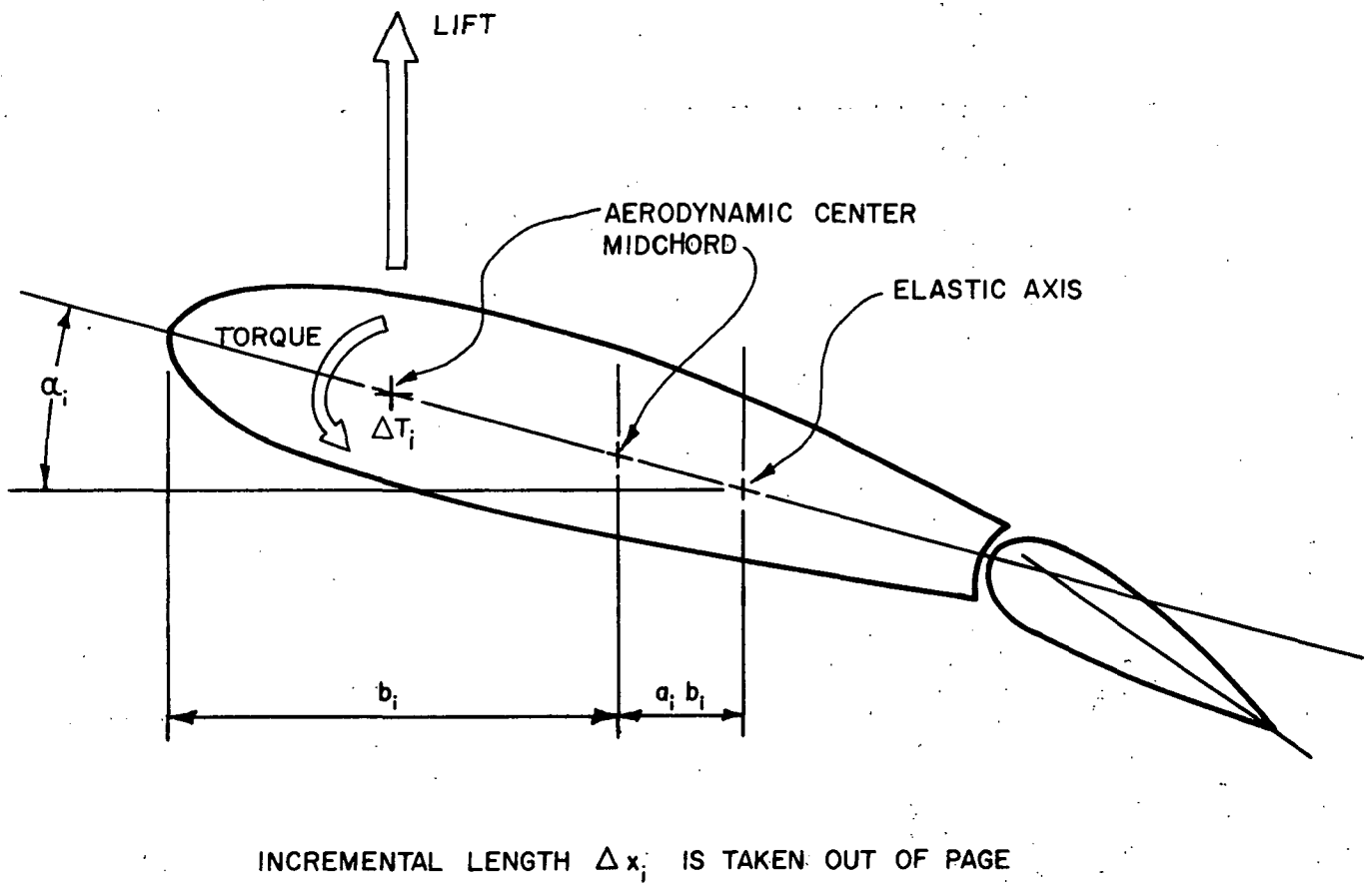

Figure 62. Section wing loading and geometry.

If [B] is the matrix of torsional influence coefficients, then

$$[\alpha] = [B][\Delta T] \quad . \tag{205}$$

Substituting equation (204) into (205) gives

$$[\alpha] = \lambda[A][B][\alpha] \quad . \tag{206}$$

Equation (206) can be solved for λ by iterating on α; this will in turn give the desired divergence velocity.

Divergence velocity is plotted against torsional stiffness (GJ) in Figure 63. As shown, for an aluminum wing at the preliminary inertia estimate of $J = 310\ in^4$, the critical speed is 579.035 mph. As in the case of flutter, it can be assumed that torsional divergence does not appear to be a problem.

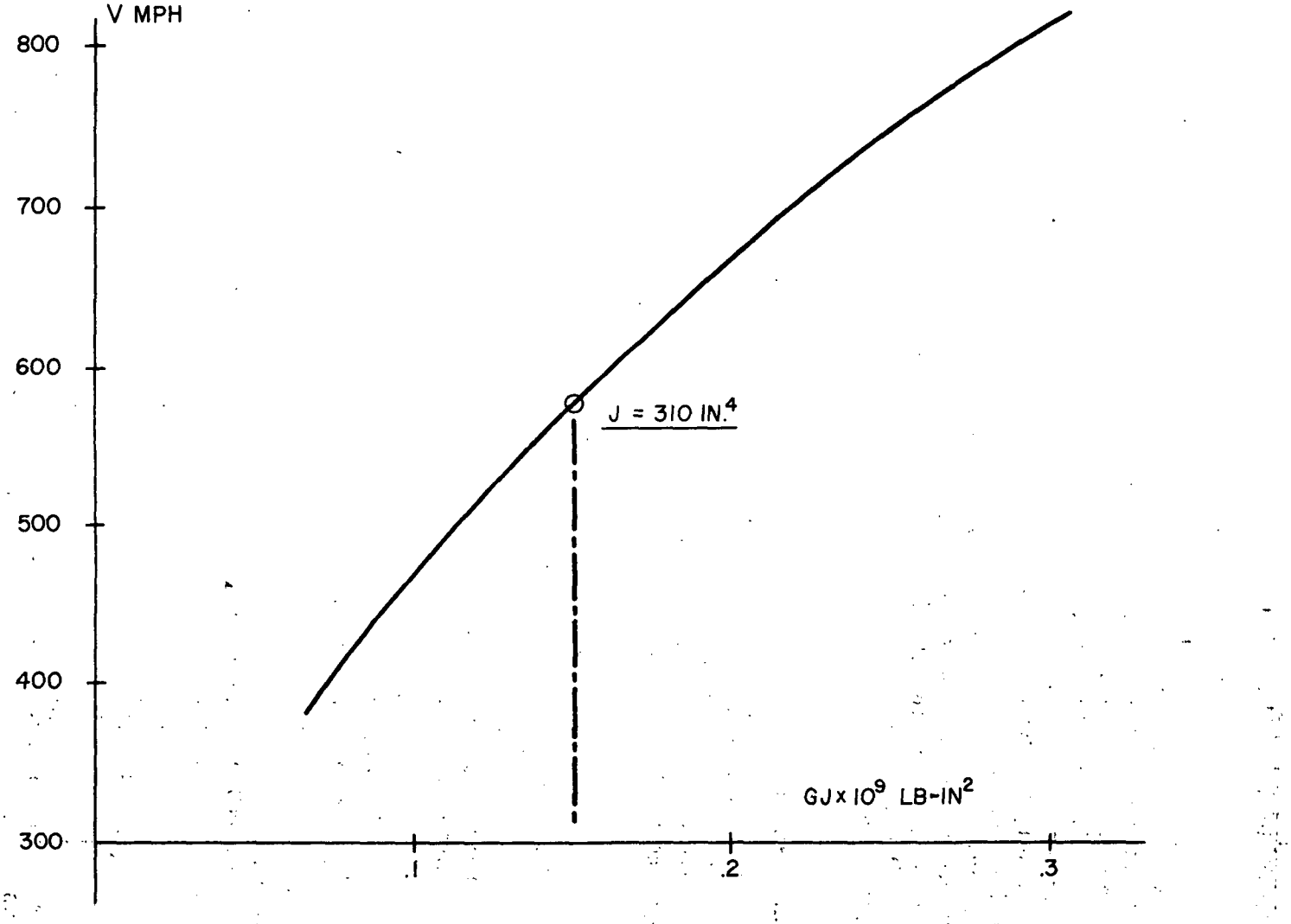

Figure 63. Torsional stiffness and divergence velocity (uniform span properties).

CONSTRUCTION TYPES AND FABRICATION METHODS

One of the first problems encountered in aircraft design is the determination of the aerodynamic and inertia loads which the airframe must resist. Once these loads are known, the aircraft can be analyzed for stress and deformation integrity. This essentially is a twofold problem of determining the shear, bending, and torsion loads carried by the structure in static equilibrium and then accounting for dynamic effects with an appropriate acceleration or load factor. The Federal Aviation Agency has established rules and regulations which govern structural design velocities and the various flight conditions which should be investigated in structural analysis. It is the purpose of the following discussion to establish the load combinations which were investigated and to calculate the appropriate load factors.

Wing Loading

The wing is subjected to combinations of bending, shear, and torsion loading, which fluctuate according to flight conditions. Referring to Figure 64, the relationship for the air shear load at any station is given as

$$V_{k+1} = q \sum_{i=1}^{i=k} \bar{C}_{Ni} \bar{C}_i \Delta X_i \quad . \tag{207}$$

The shear load due to structural weight and various mechanical and electrical hardware becomes

$$W_{k+1} = \sum_{i=1}^{i=k} (P_i + W_i)\Delta X_i \quad . \tag{208}$$

For normal flight conditions, the net shear load per station will be the algebraic sum of equations (207) and (208). This gives

$$S_{k+1} = q \sum_{i=1}^{i=k} \bar{C}_{Ni} \bar{C}_i \Delta X_i - \sum_{i=1}^{i=k} (P_i + W_i)\Delta X_i \quad . \tag{209}$$

The dynamic pressure used in 207 must correspond to the dynamic pressure at unity load factor, which becomes

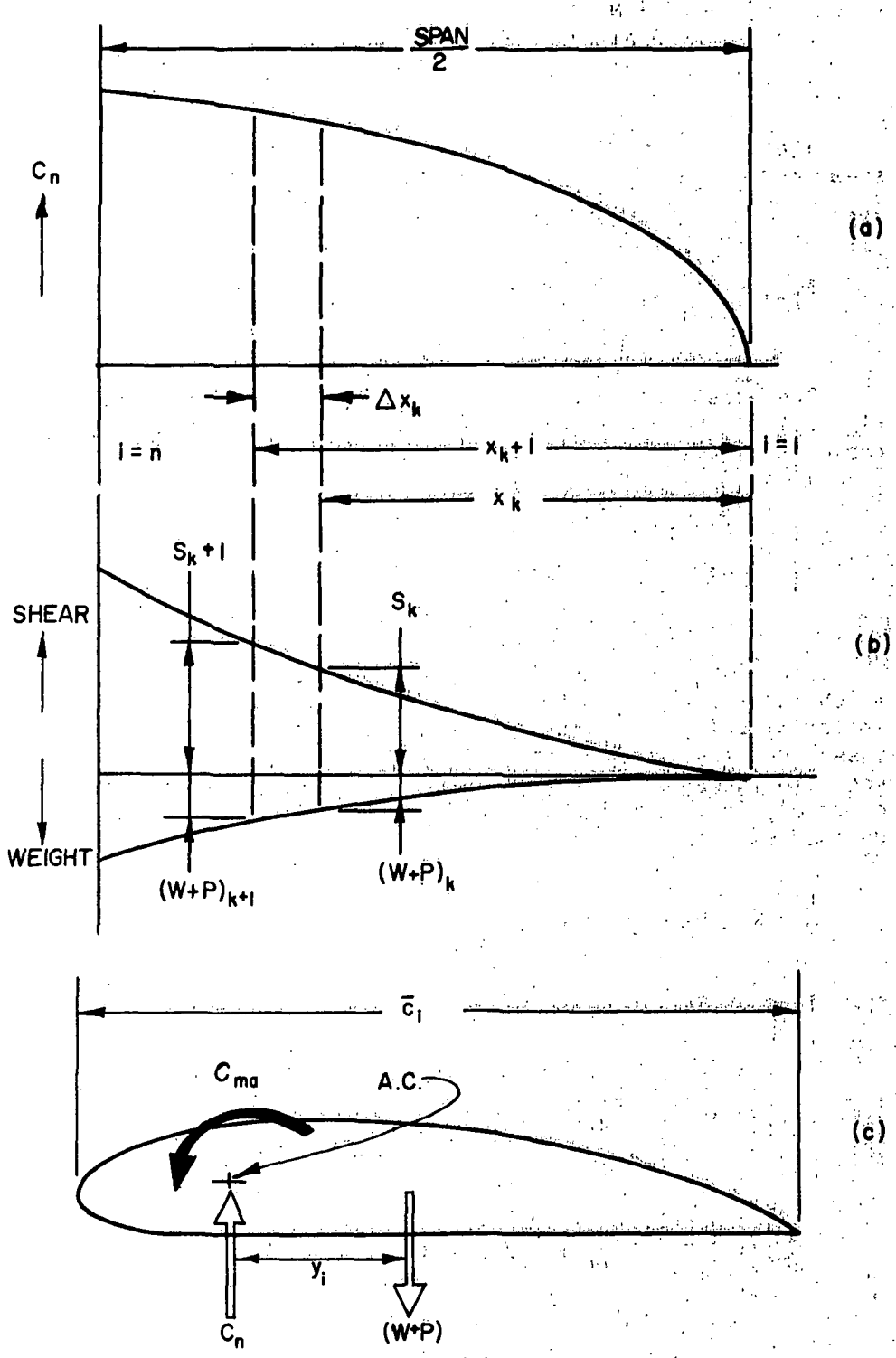

Figure 64. Wing loading.

$$q = (W_g/z)/\left(\sum_{i=1}^{i=N} \bar{C}_{Ni}\bar{C}_i\Delta X_i\right) \quad . \tag{210}$$

The bending moment by station will equal the area under the shear curve. Applying numerical techniques yields

$$M_{k+1} = \sum_{i=1}^{i=k} [(S_{i+1} + S_i)/2]\Delta X_i \quad . \tag{211}$$

The torsional loads can be determined by considering Figure 64. The torsional twisting moment about the aerodynamic center at station k will be

$$T_i = C_{MA}q \sum_{i=1}^{i=k} \bar{C}_i^{\,2}\Delta X_i - \sum_{i=1}^{i=k} (P_i + W_i)y_i\Delta x_i \quad . \tag{212}$$

Equations (209), (211), and (212) determine the external loads which the structure must resist for static equilibrium or for a load factor of unity. The actual design loads are obtained by multiplying these equations by the appropriate load factor for the flight condition in question. It is also necessary to account for a factor of safety in the design. If a combined load, safety factor $\bar{N}$ is defined such that

$$\bar{N} = N \times \text{Safety Factor}, \tag{213}$$

the final design loads become

$$S_{k+1} = \left[q \sum_{i=1}^{i=k} \bar{C}_{Ni}\bar{C}_i\Delta X_i - \sum_{i=1}^{i=k} (P_i + W_i)\Delta X_i\right]\bar{N} \tag{214}$$

$$M_{k+1} = \left[\sum_{i=1}^{i=k} (S_{i+1} + S_i/z)\Delta X_i\right]\bar{N} \tag{215}$$

$$T_k = \left[C_{MA}q \sum_{i=1}^{i=k} \bar{C}_i^{\,2}\Delta X_i - \sum_{i=1}^{i=k} (P_i + W_i)y_i\Delta x_i\right]\bar{N} \tag{216}$$

A weight analysis, restricted to the root requirements for a symmetrical box beam, was performed on the Piper 235 Cherokee wing loading. The essential design parameters were

1. Airfoil - NACA 23012
2. Load Factor - 4.4
3. Box Beam Structural Chord - 34.5 inches
4. Effective Beam Height - 8 inches
5. Rib Spacing - 12.5 inches
6. Loading at Center of Gravity

    a. Torque - 36,350 in/lb.
    b. Lift Force - 1,450 lbs.
    c. Drag Force - 171 lbs.

Figure 65 illustrates a section of minimum weight 75TS aluminum beam. For a minimum factor of safety of 1.52, the beam weighs 8.78 lb/ft.

Load Factors and Flight Conditions

The next consideration is the determination of the appropriate load factors to be used and the flight conditions which must be investigated. All formulas applied here are specified in Part 23 of Reference 37. All flight conditions cited will be equal to or more severe than those recommended by the Federal Aviation Agency. The minimum structural design velocities are given as follows:

$$V_{CMIN} = 38W_g/S_w = 156.5 \text{ MPH} \quad (217)$$

$$V_{DMIN} = 1.4V_{CMIN} = 219 \text{ MPH} \quad (218)$$

$$V_{STALL} = 65 \text{ MPH} \quad (219)$$

$$V_A = NV_S = 126.5 \text{ MPH} \quad (220)$$

$$V_f = V_c = 156.5 \text{ MPH}. \quad (221)$$

The positive limit maneuvering load factor is given as

$$N_l = 2.1 + 24{,}000/W_g + 10{,}000 = 3.96 \quad (222)$$

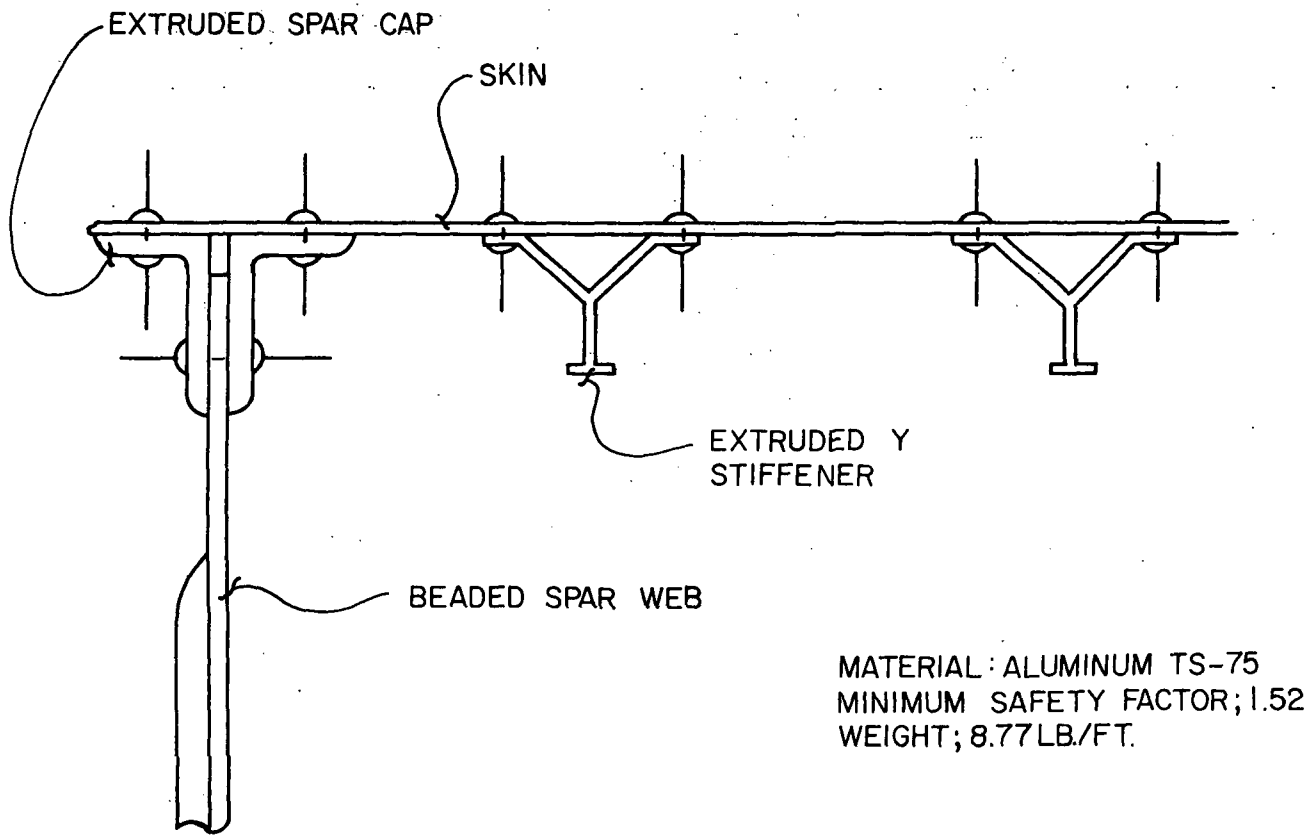

Figure 65. Riveted aluminum structure.

subject to

$$2.5 \leq N_1 \leq 3.8$$

Therefore, $n_1 = 3.8$ will be used. The positive limit load factor with flaps is given as

$$N_f = .5N_1 \qquad N_f \leq 2.0. \tag{223}$$

The gust load factor is computed as

$$N_g = 1 + KUV_M/575(W_g/S_w) \tag{224}$$

where

$$K = 1.33 - 2.67/(W_g/S_w)^{.75} \tag{225}$$

For gust velocities of 15 fps and 30 fps

$$N_3 = 3.11(+30 \text{ fps}) \tag{226}$$

$$N_4 = 2.64(+15 \text{ fps}) \tag{227}$$

$$N_5 = -1.1(-30 \text{ fps}) \tag{228}$$

$$N_6 = -.64(-15 \text{ fps}) \tag{229}$$

The velocities and load factors as calculated in equations (217) through (229) are plotted on the V-N diagram of Figure 66.

Reference 37 recommends that the airplane be designed for the following symmetrical flight conditions:

1. The conditions under A, D, E, and F from the V-N flight diagram, and
2. The condition of flaps extended at V_f for a load factor of 2.0.

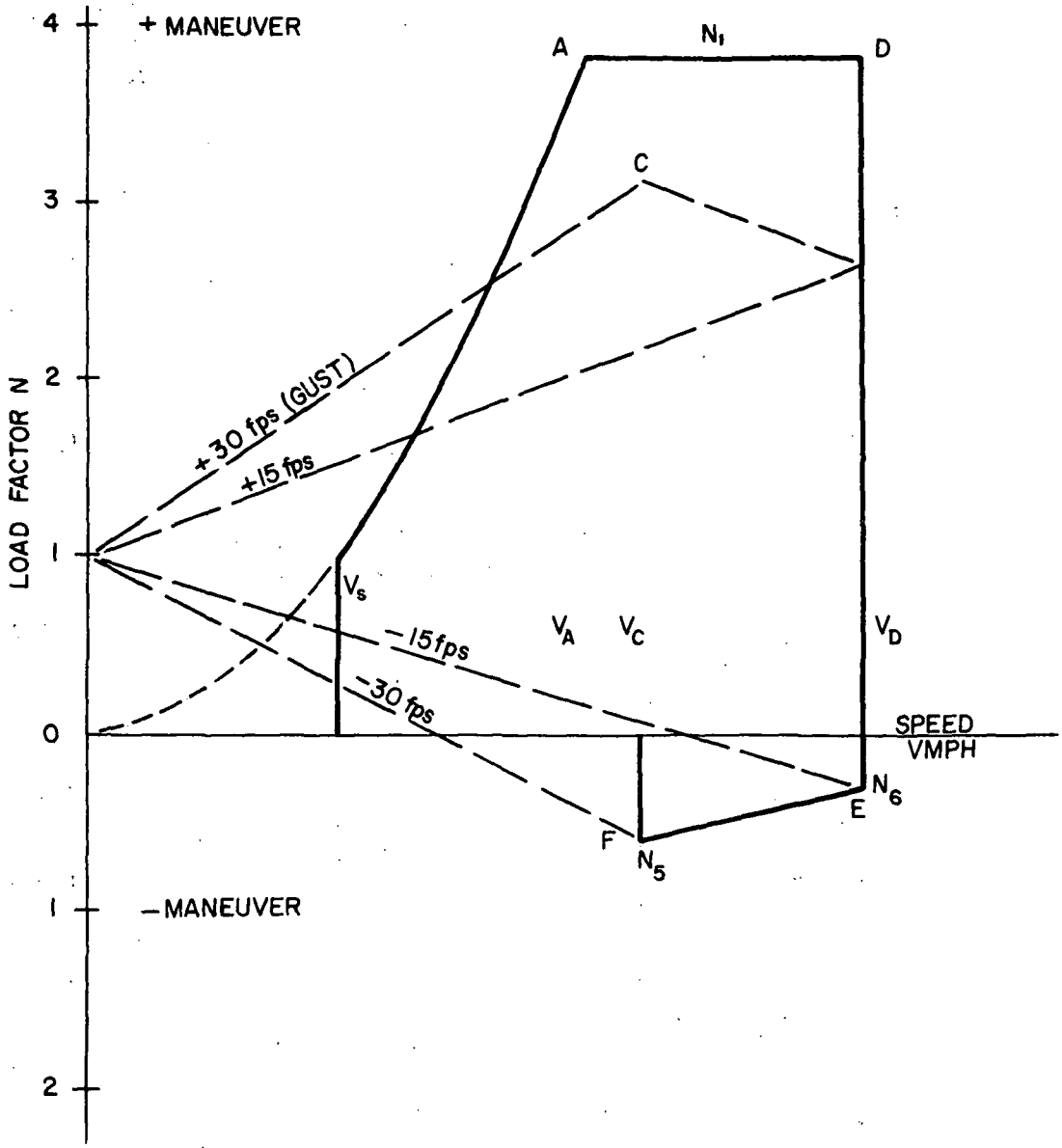

V_S = 65 MPH
V_A = 126.5 MPH
V_C = 156.5 MPH
V_D = 219 MPH

N_1 = 3.8
N_5 = -1.1
N_6 = -.64

Figure 66. Velocity-load factor diagram.

The symmetrical conditions listed above apply to the entire airplane. In addition, the lift and control sections of the structure were equipped for the following unsymmetrical flight conditions:.

1. The aft fuselage-to-wing attachment must be designed for the case of flap extended at maximum flap surface loading.

2. The wing and wing carry-through structure must be designed for 100% of condition A loading on one side of the plane of symmetry and 70% on the opposite side.

3. The wing and wing carry-through structure must be designed for the loads resulting from a combination of 75% of the positive maneuvering wing loading on both sides of the plane of symmetry and the maximum wing torsion resulting from aileron displacement.

4. The wing flap shall be designed for both of the flight conditions and load magnitudes given in Figure 67.

5. The horizontal tail shall be designed for positive and negative loading of the magnitude and distribution of Figure 68, where loading is symmetrical. In addition, it shall be designed for 100% of the a and b loading on one side of the plane of symmetry and 75% on the other.

6. The vertical tail shall be designed for positive and negative loading of the magnitude and distribution of Figure 69-a and 69-b, where loading is symmetrical.

7. The aileron shall be designed for the maximum aileron surface loading multiplied by n_1 load factor.

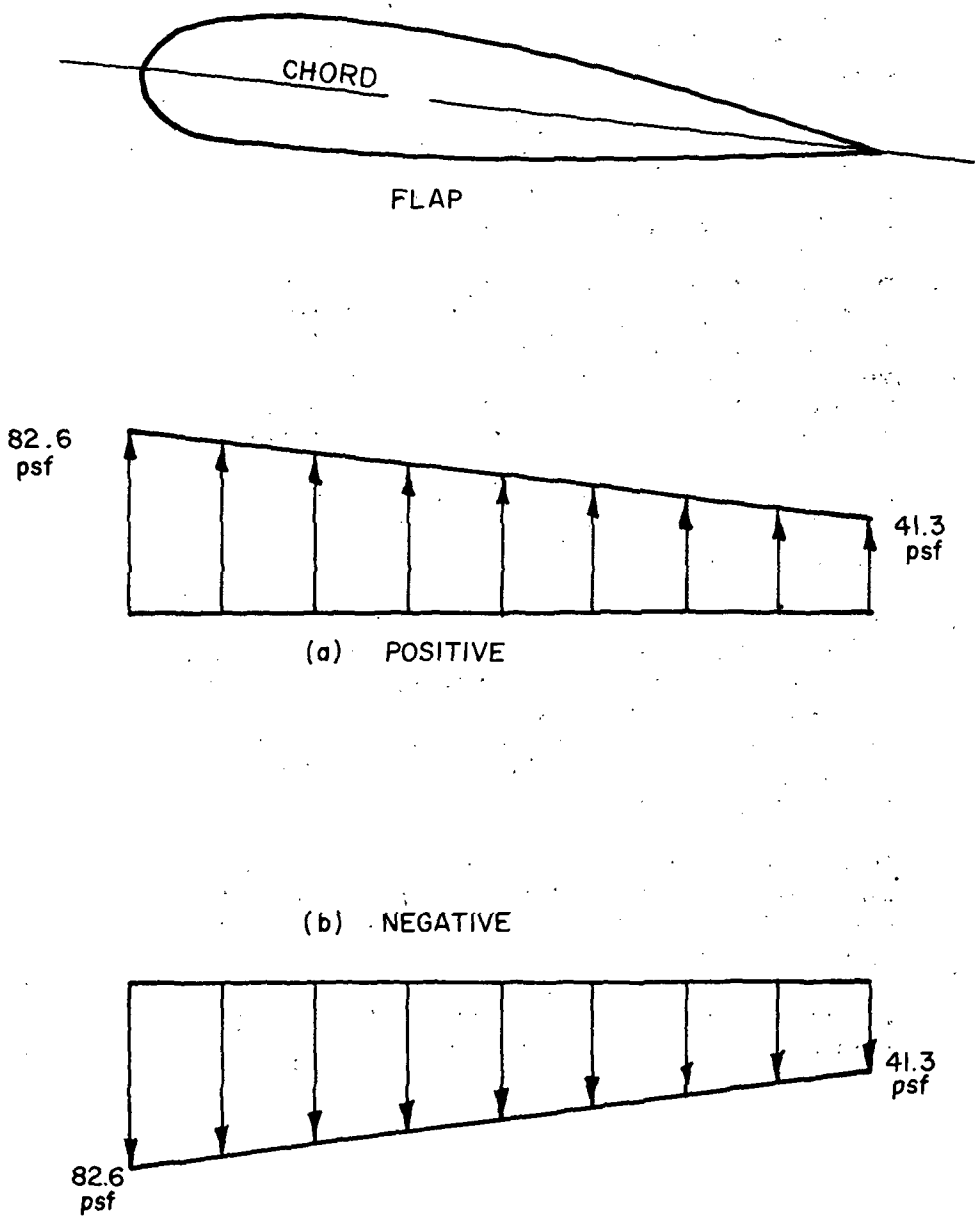

Figure 67. Design flap load distribution.

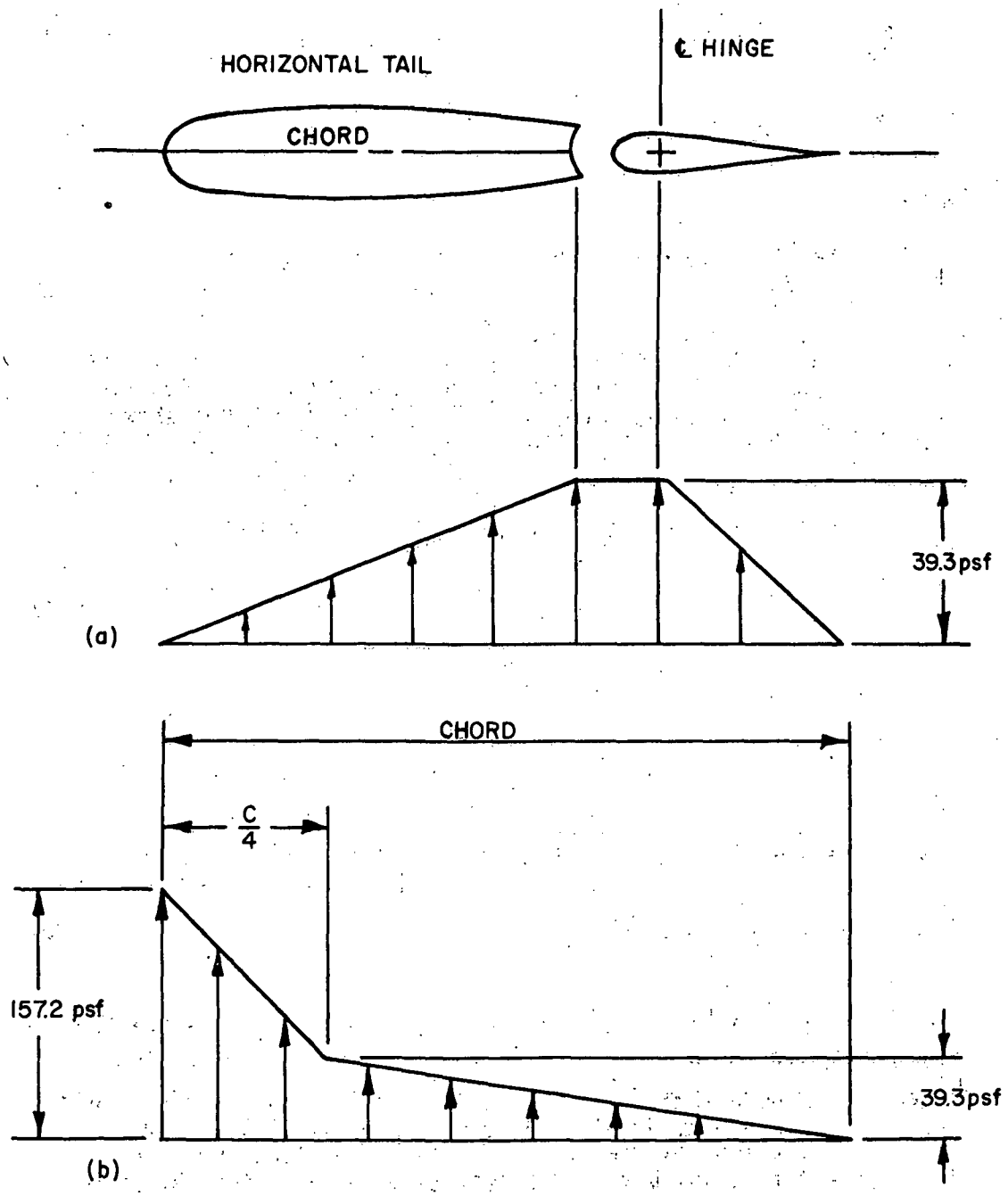

Figure 68. Design loads for the horizontal tail.

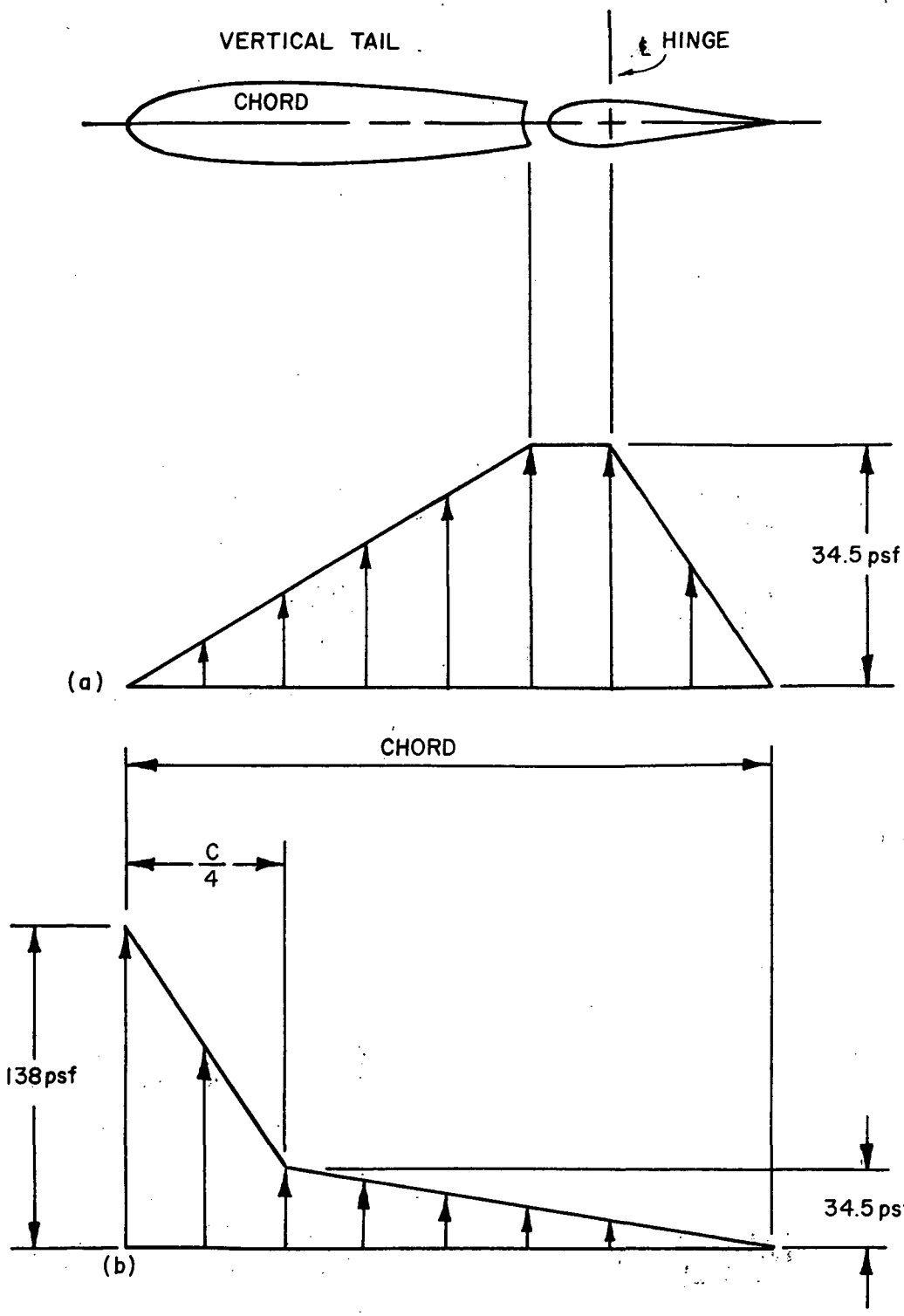

Figure 69. Vertical tail design loads.

Since labor cost represents the largest portion of structural input, materials and techniques which show promise of minimizing labor requirements as well as reducing weight were investigated for use in the constant attitude, simple-to-fly light aircraft. Ultimately, the decision was made to use standard riveted aluminum construction; however, the results of the study on construction techniques and materials not widely used in light airplane fabrication for primary structural members revealed some promise for use in future designs.

Three construction types--reinforced plastic construction, sandwich construction, and adhesive bonding--and three fabrication methods--bag molding, filament winding, and matched die molding--were considered. All three fabrication methods are suitable for use with reinforced plastic and sandwich assemblies. For quantities of 1,000 or less, the usual method of fabrication is bag molding or filament winding because of lower tooling costs. Either method is suitable for single unit or quantity production.

Several research studies have been made in recent years to obtain realistic comparisons between reinforced plastic and aluminum construction. One of the most informative of these was conducted by Mr. Charles Tanis at Wright-Patterson Air Force Base. His report, "A New Method for Manufacturing Airframe Structures," discussed the design, construction, and testing of a filament wound honeycomb wing section for the Navy T-2B aircraft. The test article was 92.5" long, 44" wide at the tip, and 62" wide at the root. Wing loading for the test article was 300 lbs/ft^2, compared to wing loadings of 15 lb/ft^2 for the average light airplane. Although the difference in wing loading is significant, it is felt that the results are representative of the magnitude of weight savings which could be expected using filament wound techniques. The entire section was manufactured using roving tension and matrix cure or secondary adhesive bonding; no mechanical fasteners were used. The completed structure reflected a weight savings of 65% over the aluminum structure in current use.

Reinforced Plastic Construction

Reinforced plastics offer several advantages as well as disadvantages over conventional riveted aluminum construction.

ADVANTAGES

1. High strength/weight and high modulus/weight
2. Excellent forming characteristics

3. Excellent adhesive properties
4. Low tooling costs
5. Exterior surfaces free of irregularities and fasteners

DISADVANTAGES

1. No clearly defined yield point
2. Restricted to low temperature applications
3. High material cost

In structural design for minimum weight, the factors normally considered first in material evaluation are the strength-to-weight ratio and modulus-to-weight ratio. These values are usually expressed as tensile strength and tensile modulus to material density with units in inches; these numbers would, in effect, represent the length of a vertical member of uniform cross section which would fail in tension under its own weight. Although restricted to unidirectional loading, these factors are useful as a starting point in weighing the relative merits of different materials. Figure 70 shows that glass-reinforced plastics are superior to titanium for applications using unidirectional filaments. Figure 71 illustrates that the modulus-to-weight ratios are better than aluminum for some materials and at least compatible for all of the filament-reinforced materials with the exception of 181 E-glass. These comparisons are somewhat misleading because of the directional characteristics of the fiber-reinforced plastics.

To take full account of the directional properties of orthotropic composites, careful attention must be given to fiber orientation to load. When designing with isotropic materials such as aluminum, it is customary to base strength predictions on a comparison between principal loads and the ultimate or yield strength of the material. When using orthotropic materials, it is necessary to compare loads and strengths for all angular directions. Two methods of analysis and design are currently being used to account for variation of directional properties. The first method makes use of the theory that a layup of directional fibers at angular spacings of $\theta = \pi/n$, where n is an integer greater than 2, is isotropic in the plane of the fiber. That is to say that laminates fabricated at equal angles such as 60°, 45°, and 30° are isotropic. The second approach is to take full advantage of the directional properties by laminating multiple orientations to give the highest strength and modulus is the direction of principal loads.

Figure 72 illustrates a directional orientation of 143 E-glass fabric designed to increase zero degrees shear properties while maintaining good zero degree compression properties. This particular design would result in a more uniform distribution of strength, but the strength values would be lower than those for the unidirectional

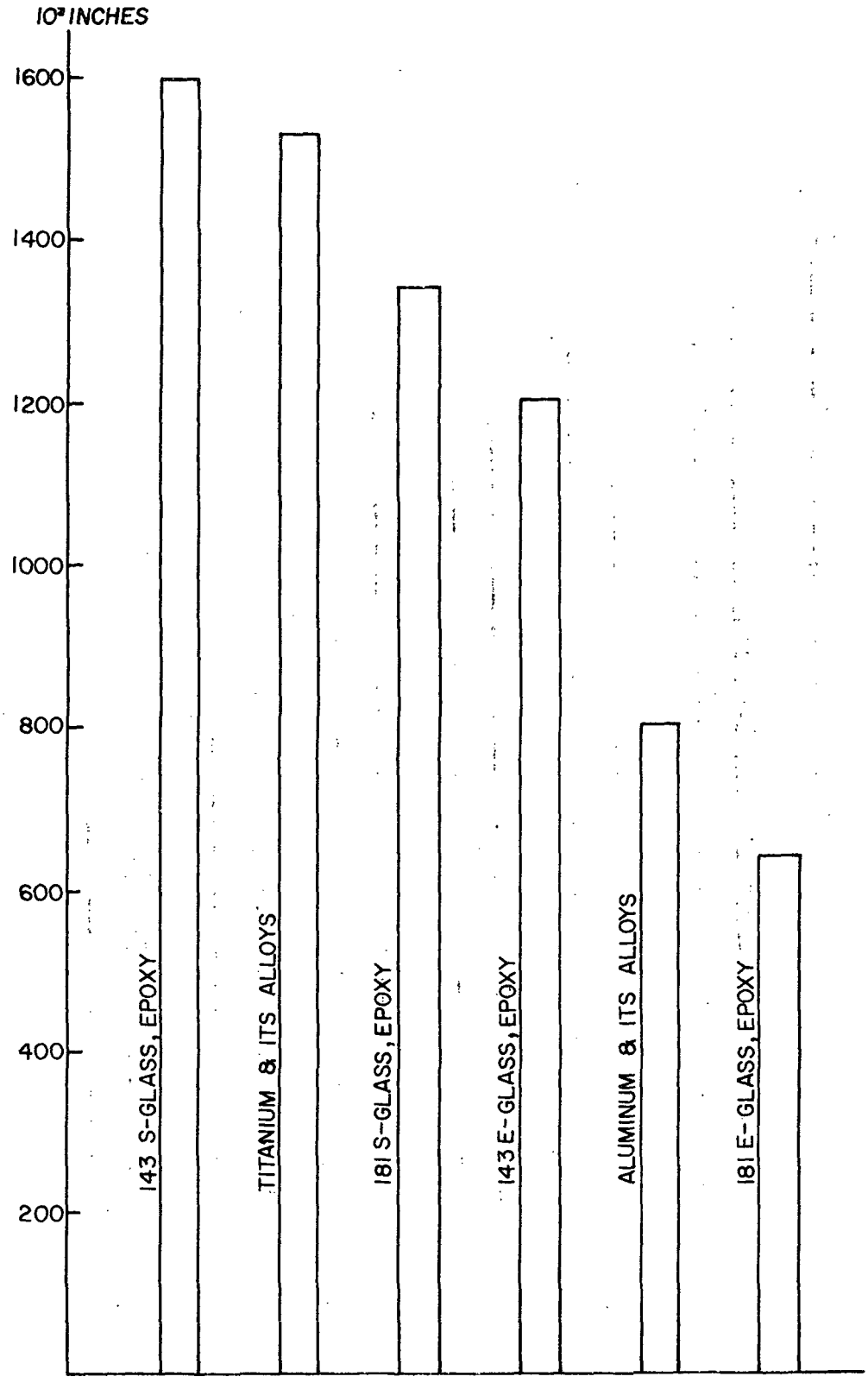

Figure 70. Specific strength.

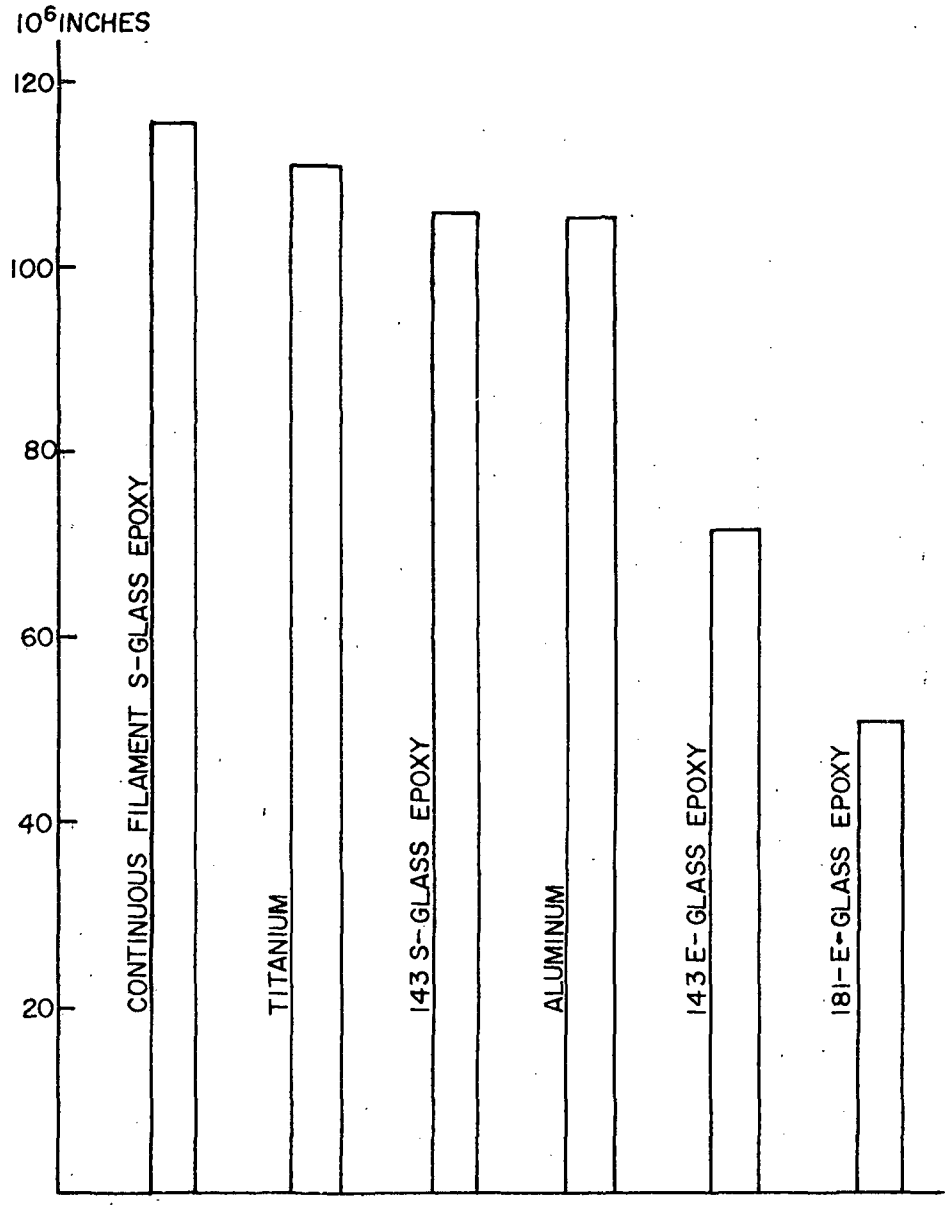

Figure 71. Specific modulus.

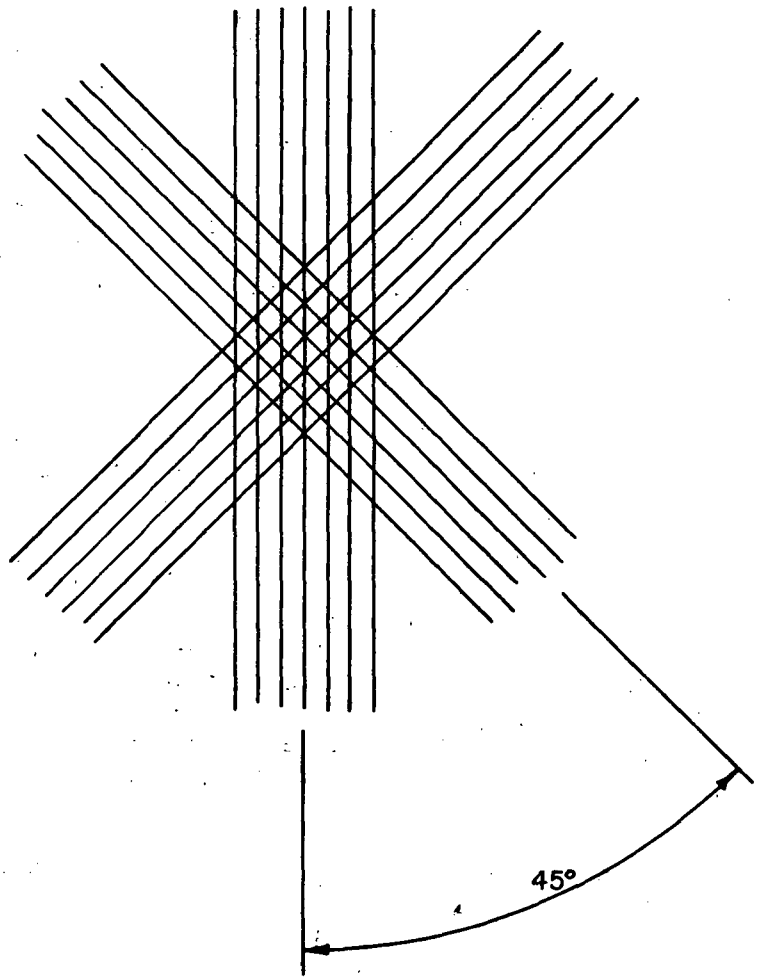

Figure 72. Direction controlled laminate (143 E-glass epoxy).

case. The increase in uniformity of directional properties coupled with a decrease in unidirectional properties is typical of directional controlled laminates.

Designing effectively with fiber-reinforced plastics requires that a variety of construction techniques be used to take full advantage of material characteristics. The fact that fiber-reinforced plastics are orthotropic is an advantage as well as a disadvantage. This characteristic permits the designer to tailor his material to meet a variety of loading conditions; but, it also means that the excellent strength-to-weight ratios can only be fully realized for unidirectional loading. This disadvantage can be overcome to a great extent through the use of filament winding techniques which offer a high degree of load-to-fiber orientation. One of the best advantages of using these materials is the relative ease with which complex shapes can be formed and molded to a smooth exterior without expensive tooling or machining. Another advantage is that the resin matrix of the plastic provides a built-in adhesive system for bonding in the uncured state. As a result of the adhesive and forming characteristics, fiber-reinforced plastics lend themselves readily to applications using sandwich construction and adhesive bonding techniques.

Sandwich Construction

Sandwich construction, using low density cores, offers excellent possibilities for use in minimum weight structural design. This type of construction is characterized by thin load carrying faces which are stabilized against buckling by a lightweight core which carries shear loads normal to the faces. At present, sandwich construction has not gained wide acceptance for use in light aircraft. This is because of high fabrication cost compared to conventional construction methods. Part of this cost is reflected in the difficulty of obtaining good adhesive bonds with contoured shapes. Because of the low crush strength of core materials currently available, faces must be preshaped to the desired contour before bonding. This results in complicated tooling and expensive assembly procedures. Because of the excellent drape and forming characteristics of reinforced plastics, sandwich panels with composite faces are cured in one operation with simple tooling.

Adhesive Bonding

Adhesive bonding has been successfully used in aircraft construction for many years. Indications have been obtained that it could be used to a much greater extent in light aircraft than current practice shows. Properly designed adhesive joints have a more uniform stress distribution than riveted joints. This uniform distribution reduces stress concentration and restricts crack propagation, the main cause

of fatigue failure. This in turn means that it is possible to design bonded joints with less material than would be required for riveted construction, which in turn leads to weight savings. The main disadvantage of adhesive bonding is a requirement for close tolerance control and critical alignment between mating parts. This disadvantage could be partially eliminated using the uncured forming characteristics of fiber-reinforced plastics to full advantage.

Bag Molding

Bag molding is a process in which a flexible form is used to apply pressure to a layup during the cure cycle. It is normally classified under three basic types: vacuum bag molding; pressure bag molding; and autoclave molding. This technique is essentially a hand layup process which applies equally well to parts cured at high or room temperature. In the case of the high temperature cure, heat can be applied by heat lamps, ovens, or other appropriate means.

Filament Winding

The filament winding process makes the best possible use of the composite directional properties. Unidirectional reinforcement in roving or tape form is wound under tension on a mandrel of desired shape. The reinforcement, preimpregnated or impregnated during the winding operation, is wound at an angle which complements the component loading to be expected. Mandrels for complicated shapes can be manufactured from soluble hard salt or other substances and removed with water after curing.

Matched Die Molding

Matched die molding is the process usually applied to large quantity production items. Male and female metal dies are used to maintain exact duplicates at high production rates. This process offers excellent cure cycle and quality controls. Parts may be produced in quantities of 5 to 50 per hour depending on part size and equipment capacity.

Cost Compatibility

The current price of E-glass epoxy laminates is approximately $2/lb, compared to 90¢/lb for aluminum. To be compatible, the difference in material cost would have to be bridged with savings in labor and tooling costs. For the present, sufficient data have not been found to permit a substantiated cost estimate on these parameters. It is known that the tooling required for plastic molding operation is generally less complex than that required for

metal forming. It is also known that plastic molding requires less labor and lower skilled labor than that required for metal fabrication. Based on these generalities and the fact that the value of labor is twice the cost of material in conventional aluminum construction, it can be assumed that the cost of a plastic structure should be at least compatible with conventional aluminum construction.

COST ANALYSIS

Introduction

The cost analysis of the aircraft has been divided into three main headings which were then subtotaled; an allowance was made for salvage; and an estimate was made of the total cost of the project. Table 27 gives a breakdown of the analysis.

TABLE 27. SUMMARY OF COST ANALYSIS

	Weight	Cost
1. Airframe and Installed Equipment (outright purchase)	1523 lb	$25,080
2. Aerodynamic Modifications (wing, tailcone, and tail)	602 lb	$ 5,278
3. Control Modifications (electronics bought and built, hardware, servos and control components)	24 lb	$ 3,378
4. Subtotal	2149 lb	$33,736
5. Salvage (weight saved by removal of equipment replaced; value of removed equipment)	450 lb	$ 100
6. Total Cost and Weight	1699 lb	$33,636

Airframe and Installed Equipment

Cost of the airframe and installed equipment is based on the retail purchase price quoted by Raleigh-Durham Aviation for a Piper Cherokee 235-C, price list dated February 1, 1969. Although Piper has introduced their new model, the 235-D, Raleigh-Durham Aviation was unable to quote a price on the new model. The price used in this report includes the basic airplane, equipped with the Executive operational group and Electronic group C.

Basic 235-C	1467 lb	$17,990
Executive operational group	20 lb	$ 1,985
Electronics group C	36 lb	$ 5,105
Total	1523 lb	$25,080

The operational and electronics groups were included in the airframe cost to simplify cost estimation for the control systems. The instruments may be replaced or altered, but it has been agreed that such alterations should be kept very close to the cost of factory installation. This is taken as a limit on the electronics cost and thus is a limit on the total aircraft cost.

The total airframe price includes the following items, among others:

a. elevator and rudder trim position indicator
b. steerable nose wheel
c. hand brakes, parking brake
d. 35 amp/hr battery, 60 amp alternator
e. single axis stability system (lateral), Auto Flite, Auto Nav
f. omni tracker
g. shoulder harness and reel
h. cabin speaker, headphone and jack, microphone and jack
i. Mark 8 90/100 NAV/COM with VOR/LOC indicator
j. Mark 12 90/100 NAV/COM
k. ADF-31 with BFO
l. VOA-40 VOS/ILS localizer indicator
m. PIPER MARKER BEACON receiver/indicator
n. electric trim on elevator
o. optional lights required for night flying
p. radio shielding
q. oil filter
r. TSO's air-driven gyro instruments
s. fire extinguisher
t. anti-static wicks and antennas
u. constant speed prop
v. toe brakes, both sides
w. mixture control and cylinder head temperature gauge
x. external power plug
y. heated pitot

Aerodynamic Modifications

Cost of the aerodynamic modifications is based upon the estimated weight of such modifications, as supplied by the structures section, and the cost per pound of such structures, taken from Pazmany. The modified components include wing, tailcone, and tail. This is expected to be the maximum cost, assuming mass production. It would undoubtedly be extremely difficult to produce it at this price in a job shop.

Item	Weight	Cost/pound	Cost
Wing	504 lb	$ 8.25	$4,158
Tailcone	18 lb	$12.20	$ 976
Tail, horizontal	80 lb	$ 8.00	$ 144
		Total	$5,278

Control System Modifications

Control system modifications costs have been figured on the basis of a component list supplied by the control section. This is not a complete list, since it outlines the major components required by the block diagram, that is, those with the most obvious functions. No specifications are currently available on the size, type, capacity, precision, accuracy, reliability, or any other variable for these components. The cost of the system and each subsystem has been figured on the basis of available catalogues for equipment in the size range considered suitable. Catalogues used were

a. Van Dusen Aircraft Supplies, General Catalogue, 1969
b. American Relays, Electronics Division; 11-69 Guidebook; Electromechanical Equipment and Components
c. Palley Supply Company, partial copy, undated catalogue.

Given below is a breakdown of weight and cost for components of the modified control system and its two non-standard subsystems, elevator control and forward speed.

General Control System

	Weight (lbs)	Cost ($)
2 Potentiometers (yoke & foot throttle) 1 KΩ, 0.1 linearity, Helipot Model A (American Relays) Rotary	.10	12.00
2 Summing Amplifiers	-	100.00
2 Actuators (Flaps) 3/4" shaft, Lear, 5 1/4" stroke, tension 1600 lbs, compression 800 lbs, 24 VDC, (Palley's LA49 TG11B), 5.5 amp.	10.00	50.00

General Control System (continued)

	Weight (lbs)	Cost ($)
1 Tachometer (Flap motor) p. 24 Van Dusen, less expensive from Palley	2.75	60.00
1 Linear Electric Actuator (Throttle lock) 2-position servo	3.00	30.00
Subtotal	16.00	252.00
Elevator Subsystem	8.00	181.00
Speed Control Subsystem	4.00	371.00
Lateral Control Subsystem (Standard)	-	500.00
Total	28 lbs	$1304.00

Elevator Control Subsystem

1 Rate Gyro 30^{o}/sec, ω_n = 16 cps, Pot 5K, 35 VDC, American Gyro R59B-1	4.00	100.00
1 Potentiometer Helipot Model A	.10	6.00
1 Amplifier - adder	-	50.00
1 Actuator (Elevator)	3.75	25.00
Total Cost	7.85	$181.00

Forward Speed Control Subsystem

2 Operational Amps. Economy multiplier - Intronics M601	-	165.00
(MIL-spec), adder Intronics 13.50	-	50.00
1 Potentiometer Helipot Model A	.1	6.00

Forward Speed Control Subsystem (continued)

	Weight (lbs)	Cost ($)
2 Transducers Gianni 45154 (American Relays) Pot Type, 0-20 spig 2 ea. 7.5KΩ	-	150.00
Total Cost	.10	$371.00

APPENDIX A

LIST OF MAJOR SYMBOLS

C	Airfoil chord
C_{ℓ}	2-D lift coefficient
C_L	3-D lift coefficient
$C_{L_{TO}}$	Lift coefficient at takeoff
C_D	Total drag coefficient
C_{d_o}	Profile drag coefficient
C_m	Pitching moment coefficient
C_s	Airfoil structural chord
L	Rib spacing
P	Flange load (tension or compression)
S_c	Compression strength
S_s	Shear strength
S_t	Tension strength
S_w	Planform area
V	Lift
W_g	Gross weight
b	Wing span
h	Structural height of box beam
n	Acceleration load factor
q	Load/unit length of flange or web
s_{xy}	Component stress
$\bar{t}$	Equivalent thickness of composite structure
t_s	Skin thickness
E	Young's Modulus

G	Polar modulus
G_{12}	Controller element for inner loop
G_{21}	Controller element for outer loop
HP_{av}	Horsepower available
HP_{req}	Horsepower required
I	Area moment of inertia
I_c	Control surface mass moment of inertia about its elastic axis
I_x	Moment of inertia about x-axis (slug-ft^2)
I_y	Moment of inertia about y-axis (slug-ft^2)
I_z	Moment of inertia about z-axis (slug-ft^2)
J	Polar moment of inertia
K	Product of inertia
K_β	Feedback gain for inner loop
K_ϕ	Feedback gain for outer loop
L	Rolling moment (ft-lbs)
L_i	$1/I_x \partial L/\partial i$ where $i = p, r, \beta, \delta_A, \delta_R$ (rad/sec)
M	Pitching moment (ft-lbs)
M_i	$1/I_y \partial M/\partial i$ where $i = u, w, \dot{w}, q, \delta_e$ (rad/sec)
N	Yawing moment (ft-lbs)
N_i	$1/I_z \partial N/\partial i$ where $i = p, r, \beta, \delta_A, \delta_R$ (rad/sec)
$N^\beta_{\delta_r}$	Numerator for β/δ_r transfer function
$N^\phi_{\delta_A}$	Numerator for ϕ/δ_A transfer function
$N_{\beta_{\beta_g}}$	Numerator for the gust transfer function β/β_g

$N^{\beta\ \phi}_{\delta_r \delta_A}$	Cross-coupling numerator ($\equiv N^{\phi\ \beta}_{\delta_A \delta_r}$)
Q	General forcing function
R	Radius from wing axis to mass distribution
R/C	Rate of climb (ft/sec)
S	Wing area (ft^2) in aerodynamic sections, Laplace operator in dynamics section
S_{TO}	Takeoff distance (ft)
$\bar{S}_x$	Static moment of inertia per unit span, subscript denotes appropriate quantity
S_x	Static moment of inertia for full span, subscript denotes appropriate quantity
T	Thrust (lbs)
T_R	Roll-mode time constant
T_S	Spiral-mode time constant
U_o	Forward airspeed (ft/sec)
$\bar{U}_x$	Energy per unit span, subscript denotes type
U_x	Energy per full span, subscript denotes type
D	Dissipation energy
V	Velocity
V_D	Maximum design velocity
W	Aircraft weight (lbs)
X	Force in direction of flight path (lbs)
X_i	$1/m\ \partial X/\partial i$ where i = u, w, $\dot{w}$, q, δ_e (1/sec)
Y	Side force (lbs)
Y_v	$1/m\ \partial Y/\partial v$ (rad/sec)
Y^*_i	$1/mU_o\ \partial Y/\partial i$ where i = p, r, δ_A, δ_R (1/rad)

Z	Force normal to direction of flight path (lbs)
Z_i	$1/m\ \partial Z/\partial i$ where $i = u, w, \dot{w}, q, \delta_e$ (1/sec)
a	Percentage of semichord between elastic axis and midchord, positive if aft of midchord
b	Semichord
c	Percentage of semichord between midchord and flap elastic axis, positive if aft of midchord
e	Percentage of semichord between midchord and flap leading edge, positive if aft of midchord
f	Subscript denotes flap
g	Dissipation energy proportionality constant
h	Transverse deflection of wing; subscript
i	Square root of -1; index denotes span position
j	Index denotes span position
k	Subscript denotes kinetic
l	Wing span
m	Mass (slugs)
p	Subscript denotes potential
P	Roll rate (deg/sec)
q	Pitch rate (deg/sec)
r	Radius from flap elastic axis to flap mass distribution
u	Perturbation velocity in x-force direction (ft/sec)
v	Perturbation velocity in y-force direction (ft/sec)
v	Velocity

w	Subscript denotes wing
w	Perturbation velocity in z-force direction (ft/sec)
$\dot{w}$	Vertical acceleration (ft/sec^2)
$f(x)$	Normalized deflection shape of wing due to bending
$F(x)$	Normalized deflection shape of wing due to twisting
(x)	Indicates quantity is a function of span station
α	Rotation of wing about its elastic axis
α	Angle of attack (degrees)
β	Sideslip angle (degrees)
β	Rotation of flap about its elastic axis
β_c	Sideslip angle command (degrees)
γ	Flight path angle (degrees)
δ_A	Aileron deflection (degrees)
δ_e	Elevator deflection (degrees)
δ_f	Flap deflection (degrees)
δ_R	Rudder deflection (degrees)
Δ	Characteristic equation of basic aircraft
Δ''	Characteristic equation of aircraft with two loops closed
ΔC_ℓ	Increment in 2-D lift coefficient
ΔC_L	Increment in 3-D lift coefficient
ΔC_{d_o}	Increment in drag coefficient
ΔC_m	Increment in pitching moment coefficient
ζ_D	Dutch roll-mode damping ratio
θ_o	Pitch angle (degrees)

μ	Ground friction coefficient
ρ	Density (slugs/ft^3)
λ	Wing taper ratio, root chord/tip chord
σ	Ratio of density at altitude to density at sea level
ϕ	Bank angle (degrees)
ϕ_c	Bank angle command (degrees)
ϕ'_{δ_A}	Transfer function for the aircraft with the inner loop closed
ψ	Yaw angle (degrees)
ω	Natural frequency of vibration
ω_{n_D}	Undamped natural frequency of Dutch roll mode (rad/sec)
θ	Angle of velocity vectors

APPENDIX B

LIST OF REFERENCES

1. Pazmaney, L. H. Prentice; Waterman, C.; and Tietge, F.: Potential Structural Materials and Design Concepts for Light Airplanes. NASA CR-73258, National Aeronautics and Space Administration, Washington, D. C., 1968.

2. Damon, Albert; Stoudt, Howard W.; and McFarland, Ross A.: The Human Body in Equipment Design. Harvard University Press, Cambridge, 1966.

3. Woodson, W. E.; and Conover, W. D.: Human Engineering Guide for Equipment Designers. Univ. Calif. Press, Berkeley, 1964.

4. Dreyfuss, Henry: Anthropometric Data. Whitney Publications, New York, 1960.

5. McCormick, Ernest J.: Human Factors Engineering. McGraw-Hill, New York, 1964.

6. Fitts, Paul M.: Designing Displays and Consoles to Match Man's Discrimination Capabilities. Human Factors Engineering Summer Conference, University of Michigan, 1962.

   Fitts, Paul M.: Arrangement of Controls and Displays and Layout of Workspaces. Human Factors Engineering Summer Conference, University of Michigan, 1962.

   Fitts, Paul M.; and Jones, Robert E.: Analysis of 270 Pilot-Error Experiences in Reading and Interpreting Instruments. Human Factors Engineering Summer Conference, University of Michigan, 1962.

7. Gagne, R. N.: Psychological Principles in System Development. Holt, Rinehart, and Winston, New York, 1964.

8. Morgan, C. T.; Cook, J. S.; Panis, A. Cha; and Lund, M. W.: Human Engineering Guide to Equipment Design. McGraw-Hill, New York, 1963.

9. Smetana, F. O.; and Carden, R. K.: An analytical Study of a Constant-Attitude Aircraft to Atmospheric Turbulence. Forthcoming NASA CR, 1972.

10. Blakelock, John H.: Automatic Control of Aircraft and Missiles. John Wiley and Sons, Inc., New York, 1965.

11. Jarvis, Calvin R.; Loschke, Paul C.; and Enevoldson, Einar K.: Evaluation of the Effect of a Yaw-rate Damper on the Flying Qualities of a Light Twin-engine Airplane. NASA TN D-5890, National Aeronautics and Space Administration, Washington, D. C., 1970.

12. McRuer, D. T.; Ashkenas, I. L.; and Pass, H. R.: Analysis of Multiloop Vehicular Control Systems. ASK-TDR-62-1014, Air Force Flight Dynamics Laboratory Research and Technology Division, Wright-Patterson Air Force Base, Ohio, 1964.

13. Smetana, F. O.; Montoya, R. J.; and Carden, R. K.: A Fast-Acting Electrical Servo for the Actuation of Full-Span, Fowler-Type Wing Flaps In DLC Applications - A Detail Design Study. Forthcoming NASA CR, 1972.

14. Onstott, E. D.; and Salmon, E. P.: Airplane Flying Characteristics in Turbulence. AFFDL-TR-70-143, Air Force Flight Dynamics Laboratory, Air Force Systems Command, Wright-Patterson Air Force Base, Ohio, 1971.

15. Smetana, F. O.; Summey, D. C.; and Johnson, W. D.: Riding and Handling Qualities of Light Aircraft--A Review and Analysis. NASA CR-1975, 1972.

16. Smetana, F. O.; Summey, D. C.; and Johnson, W. D.: Flight Testing Techniques for the Evaluation of Light Aircraft Stability Derivatives--A Review and Analysis. NASA CR-2016, 1972.

17. Sanders, Karl L.: High-lift Devices, a Weight and Performance Trade-off Methodology. SAWE paper 761, Society of Aeronautical Weight Engineers, Los Angeles, California, 1969.

18. Fisher, Jack W.: Flight Test Results on the Use of High Lift Boundary Layer Control Applied to a Modified Liaison Airplane. Cessna Aircraft Company Report Number 1339-7, Cessna Aircraft Company, Witchita, Kansas, 1956.

19. Abbott, Ira H.; von Doenhoff, Albert E.; and Stivers, Jr., Louis S.: Summary of Airfoil Data. NACA Report 824, National Advisory Committee for Aeronautics, Washington, D. C., 1945.

20. Young, A. D.: The Aerodynamic Characteristics of Flaps. RM2622, Aeronautical Research Council Reports and Memoranda, London, England, 1947.

21. Hoak, D. E.; and Ellison, D. E.: USAF Stability and Control Datcom. Air Force Flight Dynamics Laboratory, Flight Control Division, Wright-Patterson Air Force Base, Ohio, 1970.

22. Cahill, Jones F.: Summary of Section Data on Trailing-edge High-lift Devices. NACA Report 938, National Advisory Committee for Aeronautics, Washington, D. C., 1948.

23. Lowry, John G.: Wind-tunnel Investigation of a NACA 23012 Airfoil with Several Arrangements of Slotted Flaps with Extended Lips. NACA TN 808, National Advisory Committee for Aeronautics, Washington, D. C., 1941.

24. Hartman, Edwin P.; Biermann, David: The Aerodynamic Characteristics of Full-scale Propellers Having 2, 3, and 4 blades of Clark Y and R.A.F. 6 Airfoil Sections. NACA Report 640, National Advisory Committee for Aeronautics, Washington, D. C., 1937.

25. Dommasch, Daniel O.; Sherby, Sydney S.; and Connolly, Thomas F.: Airplane Aerodynamics, fourth edition. Pitman Publishing Corporation, New York, 1967.

26. Jex, H. R.; McDonnell, J. D.; and Phatak, A. V.: A Critical Tracking Task for Man-Machine Research Related to Operator's Effective Delay Time. NASA SP-128, 1966.

27. McRuer, Duane: Some Neuromuscular Subsystem Dynamics. NASA SP-128, 1966.

28. Pew, R. W.; Daffendack, J. C.; and Fench, L. K.: Sine Wave Tracking Revisited. Conference on Manual Control. NASA SP-128, 1966.

29. Shortal, Joseph A.: Wind Tunnel and Flight Test of Slot-lip Ailerons. NACA Report 602, 1937.

30. Weick, Fred E.; and Jones, Robert T.: The Effect of Lateral Controls in Producing Motion of an Airplane as Computed from Wind Tunnel Data. NACA Report 570, 1936.

31. Anon.: Dynamics of the Airframe. Bu Aer Report AE-61-4 II, Sept. 1952. Available from Northrop Corp., Aircraft Div., 3901 West Broadway, Hawthorne, Calif. 90250.

32. Shanley, F.: Weight-strength Analysis of Aircraft Structures. McGraw-Hill Book Co., New York, 1952.

33. Scanlan, R. H.; and Rosenbaum, R.: Aircraft Vibration and Flutter. Dover Publications, New York, 1951.

34. Theodorsen, T.: General Theory of Aerodynamic Instability and the Mechanism of Flutter. NACA TR 496, 1934.

35. Küssner, H. G.; and Schwarz, I.: The Oscillating Wing with Aerodynamically Balanced Elevator. NACA TM 991, 1941.

36. Garrick, I. E.: Bending Torsion Flutter Calculations Modified by Subsonic Compressibility Corrections. NACA TN 1034, 1946.

37. Airworthiness Standards: Normal, Utility, and Acrobatic Category Airplanes. Federal Aviation Regulations Part 23. Federal Aviation Agency, Washington, D. C., 1967.

38. Muzzey, C. L.; and Kidd, E. A.: Measurement and Interpretation of Flight Test Data for Dynamic Stability and Control. Cornell Aeronautical Laboratory, Inc., Buffalo, New York, 1954.

39. Gibson, J. E.; and Tuteur, F. B.: Control System Components. McGraw-Hill Book Co., New York, 1958.

40. Williams, J. C. III; Summey, D. C.; and Perkins, J. N.: A Study of NACA and NASA Published Information of Pertinence in the Design of Light Aircraft. Vol. II - Aerodynamics and Aerodynamic Loads. NASA CR 1485, 1970.

41. Stevens, Frederick; and Stevenson, M. K.: A Design Method for Automatic Longitudinal Control Systems. Aeronautical Engineering Review, 1951.

42. Takahoshi, Y.; Rabins, M. J.; and Auslander, D. M.: Control and Dynamic Systems. Addisson-Wesley Publishing Co., Reading, Massachusetts, 1970.

43. Humphreys, D. E.: Design for Improvements to Static Performance and Lateral Stability of a Constant Attitude Light Aircraft. Ph. D. Thesis, North Carolina State University. 1971.

APPENDIX C

DEVELOPMENT OF MULTILOOP ANALYSIS METHODS

The differential equations that describe the aircraft in the lateral-directional mode can be written as

$$\begin{aligned} a_{11}q_1 + a_{12}q_2 + a_{13}q_3 &= F_{11}\delta_1 + F_{12}\delta_2 + E_{11}\eta_1 + E_{12}\eta_2 \\ a_{21}q_1 + a_{22}q_2 + a_{23}q_3 &= F_{21}\delta_1 + F_{22}\delta_2 + E_{21}\eta_1 + E_{22}\eta_2 \\ a_{31}q_1 + a_{32}q_2 + a_{33}q_3 &= F_{31}\delta_1 + F_{32}\delta_2 + E_{31}\eta_1 + E_{32}\eta_2 \end{aligned} \tag{230}$$

where a_{ij} is in general a function of s in the Laplace domain and q_i is an aircraft output variable (i.e., β, ϕ, or r), δ_i is a control surface deflection, and η_i is a disturbance input.

In matrix notation, equation (230) reduces to

$$[a]\,[q] = [F]\,[\delta] + [E]\,[\eta]$$

or

$$[q] = [a]^{-1}\left[[F]\,[\delta] + [E]\,[\eta]\right] . \tag{231}$$

Equation (231) is shown in block diagram form in Figure 73.

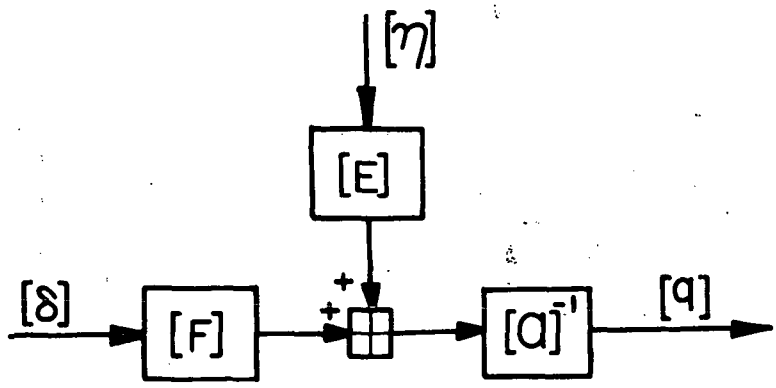

Figure 73. Open-loop block diagram for general multiloop system.

Now, if the output motion matrix [q] is fedback, and a controller matrix [G] is added to the forward loop, a closed-loop control system is developed. The general block diagram for the controlled system, with the commands fed through a command matrix [J], is shown in Figure 74.

From Figure 74 one sees that the equation for the control surface deflection matrix is

$$[\delta] = [G]\ [J]\ [q_c] - [G]\ [q] \quad . \tag{232}$$

Substituting this equation into equation (231) leads to

$$[q] = \left[[a] + [F]\ [G]\right]^{-1} \left[[F]\ [G]\ [J]\ [q_c] + [E]\ [n]\right] \quad . \tag{233}$$

The matrix $\left[[a] + [F]\ [G]\right]^{-1}$ is, after inversion, expressible as

$$\left[[a] + [F]\ [G]\right]^{-1} = \frac{\begin{bmatrix} \Delta_{11} & \Delta_{21} & \Delta_{31} \\ \Delta_{12} & \Delta_{22} & \Delta_{32} \\ \Delta_{13} & \Delta_{23} & \Delta_{33} \end{bmatrix}}{\Delta''} \tag{234}$$

where Δ'' is the characteristic equation of the system given by

$$\Delta'' = \Delta + \sum_{i=1}^{3} \sum_{j=1}^{2} G_{ji} N_{\substack{q_i \\ \delta_j}} + \sum_{i=1}^{3} \sum_{\substack{k=1 \\ i \neq k}}^{3} G_{1i} G_{2k} N_{\substack{q_i q_k \\ \delta_1 \delta_2}} \tag{235}$$

where Δ and $N_{\substack{q_i \\ \delta_j}}$ are the characteristic equation of the aircraft and the numerator of the q_i/δ_j transfer function, respectively. Terms of the form $N_{\substack{q_i q_k \\ \delta_1 \delta_2}}$ in equation (235) are called coupling numerators. They are formed by replacing the ith and kth columns of the [a] matrix by the first and second columns, respectively, of the [F] matrix. The G_{ji}'s are the elements of the controller matrix [G]. The numerator

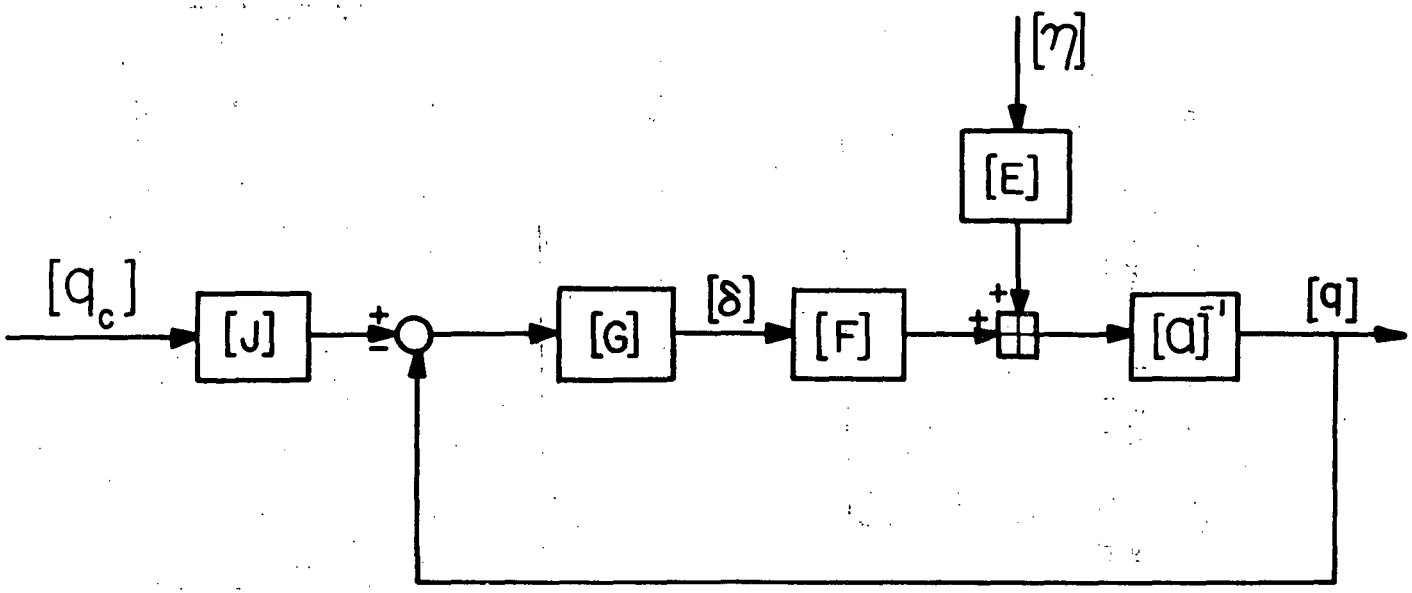

Figure 74. Closed-loop block diagram for general multiloop system.

of equation (234) is the transpose of the matrix made up of the cofactors obtained when equation (235) is written in matrix form.

This general system can be specialized to a single command, two control inputs, three outputs, two-loop closure system by setting

$$q_{2c} = q_{3c} = G_{11} = G_{22} = G_{3i} = G_{i3} = n_1 = n_2 = 0. \qquad i = 1,2,3 \ . \tag{236}$$

The block diagram for this system is shown in Figure 75.

Substituting equation (234) into equation (233), with the quantities in equation (236) set equal to zero, yields

$$\begin{bmatrix} q_1 \\ q_2 \\ q_3 \end{bmatrix} = J_1 G_{21} q_{1c} \frac{\begin{bmatrix} \Delta_{11}F_{12} + \Delta_{21}F_{22} + \Delta_{31}F_{32} \\ \Delta_{12}F_{12} + \Delta_{22}F_{22} + \Delta_{32}F_{33} \\ \Delta_{13}F_{12} + \Delta_{23}F_{22} + \Delta_{33}F_{32} \end{bmatrix}}{\Delta''} \ . \tag{237}$$

The closed-loop transfer function for the output variable q_1 is therefore

$$q_1/q_{1c} = \frac{J_1 G_{21}(F_{12}\Delta_{11} + F_{22}\Delta_{21} + F_{32}\Delta_{31})}{\Delta''} \ . \tag{238}$$

After expanding the Δ_{ij}'s and combining terms, equation (238) can be written as

$$q_1/q_{1c} = \frac{J_1 G_{21}\left[\begin{vmatrix} F_{12} & a_{12} & a_{13} \\ F_{22} & a_{22} & a_{23} \\ F_{32} & a_{32} & a_{33} \end{vmatrix} + G_{12}\begin{vmatrix} F_{12} & F_{11} & a_{13} \\ F_{22} & F_{22} & a_{23} \\ F_{32} & F_{31} & a_{33} \end{vmatrix}\right]}{\Delta''} \ . \tag{239}$$

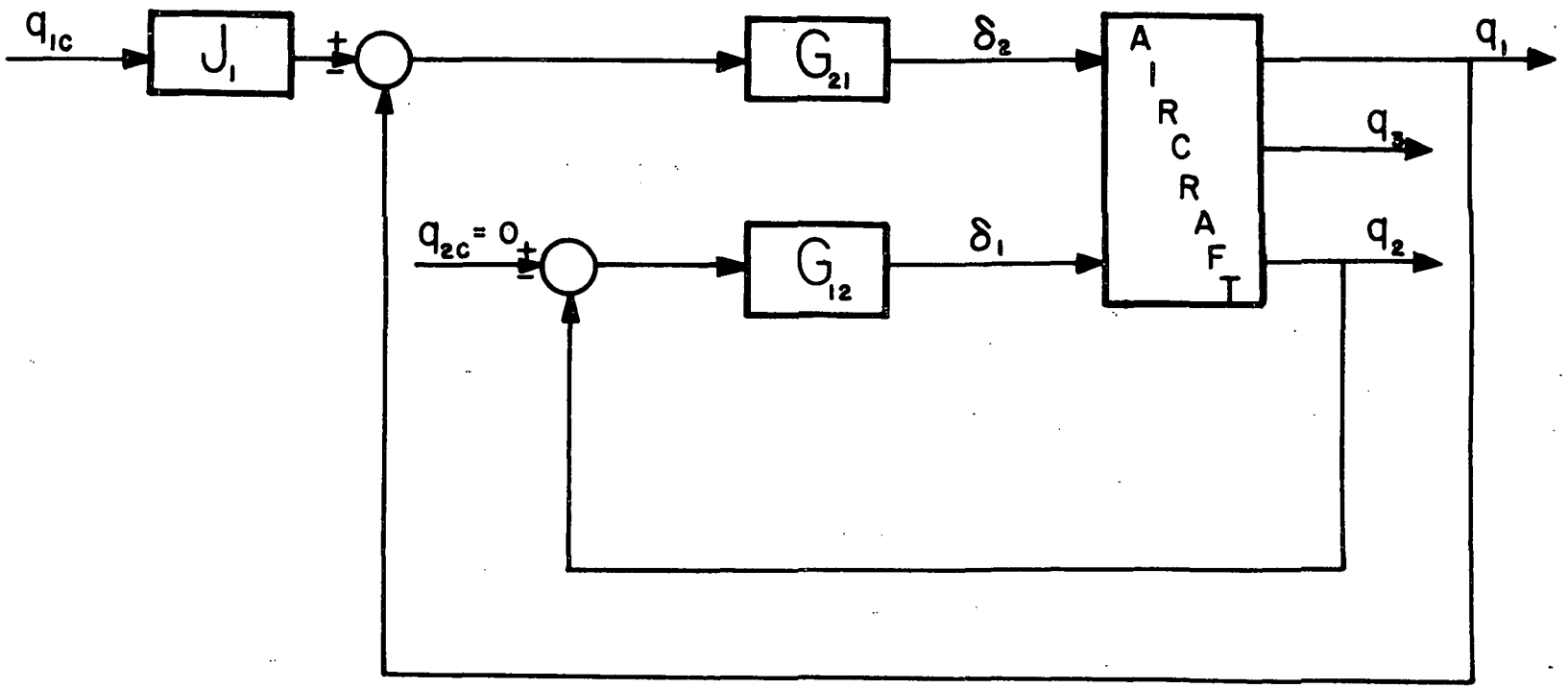

Figure 75. Block diagram for single command, two control input, three output, two-loop closure system.

The first determinant is recognized to be the numerator of the q_1/δ_2 transfer function, whereas the second determinant is the coupling numerator $N_{\delta_2\delta_1}^{q_1q_2}$. Then

$$q_1/q_{1c} = \frac{J_1G_{21}\left[N_{\substack{q1\\ \delta_2}} + G_{12}N_{\delta_2\delta_1}^{q_1q_2}\right]}{\Delta''} \tag{240}$$

where

$$\Delta'' = \Delta + G_{12}N_{\substack{q2\\ \delta_1}} + G_{21}\left(N_{\substack{q1\\ \delta_2}} + G_{12}N_{\delta_2\delta_1}^{q_1q_2}\right) . \tag{241}$$

Substituting equation (241) into equation (240) yields

$$q_1/q_{1c} = \frac{\dfrac{J_1G_{21}N_{\substack{q1\\ \delta_2}}}{\Delta}\left[1 + G_{12}\dfrac{N_{\delta_2\delta_1}^{q_1q_2}}{N_{\substack{q1\\ \delta_2}}}\right]}{1 + \dfrac{G_{12}N_{\substack{q2\\ \delta_1}}}{\Delta} + \dfrac{G_{21}N_{\substack{q1\\ \delta_2}}}{\Delta}\left[1 + \dfrac{G_{12}N_{\delta_2\delta_1}^{q_1q_2}}{N_{\substack{q1\\ \delta_2}}}\right]} \tag{242}$$

To get equation (242) into the familiar $G/(1 + GH)$ form, let

$$A = 1 + \frac{G_{12}N_{\delta_2\delta_1}^{q_1q_2}}{N_{\substack{q1\\ \delta_2}}} \tag{243}$$

$$B = 1 + \frac{G_{12}N_{\substack{q2\\ \delta_1}}}{\Delta}$$

Then,

$$q_1/q_{1c} = \frac{\dfrac{J_1 G_{21} N_{q1}\ A}{\dfrac{\delta_2}{\Delta}}}{B + \dfrac{G_{21} N_{q1}\ A}{\dfrac{\delta_2}{\Delta}}} = \frac{\dfrac{J_1 G_{21} N_{q1}\ A}{\dfrac{\delta_2}{B\,\Delta}}}{1 + \dfrac{G_{21} N_{q1}\ A}{\dfrac{\delta_2}{B\,\Delta}}} \tag{244}$$

which is in the G/(1 + GH) form with

$$G = \frac{G_{21} N_{q1}\ A}{\dfrac{\delta_2}{B\,\Delta}} \tag{245}$$

$$H = 1$$

From equation (244), an equivalent block diagram for the multiloop system can be obtained, as shown in Figure 76. The multiloop system has now been reduced to an equivalent single-loop system and may be analyzed using standard root locus techniques.

The advantage in using this analysis technique as compared to matrix methods, is the physical insight available to the designer. The individual system components are not obscured by the mathematics. For example, comparing Figures 76 and 75, the G_{21} block represents the sensing, actuation, and equalization elements for the outer loop. The term $\frac{N_{q1}}{\frac{\delta 2}{\Delta}}$ is simply the q_1/δ_2 transfer function.

The term $1 + \frac{G_{12} N_{\delta_2 \delta_1}}{\frac{N_{q1}}{\delta_2}}$ represents the cross coupling between the outer and inner loops of the system. The last block in the forward loop of Figure 76 represents the inner loop of the system. Finally, the combination of the last three blocks in the forward loop, which is denoted by Φ'_{δ_2}, represents the equivalent aircraft system with the inner loop closed.

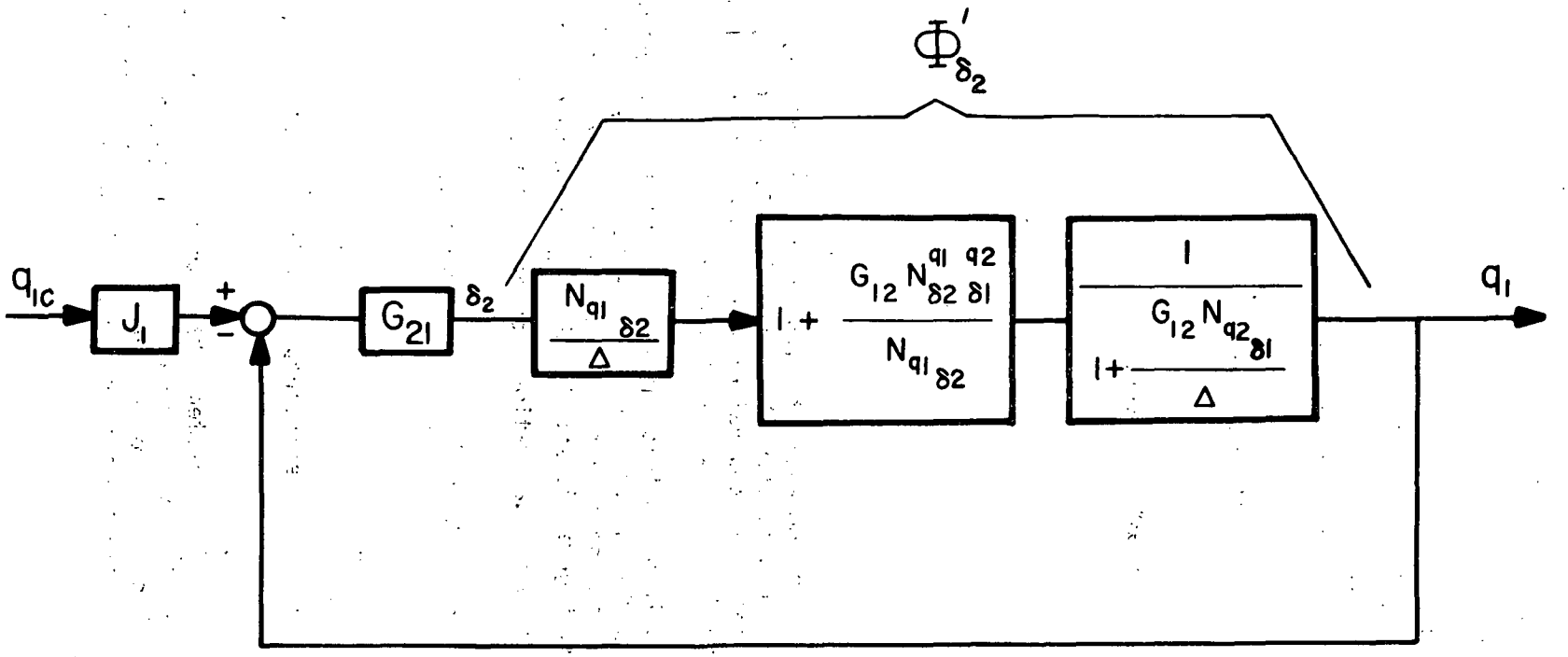

Figure 76. Equivalent block diagram for multiloop system.

APPENDIX D

Numerical Values for the Longitudinal and Lateral-Directional Stability Derivatives and Transfer Functions for the PA28-235C

	FLIGHT CONDITION					
	1	2	3	4	5	6
Speed (ft/sec)	238.	142.	89.	221.	144.	88.
Altitude (ft)	7000.	0.	0.	7000.	0.	0.
Mass (slugs)	50.5	50.5	50.5	90.2	90.2	90.2
R/C (ft/min)	0.	2180.	-500.	0.	918.	-500.
C_L	.171	.390	1.01	.360	.690	1.83
C_D	.036	.050	.140	.045	.073	.295
C_{D_o}	.035	.042	.086	.038	.048	.117
C_M	0.0026	0.011	0.003	0.007	0.013	0.011
C_T	0.037	0.152	0.044	0.045	0.147	0.124
LONGITUDINAL STABILITY DERIVATIVES						
C_{L_α}	5.34	5.34	5.34	5.34	5.34	5.34
C_{D_α}	0.16	0.35	0.81	0.30	0.52	1.28
C_{M_α}	-2.37	-2.37	-2.37	-0.86	-0.86	-0.86
$C_{L_{\dot\alpha}}$	1.44	1.44	1.44	1.44	1.44	1.44
$C_{D_{\dot\alpha}}$	0.	0.	0.	0.	0.	0.
$C_{M_{\dot\alpha}}$	-4.15	-4.15	-4.15	-3.72	-3.72	-3.72
C_{L_q}	3.74	3.74	3.74	3.07	3.07	3.07
C_{D_q}	0.	0.	0.	0.	0.	0.
C_{M_q}	-10.8	-10.8	-10.8	-7.94	-7.94	-7.94
C_{L_u}	0.	0.	0.	0.	0.	0.

	FLIGHT CONDITION					
	1	2	3	4	5	6
C_{D_u}	0.	0.	0.	0.	0.	0.
C_{M_u}	0.	0.	0.	0.	0.	0.
C_{T_u}	-0.075	-0.238	-0.663	-0.092	-0.230	-0.674
$CT_{\delta_{RPM}}$	0.00053	0.0009	0.0015	0.00078	0.00092	0.0029
$C_{L_{\delta_e}}$	-0.593	-0.593	-0.593	-0.593	-0.593	-0.593
$C_{D_{\delta_e}}$	0.	0.	0.	0.	0.	0.
$C_{M_{\delta_e}}$	1.71	1.71	1.71	1.53	1.53	1.53
$C_{L_{\delta_f}}$	1.24	1.24	0.65	1.24	1.24	0.65
$C_{D_{\delta_f}}$	0.04	0.04	0.06	0.04	0.04	0.06
$C_{M_{\delta_f}}$	-0.42	-0.42	-0.22	-0.42	-0.42	-0.22
X_u	-0.057	-0.058	-0.10	-0.037	-0.048	-0.12
X_w	0.010	0.021	0.073	0.025	0.055	0.11
$X_{\dot{w}}$	0.	0.	0.	0.	0.	0.
X_q	0.	0.	0.	0.	0.	0.
X_{δ_e}	0.	0.	0.	0.	0.	0.
X_{δ_f}	-7.79	-3.43	-1.93	-3.79	-1.97	-1.06
Z_u	-0.27	-0.42	-0.72	-0.29	-0.45	-0.73
Z_w	-4.19	-3.10	-1.97	-2.19	-1.76	-1.13
$Z_{\dot{w}}$	-0.013	-0.016	-0.016	-0.007	-0.009	-0.008
Z_q	-7.83	-5.77	-3.61	-3.36	-2.69	-1.65
Z_{δ_e}	110.	48.4	18.9	53.5	27.8	10.4
Z_{δ_f}	-229.	-101.	-20.8	-111.	-57.9	-11.5

	FLIGHT CONDITION					
	1	2	3	4	5	6
M_u	0.	0.	0.	0.	0.	0.
M_w	-0.42	-0.31	-0.19	-0.12	-0.098	-0.059
$M_{\dot{w}}$	-0.0083	-0.010	-0.010	-0.0064	-0.0079	-0.0079
M_q	-5.12	-3.77	-2.35	-3.01	-2.41	-1.48
M_{δ_e}	71.8	31.6	12.3	47.9	24.9	9.36
M_{δ_f}	-17.6	-7.76	-16.0	-13.1	-6.81	-1.35
$T_{\delta_{RPM}}$	0.155	0.163	0.171	0.099	0.095	0.181
LONGITUDINAL DENOMINATOR COEFFICIENTS						
A	1.01	1.02	1.02	1.01	1.01	1.01
B	11.4	8.48	5.78	6.69	5.41	3.64
C	119.	54.9	23.9	33.7	18.6	8.05
D	13.9	6.23	12.6	2.61	1.80	3.00
E	3.91	4.39	5.46	1.33	1.65	1.80
ELEVATOR NUMERATOR COEFFICIENTS						
B_u	1.14	0.999	1.38	1.35	1.52	1.14
C_u	-2133.	-891.	-315.	-1273.	-601.	-210.
D_u	-8202.	-2586.	-658.	-3166.	-1322.	-314.
A_w	110.	48.4	18.9	53.5	27.8	10.4
B_w	17084.	4497.	1105.	10608.	3580.	828.
C_w	1997.	448.	633.	789.	282.	306.
D_w	635.	413.	324.	460.	357.	236.
A_θ	71.8	31.6	12.3	47.9	24.9	9.36
B_θ	263.	88.	27.3	102.	43.7	13.1
C_θ	30.	13.4	11.9	7.68	4.85	4.11

	FLIGHT CONDITION					
	1	2	3	4	5	6
FLAP NUMERATOR COEFFICIENTS						
A_u	-7.89	-3.48	-1.96	-3.81	-1.98	-1.07
B_u	-90.2	-30.6	-11.6	-27.8	-13.6	-4.76
C_u	-457.	-0.44	-8.88	195.	110.	18.8
D_u	-707.	-210.	-28.9	487.	205.	26.1
A_w	-229.	-101.	-20.8	-111.	-57.9	-11.5
B_w	-5246.	-1451.	-195.	-3199.	-1105.	-137.
C_w	-603.	-159.	-103.	-236.	-88.6	-48.8
D_w	-168.	-113.	-46.4	-133.	-105.	-36.9
A_θ	-15.9	-6.85	-1.41	-12.5	-6.41	-1.28
B_θ	20.1	5.96	0.06	-16.1	-7.03	-0.46
C_θ	1.57	0.51	0.06	-1.39	-0.94	1.46
RPM NUMERATOR COEFFICIENTS						
A_u	-0.011	-0.011	-0.012	-0.007	-0.007	-0.013
B_u	-0.12	-0.091	-0.050	-0.043	-0.030	-0.022
C_u	-1.15	-0.47	-0.095	-0.12	-0.009	0.12
D_u	2.42	1.84	1.22	0.61	0.47	0.55
A_w	0.16	0.16	0.17	0.099	0.095	0.18
B_w	0.24	0.29	0.27	-0.38	-0.18	-0.16
C_w	0.036	0.075	0.097	-0.026	-0.007	-0.090
D_w	-0.012	-0.011	-0.030	-0.024	-0.028	-0.094
A_θ	-0.004	-0.004	-0.005	-0.004	-0.004	-0.007
B_θ	-0.076	-0.059	-0.041	-0.019	-0.015	-0.020
C_θ	-0.01	-0.011	-0.023	-0.002	-0.002	-0.007

	FLIGHT CONDITION					
	1	2	3	4	5	6
LONGITUDINAL DENOMINATOR CHARACTERISTICS						
ω_{SP}	10.8	7.3	4.5	5.7	4.2	2.6
ζ_{SP}	0.52	0.57	0.57	0.57	0.62	0.64
ω_{PH}	0.18	0.29	0.51	0.20	0.30	0.52
ζ_{PH}	0.32	0.18	0.53	0.18	0.12	0.30

LONGITUDINAL NUMERATOR ROOTS

$N^{u}_{\delta_e}$	-3.84 + i0	-2.89 + i0	-2.07 + i0	-2.48 + i0	-2.19 + i0	-1.49 + i0
	1874. + i0	894. + i0	230. + i0	944. + i0	399. + i0	185. + i0
$N^{\theta}_{\delta_e}$	-3.55 + i0	-2.62 + i0	-1.62 + i0	-2.05 + i0	-1.64 + i0	-0.92 + i0
	-0.12 + i0	-0.16 + i0	-0.60 + i0	-0.078+ i0	-0.12 + i0	-0.48 + i0
$N^{\omega}_{\delta_e}$	-0.058± i0.18	-0.049± i0.30	-0.29 ± i0.46	-0.037± i0.20	-0.039± i0.31	-0.18 ± i0.50
	-155. ± i0	-92.8 ± i0	-57.9 ± i0	-198. ± i0	-129. ± i0	-78.9 ± i0
$N^{u}_{\delta_f}$	-4.45 ± i3.95	0.33 ± i2.50	-0.17 ± i1.61	-2.06 + i0	-1.62 + i0	-1.14 + i0
	-2.53 + i0	-9.45 + i0	-5.59 ± i0	-10.9 + i0	-11.0 + i0	-6.55 + i0
				5.68 + i0	5.79 + i0	3.25 + i0
$N^{\theta}_{\delta_f}$	-1.33 + i0	0.95 + i0	0.22 + i0	-0.093+ i0	-0.16 + i0	-0.50 ± i0
	-0.074+ i0	-0.078+ i0	-0.18 + i0	-1.19 + i0	-0.94 + i0	
$N^{\omega}_{\delta_f}$	-0.051± i0.17	-0.052± i0.28	-0.27 ± i0.43	-0.036± i0.20	-0.038± i.31	-0.17 ± i0.50
	-22.8 ± i0	-14.3 ± i0	-8.84 ± i0	-28.7 ± i0	-19.0 ± i0	-11.6 ± i0
$N^{u}_{\delta_{RPM}}$	-6.36 ± i9.29	-5.16 + i6.25	-3.66 ± i4.22	-4.28 ± i4.32	-3.73 ± i3.10	-2.75 ± i1.96
	1.74 + i0	2.42 + i0	3.21 + i0	2.36 + i0	2.98 + i0	3.78 + i0
$N^{\theta}_{\delta_{RPM}}$	-0.13 + i0	-0.19 + i0	-0.60 + i0	-0.09 + i0	-0.13 + i0	-0.40 + i0
	-19.8 + i0	-13.5 + i0	-8.44 + i0	-4.98 + i0	-3.84 + i0	-2.36 + i0
$N^{\omega}_{\delta_{RPM}}$	-0.38 + i0	-0.46 + i0	-0.89 ± i0.34	-0.041± i0.24	-0.05 ± i.038	-0.29 ± i0.52
	-1.34 + i0	-1.41 + i0	0.19 + i0	3.91 + i0	2.04 + i0	1.46 + i0
	0.16 + i0	0.10 + i0				

	FLIGHT CONDITION					
	1	2	3	4	5	6
LATERAL STABILITY DERIVATIVES						
$C_{y_{\delta_A}}$	.000	.000	.000	.000	.000	.000
$C_{L_{\delta_A}}$	.114	.114	.114	.114	.114	.114
$C_{n_{\delta_A}}$	-.008	-.019	-.050	-.018	-.034	-.091
$C_{y_{\delta_R}}$	.123	.123	.123	.123	.123	.123
$C_{L_{\delta_R}}$	.011	.011	.011	.011	.011	.011
$C_{n_{\delta_R}}$	-.106	-.106	-.106	-.095	-.095	-.095
C_{y_β}	-.253	-.253	-.253	-.253	-.253	-.253
C_{L_β}	-.032	-.048	-.095	-.046	-.071	-.157
C_{n_β}	.106	.107	.119	.087	.092	.130
C_{y_p}	-.121	-.113	-.090	-.114	-.101	-.061
C_{L_p}	-.391	-.393	-.404	-.392	-.396	-.424
C_{n_p}	.001	-.004	-.067	-.017	-.049	-.174
C_{y_R}	.173	.204	.293	.178	.226	.389
C_{L_R}	.062	.119	.282	.110	.196	.496
C_{n_R}	-.109	-.114	-.146	-.092	-.103	-.183
Y_v	-.197	-.145	-.090	-.103	-.082	-.050
Y_p	-.006	-.007	-.005	-.003	-.003	-.002
Y_r	.009	.013	.019	.005	.008	.014
Y_{δ_A}	.000	.000	.000	.000	.000	.000
Y_{δ_R}	.095	.070	.044	.050	.040	.024
L_β	-9.63	-6.40	-4.89	-11.1	-8.90	-7.37

	FLIGHT CONDITION					
	1	2	3	4	5	6
L_p	-7.90	-5.84	-3.75	-6.83	-5.51	-3.61
L_R	1.25	1.78	2.62	1.91	2.74	4.23
L_{δ_A}	34.1	15.0	5.86	27.4	14.2	5.35
L_{δ_R}	3.17	1.39	.545	2.55	1.32	.498
N_β	14.4	6.46	2.79	9.49	5.19	2.75
N_p	.009	-.031	-.286	-.138	-.307	-.669
N_R	-1.00	-.775	-.618	-.726	-.646	-.704
N_{δ_A}	-1.16	-1.16	-1.18	-1.94	-1.94	-1.93
N_{δ_R}	-14.4	-6.37	-2.48	-10.2	-5.33	-2.00
I_x	1000.	1000.	1000.	1080.	1080.	1080.
I_y	1200.	1200.	1200.	1400.	1400.	1400.
I_z	2200.	2200.	2200.	2400.	2400.	2400.
I_{xz}	50.0	50.0	50.0	60.0	60.0	60.0
LATERAL DENOMINATOR COEFFICIENTS						
A	.998	.998	.998	.998	.998	.998
B	9.07	6.72	4.41	7.62	6.19	4.03
C	23.7	11.7	6.06	15.1	9.81	8.12
D	116.	39.2	13.7	68.2	33.3	17.7
E	-1.15	-3.63	-1.14	-1.46	-2.63	-1.84
AILERON NUMERATOR COEFFICIENTS						
B_β	.171	.706	.993	1.16	1.52	1.76
C_β	13.4	10.3	8.12	20.9	18.0	12.4
D_β	4.45	1.67	.397	2.35	.505	-1.24

	FLIGHT CONDITION					
	1	2	3	4	5	6
A_{ψ}	-.393	-.827	-1.04	-1.26	-1.58	-1.80
B_{ψ}	-8.98	-7.43	-6.20	-17.2	-15.2	-10.6
C_{ψ}	-4.85	-1.72	-.617	-2.56	-1.45	-.536
D_{ψ}	65.3	19.6	3.82	34.7	12.6	.180
A_{ϕ}	34.1	14.9	5.80	27.3	14.1	5.24
B_{ϕ}	39.6	11.7	1.05	19.0	5.05	-4.16
C_{ϕ}	485.	89.9	10.4	239.	56.6	.264
RUDDER NUMERATOR COEFFICIENTS						
A_{β}	.095	.070	.044	.050	.040	.024
B_{β}	15.1	6.71	2.61	10.5	5.49	2.06
C_{β}	114.	37.0	9.71	70.7	29.9	7.83
D_{β}	-2.03	-4.40	-1.90	-2.58	-3.77	-2.69
A_{ψ}	-14.4	-6.33	-2.47	-10.1	-5.29	-1.99
B_{ψ}	-115.	-37.7	-9.59	-71.0	-30.0	-7.62
C_{ψ}	-11.0	-2.50	-.275	-3.63	-1.05	.012
D_{ψ}	-12.6	-6.96	-3.84	-13.1	-9.03	-4.87
A_{ϕ}	2.45	1.07	.420	1.98	1.02	.386
B_{ϕ}	-15.3	-10.5	-6.35	-18.1	-14.0	-8.30
C_{ϕ}	-94.7	-32.3	-10.8	-91.0	-41.0	-13.4
LATERAL DENOMINATOR CHARACTERISTICS						
ζ_D	.15	.18	.18	.12	.15	.20
ω_{n_D}	3.8	2.6	1.9	3.1	2.5	2.3
$1/T_R$	-7.9	-5.9	-3.8	-6.9	-5.5	-3.5
$1/T_S$	.010	.090	.080	.021	.077	.099

LATERAL NUMERATOR ROOTS

$N^{\phi}_{\delta_A}$	-.58 ± 13.0	-.65 ± 12.8	-.32 ± 11.6	-.55 ± 13.2	-.43 ± 12.0	-.24 ± 11.5
$N^{\beta}_{\delta_A}$	+23.2 + 10 -.40 + 10	+43.0 + 10 -.33 + 10	-41.7 + 10 -.27 + 10	+29.5 + 10 -.30 + 10	-90.0 + 10 -.17 + 10	-23.0 + 10 -.17 + 10
$N^{r}_{\delta_A}$	+2.5 + 10 -2.6 + 10 +20.9 + 10	+1.8 + 10 -2.1 + 10 +69.0 + 10	+1.3 + 10 -1.5 + 10 -18.4 + 10	+2.1 + 10 -2.1 + 10 +26.0 + 10	+1.1 + 10 -1.3 + 10 -49.3 + 10	+.94 + 10 -1.1 + 10 -15.5 + 10
$N^{\phi}_{\delta_r}$	-3.4 + 10 +12.8 + 10	-3.0 + 10 +13.9 + 10	-1.6 + 10 +19.7 + 10	-4.0 + 10 +16.4 + 10	-2.4 + 10 +22.4 + 10	-1.6 + 10 +29.5 + 10
$N^{\beta}_{\delta_r}$	-5.5 + 10 -135. + 10 +.03 + 10	-6.3 + 10 -115. + 10 +.07 + 10	-3.5 + 10 -64.5 + 10 +.19 + 10	-6.5 + 10 -251. + 10 +.04 + 10	-5.3 + 10 -146. + 10 +.14 + 10	-3.9 + 10 -102. + 10 +.29 + 10
$N^{r}_{\delta_r}$	-.03 ± 1.39 -5.6 + 10	-.04 ± 1.39 -6.4 + 10	+.03 ± 1.61 -3.6 + 10	-.02 ± 1.43 -6.6 + 10	+.009± 1.56 -5.4 + 10	+.06 ± 1.74 -4.0 + 10

APPENDIX E

Numerical Values for the Longitudinal and Lateral-Directional Stability Derivatives and Transfer Functions for the Modified PA28-235C

	FLIGHT CONDITION					
	1	2	3	4	5	6
Speed (ft/sec)	198.	168.	95.	235.	137.	96.
Altitude (ft)	7000.	0.	0.	0.	0.	0.
Mass (slugs)	50.5	50.5	50.5	90.2	90.2	90.2
C_L	.337	.378	1.17	.426	1.01	2.05
C_D	.048	.087	.124	.052	.140	.266
C_{D_o}	.043	.081	.069	.045	.099	.098
C_M	0.005	0.016	0.002	0.006	0.030	0.011
C_T	0.048	0.141	0.019	0.052	0.266	0.088
LONGITUDINAL STABILITY DERIVATIVES						
C_{L_α}	6.27	6.90	6.53	6.32	7.20	7.05
C_{D_α}	0.173	0.187	0.655	0.21	0.56	1.17
C_{M_α}	-2.38	-2.16	-2.29	-1.18	-0.72	-0.79
$C_{L_{\dot\alpha}}$	3.16	3.54	3.31	3.19	3.71	3.62
$C_{D_{\dot\alpha}}$	0.	0.	0.	0.	0.	0.
$C_{M_{\dot\alpha}}$	-14.2	-15.8	-14.9	-13.7	-15.9	-15.5
C_{L_q}	8.41	8.41	8.41	8.19	8.22	8.21
C_{D_q}	0.	0.	0.	0.	0.	0.
C_{M_q}	-37.7	-37.7	-37.7	-35.1	-35.2	-35.2
C_{L_u}	0.	0.	0.	0.	0.	0.
C_{D_u}	0.	0.	0.	0.	0.	0.

	FLIGHT CONDITION					
	1	2	3	4	5	6
C_{M_u}	0.	0.	0.	0.	0.	0.
C_{T_u}	-0.16	-0.20	-0.75	-0.10	-0.35	-0.73
$C_{T_{\delta_{RPM}}}$	0.0017	0.0015	0.0015	0.0012	0.0015	0.0025
$C_{L_{\delta_e}}$	-0.937	-0.937	-0.937	-0.937	-0.937	-0.937
$C_{D_{\delta_e}}$	0.	0.	0.	0.	0.	0.
$C_{M_{\delta_e}}$	4.20	4.20	4.20	4.02	4.02	4.02
$C_{L_{\delta_f}}$	2.97	3.22	3.41	3.03	3.37	3.76
$C_{D_{\delta_f}}$	0.09	0.14	0.37	0.11	0.33	0.69
$C_{M_{\delta_f}}$	-1.22	-1.39	-1.32	-1.24	-1.28	-1.31
X_u	-0.047	-0.088	-0.071	-0.034	-0.065	-0.087
X_w	0.079	0.097	0.150	0.069	0.104	0.144
X_q	0.	0.	0.	0.	0.	0.
X_{δ_e}	0.	0.	0.	0.	0.	0.
X_{δ_f}	-8.84	-11.6	-10.0	-8.68	-10.5	-10.8
Z_u	-0.325	-0.38	-0.68	-0.27	-0.469	-0.67
Z_w	-3.04	-3.54	-1.91	-2.05	-1.70	-1.19
$Z_{\dot{w}}$	-0.015	-0.021	-0.020	-0.009	-0.013	-0.012
Z_q	-8.12	-8.51	-4.82	-5.27	-3.80	-2.67
Z_{δ_e}	89.3	79.6	25.5	70.9	29.7	14.6
Z_{δ_f}	-28.3	-274.	-93.1	-229.	-107.	-58.7
M_u	0.	0.	0.	0.	0.	0.
M_w	-0.175	-0.166	-0.10	-0.089	-0.039	-0.030
$M_{\dot{w}}$	-0.011	-0.015	-0.014	-0.009	-0.013	-0.012
M_q	-5.56	-5.83	-3.30	-5.33	-3.84	-2.69

	FLIGHT CONDITION					
	1	2	3	4	5	6
M_{δ_e}	61.2	54.6	17.5	71.7	30.0	14.8
M_{δ_f}	-17.8	-18.	-5.51	-22.1	-9.59	-4.80
$T_{\delta_{RPM}}$	0.20	0.18	0.10	0.095	0.084	0.099
LONGITUDINAL DENOMINATOR COEFFICIENTS						
A	1.02	1.02	1.02	1.01	1.01	1.01
B	10.8	12.	7.01	9.52	7.39	5.37
C	51.8	48.9	18.7	32.1	12.6	7.67
D	8.08	6.65	8.60	2.30	1.68	2.54
E	2.13	2.33	2.84	0.92	0.84	0.95
ELEVATOR NUMERATOR COEFFICIENTS						
A_u	0.	0.	0.	0.	0.	0.
B_u	7.08	7.70	3.84	4.92	3.10	2.10
C_u	-1010.	-853.	-311.	-1136.	-532.	-269.
D_u	-5494.	-5748.	-980.	-4521.	-1604.	-542.
A_w	89.3	79.6	25.5	70.9	29.7	14.6
B_w	12108.	9178.	1679.	16855.	4118.	1426.
C_w	1875.	1104.	864.	1117.	373.	461.
D_w	663.	645.	426.	641.	447.	339.
A_θ	61.2	54.6	17.5	71.7	30.	14.8
B_θ	180.	188.	39.4	145.	53.2	21.5
C_θ	28.1	28.5	17.	10.7	7.22	6.51
FLAP NUMERATOR COEFFICIENTS						
A_u	-8.98	-11.9	-10.2	-8.76	-10.6	-10.9
B_u	-117.	-164.	-79.3	-97.9	-87.1	-63.0

	FLIGHT CONDITION					
	1	2	3	4	5	6
C_u	-351.	-522.	-136.	-57.6	-30.6	-20.1
D_u	144.	591.	32.5	801.	392.	123.
A_w	-283.	-274.	-93.1	-229.	-107.	-58.7
B_w	-4979.	-4504.	-844.	-6318.	-1696.	-617.
C_w	-753.	-557.	-393.	-409.	-150.	-180.
D_w	-214.	-239.	-154.	-211.	-158.	-122.
A_θ	-15.	-14.4	-4.34	-20.3	-8.36	-4.14
B_θ	-6.85	-20.3	-3.47	-26.3	-13.2	-5.31
C_θ	-1.81	-4.31	-2.11	-2.35	-2.20	-2.00
RPM NUMERATOR COEFFICIENTS						
A_u	-0.014	-0.013	-0.007	-0.007	-0.006	-0.007
B_u	-0.13	-0.13	-0.030	-0.056	-0.034	-0.021
C_u	-0.49	-0.35	0.018	-0.10	0.045	0.091
D_u	1.46	1.28	0.42	0.45	0.24	0.21
A_w	0.20	0.18	0.10	0.095	0.084	0.099
B_w	0.51	0.58	0.23	-0.13	0.007	0.029
C_w	0.093	0.12	0.094	-0.002	0.015	-0.001
D_w	-0.019	-0.015	-0.017	-0.02	-0.023	-0.044
A_θ	-0.006	-0.006	-0.003	-0.004	-0.004	-0.004
B_θ	-0.046	-0.041	-0.015	-0.014	-0.008	-0.008
C_θ	-0.008	-0.007	-0.007	-0.001	-0.001	-0.002

	FLIGHT CONDITION					
	1	2	3	4	5	6
LONGITUDINAL DENOMINATOR CHARACTERISTICS						
ω_{SP}	7.0	6.8	3.9	5.6	-4.76 *	-3.07 *
ζ	0.75	0.85	0.82	0.84	-2.44	-1.94
ω_{PH}	0.21	0.22	0.43	0.17	0.27	0.40
ζ_{PH}	0.37	0.29	0.56	0.19	0.19	0.36

* indicates a non-oscillatory mode:

$\zeta > 1$ roots are given in brackets

LONGITUDINAL NUMERATOR ROOTS

$N^{u}_{\delta_e}$	-5.25 + i0	-6.37 + i0	-3.04 + i0	-3191. + i0	-2.96 + i0	-1.98 + i0
	148. + i0	117. + i0	84. + i0	235. + i0	175. + i0	130. + i0
$N^{\theta}_{\delta_e}$	-2.78 + i0	-3.28 + i0	-1.67 + i0	-1.95 + i0	-1.63 + i0	-1.02 + i0
	-0.17 + i0	-0.16 + i0	-0.58 + i0	-0.077+ i0	-0.15 + i0	-0.43 + i0
$N^{\omega}_{\delta_e}$	-0.077± i0.22	-0.060± i0.26	-0.26 ± i0.43	-0.033± i0.19	-0.045± i0.33	-0.16 ± i0.46
	-135. + i0	-115. ± i0	-65. + i0	-238. ± i0	-139. + i0	-97. + i0
$N^{u}_{\delta_f}$	-5.76 + i0	-7.34 ± i1.71	-3.05 ± i0	-4.08 + i0	-2.93 ± i0	-1.98 + i0
	-7.64 + i0	0.88 + i0	-4.91 + i0	-9.47 + i0	-7.09 + i0	-4.95 + i0
	0.36 + i0		0.21 + i0	2.37 + i0	1.78 + i0	1.15 + i0
$N^{\theta}_{\delta_f}$	-0.22 ± i0.26	-0.26 + i0	-0.40 ± i0.57	-0.097 +i0	-0.19 + i0	-0.64 + i0.27
		-1.15 + i0		-1.20 + i0	-1.39 + i0	
$N^{\omega}_{\delta_f}$	-0.075± i0.19	-0.061± i0.23	-0.23 ± i0.37	-0.032± i0.18	-0.041± i0.30	-0.14 ± i0.43
	-17.4 + i0	-16.3 + i0	-8.59 + i0	-27.5 + i0	-15.8 + i0	-10.2 + i0
$N^{u}_{\delta_{RPM}}$	-5.64 ± i4.83	-6.10 ± i3.82	-3.65 ± i2.49	-5.16 ± i2.91	-2.59 + i0	-1.96 + i0
	1.86 + i0	1.97 + i0	3.03 + i0	1.94 + i0	-5.81 + i0	-4.41 + i0
$N^{\theta}_{\delta_{RPM}}$	-0.18 + i0	-0.17 + i0	-0.54 + i0	-0.08 + i0	-0.15 + i0	-0.37 + i0
	-8.17 + i0	-7.19 + i0	-4.27 + i0	-3.88 + i0	-2.08 + i0	-1.57 + i0
$N^{\omega}_{\delta_{RPM}}$	-0.34 + i0	-0.31 + i0	-0.75 + i0	-0.06 ± i0.37	-0.31 ± i0.64	-0.49 ± i0.64
	-2.32 + i0	-3.09 + i0	-1.71 + i0	1.44 + i0	0.54 + i0	0.68 + i0
	0.12 + i0	0.09 + i0	0.14 + i0			

	FLIGHT CONDITION					
	1	2	3	4	5	6
LATERAL STABILITY DERIVATIVES						
$C_{y_{\delta_A}}$	.000	.000	.000	.000	.000	.000
$C_{L_{\delta_A}}$	1.48	1.61	1.70	1.51	1.68	1.87
$C_{n_{\delta_A}}$	-.046	-.068	-.184	-.057	-.164	-.334
$C_{y_{\delta_R}}$	.164	.164	.164	.164	.164	.164
$C_{L_{\delta_R}}$	.014	.014	.014	.014	.014	.014
$C_{n_{\delta_R}}$	-.167	-.167	-.167	-.159	-.159	-.159
C_{y_β}	-.347	-.347	-.347	-.347	-.347	-.347
C_{L_β}	-.051	-.054	-.114	-.058	-.102	-.181
C_{n_β}	.143	.143	.156	.124	.132	.164
C_{y_p}	-.149	-.162	-.122	-.147	-.142	-.100
C_{L_p}	-.497	-.540	-.523	-.501	-.563	-.571
C_{n_p}	-.030	-.053	-.090	-.037	-.113	-.164
C_{y_R}	.318	.324	.439	.316	.400	.550
C_{L_R}	.121	.132	.354	.144	.307	.597
C_{n_R}	-.194	-.207	-.224	-.179	-.212	-.266
Y_v	-.167	-.175	-.099	-.111	-.080	-.056
Y_p	-.006	-.007	-.005	-.003	-.003	-.002
Y_r	.012	.015	.021	.006	.010	.014
Y_{δ_A}	.000	.000	.000	.000	.000	.000
Y_{δ_R}	.079	.082	.047	.052	.037	.026
L_β	-7.06	-6.68	-4.51	-11.07	-8.17	-7.11
L_p	-5.54	-6.31	-3.46	- 6.50	-5.24	-3.73
L_R	1.35	1.54	2.34	1.87	2.86	3.90

	FLIGHT CONDITION					
	1	2	3	4	5	6
L_{δ_A}	204.	197.38	67.1	288.	134.	73.8
L_{δ_R}	1.95	1.74	.558	2.70	1.13	.558
N_β	9.27	8.28	2.88	10.4	4.65	2.84
N_p	-.156	-.291	-.282	-.213	-.465	-.474
N_R	-1.01	-1.13	-.696	-1.02	-.871	-.766
N_{δ_A}	-2.99	-3.94	-3.40	-4.81	-5.79	-5.79
N_{δ_R}	-10.7	-9.59	-3.08	-13.3	-5.59	-2.75
I_x	1120.	1120.	1120.	1145.	1145.	1145.
I_z	2385.	2385.	2385.	2600.	2600.	2600.
I_{xz}	62.1	62.1	62.1	75.5	75.5	75.5
DENOMINATOR COEFFICIENTS						
A	.998	.998	.998	.998	.998	.998
B	6.70	7.60	4.21	7.60	6.14	4.47
C	15.8	16.8	6.16	17.9	10.7	7.55
D	53.9	55.7	12.9	71.8	30.1	16.4
E	-.868	-2.43	-.890	-1.11	-2.15	-1.48
AILERON NUMERATOR COEFFICIENTS						
B_β	-3.48	-2.71	1.22	-4.45	1.35	3.39
C_β	80.0	116.	52.4	130.	123.	80.3
D_β	33.1	39.1	13.9	39.2	21.2	12.9
A_ψ	2.32	1.19	-1.65	3.55	-1.88	-3.64
B_ψ	-48.2	-82.1	-30.8	-92.3	-93.3	-56.8
C_ψ	-19.1	-27.0	-4.10	-19.8	-9.71	-3.65
D_ψ	304.	305.	60.1	403.	135.	56.3

	FLIGHT CONDITION					
	1	2	3	4	5	6
A_ϕ	204.	197.	66.9	287.	134.	73.4
B_ϕ	237.	252.	45.4	319.	111.	38.1
C_ϕ	1883.	1621.	178.	2960.	581.	168.
RUDDER NUMERATOR COEFFICIENTS						
A_β	.079	.082	.046	.052	.037	.026
B_β	11.0	10.0	3.19	13.5	5.72	2.81
C_β	60.0	60.8	11.0	87.4	29.8	10.7
D_β	-2.04	-4.07	-1.98	-3.04	-4.24	-3.13
A_ψ	-10.7	-9.55	-3.06	-13.2	-5.56	-2.73
B_ψ	-61.0	-62.1	-11.0	-88.3	-30.1	-10.6
C_ψ	-5.55	-5.85	-.475	-5.68	-1.17	-.173
D_ψ	-9.44	-9.43	-4.14	-16.3	-9.44	-6.00
A_ϕ	1.35	1.20	.387	1.82	.764	.376
B_ϕ	-12.8	-13.1	-7.01	-22.6	-15.2	-10.5
C_ϕ	-58.9	-50.7	-12.5	-120.	-40.9	-18.1
DENOMINATOR CHARACTERISTICS						
ζ_D	.18	.22	.19	.16	.21	.21
ω_{n_D}	3.1	3.0	1.9	3.3	2.4	2.2
$1/T_R$	-5.6	-6.3	-3.5	-6.6	-5.2	-3.7
$1/T_S$	.016	.043	.067	.015	.069	.086

LATERAL NUMERATOR ROOTS

$N^{\phi}_{\delta_A}$	$-.58 \pm i3.7$	$-.42 \pm 12.4$	$-.07 \pm i1.3$	$-.34 \pm i2.9$	$-.19 \pm i2.0$	$+.12 + i0$ $+.71 + i0$
$N^{\beta}_{\delta_A}$	$-76.4 + i0$ $-.34 + i0$	$-14.2 + i0$ $-.17 + i0$	$-7.7 + i0$ $-.05 + i0$	$-17.6 + i0$ $-.11 + i0$	$-11.6 + i0$ $-.03 + i0$	$-6.8 + i0$ $+.10 + i0$
$N^{r}_{\delta_A}$	$-3.2 + i0$ $-22.0 + i0$ $-2.3 + i0$	$-2.0 + i0$ $-8.4 + i0$ $+1.4 + i0$	$-.90 + i0$ $-5.7 + i0$ $+.70 + i0$	$-1.6 + i0$ $-13.3 + i0$ $-1.3 + i0$	$-1.0 + i0$ $-9.4 + i0$ $+.83 + i0$	$-.16 + i0$ $-5.9 + i0$ $+.11 + i0$
$N^{\phi}_{\delta_r}$	$-3.8 + i0$ $+10.1 + i0$	$-2.5 + i0$ $+12.2 + i0$	$-1.5 + i0$ $+16.6 + i0$	$-3.6 + i0$ $+12.7 + i0$	$-2.5 + i0$ $+16.1 + i0$	$-1.5 + i0$ $+23.0 + i0$
$N^{\beta}_{\delta_r}$	$-7.9 + i0$ $-150. + i0$ $+.02 + i0$	$-5.8 + i0$ $-89.4 + i0$ $+.12 + i0$	$-3.8 + i0$ $-55.7 + i0$ $+.20 + i0$	$-6.8 + i0$ $-203. + i0$ $+.04 + i0$	$-5.6 + i0$ $-132. + i0$ $+.13 + i0$	$-3.9 + i0$ $-80.7 + i0$ $+.35 + i0$
$N^{r}_{\delta_r}$	$-.04 \pm i.32$ $-8.0 + i0$	$-.02 \pm i.43$ $-5.9 + i0$	$+.04 \pm i.63$ $-4.0 + i0$	$-.01 \pm i.43$ $-6.9 + i0$	$+.009 \pm i.55$ $-5.7 + i0$	$+.08 \pm i.78$ $-4.0 + i0$

APPENDIX F

CONTROL SYSTEM BACKUPS

Although the primary control system is designed to be highly reliable, it is not possible to build any device which never fails. Thus it is necessary to consider the results of a situation in which some portion, or all of the simple to fly control system fails to operate properly. It would be inexcusable to design the aircraft in such a way that it would be impossible to safely land it after a control system failure. One could consider failures of individual component failures, and attempt to find solutions for each problem. There are so many components and circuits in the system that such extensive emergency procedures would be far beyond the capabilities of the average pilot. It should be sufficient to consider only failures of large groups of components, as it is unlikely that single component failures will be more serious than subsystem failures. It is expected that two or three options for backup control will be sufficient to cover all possible failures and will be all that the pilot could be expected to handle in an emergency.

Only two types of failures will be considered, regardless of the actual component failures: forward loop failures and feedback loop failures. The possible control system failures are thus forward speed forward loop or feedback failure, rate of climb forward loop or feedback failure, pitch attitude forward loop or feedback failure, sideslip forward loop or feedback failure, and roll angle forward loop or feedback failure.

The analysis by Humphreys Ref. 43 shows that failures in the bank angle and sideslip angle feedback loop do not degrade aircraft performance or control sufficiently to require any backup. Such failures will degrade the dynamic stability of the aircraft somewhat. If the inner (β) loop feedback fails, the outer loop still acts as a wings leveler and maintains a positive spiral stability, while the rudder obeys only the command. The command is simply $\beta = 0^{\circ}$, so the rudder remains undeflected. As a result, the sideslip can become large with large aileron deflections. The airframe still has its natural damping in yaw, which is considerable. Slow turns would be advisable in this situation, to reduce the amount of sideslip occurring. The Dutch roll will be excited as would any aircraft, but the airframe has better-than-average Dutch roll damping, so there should be no problem. A failure of the outer (ϕ) loop changes it from a bank angle command system to an aileron deflection command system. Specifically, a 1° step in ϕ_c results in a steady state aileron deflection of 0.442° in about 0.54 seconds (to within 5%), with an overshot of about 100%. The failure of the outer loop eliminates the artificial spiral stability and slows down the roll performance, but the Dutch roll will still be stabilized by the feedback of β, $\dot{\beta}$, and $\ddot{\beta}$. There is a chance that the dynamics of the aileron in following a ϕ command will lead to pilot induced oscillations (because of the 0.54 second

lag), but this is not expected to be serious. If it should turn out to be a bad problem, provision would have to be made to disengage the command shaping network when the ϕ loop feedback failed, and replace it with something like an $\frac{s+50}{71.4}$ network.

At this point, it seems that failures in the feedback loops require no provision for backup systems, except to insure that a failed feedback loop produces negligible output.

Failures in the forward loop, however, are far more serious. Rather than merely degrading the dynamics of the aircraft, they make it completely uncontrollable. Provision must be made to allow control of the aircraft. If the rudder control (β) system forward loop fails and the aileron control (ϕ) system forward loop does not fail, the high adverse yaw of the full span ailerons will make the aircraft very difficult to turn. Therefore, it is necessary to provide for manual rudder control as a backup. If the aileron control system forward loop fails and the rudder control forward loop does not, it will be impossible to turn the aircraft. Provision must be made for manual roll control. If both rudder and aileron forward loops fail, some provision must be made to turn the aircraft, using roll and/or yaw control. No mention has been made yet of the longitudinal controllers, airspeed, rate of climb, and pitch attitude, mainly because their design has not been documented previous to this report. These systems tend to be more complex electronically and aerodynamically, than the lateral controllers. It is impossible to analyze them in any detail without complete details on their design and operation. However, provision can be made to allow reasonably safe descent of the aircraft should any or all of the longitudinal controllers fail.

Manual roll control by manual deflection of the full span Fowler flap is impossible because of the very high forces and moments to be overcome. The flap is deflected by a ball screw, driven by a 1/2 horsepower electric motor. Eight degrees of aileron deflection (each flap moving 8°) is required to attain a reasonable roll rate in a reasonable time. For this deflection, 36.48 radians deflection of each ball screw is required. The yoke deflection required for this deflection could be as much as 60°. The required gear ratio between yoke and ball screw is thus 34.84:1. Any friction in the flap mechanism would be magnified enough to make the yoke difficult to deflect, but with the flap aerodynamic load added, the task becomes nearly impossible. Some control besides the flaps must be used to roll the aircraft. Spoilers are the logical answer, being simple and easy to build, lightweight, and easy to deflect. The details of the actual spoiler design will be covered later. It will be shown that the spoiler has sufficient favorable yaw that no rudder control is required to enter a turn. Thus, when both roll and yaw control fail, only roll control need be assumed.

There is a problem involved in assuming manual control. The automatic portion of the forward loop, which has malfunctioned, must be mechanically and electrically disconnected from its system. The backup must be engaged. When roll control fails, the yoke must be connected to the spoiler, and the circuit to the flap servos must be broken. When yaw control fails, the yoke must be connected to the rudder, and the rudder servo must be disconnected, electrically and mechanically, from the system. If both fail, both must be disengaged, but only the spoiler need be engaged. The spoiler and rudder loads are low enough that the control feel springs need not be disengaged from the yoke when the backup is engaged. Note that the lateral control backups are connected only to the yoke twisting control, not the fore and aft motion which corresponds to rate of climb. In the case where yaw control only fails, twisting of the yoke will command a bank angle (ϕ) and a rudder deflection. Thus, rudder deflection is applied to neutralize the adverse yaw of the ailerons.

It will not be difficult to implement the backup controllers, as the cables and pulleys for controls similar to our backups already exist in the Piper Cherokee. Figure 77 illustrates the layout of the pulleys and cables required to implement the system. Twisting of the yoke will translate the cable attached to the yoke, the pulley around which this cable wraps, and the shaft which supports this pulley. The pulleys going to the rudder and spoiler are not fixed to this shaft: they freewheel on the shaft except when the backup is engaged.

The backup works by locking the spoiler pulley to the shaft if roll control or roll and yaw control fail, and by locking the rudder pulley to the shaft if yaw control only fails. It will be necessary to design linkages so that the pilot can manually engage either backup. It will be necessary to use sprocket and chain at the pulley location instead of pulley and cable, to avoid slippage.

As previously stated, various individual failures in the longitudinal controllers will not be considered; only the complete system failure will be considered. This failure we call the deadstick landing; without control over thrust, one can only try to set the aircraft up so that it will glide to earth as gently as possible. The pilot, of this aircraft, long accustomed to the easy fly control system, cannot suddenly be expected to manipulate the surfaces himself in such a time of stress. Thus, the backup controller for the longitudinal controller set flaps and stabilator to a preselected position, allowing a gentle glide to earth. The pilot need only steer, which is probably all he could be expected to do in the circumstances. The preselected positions for flaps and elevator where chosen to give the lowest descent speed possible over the range of possible loadings.

The rates of descent indicate a hard landing, especially at max gross weight. It is doubtful, however, that the average private pilot could do better in a conventional aircraft in such an emergency.

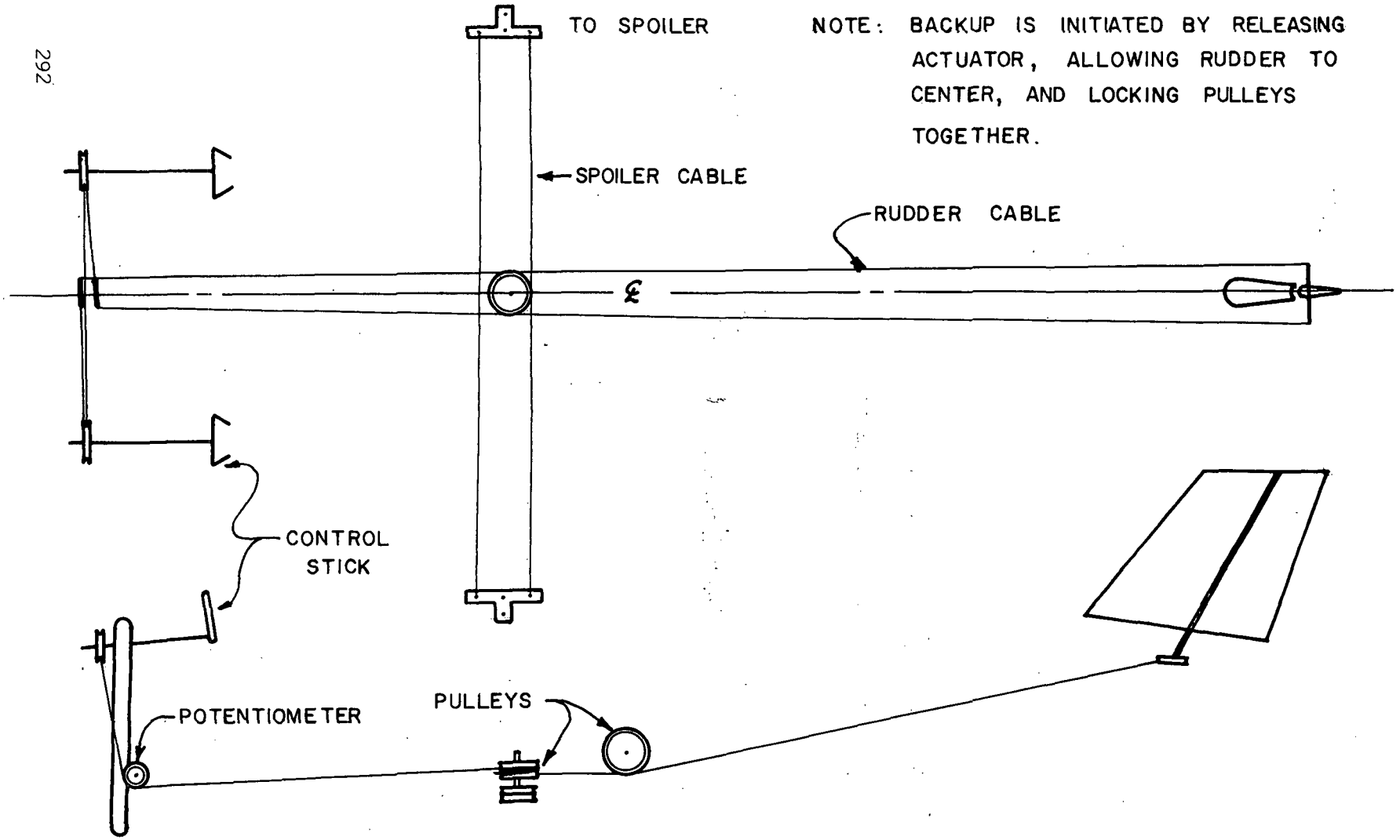

Figure 77. Spoiler and rudder backup.

APPENDIX G

Characteristics of the Fixed Elements of Subsystem 1.

Examination of Figure 3 indicates that several components can be specified on a nominal basis prior to the synthesis phase. These are: the transducers, T_u and T_w; the airspeed and rate of climb error generators; the summing junctions; the flap and engine throttle actuators; and the rate of climb and forward airspeed sensors. Two types of specifications are required, one static and one dynamic. The first type is dictated by the accuracy requirements at the different points of the subsystem and by the maximum values of the mechanical and electrical variables which are related at these points. The second type depends on the relationship between the time domain behavior of the individual components and that of the closed loop channels of the control subsystem. The components proposed are all standard and their theory of operation and representation follows normal practice found in the literature.

The forward airspeed transducer (T_u) consists of a high impedance, single turn, wire wound potentiometer with one of its ends tied to ground and the other tied to the positive supply voltage (+30 volts). The output wiper rotates as a function of the deflection of the foot throttle the linear travel of which is 6 inches. Assuming a linear potentiometer with total circular travel of 300 degrees, the relationship between foot throttle depression and potentiometer wiper position can be expressed as

$$K_1 = \frac{\text{Maximum wiper travel}}{\text{Maximum foot throttle travel}} \tag{246}$$

$$= 50 \text{ degrees/inch.} \tag{247}$$

The excitation of the potentimeter yields a transducing gain of

$$K_{T_u} = \frac{\text{Maximum excitation voltage}}{\text{Maximum wiper travel}} \tag{248}$$

$$= .1 \text{ volt/degree.} \tag{249}$$

The maximum airspeed for this aircraft is 235.14 fps and the minimum airspeed is 96.16 fps. Hence the forward speed range is related to the electrical output of the potentiometer thusly

$$K_2 = \frac{u_{max}}{\text{Maximum excitation voltage}} \tag{250}$$

$$= 7.84 \text{ fps/volt.} \tag{251}$$

The minimum airspeed constraints the in flight operational range of the output wiper of the potentiometer in the following fashion: the command voltage equivalent to 96.16 fps is 12.25 volts and according to equation 249 this requires a wiper position of 122.5 degrees; therefore the wiper must be maintained between 122.5 and 300 degrees during the flight of the aircraft. This will be insured by the use of a one way stop which disengages upon the landing of the aircraft. The overall gain relating forward airspeed command to foot throttle depression is obtained by multiplying equations 247, 249 and 251. This yields

$$\frac{u_c}{\delta_{FT}} = 39.2 \text{ fps/inch.} \tag{252}$$

The rate of climb transducer (T_w) consists of a high impedance, single turn, wire wound, special potentiometer with three terminals available for electrical connections. These will be labeled terminals 1, 2, and 3 for identification purpose. The output wiper rotates as a function of yoke deflection the total travel of which is 30 inches, 15 inches fore and 15 inches aft. The 300 degrees which constitute the operational range of the potentiometer are divided into two regions; from terminal 1 to 2 there is an arc of 187.5 degrees and from terminal 2 to 3 there is an arc of 112.5 degrees. Terminal 1 is tied to +30 volts; terminal 2 is tied to ground; and terminal 3 is tied to -18 volts. These connections imply that when the output wiper covers the arc 2-1 the potentiometer will output a positive rate of climb command voltage and when the wiper covers the arc 2-3 the potentiometer will output a negative rate of climb command voltage. The relationship between yoke deflection and wiper positions can be expressed as

$$K_3 = \frac{\text{Maximum wiper travel}}{\text{Maximum yoke travel}} \tag{253}$$

$$= 10 \text{ degrees/inch.} \tag{254}$$

The excitation of the potentiometer yields a transducing gain of

$$K_{T_w} = \frac{(+30)(-18)}{\text{Maximum wiper travel}} \tag{255}$$

$$= .16 \text{ volt/degree.} \tag{256}$$

The maximum rate of climb for this aircraft is 1500 fpm and the maximum rate of sink is -900 fpm. Hence the rate of climb range is related to the electrical output of the potentiometer thusly

$$K_4 = \frac{(+w_{max}) - (-w_{max})}{(+30) - (-18)} \tag{257}$$

$$= 50 \text{ fpm/volt.} \tag{258}$$

The overall gain relating rate of climb command voltage to yoke deflections is obtained by multiplying the results of equations 254, 256, and 258. This yields

$$\frac{w_c}{\delta_Y} = 80 \text{ fpm/inch.} \tag{259}$$

The forward airspeed and rate of climb error generators, and the summing junctions consist of highly accurate operational amplifiers with high input impedance and low output impedance. The external components added to these op amps; high impedance, low power, equal value resistors in their input and feedback paths; make these junctions have a unity voltage gain. The desired algebraic operation is obtained by connecting the appropriate variable to the inverting and noninverting inputs of these op amps. The dynamic behavior of these op amps as well as that of the transducers discussed above is much faster than that proposed for the overall subsystem and as such can be neglected.

The flap actuator package consists of a power amplifier, a split series dc motor and several feedback loops and compensation networks arranged in a servomechanism fashion. The motor drives the flap through a lead screw. The detailed design of this package is covered by Smetana, et al., (Ref. 13). The static specifications are:

i) position accuracy $\leq$ .20 degrees in flap position. This is based on the flap power for the design flight condition as shown in Figure 4a and on specification vi; i.e., on the basis of flap changes alone, 0.2 degree flap increment is required to obtain 20 fpm in w;

ii) actuation rate = 40 degrees/sec.

The dynamic specification is that the actuator package be representable by the transfer function

$$\frac{\delta_F}{V_2}(s) = \frac{\left(\frac{\delta_{F_{max}}}{+30}\right) 50}{(s+50)} \tag{260}$$

$$= \frac{66.5}{(s+50)} \quad \text{degrees/volt.} \tag{261}$$

where δ_F is flap deflection and V_2 is the voltage input to the servo actuator package.

The engine control subsystem consists of two parts: an actuator package controlling the engine throttle opening as a function of voltage V_1 and the existing control relationship between throttle opening and engine rpm. The control strategy in most reciprocating engines of general aviation aircrafts calls for changes in engine rpm at constant manifold pressure and this strategy has been followed in this design; however, the capability of changing manifold pressure through the existing engine control has been preserved.

The transfer function relating the electrical input V_1 to the mechanical output σ_1 in Figure 3 is in general a second order one. If, however, the damping and natural frequency of this transfer function are much higher than those of the aircraft modes; it can be represented by a pure gain transfer function as

$$\frac{\sigma_1}{V_1} = \frac{\sigma_{1\ max}}{V_{1\ max}} \tag{262}$$

$$= .166 \text{ inches/volt.} \tag{263}$$

It is found in the literature that a typical transfer function for a reciprocating engine is

$$\frac{\delta_{RPM}}{\sigma_I}(s) = \frac{5\ K_5}{(s+5)} \quad \text{rpm/inches.} \tag{264}$$

The maximum expected rpm change in this application is 1500 rpm and the maximum throttle opening is 5 inches. Hence, the constant K_5 is

$$K_5 = 300 \text{ rpm/inch} \quad . \tag{265}$$

The static specifications for the engine actuator package are:

i) position accuracy $\leq$ 5 rpm in engine output. This is based on the engine power for the design flight condition as shown in Figure 4b and on specification vi; i.e., on the basis of engine rpm change alone, a 5 rpm change is required to obtain 2.6 fps in μ;

ii) actuation rate = 300 rpm/sec based on specification v.

The forward airspeed sensor is an accelerometer with dynamic response much faster than that of the subsystem. The static specifications are:

i) threshold = .26 fps. This is based on 10% of the static accuracy requirement of the closed loop subsystem;

ii) range = 240 fps, and

iii) sensitivity = .125 volts/fps (nominal).

The rate of climb sensor is an accelerometer with dynamic response much faster than that of the closed loop subsystem. The static specifications are:

i) threshold = 2 fpm. This is based on 10% of the static accuracy requirement of the closed loop subsystem;

ii) range = $\pm$ 1500 fpm, and

iii) sensitivity = .020 volts/fpm (nominal).

It should be pointed out that these accelerometers used as the sensing elements for u and w require an integrating element to obtain these variables plus adequate compensation to suppress the resultant undesirable steady state values.

APPENDIX H

Development of the MIMO System Analysis Method for the Two Input-Two Output Case

The transfer functions that relate the output to input variables of the subsystem depicted in Figure 3 can be derived in a straight forward manner with the aid of matrix formulation. The analysis then becomes analogous to that of a single input-single output (SISO) subsystem with matrices taking the place of the single variables.

It should be noted that while in general the method developed in Appendix (C) for the analysis of the lateral control subsystem (subsystem 3) is applicable to the analysis of the forward airspeed-rate of climb control subsystem, the differences in the models used and in the design approach are such that a separate development is warranted.

The relationship between u and w and the aircraft manipulated variables δ_{RPM} and δ_F can be expressed as

$$\begin{bmatrix} u \\ w \end{bmatrix} = \begin{bmatrix} \frac{u}{\delta_{RPM}} & \frac{u}{\delta_F} \\ \frac{w}{\delta_{RPM}} & \frac{w}{\delta_F} \end{bmatrix} \begin{bmatrix} \delta_{RPM} \\ \delta_F \end{bmatrix} \tag{266}$$

where

$$\begin{bmatrix} \delta_{RPM} \\ \delta_F \end{bmatrix} = \begin{bmatrix} \frac{\delta_{RPM}}{V_1} & V_1 \\ \frac{\delta_F}{V_2} & V_2 \end{bmatrix} ; \tag{267}$$

but V_1 and V_2 can be expressed in terms of ε_u and ε_w as

$$\begin{bmatrix} V_1 \\ V_2 \end{bmatrix} = \begin{bmatrix} G_{11_s} & G_{21_s} \\ G_{12_s} & G_{22_s} \end{bmatrix} \begin{bmatrix} \varepsilon_u \\ \varepsilon_w \end{bmatrix} \tag{268}$$

where

$$\begin{bmatrix} \varepsilon_u \\ \varepsilon_w \end{bmatrix} = \begin{bmatrix} u_c - u \\ w_c - w \end{bmatrix} \tag{269}$$

is the error matrix. Substituting matrix equation 268 into 267 and substituting the result into matrix equation 266 one gets:

$$\begin{bmatrix} u \\ w \end{bmatrix} = \begin{bmatrix} \frac{u}{\delta_{RPM}} & \frac{u}{\delta_F} \\ \frac{w}{\delta_{RPM}} & \frac{w}{\delta_F} \end{bmatrix} \begin{bmatrix} \frac{\delta_{RPM}}{V_1} G_{11_s} & \frac{\delta_{RPM}}{V_1} G_{21_s} \\ \frac{\delta_F}{V_2} G_{12_s} & \frac{\delta_F}{V_2} G_{22_s} \end{bmatrix} \begin{bmatrix} \varepsilon_u \\ \varepsilon_w \end{bmatrix} \tag{270}$$

This equation can be written as

$$\begin{bmatrix} u \\ w \end{bmatrix} = [D] \begin{bmatrix} \varepsilon_u \\ \varepsilon_w \end{bmatrix} \tag{271}$$

where $[D]$ is the forward path transfer function matrix resulting from the matrix multiplication indicated in equation 270; i.e.,

$$[D] = \begin{bmatrix} D_{11} & D_{12} \\ D_{21} & D_{22} \end{bmatrix} \tag{272}$$

and

$$D_{11} = \frac{u}{\delta_{RPM}} \frac{\delta_{RPM}}{V_1} G_{11_s} + \frac{u}{\delta_F} \frac{\delta_F}{V_2} G_{12_s}$$

$$D_{12} = \frac{u}{\delta_{RPM}} \frac{\delta_{RPM}}{V_1} G_{21_s} + \frac{u}{\delta_F} \frac{\delta_F}{V_2} G_{22_s} \tag{273}$$

$$D_{21} = \frac{w}{\delta_{RPM}} \frac{\delta_{RPM}}{V_1} G_{11_s} \frac{w}{\delta_F} \frac{\delta_F}{V_2} G_{12_s}$$

$$D_{22} = \frac{w}{\delta_{RPM}} \frac{\delta_{RPM}}{V_1} G_{21_s} \frac{w}{\delta_F} \frac{\delta_F}{V_2} G_{22_s}$$

If equation 269 is substituted into equation 271, one gets

$$\begin{bmatrix} u \\ w \end{bmatrix} = \left[I + D\right]^{-1} \left[D\right] \begin{bmatrix} u_c \\ w_c \end{bmatrix} \tag{274}$$

$$= \left[W\right] \begin{bmatrix} u_c \\ w_c \end{bmatrix} \tag{275}$$

where I is the identity matrix and $\left[W\right]$, the closed loop transfer matrix, is the resultant of the matrix operations indicated in equation 274; i.e.,

$$\left[W\right] = \begin{bmatrix} W_{11} & W_{12} \\ W_{21} & W_{22} \end{bmatrix} \tag{276}$$

Once this matrix inversion and multiplication is performed, it is found that

$$W_{11} = \frac{1}{\beta}\left(1 + D_{22}\right) D_{11} + D_{12}\, D_{21}\right)$$

$$W_{12} = \frac{1}{\beta}\left(1 + D_{22}\right) D_{12} + D_{12}\, D_{22}\right)$$

$$W_{21} = \frac{1}{\beta}\left(D_{21}\, D_{11} + \left(1 + D_{11}\right) D_{21}\right) \qquad (277)$$

$$W_{22} = \frac{1}{\beta}\left(D_{21}\, D_{12} + \left(1 + D_{11}\right) D_{22}\right)$$

where $\beta = \left(\left(1 + D_{11}\right)\left(1 + D_{22}\right) - D_{12}\, D_{21}\right)$.

It can be seen from equation 275 that in order to obtain noninteraction of the control channels the matrix $[W]$ must be diagonal. It is proven in the literature that this condition implies that the matrix $[D]$ must also be diagonal. This implication can be easily verified by considering the resultant simplification of equation set 277 when $D_{12} = D_{21} = 0$. The result is

$$[W] = \begin{bmatrix} \dfrac{D_{11}}{1 + D_{11}} & 0 \\ 0 & \dfrac{D_{22}}{1 + D_{22}} \end{bmatrix} \qquad (278)$$

In equation set 273, the condition for noninteraction yields the following relationships between the components of the controller transfer matrix:

$$G_{12_s} = - \frac{\dfrac{w}{\delta_{RPM}} \quad \dfrac{\delta_{RPM}}{V_1}\; G_{11_s}}{\dfrac{w}{\delta_F} \quad \dfrac{\delta_F}{V_2}} \qquad (279)$$

and

$$G_{21_s} = \frac{-\frac{u}{\delta_F}\frac{\delta_F}{V_2}G_{22_s}}{\frac{u}{\delta_{RPM}}\frac{\delta_{RPM}}{V_1}} \quad . \tag{280}$$

Substituting equations 279 and 280 into the expressions for D_{11} and D_{22} respectively, one gets

$$D_{11} = \frac{(\frac{u}{\delta_{RPM}}\frac{w}{\delta_F} - \frac{w}{\delta_{RPM}}\frac{u}{\delta_F})\frac{\delta_{RPM}}{V_1}}{\frac{w}{\delta_F}} G_{11_s} \tag{281}$$

and

$$D_{22} = \frac{(\frac{u}{\delta_{RPM}}\frac{w}{\delta_F} - \frac{w}{\delta_{RPM}}\frac{u}{\delta_F})\frac{\delta_F}{V_2}}{\frac{u}{\delta_{RPM}}} G_{22_s} \quad . \tag{282}$$

Equations 279 through 282 can be written in a more compact form by substituting the values for $\frac{\delta_{RPM}}{V_1}$ and $\frac{\delta_F}{V_2}$ given in Appendix G and by using the standard nomenclature for the plant transfer functions. After these substitutions the equations become

$$G_{12_s} = -3.74\frac{N^w_{RPM}(s+50)}{N^w_F(s+5)}G_{11_s} \tag{283}$$

$$G_{21_s} = -0.267\frac{N^u_F(s+5)}{N^u_{RPM}(s+50)}G_{22_s} \tag{284}$$

$$D_{11} = \frac{249\ (N^u_{RPM}\ N^w_F - N^w_{RPM}\ N^u_F)\ G_{11_s}}{N^w_F\ (s+5)} \tag{285}$$

and

$$D_{22} = \frac{66.5\ (N^u_{RPM}\ N^w_F - N^w_{RPM}\ N^u_F)\ G_{22_s}}{N^u_{RPM}\ (s+50)} \tag{286}$$

[W] The closed loop transfer functions given by equation 275 with as given by equation 278 are:

$$\frac{u}{u_c} = \frac{D_{11}}{1 + D_{11}} \qquad \frac{u}{w_c} = 0$$

$$\frac{w}{u_c} = 0 \qquad \frac{w}{w_c} = \frac{D_{22}}{1 + D_{22}} \tag{287}$$

The design procedure consists of specifying a desired closed loop dynamic behavior for the non-zero transfer functions of equation set 287. Once this has been done, D_{11} and D_{22} can be determined and they in turn fix G_{11_s} and G_{22_s} through equations 285 and 286 respectively. Finally, G_{12_s} and G_{21_s} are determined through equations 283 and 284 respectively.

Determination of the Aircraft Transfer Functions Under the Assumption of Zero Pitch Angle

In order to carry out the design procedure outlined above, it is necessary to develop the aircraft equations of motion from which the plant transfer functions can be obtained. Under the assumption of zero pitch angle throughout the flight envelope of the aircraft and disregarding the moment equation, these equations are:

$$(s - X_u)\, u - (sX_{\dot{w}} + X_w)\, w = T_{\delta_{RPM}}\, \delta_{RPM} + X_{\delta_F}\, \delta_F$$

$$- Z_u\, u + (s(1-Z_{\dot{w}}) - Z_w)\, w = 0\, \delta_{RPM} + Z_{\delta_F}\, \delta_F \quad . \tag{288}$$

It is convenient to simplify the notation by writing these equations in the following fashion:

$$a_{11}\, u + a_{12}\, w = b_{11}\, \delta_{RPM} + b_{12}\, \delta_F$$

$$a_{21}\, u + a_{22}\, w = b_{21}\, \delta_{RPM} + b_{22}\, \delta_F \quad . \tag{289}$$

Table 28 presents a summary of the values of these coefficients for the six flight conditions. These coefficients were evaluated with the data presented in Appendix E.

TABLE 28. COEFFICIENTS OF THE REDUCED AIRCRAFT EQUATIONS OF MOTION

FC	a_{11}	a_{12}	a_{21}	a_{22}	b_{11}	b_{12}	b_{21}	b_{22}
1	(s+.047)	-.079	.325	(s+3.04)	.20	- 8.84	0.0	- 28.3
2	(s+.088)	-.097	.380	(s+3.54)	.18	-11.60	0.0	-274.0
3	(s+.071)	-.150	.680	(s+1.91)	.10	-10.00	0.0	- 93.1
4	(s+.034)	-.069	.270	(s+2.05)	.09	- 8.68	0.0	-229.0
5	(s+.065)	-.104	.469	(s+1.70)	.08	-10.50	0.0	-107.0
6	(s+.087)	-.144	.670	(s+1.19)	.09	-10.80	0.0	- 58.7

The transfer functions of interest can be written as:

$$\frac{u}{\delta_{RPM}} = \frac{N^u_{RPM}}{\Delta} = \frac{b_{11}\, a_{22} - b_{21}\, a_{12}}{\Delta} \tag{290}$$

$$\frac{u}{\delta_F} = \frac{N_F^u}{\Delta} = \frac{b_{12}\, a_{22} - b_{22}\, a_{12}}{\Delta} \tag{291}$$

$$\frac{w}{\delta_{RPM}} = \frac{N_{RPM}^w}{\Delta} = \frac{a_{11}\, b_{21} - a_{21}\, b_{11}}{\Delta} \tag{292}$$

$$\frac{w}{\delta_F} = \frac{N_F^w}{\Delta} = \frac{a_{11}\, b_{22} - a_{21}\, b_{12}}{\Delta} \tag{293}$$

where $\Delta = a_{11}\, a_{22} - a_{12}\, a_{21}$.

The numerical values for the numerators of these transfer functions are summarized in Table 29.

TABLE 29. NUMERICAL VALUES FOR THE NUMERATORS OF THE AIRCRAFT TRANSFER FUNCTIONS

FC	N_{RPM}^u	N_F^u	N_{RPM}^u	N_F^w	$(b_{11}\, b_{22} - b_{12}\, b_{21})$
1	.20(s+3.04)	- 8.84(s+3.30)	-.065	- 28.3(s-.054)	- 5.66
2	.18(s+3.54)	-11.60(s+5.83)	-.068	-274.0(s+.072)	-49.32
3	.10(s+1.91)	-10.00(s+3.30)	-.068	- 93.1(s-.002)	- 9.31
4	.09(s+2.05)	- 8.68(s+3.87)	-.025	-229.0(s+.023)	-21.75
5	.08(s+1.70)	-10.50(s+2.76)	-.040	-107.0(s+.018)	- 8.98
6	.09(s+1.19)	-10.80(s+1.97)	-.067	- 58.7(s-.036)	- 5.81

Determination of the Elements of the Controller Transfer Matrix

The term within brackets in the numerator of equations 285 and 286 can be simplified by substituting the expressions given by equations 290 through 293. The result is

$$(N^{u}_{RPM}\, N^{w}_{F} - N^{w}_{RPM}\, N^{u}_{F}) = (a_{11}\, a_{22} - a_{12}\, a_{21})\,(b_{11}\, b_{22} - b_{12}\, b_{21}). \quad (294)$$

Therefore, equations 285 and 286 become

$$D_{11} = \frac{249\,(b_{11}\, b_{22} - b_{12}\, b_{21})\,{}^{s}G_{11}}{N^{w}_{F}\,(s+5)} \quad (295)$$

and

$$D_{22} = \frac{66.5\,(b_{11}\, b_{22} - b_{12}\, b_{21})\,{}^{s}G_{22}}{N^{u}_{RPM}\,(s+50)} \quad (296)$$

At this point the design procedure calls for the specification of the desired closed loop behavior of the direct transfer functions. While a first order type response with a time constant of 2-3 seconds is desirable, it is found advantageous, from the standpoint of the realizability of the controller transfer function elements, to specify the following closed loop behavior:

$$\frac{u}{u_c} = \frac{2.5}{(s+.5)(s+5)} \quad (297)$$

and

$$\frac{w}{w_c} = \frac{2.5}{(s+.5)(s+5)} \quad (298)$$

The responses obtained from these transfer functions are acceptably close to that given by a first order system with a pole at $s = -.5$.

Comparison of these requirements with the relations of equation set 287 yields the following D_{11} and D_{22}:

$$D_{11} = D_{22} = \frac{2.5}{s\,(s+5.5)} \quad ; \quad (299)$$

but D_{11} is related to G_{11_s} by equation 295 and D_{22} is related to G_{22_s} by equation 296. Hence, substituting the data from Table 29 for the design flight condition (FC #4), one gets:

$$\frac{(99.6)(-21.75)\ 2.5}{-229\ (s+.023)(s+5)}\ G_{11_s} = \frac{2.5}{s\ (s+5.5)} \tag{300}$$

and

$$\frac{(26.58)(-21.75)\ 2.5}{.1\ (s+2.05)(s+50)}\ G_{22_s} = \frac{2.5}{s\ (s+5.5)} \tag{301}$$

Therefore

$$G_{11_s} = \frac{.105\ (s+.023)(s+5)}{s\ (s+5.5)} \tag{302}$$

and

$$G_{22_s} = \frac{-.00017(s+2.05)(s+50)}{s\ (s+5.5)} \tag{303}$$

Determination of G_{12_s} and G_{21_s} follows directly from equations 283 and 284 respectively. These are:

$$G_{12_s} = \frac{-.00004\ (s+50)}{s\ (s+5.5)} \tag{304}$$

and

$$G_{21_s} = \frac{-.004\ (s+3.87)(s+5)}{s\ (s+5.5)} \tag{305}$$

Equations 302 through 305 specify the elements of the controller transfer matrix necessary to obtain the closed loop transfer functions given by equations 297 and 298 and to obtain a zero value for the crossfeed responses.

It is important to note that the specified closed loop direct and crossfeed responses will occur only in the design flight condition. With the subsystem as developed operational, the closed loop responses for all other flight conditions can be determined by first obtaining the elements of matrix $[D]$ by means of equation set 273 with the controller matrix elements given by equations 302 through 305. Once this is done, the elements of matrix $[W]$ follow directly from equation set 277 and then the closed loop responses are obtained from equation 275.

Determination of the Transfer Functions Relating the Control Surface Deflections to the Command Variables

The determination of the elements of the transfer function matrix relating δ_{RPM} and δ_F to u_c and w_c can be done in a manner similar to that shown above. One major difference is that since the outputs in this case are the control surface deflections, one can no longer claim that

$$[H]=[I] \tag{306}$$

as was implicitly done in the previous development. The matrix equation relating the control surface deflections to the subsystem error matrix is given by

$$\begin{bmatrix} \delta_{RPM} \\ \delta_F \end{bmatrix} = [Z] \begin{bmatrix} \varepsilon_u \\ \varepsilon_w \end{bmatrix} \tag{307}$$

where

$$[Z] = \begin{bmatrix} Z_{11} & Z_{12} \\ Z_{21} & Z_{22} \end{bmatrix} \tag{308}$$

$$= \begin{bmatrix} G_{11_s} & \frac{\delta_{RPM}}{V_1} & G_{21_s} & \frac{\delta_{RPM}}{V_1} \\ G_{12_s} & \frac{\delta_F}{V_2} & G_{22_s} & \frac{\delta_F}{V_2} \end{bmatrix} \tag{309}$$

Substitution of equations 269 and 266 into equation 307 yields

$$\begin{bmatrix} \delta_{RPM} \\ \\ \delta_F \end{bmatrix} = \left[\left[I + [Z][H] \right]^{-1} [Z] \right] \begin{bmatrix} u_c \\ \\ w_c \end{bmatrix} \tag{310}$$

where

$$[H] = \begin{bmatrix} \frac{u}{\delta_{RPM}} & \frac{u}{\delta_F} \\ \\ \frac{w}{\delta_{RPM}} & \frac{w}{\delta_F} \end{bmatrix} . \tag{311}$$

Equation 310 can be written in a more compact manner as

$$\begin{bmatrix} \delta_{RPM} \\ \\ \delta_F \end{bmatrix} = [Y] \begin{bmatrix} u_c \\ \\ w_c \end{bmatrix} \tag{312}$$

where $[Y]$ is the matrix of closed loop transfer functions resulting from performing the indicated matrix inversion and multiplication. The elements of this matrix are:

$$\begin{aligned}
Y_{11} &= \frac{1}{\rho} \left((1+Z_{21}H_{12}+Z_{22}H_{22})Z_{11}+(Z_{11}H_{12}+Z_{12}H_{22})Z_{21} \right) \\
Y_{12} &= \frac{1}{\rho} \left((1+Z_{21}H_{12}+Z_{22}H_{22})Z_{12}+(Z_{11}H_{12}+Z_{12}H_{22})Z_{22} \right) \\
Y_{21} &= \frac{1}{\rho} \left((Z_{11}H_{11}+Z_{22}H_{21})Z_{11}+(1+Z_{11}H_{11}+Z_{12}H_{21})Z_{21} \right) \\
Y_{22} &= \frac{1}{\rho} \left((Z_{11}H_{11}+Z_{22}H_{21})Z_{12}+(1+Z_{11}H_{11}+Z_{12}H_{21})Z_{22} \right)
\end{aligned} \tag{313}$$

where

$$\rho = ((1+Z_{11}H_{11}+Z_{12}H_{21})(1+Z_{21}H_{12}+Z_{22}H_{22})-(Z_{21}H_{11}+Z_{22}H_{21})$$

$$(Z_{11}H_{12}+Z_{12}H_{22}))$$

is the characteristic equation of the subsystem being considered with the control surface deflections as output variables.

The elements of the transfer function matrix $[Y]$ are then determinable for all flight conditions by substitution of the pertinent data in equation set 313.

"The aeronautical and space activities of the United States shall be conducted so as to contribute . . . to the expansion of human knowledge of phenomena in the atmosphere and space. The Administration shall provide for the widest practicable and appropriate dissemination of information concerning its activities and the results thereof."

—NATIONAL AERONAUTICS AND SPACE ACT OF 1958

NASA SCIENTIFIC AND TECHNICAL PUBLICATIONS

TECHNICAL REPORTS: Scientific and technical information considered important, complete, and a lasting contribution to existing knowledge.

TECHNICAL NOTES: Information less broad in scope but nevertheless of importance as a contribution to existing knowledge.

TECHNICAL MEMORANDUMS: Information receiving limited distribution because of preliminary data, security classification, or other reasons. Also includes conference proceedings with either limited or unlimited distribution.

CONTRACTOR REPORTS: Scientific and technical information generated under a NASA contract or grant and considered an important contribution to existing knowledge.

TECHNICAL TRANSLATIONS: Information published in a foreign language considered to merit NASA distribution in English.

SPECIAL PUBLICATIONS: Information derived from or of value to NASA activities. Publications include final reports of major projects, monographs, data compilations, handbooks, sourcebooks, and special bibliographies.

TECHNOLOGY UTILIZATION PUBLICATIONS: Information on technology used by NASA that may be of particular interest in commercial and other non-aerospace applications. Publications include Tech Briefs, Technology Utilization Reports and Technology Surveys.

Details on the availability of these publications may be obtained from:

SCIENTIFIC AND TECHNICAL INFORMATION OFFICE

NATIONAL AERONAUTICS AND SPACE ADMINISTRATION

Washington, D.C. 20546